Dissection of visual signalling based on functionally specific rod photoreceptor mutants

Dissertation

der Mathematisch-Naturwissenschaftlichen Fakultät

der Eberhard Karls Universität Tübingen

zur Erlangung des Grades eines

Doktors der Naturwissenschaften

(Dr. rer. nat.)

vorgelegt von

Vithiyanjali Sothilingam

aus Jaffna, Srilanka

Tübingen

2016

Gedruckt mit Genehmigung der Mathematisch-Naturwissenschaftlichen Fakultät der Eberhard Karls Universität Tübingen.

Tag der mündlichen Qualifikation:	20.05.2016
Dekan:	Prof. Dr. Wolfgang Rosenstiel
1. Berichterstatter:	Prof. Dr. Alfred Nordheim
2. Berichterstatter:	Prof. Dr. Dipl.-Ing. Mathias Seeliger

To my family

Abbreviations

AAV	adeno-associated virus
ARVO	Association for Research in Vision and Ophthalmology
cGMP	cyclic guanosine monophosphate
CaV	calcium voltage-gated (channel)
Cacna1f	calcium voltage-gated channel subunit alpha1 f
cd	candela
CNG	cyclic nucleotide-gated (channel)
CNGA1	alpha-subunit of the cyclic nucleotide-gated (channel)
CNGB1	beta-subunit of the cyclic nucleotide-gated (channel)
CNS	central nervous system
CSNB	congenital stationary night Blindness
DKO	double knockout
DR	dynamic range
ERG	electroretinography, electroretinogram
GC	guanylyl cyclase
GCL	ganglion cell layer
Hz	hertz
HCN	hyperpolarization-activated and cyclic nucleotide-gated (channel)
I/OS	inner/outer segment border
ILM	inner limiting membrane
INL	inner nuclear layer
IPL	inner plexiform layer
IS	inner segment
KO	knockout
LCA	leber's congenital amaurosis
LGN	lateral geniculate Nucleus
NFL	nerve fiber layer
OLM	outer limiting membrane
ONL	outer nuclear layer
OP	oscillatory potentials
OPL	outer plexiform layer
OS	outer segment
PDE6	phosphodiesterase 6
PDE6a	alpha-subunit of the phosphodiesterase 6
PN	post-natal day
RP	retinitis pigmentosa
RR	refractory range
RPE	retinal pigmented epithelium
TE	treated eye
UE	untreated eye
WT	wild type

Contents

Manuscripts that are part of the thesis

Paper I:

Sothilingam V*, Garcia Garrido M*, Jiao K*, Buena-Atienza E, Sahaboglu A, Trifunović D, Balendran S, Koepfli T, Mühlfriedel R, Schön C, Biel M, Heckmann A, Beck SC, Michalakis S, Wissinger B**[§], Seeliger MW**[§], Paquet-Durand F**[§] (2015) Retinitis pigmentosa: impact of different Pde6a point mutations on the disease phenotype. Hum Mol Genet. 24:5486-5499.

Paper II:

Koch S, **Sothilingam V**, Garcia Garrido M, Tanimoto N, Becirovic E, Koch F, Seide C, Beck SC, Seeliger MW, Biel M, Mühlfriedel R[§], Michalakis S[§] (2012) Gene therapy restores vision and delays degeneration in the CNGB1(-/-) mouse model of retinitis pigmentosa. Hum Mol Genet. 21:4486-4496.

Paper III

Sothilingam V[§], Michalakis S, Garcia Garrido M, Biel M, Tanimoto N**, Seeliger MW** (2016) HCN1 Channels Enhance Rod System Responsivity in the Retina under Conditions of Light Exposure. PLoS One. 11:e0147728.

Paper IV:

Michalakis S, Shaltiel L, **Sothilingam V**, Koch S, Schludi V, Krause S, Zeitz C, Audo I, Lancelot ME, Hamel C, Meunier I, Preising MN, Friedburg C, Lorenz B, Zabouri N, Haverkamp S, Garcia Garrido M, Tanimoto N, Seeliger MW, Biel M, Wahl-Schott CA[§] (2014) Mosaic synaptopathy and functional defects in Cav1.4 heterozygous mice and human carriers of CSNB2. Hum Mol Genet. 23:1538-1550.

Paper V:

Knoflach D, Kerov V, Sartori SB, Obermair GJ, Schmuckermair C, Liu X, **Sothilingam V**, Garcia Garrido M, Baker SA, Glösmann M, Schicker K, Seeliger M, Lee A, Koschak A[§] (2013) Cav1.4 IT mouse as model for vision impairment in human congenital stationary night blindness type 2. Channels (Austin). 7:503-513.

*, ** = equal contribution; [§]= corresponding author

I. Summary

Visual signalling initiates in the rod and cone photoreceptors in the retina. The first steps include a multi-step amplification cascade starting in the outer segments upon light exposure and activating the phosphodiesterase 6 (PDE6). PDE6 reduces the level of the second messenger cyclic guanosine monophosphate (cGMP) by hydrolysis. Low levels of cGMP in turn mediate the closure of cyclic nucleotide-gated (CNG) channels as the final step of phototransduction causing a voltage change, the first electrical signal in rods. At downstream photoreceptor synaptic terminals this leads to a reduction in neurotransmitter release which activates the bipolar cells, retinal second order neurons. Thus, the focus of this thesis was to investigate rod signalling precisely by means of rod-specific mutations in rodent models and electroretinography (ERG) which measures the electrical activity of the retina including photoreceptor outer segment function and signal transmission to bipolar. This work concentrates on the role of four distinctive components located in different compartments of rods from the outer segment to the synaptic terminal.

The first part of the thesis addresses the contribution of the PDE6 and the CNG channels, located in rod outer segments, to signal generation. The role of PDE6 was studied in *Pde6a* mutants with differently compromising missense mutations in the alpha-subunit of rod PDE6 (*Pde6a*) resulting in a gradually reduced PDE6 activity in each Pde6a variant. This causes a continuously elevated level of cGMP which triggers a premature degeneration of rods and secondary cone cell death. In this regard, we have found that functionally the generation of rod-driven electrical signals are prevented, resulting in a mostly cone-driven vision in *Pde6a* variants. The remaining cone signal in each Pde6a line is ultimately determined by the speed of photoreceptor degeneration.

The role of CNG channels was addressed in the scope of AAV-mediated gene replacement therapy in the *Cngb1*$^{-/-}$ knockout model characterized by a lack of the beta subunit of the CNG channel (CNGB1) and a respective functional silencing of rod signalling. Functional assessment revealed that genetic restoration of *Cngb1* established rod electrical signals which were even translated to second and third order neurons in the retina.

The second part concerns the role of the hyperpolarization-activated and cyclic nucleotide-gated channels 1 (HCN1) situated functionally downstream at the inner

segments of rod photoreceptors. This work illustrates that a loss of HCN1 channels prolonged rod responses and subsequently saturate rod pathway. Consequently, under regular conditions, HCN1 mediates an inward current which reduces outer segment activity during bright light and enhances rod responsivity. We show here that HCN1 channels are important components of early signal processing within the photoreceptor.

The final part of the thesis describes the role of voltage-gated calcium (CaV1.4) channels. These channels control transmitter release at synaptic terminals, the final step of rod signal processing. Our functional studies describe the consequence of two mutations in the CaV1.4 channels on the synaptic activity. A complete loss of the *Cacna1f* causes a complete failure of signal transmission from photoreceptors to second-order neurons.

II. Zusammenfassung

Der Prozess der visuellen Signalübertragung beginnt in den Stäbchen- und Zapfenphotorezeptoren der Netzhaut. Lichteinfall induziert im Außensegment der Photorezeptoren eine mehrstufige Amplifikationskaskade, dabei wird auch die Phosphodiesterase 6 (PDE6) aktiviert. PDE6 reduziert den Spiegel des sekundären Botenstoffes zyklisches Guanosin Monophosphat (cGMP) über Hydrolyse. Der niedrige cGMP Spiegel bewirkt die Schließung der zyklisch-Nukleotid-gesteuerten (CNG-) Kanäle, was zu einer Spannungsänderung führt und damit das erste elektrische Signal in den Photorezeptoren erzeugt. An der Synapse des Photorezeptors wird daraufhin die Neurotransmitterfreisetzung reduziert, welches letztendlich die sekundär geschalteten Neurone in der Retina, die Bipolarzellen, aktiviert.

Der Fokus dieser Dissertation liegt darin, anhand von stäbchenspezifischen Mutationen in Nagetiermodellen und der Elektroretinographie (ERG), die Signalübertragung der Stäbchen besser zu verstehen. ERG wird hier verwendet, um die elektrische Aktivität der Retina, einschließlich der Außensegmentfunktion der Photorezeptoren und der Signalübertragung zu den Bipolarzellen zu analysieren.

Der erste Teil thematisiert die Rolle der PDE6 und der CNG Kanäle, die in den Stäbchenaußensegmenten lokalisiert sind und zur Generierung der Stäbchensignale beitragen. Hierzu wurden Pde6a Mauslinien analysiert, die verschiedene Missense-Mutationen in der alpha-Untereinheit der Stäbchen-PDE6 (Pde6a) aufweisen. Diese Mutationen führen zu einer graduellen Reduktion der PDE6 Aktivität und somit zu einem kontinuierlich erhöhten cGMP-Spiegel, der eine frühzeitige Degeneration der Stäbchen induziert und somit sekundär den Zelltod der Zapfen bewirkt. Unsere funktionellen Analysen haben ergeben, dass die Generierung von stäbchengesteuerten elektrischen Signalen in den Pde6a Mutanten beeinträchtigt war und ERG Signale daher von Zapfenantworten hervorgerufen wurden. Die Stärke der verbleibenden Zapfenantworten ist dabei abhängig von dem Fortschreiten der Zapfendegeneration.

Die Rolle der stäbchenspezifischen CNG Kanäle wurde im Rahmen einer AAV-vermittelten Genersatztherapie im Cngb1$^{-/-}$ Knockout-Modell erforscht, dem die beta-Untereinheit des CNG Kanals (CNGB1) fehlt und dies folglich zum nahezu vollständigen Funktionsverlust der Stäbchensignale führt. Unsere funktionellen

Untersuchungen zeigten, dass durch den gentherapeutischen Ersatz des Cngb1 Gens stäbchenspezifische elektrische Signale erzeugt wurden, die auch an nachgeschaltete Bipolarzellen weitergeleitet wurden.

Der zweite Teil der Doktorarbeit fokussiert die Rolle der HCN1 Kanäle. Unterschiedliche funktionelle Studien am ERG zeigten hier, dass ein Verlust von HCN1 Kanälen die Stäbchenantworten verlängert und in Folge den kompletten Stäbchensignalweg sättigt. Diese Analysen beleuchten, dass HCN1 Kanäle durch den Einwärtsstrom von Ionen die Aktivierung der Außensegmente unter starkem Lichteinfluss reduzieren und dadurch die Empfindlichkeit der Stäbchen verbessern. HCN1 Kanäle tragen so als essentielle Bestandteile zur frühen Signalverarbeitung innerhalb des Photorezeptors bei.

Der finale Teil der Dissertation befasst sich mit der Rolle der spannungsgesteuerten Calcium1.4 (CaV1.4) Kanäle, die die Transmitterfreisetzung an den Synapsen kontrollieren, dem finalen Schritt der Signalweiterleitung. Unsere ERG-Funktionsstudien beschreiben die Konsequenzen von zwei Mutationen im Cacna1f-Gen, das für den CaV1.4 Kanal kodiert. Hierbei verursacht eine vollständige Dysfunktion des Kanals eine komplette Störung der Signalübertragung von Photorezeptoren auf Bipolarzellen. Ein durch die Mutation hervorgerufener Funktionszugewinn hingegen, reduziert die synaptische Aktivität.

1. Introduction

The visual system includes the eyes, the major sensory organ, connecting pathways through to the visual cortex, and other parts of the central nervous system (CNS). Initially, light passes the optics of the eye and reaches the retina where the photo-sensing cells convert light into an electrical through a cascade of molecular mechanisms. On the way through downstream retinal neuronal cells the sensory information is further processed and then travels via the axons of the output ganglion cells through the optic nerves which are divided and partially crossed over into the optic chiasm and then proceed via the optic tracts to the lateral geniculate nucleus (LGN). From the LGN, the signals continue to the primary visual cortex where further visual processing takes place.

The structure of the eye (Fig. 1) of all vertebrates is based upon a common plan, with similarities in some of the neurons found in the retina, their interconnections, the places in the brain that receive their axon terminals (Rodieck 1998). The eye is an opaque ball, composed of three concentric layers and three chambers of fluid. The external layer consists of the sclera and the cornea; an intermediate layer also called the vascular layer consisting of the choroid, ciliary body, and iris; and an inner layer of nerve tissues, the retina. The front of the eyeball is the cornea, a transparent bulge which contributes to image-forming process by refracting light entering the eye. It merges into the sclera, which is part of the supporting wall of the eyeball and is in continuity with the dura of the central nervous system. The first anterior chamber, placed between cornea and iris, is filled with aqueous humour. After light passes through the cornea, a portion of it travels through an opening known as the pupil. The size of the pupil can be adjusted by the dilation of the iris, a diaphragm that is capable of stretching and reducing the size of the opening and hence controlling the amount of light that enters the eye. The posterior chamber is situated between the iris, the zonule fibers and the lens and is connected to the anterior chamber via the pupil (Purves et al. 2001). Light further enters the crystalline lens which is made of a fibrous material, containing about 65% water and 35% protein (Spalton et al. 1994). A major difference of the mouse eye which we focused in this study is the much larger lens in mouse than humans relative to the eye size.

The lens is suspended by zonule fibers which translate any increase or reduction in the tone of the ciliary muscle into shape changes of the lens, a process called

accommodation that allows forming sharp retinal images of objects at different distances. The third chamber, the vitreous, lies between the lens and the retina and captures 4/5 of the space inside the back part of the eye. A gelatinous substance known as the vitreous humour fills the cavity and plays an important role in nourishing the inner structures of the eye. Light passes through the vitreous to be projected on the retina, the third layer of the eye. The central cone-only region of the human retina is called the fovea and is responsible for high resolution. The region surrounding the fovea is termed macula and contains higher density of cones compared with the peripheral retina. The mouse retina lacks a distinct fovea and/or a macula.

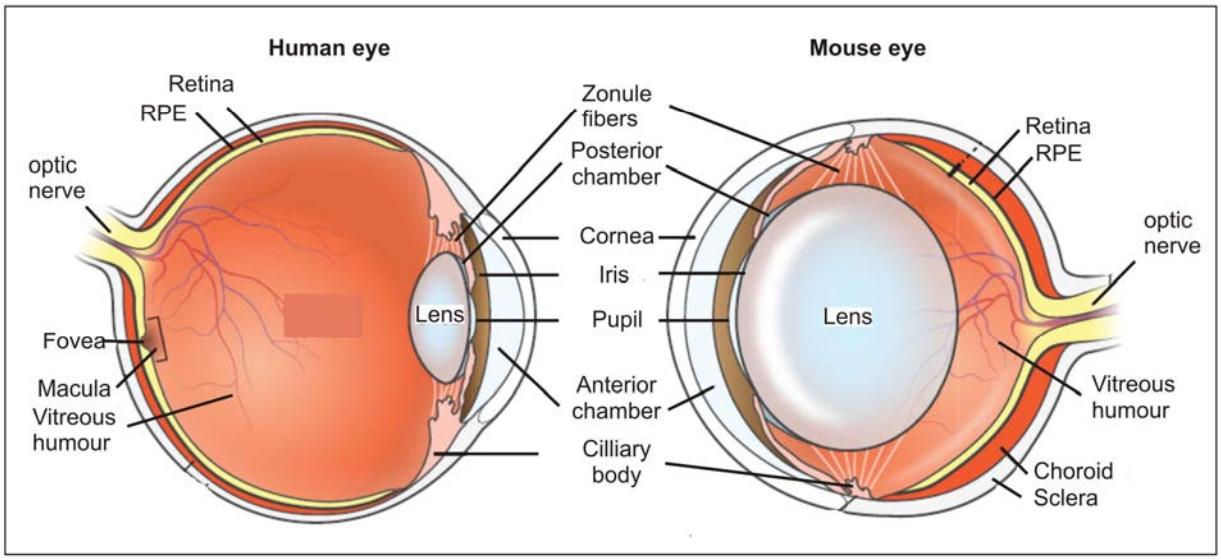

Figure 1: The structural components of the human (left) and the mouse (right) eye (modified from Veleri et al. 2015).

1.1 Anatomy of the Retina

The retina is part of the brain which is displaced into the eye during development (Dowling 1987). A radial section of the retina (Fig. 2) reveals that the light-sensing photoreceptors (the rods and cones) lie outermost in the retina against the pigment epithelium and choroid. Light must therefore travel through the thickness of the retina before striking and activating the photoreceptors (Kolb 2005). The sensory signals are then further processed through downstream retinal neuronal cells including bipolar, horizontal, amacrine and ultimately via the output ganglion cells to the CNS (Fig. 2B). The several classes of retinal neurons are organized into three cellular (nuclear) layers which are separated by two synaptic layers (plexiform layers). The primary layers from the outermost surface to the innermost surface are (Fig. 2A):

a. retinal pigment epithelium (RPE)
b. outer and the inner segments (OS/IS)
c. outer limiting membrane (OLM)
d. outer nuclear layer (ONL)
e. outer plexiform layer (OPL)
f. inner nuclear layer (INL)
g. inner plexiform layer (IPL)
h. layer of ganglion cells (GCL)
i. nerve fiber layer (NFL)

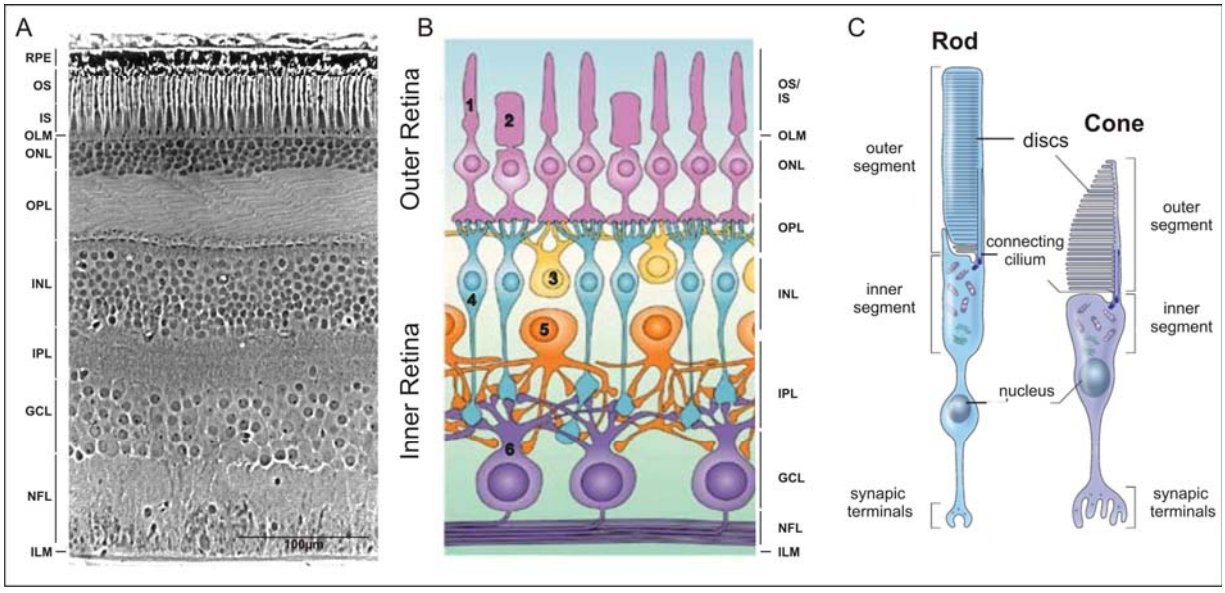

Figure 2: The structure of the retina. (A) Histology of the retinal layers (modified from Boycott and Dowling 1969). Scale bar: 100µm. (B) Neuronal organization of the retina (modified from Wässle 2004): (1) rod photoreceptors, (2) cone photoreceptors, (3) horizontal cells, (4) bipolar cells, (5) amacrine cells, (6) ganglion cells. (C) Scheme of a rod (left) and a cone (right) photoreceptor cell (from Veleri et al. 2015).

The retina can be subdivided into an inner and an outer part. The outer part of the retina contains four different layers: including the retinal pigment epithelium, the photoreceptor outer and inner segments, the outer nuclear layer, and the outer plexiform layer (Fig. 2).

The retinal pigment epithelium (RPE) is a single sheet of cells at the outermost retinal surface containing pigment granules. The RPE is located between the outer segments of the photoreceptors and the choroid. As an important part of the blood-retina barrier, the RPE transports ions, water, and metabolic end products from the subretinal space to the blood while it takes up nutrients from the blood and delivers them to photoreceptors. Furthermore, it improves the quality of vision by absorbing stray light in melanin granules. The phagocytosis of the expended photoreceptor outer segments as well as the protection against free radicals is an additional task of the RPE (Bok 1993, Boulton and Dayhaw-Barker 2001, Futter et al. 2004).

The photoreceptors, rods and cones, are the light-converting sensory cells which are physiologically divided in two parts: The distal part (inner and outer segments) is optimized for capturing light, whereas the proximal part (cell bodies and synaptic terminals) is specified to pass the information to the inner retina. Both photoreceptors have basically similar structures (Kaneko 1979), but they differ in shape as cones usually are shorter and thicker than the long, slim rods (Fig. 2C).

The outer segments (OS) of the photoreceptors are actually modified cilia (Richardson 1969) which are in contact with apical processes from the retinal pigment epithelium. These connections are necessary for the constant renewal processes of OS segments. In rods, the entire OS is replaced every 8-14 days, and in cones, a complete renewal takes about 9 months to one year (Rodieck 1998).

While the rod OSs contain a set of membranous discs which resemble a stack of coins, the OSs of cones are mainly infoldings of the surface membrane (Fig. 2C). The rhodopsin, the visual pigment in the discs of rods, is sensitive to blue-green light (Detwiler 1943). In mammals, usually only one type of rods can be found but there are two or three types of cones. Primates exhibit three types of cones which are maximally sensitive for long wavelengths, middle wavelengths or short wavelengths (Curcio et al. 1987). Most other mammals including rodents typically use only short wavelength-sensitive (SWS) cones, equivalent to blue cones, and medium

wavelength-sensitive (MWS) cones, corresponding to green cones, but no red cones exist.

The inner segments (IS) of the photoreceptors contain components that provide energy for the high metabolic OSs (e.g. mitochondria) or visual pigment molecules that are synthesised and transported to the OS. Both segments are connected by a cilium arising from the basal body of the IS.

The number and ratio of photoreceptor subtype varies among species, dependent on whether an animal is primarily diurnal or nocturnal. The murine retina, similar to human, is rod-dominated and consists to about 97.2 % of rods and to about 2.8 % of cones (Carter-Dawson and LaVail 1979).

The outer limiting membrane (OLM) builds a narrow zone of junctions between Müller cells and the ciliary region of photoreceptor outer segments and is thought to play a role in maintaining the structure of the retina through mechanical strength. It also separates the IS from the outer nuclear layer.

The outer nuclear layer (ONL) consists of the cell bodies of the photoreceptors, mostly of the rod cell bodies. Cone cell bodies are commonly situated in the distal part of the ONL, and their outer segments in the region of the rod inner segments.

The outer plexiform layer (OPL) includes the synaptic terminals of photoreceptors which connect to the dendrites of bipolar and horizontal cells, and Müller cell processes. The synaptic terminals differ between the photoreceptors: the so-called rod spherules contain a single invagination of the cell membrane, a synaptic cleft, whereas the cone endings, the pedicles, are complex structures with a number of invaginations.

The inner retina also consists of four different layers, including the inner nuclear layer, the inner plexiform layer, the ganglion cell layer and the nerve fiber layer (Fig. 2).

The inner nuclear layer (INL) is formed by cell bodies of four types of cells: horizontal cells, bipolar cells, amacrine cells and Müller cells. Horizontal cells are laterally connecting neurons which are involved in contrast vision. Bipolar cells collect and process information from the outer retina and relay it to the amacrine and/or ganglion cells in the proximal inner retina.

The inner plexiform layer (IPL) is formed by synaptic connections between bipolar, amacrine, and ganglion cells. Most amacrine cells can be found in the proximal part

of the INL and are the second laterally orientated neurons, but some are dislocated in the ganglion cell layer. Müller cells are the retinal glial cells which support the structure of the retina. They extend through the entire retina, but their nuclei are located in the INL. Müller cells are also associated with nutrition of the photoreceptor IS and act as ionic reservoir (spatial-buffering) during the light-dependent ion fluctuations (Frishman 2006).

The ganglion cell layer (GCL) consists of ganglion cells that collect all visual information processed in the retina and pass it to the brain via the optic nerve. Their cell bodies are located mainly in the GCL, and their dendrites form synapses with bipolar and amacrine cells, located in the IPL (Wässle 2004).

The nerve fiber layer (NFL) represents the innermost layer of the retina and is formed by retinal ganglion cell axons converging from all parts of the retina toward the optic disc.

The inner limiting membrane (ILM) is formed by the proximal end feet of the Müller cells and the astrocytes which act as a diffusion barrier between the neural retina and vitreous humour.

1.2 Physiologies of the Retina

The anatomy of the retina is the result of an evolutionary optimization for the best possible early processing of visual information (Wässle and Boycott 1991, Masland 2001). The highly-sensitive rods are responsible for night vision and increase sensitivity of our visual system, even capable of recognizing a single photon. The less-sensitive cones function best under daylight conditions and permit colour and contrast vision. In most sensory systems, activation of a receptor by the appropriate stimulus causes a depolarization of the membrane potential, stimulating an action potential, a sequence of electrical pulses, and transmitter release onto the neurons it contacts. In the retina, however, photoreceptors do not exhibit action potentials. Light activation leads to a graded change in membrane potential and a corresponding change in the rate of transmitter release onto postsynaptic neurons (Purves 2001). First action potentials (spikes) are found at the level of ganglion cells, but current studies showed clear evidence for early spiking neurons, such as on the level of amacrine cells or bipolar cells (Baden et al. 2013, Reifler et al. 2015). The conversion from ‘analog’ to ‘digital’ coding is a fundamental transformation carried out by the visual system, but the mechanisms are still not well understood.

1.2.1 Phototransduction

The phototransduction events describe the first conversion of the light signal into a sensory signal in photoreceptor outer segments. The cascade is broadly similar in rods and cones and due to the complexity, here only the key proteins associated with rod phototransduction are shown (Fig. 3). During darkness, the presence of high levels of second messenger cyclic guanosine monophosphate (cGMP) results in an opening of CNG channels, which causes an inward current of cations in the outer segment of rods and ultimately a constant depolarization. Steady intracellular concentrations of ions are maintained by Na^+-K^+ pumps and K^+ flows through non-gated K^+ channels (I_K) located in the inner segments. The ion flow during darkness is termed as dark current (Penn and Hagins 1969). Ca^{2+} influx through cyclic nucleotide-gated (CNG) channels further inactivates the guanylyl cyclase (GC) which is responsible for cGMP synthesis.

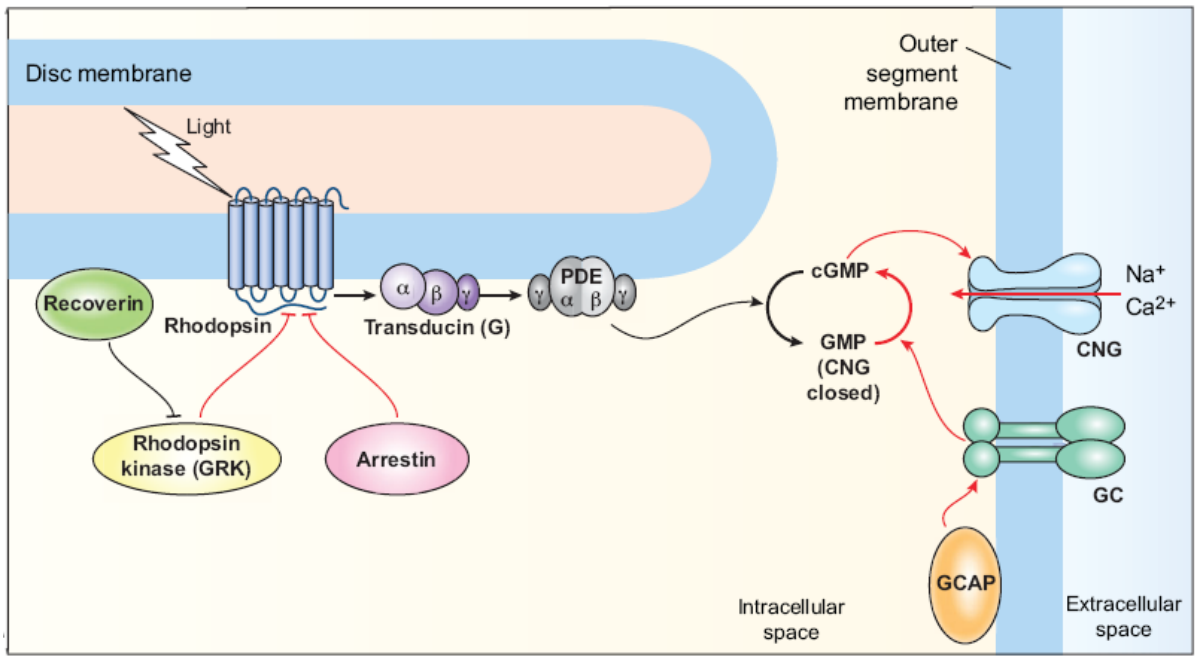

Figure 3: Phototransduction cascade in PR outer segments (from Veleri et al. 2015).

Phototransduction starts with the capture of photons and a conformational change of the rhodopsins. The activation of rhodopsin leads to a dissociation of the transducin (G-protein) subunits ßγ from Gα, and the sequential activation of the phosphodiesterase (PDE6) which catalyse the hydrolysis of the cGMP. The reduction of the cGMP level causes a closure of the CNG channels, consequently diminishing the dark current and hyperpolarizing the membrane potential. This voltage change causes a modulation of the neurotransmitter release at downstream synaptic endings

of rods (not shown here). The termination of the phototransduction cascade includes processes like the inactivation of rhodopsin and transducin-phosphodiesterase complex.

1.2.2 Signal Pathways

The major rod and cone pathway (reviewed in Wässle 2004) are anatomically well established (Fig. 4):

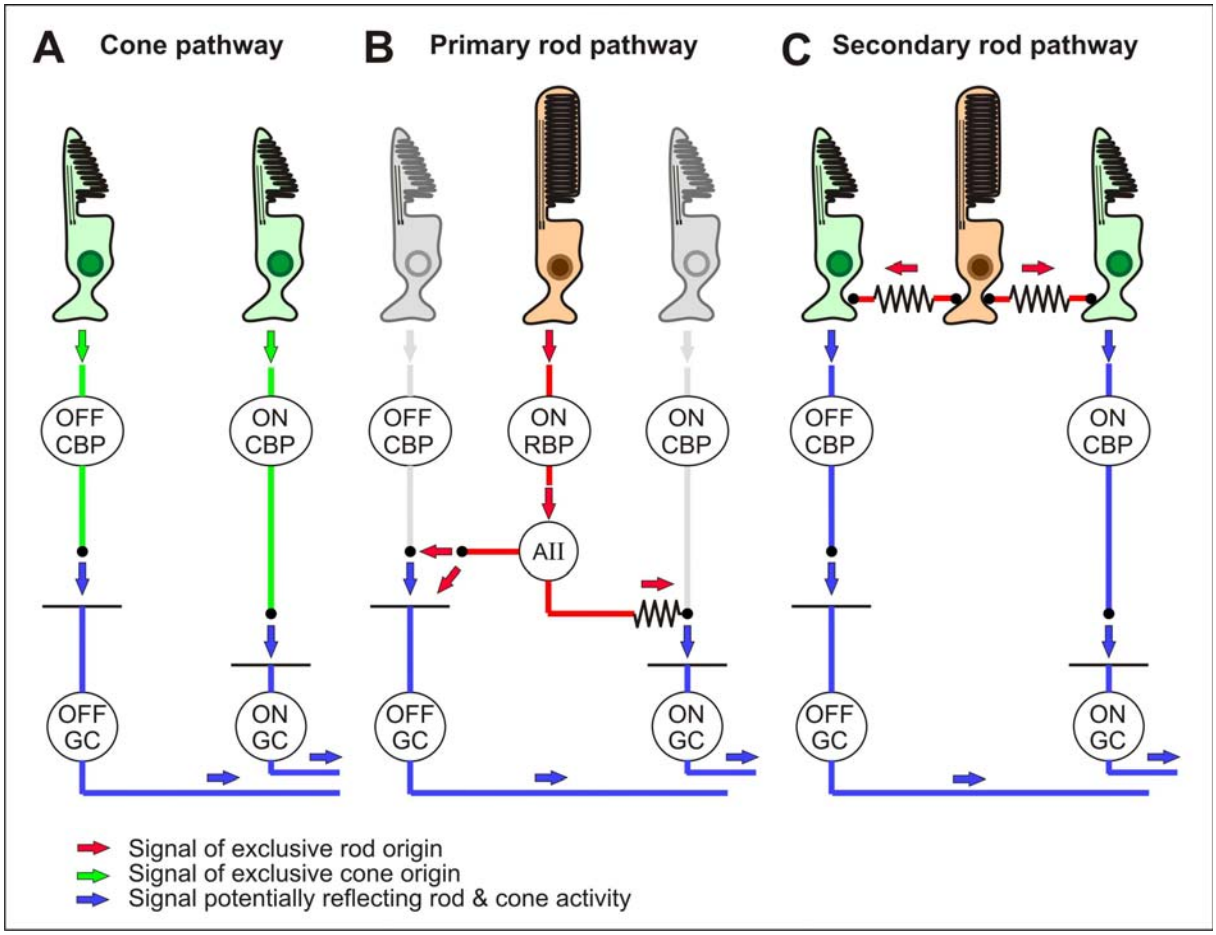

Figure 4: The major cone and rod signal pathways (modified from Seeliger et al. 2010).

In the cone pathway (A, green arrows) light-activated cones connect to ON bipolar cells, which are activated through depolarization whereas light-inhibited OFF bipolar cells are still silenced through hyperpolarization. There are roughly 9 distinct forms of cone bipolar cells, while there is only one rod bipolar cell type, due to the later evolutionary development of rods. ON- or OFF bipolar cells of cones finally connect to corresponding third order ON- or OFF ganglion cells.

The classical primary rod pathway (B, red arrows) manages vision at very dim light conditions and connects rods via rod (ON) bipolar cells to AII amacrine cells and eventually enters the cone ON pathway. It also suppresses cone OFF signalling.
The secondary rod pathway (C) becomes operational at higher illuminations. Rod signals access the cone ON pathway via rod-cone electrical coupling through gap junctions. A third pathway connecting rods to certain types of ON- and OFF-bipolar cells has also been described but awaits further clarification and is not shown for sake of clarity (Tsukamoto et al. 2001, Tsukamoto and Omi 2014).

1.3 Pathologies of the Retina

Mutations in genes that affect the function of photoreceptors impair the processing of visual information in photoreceptors and may even lead to retinal degenerative disorders up to blindness. Hereditary retinal disorders are a clinically and genetically heterogeneous group, usually caused by monogenic defects and currently untreatable (Fig. 5). The group include stationary and progressive forms with diffuse and localized manifestations.

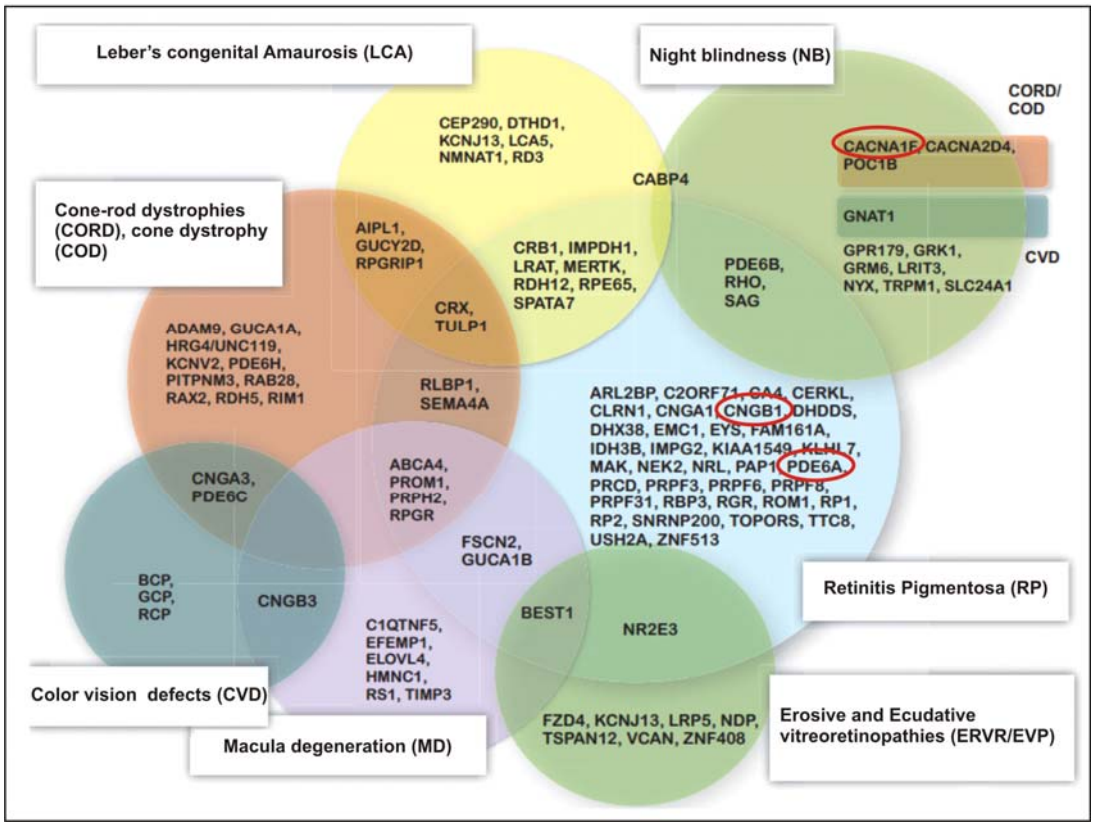

Figure 5: Groups of inherited retinal disorders and genes involved (from Berger et al. 2010; update 2014).

1.3.1 Retinitis Pigmentosa

Retinitis Pigmentosa (RP) is the most common form of inherited retinal disorders that is characterized by a progressive degeneration type (Pagon 1988, Hartong et al. 2006) and can appear in an autosomal-dominant, autosomal recessive, an X-linked form or in a syndromic manner as in e.g. Usher-Syndrome or Bardet-Biedl-Syndrome (Daiger et al. 2013). Currently more than 50 genes are known to cause RP (Berger et al. 2010); many of them are preferentially or even exclusively expressed in rod photoreceptors (Hartong et al. 2006). These genes encode for proteins such as the rod PDE6 (Bayes et al. 1995, Dryja et al. 1999, 2009, Dvir et al. 2010) or the rod CNG channel (Dryja et al. 1995, Travis et al. 1998) which are vital for phototransduction processes. The other minor fraction of RP genes encode for proteins that impair other cell types, e.g. RPE cells. RP is characterized by a primary loss of photoreceptors followed by degeneration of the outer layers of the retina, whereas the inner retina is widely preserved until late in the course of the disease (Santos et al. 1997, Milam et al. 1998). In human, there is a large variability in the age of onset, progression, retinal appearance, and final visual outcome. This variability is also consistent in mouse models where the severity of disease phenotype varies among animal models for RP, known so far.

1.3.2 Congenital Stationary Night Blindness

Congenital stationary night blindness (CSNB) is a further group of hereditary retinal disorders and has a non-progressive course. CSNB can be classified in two groups. The complete CSNB type 1 predominantly affects the inner retina, including changes proximal to photoreceptors. Most of the genes encode for proteins located in ON-bipolar cells, such as the *NYX* gene which encodes a protein involved in retinal synapse formation or synaptic transmission (Bech-Hansen et al. 2000, Pusch et al. 2000). However, the X-linked incomplete CSNB type 2 (CSNB2) can be caused by a mutation in the *CACNA1F* gene encoding for an L-type calcium channel located at the synaptic terminals of the photoreceptors (Strom et al. 1998, Bech-Hansen et al. 1998). Due to the X-chromosomal recessive inheritance males are far more frequently affected than females. However clinical symptoms are occasionally also observed in female carriers (Rigaudiere et al. 2003, Hemara-Wahanui et al. 2005, Michalakis et al. 2013).

2. Methods: Electroretinography (ERG)

The ERG measures temporally consecutive activities of photoreceptor based processes and the subsequent signal transmission to the neuronal network of the retina (Klinke and Silbernagel 2001) which are described in Chapter 1.2. For this reason, ERG is an appropriate biomarker to assess the contribution of four key components to different steps in visual processing.

The cellular origins of major ERG components were initially demonstrated by Granit 1934 and were further established by a wide range of scientists (Tomita 1981, Miyake 2006, Frishman 2006) leading to a better understanding of visual signal processing within the retina. That is precisely why ERG is nowadays an established diagnostic technique in clinical ophthalmology and in basic research (Frishman 2006, Tanimoto et al. 2009, McCulloch et al. 2015).

2.1 Principle of ERG

The ERG reflects a sum response of event-related transient electrical activity of the entire retina to a light stimulation (Tanimoto et al. 2009). The electrical response of the eye is generated by radial currents that originate either directly from retinal neurons or their supporting cells, the Müller cells, which buffer the large extracellular ion concentrations (Frishman 2006). One main factor regarding the contribution of different retinal neurons to the ERG is their orientation. According to the radial current, radially oriented retinal neurons like photoreceptors and bipolar cells have larger contributions to the ERG than tangentially positioned cells like horizontal and amacrine cells. The correlation of the cellular actions of the retina to respective ERG signal components are illustrated for our settings (Fig. 6):

(A) In the dark, the photoreceptor is in a depolarized state due to maximally opened CNG channels which allow an inward current. At synaptic terminals this results in a high downstream synaptic activity, indicated by the amount of transmitter release. Consequently, this leads to a baseline ERG.

(B) Stimulation by a bright light diminishes the dark current in the outer segments by closure of CNG channels and hyperpolarizes the membrane potential. This in turn is translated to an initial negative deflection (the leading edge of a-wave) in the ERG.

(C) Further downstream in the photoreceptor the strong hyperpolarization leads to a great reduction of synaptic activity, which activates post-synaptic depolarizing (ON-) bipolar cells leading to a large positive deflection (b-wave).

(D) Despite unchanged CNG activity, the voltage change is sensed by the HCN1 channels. After a certain time delay they become active and the HCN1-mediated inward current drives the membrane potential of the photoreceptor back to the depolarized state inducing an increased synaptic activity and a decreased ON-bipolar cell function. The result is a substantial, but not complete, reduction of the ERG b-wave signal.

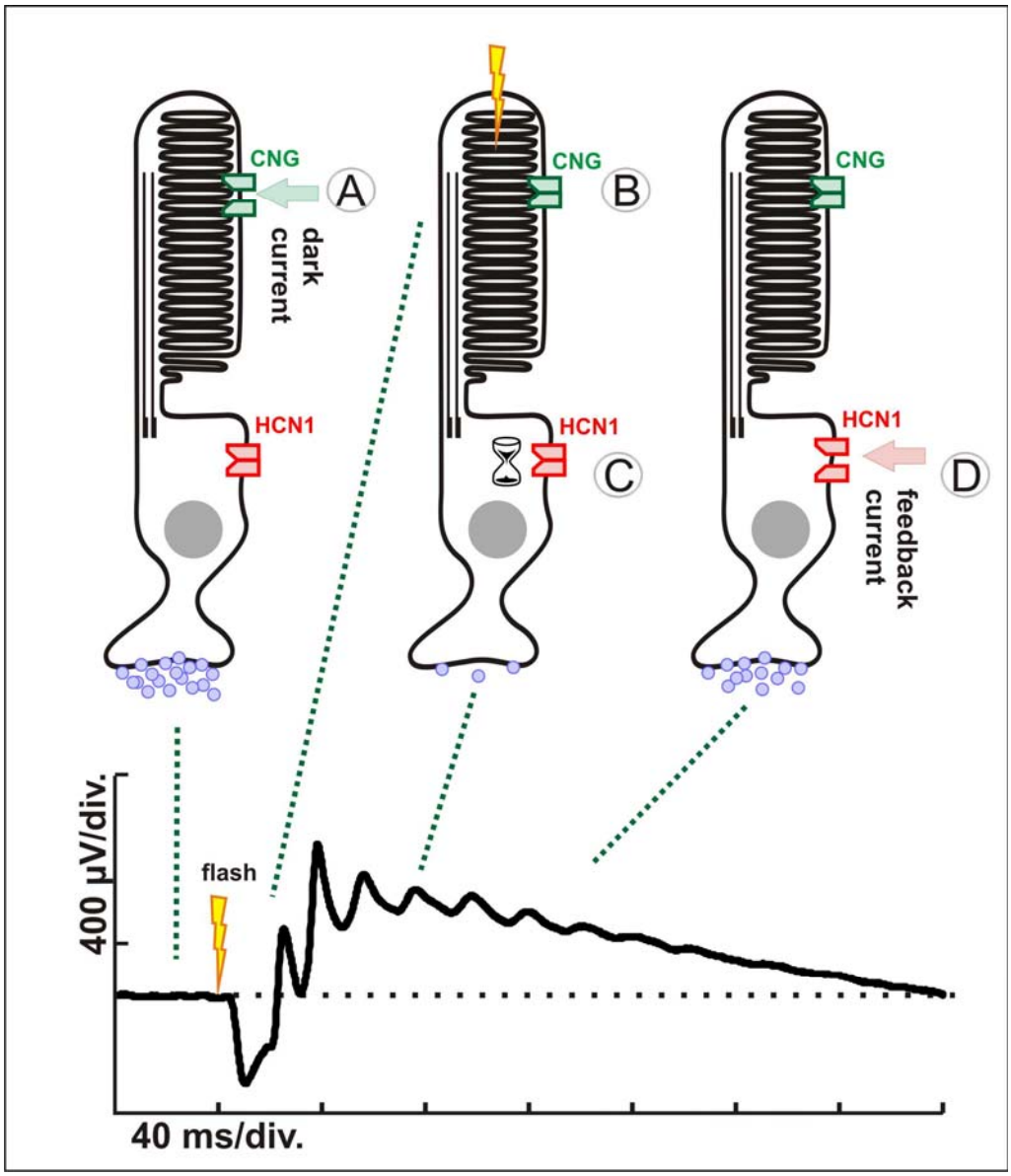

Figure 6: Correlation of cellular electrical activities in the retina to ERG components (modified from Seeliger et al. 2010).

2.2 Preparations before ERG Examination

Preparations before the measurement start with an over night dark adaptation or a minimum of 6 hours (Tanimoto et al. 2009 and 2013). On the day of ERG examination, a subcutaneous injection of a mixture of Ketamine (66.7 mg/kg body weight), Xylazine (11.7 mg/kg body weigh), and physiological saline is given for anaesthesia as previously described (Tanimoto et al. 2009). After a stable anaesthesia the pupils are dilated with tropicamide eye drops (Mydriaticum Stulln, Pharma Stulln, Stulln, Germany).

The ERG equipment in our lab is from Multiliner Vision, VIASYS Healthcare GmbH, Hoechberg (Germany) and consists of a Ganzfeld bowl which uniformly stimulates the entire retina, a direct current amplifier as well as a PC-based control and recording unit (Fig. 7). Additionally to this equipment we use a small box which is essential for the ERG analysis on small animal models like for e. g. mice. The box is covered with a heating pad which enables the control of body temperature (a sensitive parameter) of the anaesthetized mouse during ERG.

Figure 7: The Ganzfeld ERG recording unit.

For the ERG measurement, the mouse is symmetrically placed on the small box. Two active electrodes (e.g. ring electrode made of gold wire) and two short (disposable stainless) needle electrodes for a reference and a ground electrode are needed. The first needle electrode is applied as reference at the forehead region as well as a second ground electrode at the back near the tails. The positioning of the active electrodes includes moistening of these electrodes with methylcellulose and positioning of them on the surface of both corneas. After the impedance of each electrode is checked, the small box is placed into the Ganzfeld bowl and the mouse eyes were placed well into the center. ERG responses are obtained from both eyes simultaneously, due to a verification of proper positioning of active electrodes by comparing ERG responses between right and left eyes. Furthermore the measurement of both eyes is particularly necessary in case of experiments with therapeutic aims, where the untreated eye could be used as an internal control (Michalakis et al. 2010, Koch et al. 2012).

2.3 ERG Recording Protocols

Important factors that determine the contribution of the retinal neurons to ERG include stimulus conditions, background illumination (which influences retinal adaptation levels) and duration of the stimulus. Therefore it is essential that appropriate ERG protocols have to be tailored in order to specifically analyze visual signals of retinal neurons. Additionally, specific mouse mutants lacking either rod or cone system functionality enable a dissection of rod and cone mediated visual signalling in ERG (Tanimoto et al. 2009).

ERG recordings are usually divided into two groups according to the frequency of stimuli, the so-called single flash which represents an intensity series and the flicker ERG with a change in frequency from very low to high. In our laboratory, ERG examinations start with scotopic measurements (without background illumination) which enable the assessment of rod system dominated activity (Fig. 8A). Accordingly, single flash ERG responses at light levels up to 10 mcd*s/m^2 reflect pure rod system activity (orange marked area) and ERG traces above 10 mcd*s/m^2 represent mixed rod and cone system activities (Fig. 8A, orange and green marked area). After a certain light-adaptation period (about 10 min) photopic ERG measurements were continued under a steady background illumination of 30 cd*s/m^2 starting at 10

mcd*s/m^2 and allowing to obtain information exclusively about cone system contributions (Fig. 8B, green marked area). The rod system is usually saturated and cannot react under these conditions (Tanimoto et al. 2009 and 2013). The contributions of rod and cone system functionality are altered when specific genetic defects in mice cause a strong desensitization of rod photoreceptors (Seeliger et al. 2001, Samardzija et al. 2009).

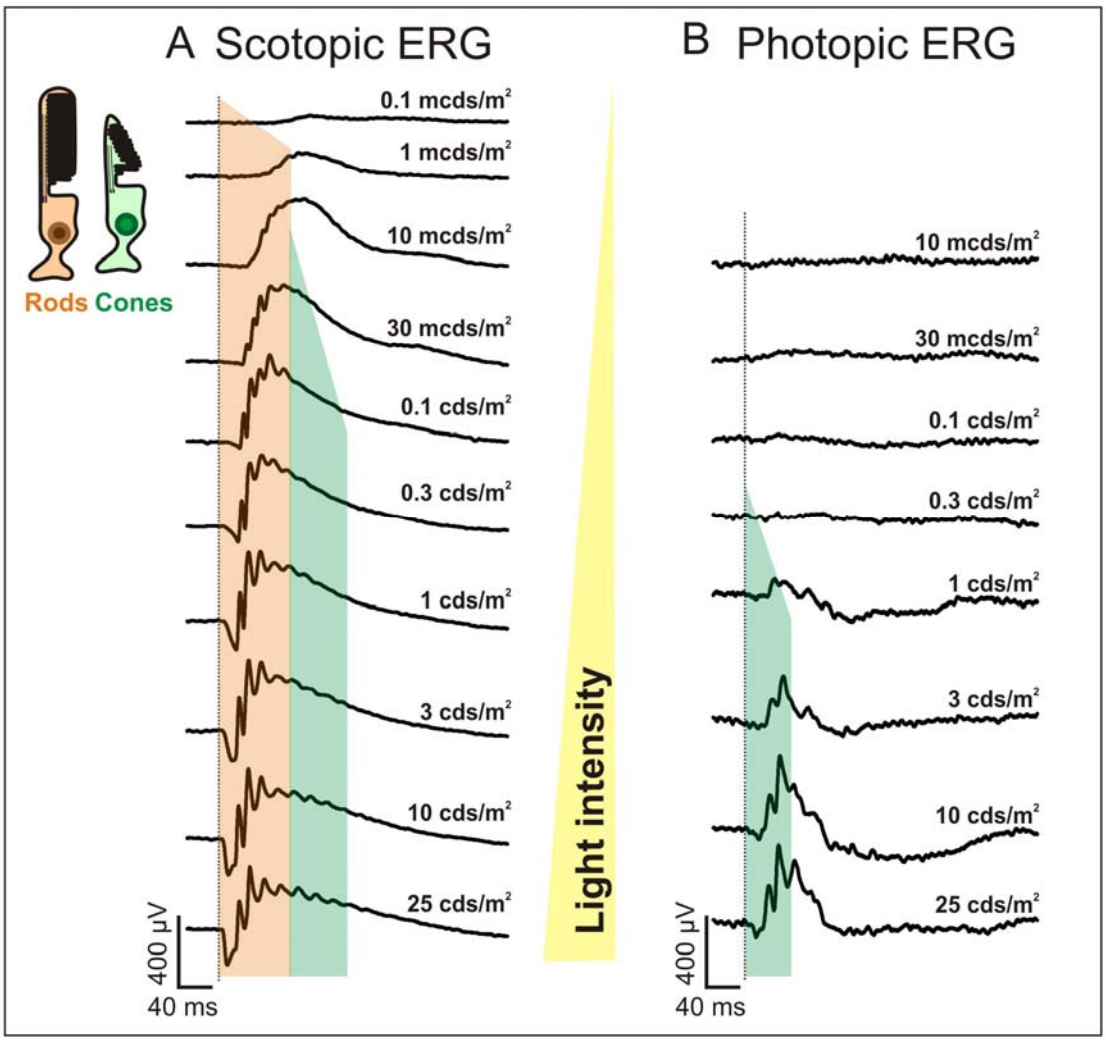

Figure 8: The rod system and cone system contribution to scotopic (A) and photopic (B) single flash ERG.

As initially mentioned in Chapter 2.1 the flash of light elicits a biphasic ERG waveform which is typically composed of an initial negative component, the a-wave, and a subsequent positive component, called b-wave (Fig. 9A). A third component of the ERG are the oscillatory potentials (OPs), a number of higher-frequent and low-amplitude wavelets on top of the b-wave which vary in size and in number with

increasing stimulus intensities (Frishman 2006, Tanimoto et al. 2009 and 2013). The initial a-wave is dominated by photoreceptor outer segment activity and the following b-wave component reflects the activity of ON bipolar cells. In particular cases, a specific reduction of the b-wave is a reliable marker to diagnostically identify defects in synaptic transmission originating either from photoreceptor presynaptic endings or from postsynaptically connected bipolar cells (Pardue and Peachey 2014).

Single-flash protocols are considered a minimum requirement to dissect rod from cone signalling, but additional flicker ERG protocols can be performed to further examine the major bipolar cell contributions of the rod and cone pathway (Tanimoto et al. 2015). Specific flicker ERG protocols are described in the Results, Chapter 4.2.2.

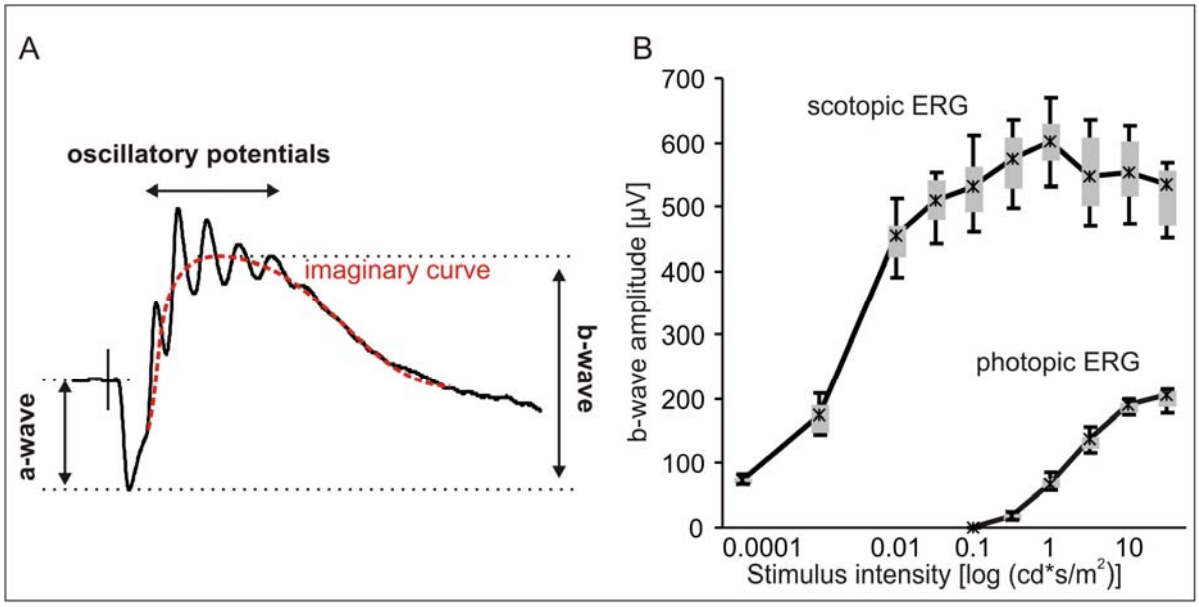

Figure 9: (A) Major components of the ERG (adopted from Tanimoto et al. 2009). (B) Box-and-whisker-plot of single-flash intensity series of a wild type group (kindly provided from Dr. Tanimoto).

2.4 ERG Data Analysis and Presentation

In our lab, ERG data are initially analyzed by evaluating the b-wave amplitudes (from the trough to the peak [in microvolt]) and the implicit time (time, expressed in milliseconds, between the start of the stimulus and the peak of the b-wave). The b-wave analysis is a useful first indication of the overall retinal functionality, as neuronal activities of the inner retina are dependent on photoreceptor function. In particular cases where photoreceptor activity is impaired, we additionally examine the a-wave amplitude and implicit time.

The configuration of the murine ERG is in principle comparable to human ERG; however, the b-wave and the superimposed OPs are large in mice. Due to the relatively large OPs an imaginary curve (Fig. 9A, red dashed curve) which approximately runs through the midpoints of all OPs is fitted on the b-wave of both the dark-adapted and light-adapted single-flash intensity series. The analyzed data of all mice in each group are then summarized in amplitude vs. log intensity (VlogI) curve (Fig. 9B) and an implicit time plot, respectively. We usually use the box-and-whisker plot, including the 5, 25, 50 (median), 75, and 95% quantiles, which provides a proper data presentation independent of the underlying statistical distribution than the mean and standard deviation (Tanimoto et al. 2009).

3. Objectives

The aim of the thesis is to explore the role of four selected signalling components located in different compartments of the photoreceptor cell, each contributing to a different step in visual processing. The structure of the thesis follows this functional order by a division into three parts reflecting the sequence of signal flow (Fig. 10):

The origin of rod vision: From biochemistry to electricity

The process from the reception of light in the opsin complex to the generation of an early electrical visual signal is known for quite some time. Nevertheless, many details in this sequence are still not clear even today. The first aim of this work was thus to characterize some of the key elements of phototransduction located in rod outer segments.

PDE6, the rod phosphodiesterase, is situated close to the end of the photo-transduction cascade. The primary role of this protein is to control the concentration of the second messenger cGMP, which drives the cyclic nucleotide-gated (CNG) channels in the outer segment membrane. Here, different point mutations in the alpha subunit of the PDE6 were examined for the degree of remaining PDE6 function. Our hypothesis was that the overall function in a compound heterozygous line is determined by the average of the remaining function associated with each mutated *Pde6a* allele. This way, mutant lines with intermediate functional characteristics should arise from such cross-breeding. Further, we asked whether the broad range of cGMP levels present in the original and newly generated mutants would permit any visual activity.

Secondly, we investigated the role of CNG channels located in the outer segment membrane of rod photoreceptors. These channels mediate light-driven responses by a translation from biochemical activation to electrical signalling. While in the absence of such channels no rod vision is possible, the hypothesis was that a gene replacement approach may be able to rescue this deficiency. In Paper II, we thus examined the different functional aspects of visual restoration in the *Cngb1*$^{-/-}$ model lacking the beta-subunit of the rod CNG channel.

Early adaptation in rod vision: Signal processing within the photoreceptor cell

The processing of sensory signals is of equal importance to the sheer generation of signals. In vision, an extended activation of retinal pathways leads to a failure to detect or follow changes in the environment during this period of ‘blinding’. In the rod

pathway, adaptation occurs at several sites to limit periods of unresponsiveness. A recently discovered key protein in this regard is the HCN1 channel located in the rod inner segment. HCN1 channels limit prolonged activation of photoreceptors by a modulation of the net current driving the synaptic output. In Paper III, we assessed the details of this rod-intrinsic adaptation by HCN1 channels without cone photoreceptor interference in the *Hcn1*$^{-/-}$*Cnga3*$^{-/-}$ double knockout line devoid of any cone system function.

Synaptic transmission in rod vision: Key players at the photoreceptor output terminals

The synaptic region is the site where visual signals leave the photoreceptor and continue to second order neurons. Specifically, neurotransmitter originating from the presynaptic terminals elicits postsynaptic signals in downstream bipolar cells. Key regulators of the respective activity at rod synaptic terminals are CaV1.4 L-type calcium channels. In Paper IV and V, we examined two mutations in *Cacna1f* for differences in remaining function. Our main interest was whether the overall function in a knockout line differs from that in a line carrying a known gain-of-function mutation.

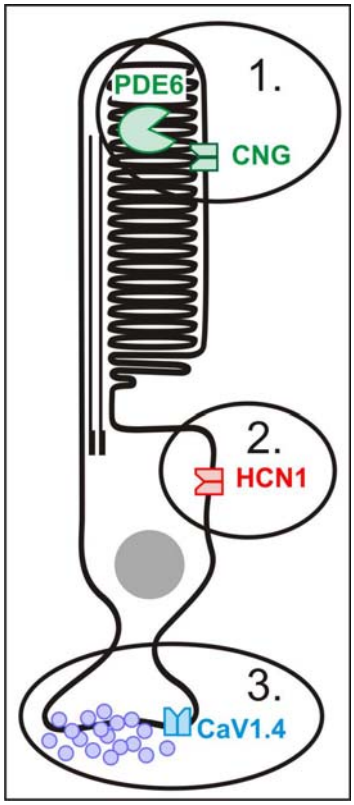

Figure 10: Localization of key signal components in the rod photoreceptor cell, analyzed in this work.

4. Results

4.1 The origin of rod vision: From biochemistry to electricity (Paper I and II)

4.1.1 Background (Paper I)

The transduction of light is initiated by a series of biochemical reactions in the rod photoreceptor cell. Triggered by activation of rhodopsin, a multi-step amplifying cascade drives current changes via cGMP-gated membrane-bound ion channels, leading eventually to a change in synaptic activity. In this process, the rod-specific phosphodiesterase-6 (PDE6) is the main cGMP hydrolysing enzyme and regulates the intracellular cGMP concentration (Lagnado and Baylor 1992, Zhang and Cote 2005). PDE6 is a heterotetrameric complex composed of one alpha and one beta catalytic as well as two gamma inhibitory subunits (Deterre et al. 1988). Mutations affecting PDE6 functionality were found in 2-4 % of patients with autosomal recessive RP (arRP) (Drya et al. 1999) and are known to lead to premature retinal degeneration with a similar course: rods are directly affected by the disease, but cones nevertheless, undergo a secondary degeneration in areas where rods are completely lost (bystander effect).

In this work, we therefore explored the differential functional effects of such mutations on visual signalling which is additionally impaired due to degeneration. For this purpose, four mouse lines that carry different knockin mutations in the alpha-subunit of PDE6 (*Pde6a*) were identified or newly generated. Two existing PDE6a-deficient mouse lines were included, the *A.B6-Tyr+/J-Pde6a*$^{nmf282/nmf282}$ (V685M) and the *C57BL/6J-Pde6a*$^{nmf283/nmf283}$ (D670G) lines originally identified at the Jackson Laboratory. The other two *Pde6a* mutant lines were generated anew from Paquet-Durand and colleagues: the *B6-Pde6a*$^{tm\ R562W/tm\ R562W}$ variant (R562W) and the *B6-Tyr+/J-Pde6a*$^{tm\ R562W/nmf282}$ (V685M/R562W). All *Pde6a* mutants are in the following referred to by the position and the type of the underlying amino acid exchange, i.e. V685M, D670G, R562W and V685M/R562W.

4.1.2 Results (Paper I)

To assess residual enzymatic function via the expression level of the PDE6a protein Paquet-Durand and co-workers performed specific staining in all four *Pde6a* variants and WT retina (Fig. 3 A-E). A gradual decrease in PDE6a levels was found, ranging from almost undetectable expression in V685M and V685M/R562W mutants and intermediate expression in the R562W variant to strong (but clearly lower than wt) expression in D670G retinae. PDE6a expression levels correlated well with an increase in cGMP accumulation (Paquet-Durand and colleagues, Fig. 3 F-J) as a consequence of subnormal PDE6 activity. Except in wild type retina, all four *Pde6a* variants had strongly elevated cGMP levels, with V685M displaying the highest level and D670G the lowest level. The cGMP concentrations of R562W and V685M/R562W lay in between these extreme values.

Based on these *ex vivo* expression studies, we assessed retinal function with scotopic and photopic electroretinography (Fig. 7). Responses were best preserved in D670G animals (marked in blue), greatly reduced in R562W mice (marked in green), and completely missing in V685M mutants (marked in red). The responses of the V685M/R562W intermediate mutants lay in between the R562W and V685M variants. A comparison of the size of ERG amplitudes of different *Pde6a* variants with age-matched C57/BL6 wild type mice revealed, that amplitudes of the *Pde6a* mutants were substantially reduced and represent 1/3 to 1/4 of wild type animals. Next, we wanted to specify whether retinal function is of rod or cone origin. Under scotopic conditions no ERG responses were visible at -2 log cd*s/m^2 and below which is suggestive for a missing rod signalling (Fig. 7A). A further comparison of scotopic and photopic ERG amplitudes and waveforms showed that both ERG signals were largely similar in size and shape. Additionally they resemble in shape those of *rho*$^{-/-}$ mice, functional controls for cone-only responses (Fig. 7C). Together, these findings argue for a mostly cone driven signalling in the *Pde6a* lines.

In vivo morphological analysis performed by Garcia Garrido (Fig. 6) and immuno-histological analyses (by Paquet-Durand and colleagues, Fig. 4 and 5) give indications for strong photoreceptor degeneration in *Pde6a* mutants, particularly occurring in a graded manner. This indicates that different degrees of remaining cone function, assessed by ERG, originate from a variable speed in degenerative processes at PN30.

In summary, insufficient PDE6 activity lead to an unphysiologically elevated level of cGMP in rod photoreceptors of all four *Pde6a* variants. Essentially, this prevent light-driven responses of rod origin even in very mild forms of PDE6a functional loss, so that PDE6-deficiency did not lead to differences in rod function, but only determined the speed of photoreceptor degeneration which in turn is reflected by the remaining cone ERG signals at P30 (Fig. 7).

4.1.3 Contribution Paper I

- Performed the *in vivo* functional analysis by means of ERG in all of the *Pde6a* mutant variants (D670G, R562W, V685M/R562W and V685M).
- Developed the hypotheses (together with co-authors)
- Analyzed the data
- Wrote the manuscript including revisions (together with co-authors)

4.1.4 Background (Paper II)

At the end of the phototransduction in the outer segments, the rod CNG channel, consisting of three CNGA1 and one CNGB1 subunits, translates the intracellular cGMP level into a voltage change (Biel and Michalakis 2007). In the dark-adapted state of rods, there is an inward current (the so-called 'dark current') mediated by the CNG channel which allows influx of Na^+ and Ca^{2+}. Upon light, cGMP levels decrease via PDE6 hydrolysis which causes CNG channels to close, resulting in a hyperpolarization of the cell membrane, the origin of photoreceptor electrical signalling. Mutations in the genes encoding for each of the CNG channel subunits cause arRP in humans (Biel and Michalakis 2007). In the *Cngb1*$^{-/-}$ mouse, lack of the CNGB1subunits resulted in a lack of CNG channels which impaired rod signalling. In this work, we specifically analyze the gain of rod signalling after an AAV-mediated gene replacement approach in the *Cngb1*$^{-/-}$ mouse. Application of this vector using the described technique produced a transfected area of about one third of the retina, which was verified via an analysis of the topographic expression of the CNGB1 protein (Koch, Fig. 1). A more detailed immunohistochemical breakdown revealed that these channels contained both α and β subunits and were correctly localized at rod outer segments (Fig. 2). Importantly, after treatment cGMP in the retina was

normalized to physiological levels, indicative for the crucial role of CNG channels in its regulation (Fig. 6G vs. F).

4.1.5 Results (Paper II)

To assess whether restoration of the CNG channel indeed established rod-derived signals, ERG examination were performed. Our functional analysis confirmed very well that rod-mediated responses became recordable in treated eyes (TEs), whereas no such activity was found in the untreated collateral eyes (UEs) (Fig. 4). Here, it became evident that rod responses integrated into the corresponding rod-specific dim light range and took over its entire activity (Fig. 4A and B; up to -2 log cd*s/m^2). At intermediate and brighter light conditions, however, rod activity interferes into the existing cone-dominated signals resulting in a change in the contribution of the rod and cone function to the net sum response which importantly remained stable (Fig. 4B; >-2 log cd*s/m^2). Additionally, it was observed that rod ERG response was always higher in amplitude (in TE) than the corresponding cone-dominated responses (in UE) at each light-intensity. This indicated that in this setting, rod system mediated signals dominate over the cone-system activity at intermediate light intensities (up to about 0.5 log cd*s/m^2). Finally, it was found that the size of the ERG amplitude after gene therapy was approximately proportional to the size of the treated area (one-third). A behavioural test was conducted to assess the transmission of retinal information to more proximal parts of the CNS. Indeed, the presence of perception-guided behaviour was found (Koch, Fig 5), highlighting the role of CNG channels for rod vision.

Taken together, rod function was successfully induced in the Cn*gb1*$^{-/-}$ mouse line via gene replacement therapy. The novel light-driven rod CNG activity resulted in regular rod-mediated electrical responses, transmission to respective brain areas, and finally vision-guided behaviour.

4.1.6 Contribution (Paper II)

- Performed the *in vivo* functional analysis by means of ERG in all treated *Cngb1*$^{-/-}$ mice
- Evaluated the data
- Prepared eye cups for *ex vivo* immunohistological analysis
- Contributed substantial text passages for manuscript including revisions

4.2 Early adaptation in rod vision: Signal processing within the photoreceptor cell (Paper III)

4.2.1 Background

Hyperpolarization-activated and cyclic nucleotide-gated channels 1 (HCN1) are ubiquitously expressed in tissues where time-dependent activity is needed, such as cardiac pacemaker cells. In rod photoreceptors, the voltage-gated HCN1 channels are located in the inner segments (Müller et al. 2003, Knop et al. 2008). Light triggers a closure of CNG channels in the outer retina which hyperpolarizes the membrane potential. In reaction to this voltage change, HCN1 channels open after a delay of approximately 30 ms in warm-blooded animals (Schneeweiß and Schnapf 1995, Demontis et al. 1999). This way, they counteract prolonged photoreceptor activation via an inward current that partially restores outward flow from synaptic endings. Nevertheless, the HCN1-mediated currents do not affect rod photoreceptor outer segment activity (Knop et al. 2008).

4.2.2 Results

To dissect the functional role of HCN1 channels on rod system responses, we generated double mutants by crossbreeding *Hcn1*$^{-/-}$ with *Cnga3*$^{-/-}$ mice, a line in which cones are non-functional. Retinal function in the resulting *Hcn1*$^{-/-}$*Cnga3*$^{-/-}$ double knockout animals (DKO) was followed by ERG. As a first step we had to verify that the ERG responses in the rod-specific DKO line are comparable to that in the single *Hcn1*$^{-/-}$ mutants. Indeed, a substantial effect of HCN1 deficiency was particularly obvious at higher flash intensities above 30 mcd*s/m^2 (Fig. 2A-C), the conditions where its function normally has the largest impact. Regarding the timing of HCN1, the effect of HCN1 deficiency is greatest in later parts of the ERG response (Fig. 2D). As projected, the elimination of cone intrusion, which is normally strongest in later parts of the scotopic ERG waveform, enabled a more detailed analysis of rod-specific HCN1 actions in the DKO line. Next, we determined the temporal resolution of rod-specific vision in DKOs based on the ability to respond to repetitive light stimuli of 10 mcd*s/m^2 under scotopic conditions. In order to reproduce a train of input signals correctly, the output response has to return to the initial state (i.e. the state that was present before a stimulus was applied) before the next stimulus occurs. A system reaches its temporal limit if the next stimulus occurs prematurely, so that the

baseline does not return to the initial resting state. The higher the rate of stimuli (i.e. the frequency) becomes, the higher the new baseline between stimulus-induced responses is elevated above the initial state. Since the width of the response to a single stimulus is a major factor in this regard (Tanimoto et al. 2012), the prolongation of waveforms in the absence of HCN1 channels is expected to considerably reduce temporal resolution in the respective mutants. Paper III illustrates the experiments in the DKOs. In Fig. 3, the signal baseline level before onset of the following response is marked by a red line. The refractory range (RR) is given by the difference between the initial state (black dotted line) and the new signal baseline level (red line). A RR>0 indicates that the system operates outside its capability of temporal resolution. In this case, the increasing RR does limit the dynamic range (DR; green shaded area). The DR is the remaining output range of the system available for the response to a subsequent stimulus. In ERG data, the DR corresponds to the maximally achievable flicker amplitude. Here, single *Cnga3*$^{-/-}$ mice were not able to respond to frequencies above about 15Hz (Fig. 3B). In DKOs, the prolongation of the rod response waveform due to HCN1 deficiency increased its RR already at much lower frequencies, thereby reducing the DR and thus the overall flicker amplitude (Fig. 3C). We observed no differences to single *Hcn1*$^{-/-}$ mutants in this regard (for data see Seeliger et al. 2011).

Finally, we assessed the flicker characteristics of DKOs to brighter light stimuli of 3 cd*s/m^2, but still under scotopic conditions (Tanimoto et al. 2009 and 2015). As these stimuli produce much wider waveforms, rods in *Cnga3*$^{-/-}$ were able to respond only to low frequencies of up to 3 Hz (Fig. 4A, red bar) (Tanimoto et al. 20015). In DKOs, rod response waveforms were again prolonged and thus the temporal resolution to respond to flicker stimuli in comparison is strongly reduced (Fig 4A, right). Taken together, the data from the newly generated *Hcn1*$^{-/-}$*Cnga3*$^{-/-}$ double mutants show that HCN1 channels constitute an early site of adaptation in rod vision, which is important to limit the duration of rod system saturation.

4.2.3 Contribution

- Designed the study under supervision of Dr. Tanimoto
- Performed the ERG in *Hcn1*$^{-/-}$*Cnga3*$^{-/-}$ and *Cnga3*$^{-/-}$ control animals
- Analyzed the data
- Wrote the manuscript including revisions (with input from co-authors)

4.3 Synaptic transmission in rod vision: Key players at the photoreceptor output terminals (Paper IV and V)

4.3.1 Background

The light information provided by rod outer segments is normally transferred across the first synapse of the visual system from photoreceptors to bipolar cells. At the synaptic endings (rod spherules), the voltage-gated CaV1.4 L-type calcium channels sense the change in membrane potential of photoreceptors and in turn drive Ca^{2+}-dependent exocytosis of neurotransmitter-containing vesicles (Baumann et al. 2004). The multi-subunit complex of the CaV1.4 channel is composed of the central pore-forming alpha1-subunit, the auxiliary beta- and alpha2delta-subunits, as well as the γ-subunit (Strom et al. 1998, Baumann et al. 2004, Catterall et al. 2005).

Here, we set out to explore the functional difference between a *Cav1.4* knockout model including a disruption of the *Cacna1f* gene and a *Cav1.4* knock-in model (*Cav1.4* IT) carrying a point mutation coding for the Isoleucin to Threonin amino acid exchange at position 745. The missense mutation features a pronounced hyperpolarization shift in CaV1.4 channel activation (Hemara-Wahanui et al. 2005). Both *Cav1.4* knock-out and knock-in mouse lines were originally obtained from Dr Marion Maw, University of Otago, Dunedin, New Zealand (Specht et al. 2009)

4.3.2 Results

In Paper IV, the impact of a loss of the *Cacna1f* gene on retinal structure and function was analyzed. Our studies, regarding the assessment of rod function under scotopic conditions revealed that ERG responses of *Cav1.4*-deficient mice lack the b-wave (positive component), reflecting a complete loss of rod signal transmission to the corresponding rod bipolar cells (Fig. 1C). In contrast, the amplitude of the a-wave (negative component) in *Cav1.4*-deficient mice was only slightly reduced to that of wild type animals, indicating that rod photoreceptor outer segment activity was not substantially impaired in these mice.

In Paper V, we investigated *Cav1.4* IT mice in a similar way. Functional genetics data in these mice supplied evidence for a strong shift in CaV1.4 channel sensitivity due to the missense mutation (Hemara-Wahanui et al. 2005). Consequently, these channels are activated at higher hyperpolarization levels with slower inactivation kinetics. The

functional analysis corroborated these findings in vivo, reflecting a defective rod synaptic signal transmission. The scotopic ERG revealed a minute but distinct positive peak, but no regular a- or b-wave (Paper V; Fig. 1).

Dysfunction of the synaptic transmission typically reduces only the b-wave whereas the corresponding a-wave, reflecting photoreceptor outer segment activity, stays intact in *in vivo* functional analyses (Pardue and Peachey 2014). In our ERG examinations, however, the a-wave was reduced to a different extent in both *Cav1.4* mutants. This is possibly due to differences in morphological alterations among the two lines, confirmed by Knoflach and co-workers in Paper IV (Fig. 3) and Michalakis and colleagues in Paper V (Figs. 2 and 4).

In summary, we show here that a complete functional loss of CaV1.4 channel activity results in an absence of rod synaptic transmission, while a shift in channel activation only partially interrupts signal transfer.

4.3.3 Contribution (Paper IV and V)

- Performed the *in vivo* functional ERG in male *Cav1.4* knockout mice and corresponding controls (Paper IV)
- Performed the *in vivo* functional ERG in *Cav1.4* IT mice and corresponding controls (Paper V)
- Analyzed the functional data for all animal groups and prepared figures
- Contributed text passages for the manuscript and its revised versions

5. Discussion

The architecture of the retina is the result of an evolutionary optimization for the best possible perception of visual cues in higher brain areas (Wässle and Boycott 1991, Masland 2001). In the outer retina, light responses elicited in photoreceptors are fed into a network of downstream neurons. Already at these early stages, signal processing sets in to assist extraction of important features from visual scenes. In particular, known concepts in this regard include selective signal amplification to provide detection at the single photon level, and lateral interaction of neurons to generate contrast information and to allow for motion detection. To date, a number of mechanisms of visual signal processing still remain to be further clarified, and several others may even be unknown.

The focus of this thesis was on the description of novel aspects of signal processing within the rod cell. In particular, we assessed the contributions of key proteins located in different photoreceptor compartments, specifically PDE6, CNG channels, HCN1 channels, and CaV1.4 channels, to visual signalling.

In the rod outer segment, the biochemical light reception cascade involves a sequence of amplification steps, starting with the activation of the rhodopsin complex, and ending with the closure of rod CNG channels. Towards the end of this biochemical cascade, PDE6 mediates the visual information by hydrolysis of cGMP (Beavo 1995, Farber 1995). While the function of these proteins has been extensively studied, there is little known about the interplay of cGMP levels, CNG channel function, and calcium levels. In Paper I, different degree of subnormal PDE6 catalytic activity in *Pde6a* mutants determines the level of intracellular cGMP in an *in vivo* situation. Since the concentration of cGMP in rod photoreceptors substantially controls the gating of CNG channels, the question arises whether any light-evoked rod signals may be generated in such *Pde6a* mutants. The unphysiologically elevated cGMP levels suggest that even maximally intense light stimulation may not be capable to close CNG channels, resulting in a total inability of rods to respond electrically. In some of the PDE6 mutants with substantial remaining activity, one cannot exclude that rods are less desensitized and may be activated by very strong light stimulation. Such effects have been described in rodents with insufficient retinal availability of 11-cis-retinal, the functional form of vitamin A in the photoreceptors. In this case, the limited chromophore decreases the amount of rhodopsin, which in turn

diminishes rod sensitivity (Thomas and Lamb 1999, Seeliger et al. 2001). In any case, our data show that the elevation of cGMP due to reduced PDE6 activity is at least effective to prevent rods from responding to dim light stimuli. To assess whether their sensitivity is reduced to a degree that they respond under normally cone-isolating lighting conditions, crossbreeding of *Ped6a* mutant mice with selective rod- or cone-only mouse models, such as *rho*$^{-/-}$ (Humphries et al. 1997, Jaissle et al. 2001) or *Cnga*3$^{-/-}$ (Biel et al. 1999) may be necessary. If rods contribute to light responses in *Pde6a* mutants, similar ERG responses would be obtained in *Pde6a* mutants and *Pde6a*/*Cnga*3$^{-/-}$ double mutants. Alternatively, if rod signals are completely absent, ERGs from *Pde6a* lines would equal those of *Pde6a/rho*$^{-/-}$ double mutant mice.

The CNG channels in rod outer segments are on the one hand responsible for the electrical current. On the other hand, they allow for the influx of Ca^{2+}, which contributes to a Ca^{2+}-dependent inactivation of GC and in turn a decrease in GMP synthesis. Similar to PDE6 dysfunction where channels are constitutively open, a lack of CNG channels also leads to elevated cGMP levels and to impaired rod vision (Hüttl et al. 2005). Consequently, the introduction of the missing CNG channels should normalize cGMP levels and allow for regular light-driven rod function. Paper II describes this approach based on an AAV-mediated gene therapy. Subsequent to treatment, cGMP was downregulated to normal levels, and rod electrical activity became apparent in ERG recordings under rod-specific conditions. The studies on both CNG channels and PDE6 highlight that a proper regulation of the intracellular cGMP concentration is crucial for rod vision, and dysfunction of either PDE6 or the CNG channel impaired rod signalling.

The electrical signal generated in rod outer segments is then transmitted to the synaptic region. In Paper III, we describe how the underlying current is tightly controlled and modulated after light exposure by HCN1 channels. HCN1 channels are strongly expressed in photoreceptor inner segments. They use current feedback to shape the photoreceptor voltage responses (Fain et al. 1978, Demontis et al. 1999). Such feedback mechanisms are common strategies to regulate saturation of the retinal networks (Fain et al. 2001, Reuter 2011). A further modulatory role is known from BK channels which are expressed in A17 amacrine cells (Tanimoto et al.

2012). These channels modulate rod bipolar output signals entering the primary rod pathway via AII amacrine cell (see Introduction, Fig. 4B).

In Paper III, we explored the adaptive power of HCN1 channels on rod-specific signalling in a model with additional genetic inactivation of cone function. The detailed investigation complemented previous work (Knop et al. 2008, Seeliger et al. 2011) and showed that HCN1 channels have a major impact on rod vision particularly under constant light exposure where the HCN1 channels allow inward currents in the inner segment. During the period of unresponsiveness of rods due to closure of CNG channels in the outer segment they limit prolonged activation of photoreceptors by a modulation of the net current driving the synaptic output.

The net current in photoreceptors is governed by the interplay of several ion channel types. Thus, in the absence of HCN1 channels, there may be a further mechanism which counterbalances the lack of HCN1. The resting potential of photoreceptors in the dark is driven by an inward-current through CNG channels and an outward flow of ions via potassium currents I_{Kx}. During light exposure, CNG channel closes and I_{Kx} conducts the membrane potential to more hyperpolarized levels together with the electrogenic Na^+/K^+-ATPase. This leads to the conjecture that inward-rectifying potassium currents may exist. Indeed, such currents were recorded in mouse rods (Knop et al. 2008, Demontis et al. 2009). However, their magnitude would only be sufficient to reach E_K but not the resting potential. Consequently, the full recovery to the resting state is determined by the speed of cGMP restoration, regulated by outer segment components like PDE6, GC and CNG channels, respectively.

The HCN1 feedback mechanism, mediating adaptation in rod vision at the level of the photoreceptor, is important to limit the duration of rod system saturation without compromising maximal sensitivity. Evolutionary, such adaptive mechanisms may play a decisive role in wildlife for both predators and prey, where the rapid return to useful visual perception after a period of saturation is of great advantage.

The step of signal transmission at the rod photoreceptor synaptic terminals was addressed in Papers IV and V, both concerning the role of CaV1.4 channels. These voltage-gated channels drive a Ca^{2+}-inward current and control the neurotransmitter release which finally governs the signal transfer from rods to downstream bipolar cells. They are strongly active at depolarized membrane potentials and reduce their conductance upon light-induced hyperpolarization. Paper IV describes the

interruption of rod signalling following a complete loss of CaV1.4 channels, whereas Paper V reports a gain-of-function mutation that causes a shift in CaV1.4 channel sensitivity, resulting in a subtotal reduction of synaptic activity. These papers demonstrate very nicely that regular transmitter release at rod synaptic terminals requires a certain working range of the CaV1.4 channels. A modification in the direction of either a reduced or enhanced sensitivity of the CaV1.4 channels may completely suppress or at least reduce the dynamic range of rod synaptic activity.
Dysfunction of the synaptic transmission normally is not accompanied with decreased outer segment activity, so that the corresponding a-wave stays intact in *in vivo* functional analyses (Chang et al. 2006, Pardue and Peachey 2014). Our investigations, however, showed a variable preservation of the a-wave in the CACNA1F-mutants, possibly due to differences in morphological alterations among the two lines (Paper IV: Figs. 2 and 3; Paper V: Figs. 2 and 4). Specifically, degenerations at the synaptic region may degrade the current flow in the photoreceptor which is the basis for maintaining the membrane potential. If the degeneration is not uniform, a mosaic retina may develop which is characterized by adjacent functional and non-functional retinal neurons. Correspondingly, the extent of the remaining healthy areas in the retina may determine the residual status of the outer segment currents, which is reflected in the initial a-wave.

In this thesis, the contribution of different proteins for visual signalling in rod photoreceptors was investigated. For the dissection of visual signalling, functionally specific genetic mutants were used as fundamental tools to provide physiological insights into the steps of signal transfer. We found that the loss of outer segment activity due to failure of PDE6 or CNG channel function resulted in an inability of rods to generate an electrical signal. Further, the ablation of HCN1 channels located in the inner segments led to a sustained duration of rod electrical signals and saturated downstream visual pathways. Finally, we elaborated that CaV1.4 channels that control the biochemical signal transfer at rod photoreceptor synapses require a certain working range for this process.

6. References

B

Baden T, Euler T, Weckström M, Lagnado L. Spikes and ribbon synapses in early vision. Trends Neurosci. 2013;36:480-488.

Baumann L, Gerstner A, Zong X, Biel M, Wahl-Schott C. Functional characterization of the L-type Ca2+ channel Cav1.4alpha1 from mouse retina. Invest Ophthalmol Vis Sci. 2004;45:708-713.

Bayes M, Giordano M, Balcells S, Grinberg D, Vilageliu L, Martinez I, Ayuso C, Benitez J, Ramos-Arroyo MA and Chivelet P. Homozygous tandem duplication within the gene encoding the beta-subunit of rod phosphodiesterase as a cause for autosomal recessive retinitis pigmentosa. Hum Mutat. 1995;5:228-234.

Beavo JA. Cyclic nucleotide phosphodiesterases: functional implications of multiple isoforms. Physiol Rev. 1995;75:725-748.

Bech-Hansen N, Naylor M, Maybaum T, Pearce W, Koop B, Fishman G, Mets M, Musarella M, Boycott K. Loss-of-function mutations in a calcium-channel alpha1-subunit gene in Xp11.23 cause incomplete X-linked congenital stationary night blindness. Nat Genet. 1998;19: 264-267.

Bech-Hansen N, Naylor M, Maybaum T, Sparkes R, Koop B, Birch D, Bergen A, Prinsen C, Polomeno R, Gal A, Drack A, Musarella M, Jacobson S, Young R, Weleber R. Mutations in NYX, encoding the leucine-rich proteoglycan nyctalopin, cause X-linked complete congenital stationary night blindness. Nat Genet. 2000;26:319-323.

Berger W, Kloeckener-Gruissem B, Neidhardt J. The molecular basis of human retinal and vitreoretinal diseases. Prog Retin Eye Res. 2010;29:335-375.

Biel M, Michalakis S. Function and dysfunction of CNG channels: insights from channelopathies and mouse models. Mol Neurobiol. 2007;35:266-277.

Biel M, Seeliger M, Pfeifer A, Kohler K, Gerstner A, Ludwig A, Jaissle G, Fauser S, Zrenner E, Hofmann F. Selective loss of cone function in mice lacking the cyclic nucleotide-gated channel CNG3. Proc Natl Acad Sci U S A. 1999;96:7553-7557.

Bok D. The retinal pigment epithelium: a versatile partner of vision. J Cell Sci Suppl. 1993;17:189-195.

Boulton M, Dayhaw-Barker P. The role of the retinal pigment epithelium: topographical variation and ageing changes. Eye (Lond). 2001;15:384-389.

Boycott BB, Dowling JE. Organization of the primate retina:Light microscopy. Philosophical Transactions of the Royal Society of London.1969;255:109-184.

C

Carter-Dawson LD, LaVail MM. Rods and cones in the mouse retina. I. Structural analysis using light and electron microscopy. J Comp Neurol. 1979;188:245-262.

Catterall WA., Perez-Reyes E, Snutch TP, Striessnig J. International Union of Pharmacology. XLVIII. Nomenclature and structure-function relationships of voltage-gated calcium channels. Pharmacol Rev. 2005;57:411–425.

Curcio CA, Sloan KR Jr, Packer O, Hendrickson AE, Kalina RE. Distribution of cones in human and monkey retina: individual variability and radial asymmetry. Science. 1987; 236:579-582.

D

Daiger SP, Sullivan LS, Bowne SJ. Genes and mutations causing retinitis pigmentosa. Clin Genet. 2013;84:132-141.

Della Santina L, Piano I, Cangiano L, Caputo A, Ludwig A, Cervetto L, Gargini C. Processing of retinal signals in normal and HCN deficient mice. PLOS ONE. 2012;7: e29812

Demontis GC, Longoni B, Barcaro U, Cervetto L. Properties and functional roles of hyperpolarization-gated currents in guinea-pig retinal rods. J Physiol. 1999;515:813-828.

Demontis GC, Gargini C, Paolucci L, Cervetto, L. Selective HCN1 channels inhibition by ivabradine in mouse rod photoreceptors. Invest Ophthalmol Vis Sci. 2009;50:1948-1955.

Deterre P, Bigay J, Forquet F, Robert M, Chabre M. cGMP phosphodiesterase of retinal rods is regulated by two inhibitory subunits. Proc Natl Acad Sci U S A. 1988;85:2424-2428.

Detwiler SR: Vertebrate Photoreceptors. Macmillan, New York. 1943.

Detwiler SR. The Eye and its structural Adaptations. Proc Am Philos Soc. 1955; 99: 224-238.

Dowling JE. The Retina: An Approachable Part of the Brain. Harvard University Press. 1987.

Dryja TP, Finn JT, Peng YW, McGee TL, Berson EL, Yau KW. Mutations in the gene encoding the alpha subunit of the rod cGMP-gated channel in autosomal recessive retinitis pigmentosa. Proc Natl Acad Sci USA. 1995;92:10177-10181.

Dryja TP, Rucinski DE, Chen SH, Berson EL. Frequency of mutations in the gene encoding the alpha subunit of rod cGMP-phosphodiesterase in autosomal recessive retinitis pigmentosa. Invest Ophthalmol Vis Sci. 1999;40:1859-1865.

Dvir L, Srour G, Abu-Ras R, Miller B, Shalev SA, Ben-Yosef T. Autosomal-recessive early-onset retinitis pigmentosa caused by a mutation in PDE6G, the gene encoding the gamma subunit of rod cGMP phosphodiesterase. Am J Hum Genet. 2010;87:258-264.

F

Faber DB. From mice to men: the cyclic GMP phosphodiesterase gene in vision and disease. Invest Ophthalmol Visual Sci.1995;36:263-275.

Fain GL, Quandt FN, Bastian BL., Gerschenfeld HM. Contribution of a caesium-sensitive conductance increase to the rod photoresponse. Nature. 1978;272:467-469.

Fain GL, Matthews HR, Cornwall MC, Koutalos Y. Adaptation in vertebrate photoreceptors. Physiol Rev. 2001;81:117-151.

Frishman LJ. Origins of the electroretinogram. In: Heckenlively JR, Arden GB (eds) Principles and practice of clinical electrophysiology of vision. 2nd edn. MIT press. Massachusets. 2006;139-183.

Futter CE, Ramalho JS, Jaissle GB, Seeliger MW, Seabra, MC. The role of Rab27a in the Regulation of Melanosome Distribution within Retinal Pigment Epithelial Cells. Mol Biol Cell. 2004;15:2264-2275.

G

Gouras P. Electroretinography: Some basic principles. Invest Ophthalmol. 1970;9: 557-569.

Granit R. The components of the retinal action potential in mammals and their relation to the discharge in the optic nerve. J Physiol. 1933;77:207-239.

H

Hartong DT, Berson EL, Dryja TP. Retinitis pigmentosa. Lancet. 2006;368:1795-1809.

Hemara-Wahanui A, Berjukow S, Hope CI, Dearden PK, Wu SB, Wilson-Wheeler J, Sharp DM, Lundon-Treweek P, Clover GM, Hoda JC, Striessnig J, Marksteiner R, Hering S, Maw MA. A CACNA1F mutation identified in an X-linked retinal disorder shifts the voltage dependence of Cav1.4 channel activation. Proc Natl Acad Sci USA. 2005;102:7553-7558.

Hüttl S, Michalakis S, Seeliger M, Luo DG, Acar N, Geiger H, Hudl K, Mader R, Haverkamp S, Moser M, Pfeifer A, Gerstner A, Yau KW, Biel M. Impaired channel targeting and retinal degeneration in mice lacking the cyclic nucleotide-gated channel subunit CNGB1. J Neurosci. 2005;25:130-138.

Humphries MM, Rancourt D, Farrar GJ, Kenna P, Hazel M, Bush RA, Sieving PA, Sheils DM, McNally N, Creighton P, Erven A, Boros A, Gulya K, Capecchi MR,

Humphries P. Retinopathy induced in mice by targeted disruption of the rhodopsin gene. Nat Genet. 1997;15:216-219.

J

Jaissle GB, May CA, Reinhard J, Kohler K, Fauser S, Lutjen-Drecoll E, Zrenner E and Seeliger MW. Evaluation of the rhodopsin knockout mouse as a model of pure cone function. Invest Ophthalmol Vis Sci. 2001;42:506-513.

K

Kaneko A. Physiology of the Retina. Ann Rev Neurosci. 1979;2:169-191.

Klinke R, Silbernagel S. Lehrbuch der Physiologie. Thieme, Stuttgart. 2001.

Knoflach D, Kerov V, Sartori SB, Obermair GJ, Schmuckermair C, Liu X, Sothilingam V, Garcia Garrido M, Baker SA, Glösmann M, Schicker K, Seeliger M, Lee A, Koschak A. Cav1.4 IT mouse as model for vision impairment in human congenital stationary night blindness type 2. Channels (Austin). 2013;7:503-513.

Koschak A, Reimer D, Walter D, Hoda JC, Heinzle T, Grabner M, Striessnig J. Cav1.4alpha1 subunits can form slowly inactivating dihydropyridine-sensitive L-type Ca2+ channels lacking Ca2+-dependent inactivation. J Neurosci. 2003;23:6041-6049.

Knop GC, Seeliger MW, Thiel F, Mataruga A, Kaupp UB, Friedburg C, Tanimoto N, Müller F. Light responses in the mouse retina are prolonged upon targeted deletion of the HCN1 channel gene. Eur J Neurosci. 2008;28:2221-2230.

Koch S, Sothilingam V, Garcia Garrido M, Tanimoto N, Becirovic E, Koch F, Seide C, Beck SC, Seeliger MW, Biel M, Mühlfriedel R, Michalakis S. Gene therapy restores vision and delays degeneration in the CNGB1(-/-) mouse model of retinitis pigmentosa. Hum Mol Genet. 2012;21:4486-4496.

Kolb H. Simple Anatomy of the Retina. Authors In: Kolb H, Fernandez E, Nelson R Webvision: The Organization of the Retina and Visual System [Internet]. Salt Lake City (UT): University of Utah Health Sciences Center; 1995-2005 [updated 2012].

L

Lagnado L, Baylor D. Signal flow in visual transduction. Neuron. 1992;8:995-1002.

M

Masland RH. Neuronal diversity in the retina. Curr Opin Neurobiol. 2001;11, 431-436.

McCulloch DL, Marmor MF, Brigell MG, Hamilton R, Holder GE, Tzekov R, Bach M. ISCEV Standard for full-field clinical electroretinography (2015 update). Doc Ophthalmol. 2015;130:1-12.

Michalakis S, Mühlfriedel R, Tanimoto N, Krishnamoorthy V, Koch S, Fischer MD, Becirovic E, Bai L, Huber G, Beck SC, Fahl E, Büning H, Paquet-Durand F, Zong X, Gollisch T, Biel M, Seeliger MW. Restoration of cone vision in the CNGA3-/- mouse model of congenital complete lack of cone photoreceptor function. Mol Ther. 2010;18:2057-2063.

Michalakis S, Shaltiel L, Sothilingam V, Koch S, Schludi V, Krause S, Zeitz C, Audo I, Lancelot ME, Hamel C, Meunier I, Preising MN, Friedburg C, Lorenz B, Zabouri N, Haverkamp S, Garcia Garrido M, Tanimoto N, Seeliger MW, Biel M, Wahl-Schott CA. Mosaic synaptopathy and functional defects in Cav1.4 heterozygous mice and human carriers of CSNB2. Hum Mol Genet. 2014;23:1538-1550.

Milam AH, Li ZY, Fariss RN. Histopathology of the human retina in retinitis pigmentosa. Prog Retin Eye Res. 1998;17:175-205.

Miyake Y. Electrodiagnosis of Retinal Disease. New York: Springer; 2006.

Müller F, Scholten A, Ivanova E, Haverkamp S, Kremmer E, Kaupp UB. HCN channels are expressed differentially in retinal bipolar cells and concentrated at synaptic terminals. Eur J Neurosci. 2003;17:2084-2096.

P

Pagon RA. Retinitis pigmentosa. Surv Ophthalmol. 1988;33:137-77.
Pardue MT, Peachey NS. Mouse b-wave mutants. Doc Ophthalmol. 2014;128:77-89.

Penn RD, Hagins WA. Signal transmission along retinal rods and the origin of the electroretinographic a-wave. Nature.1969;223:201-204.

Purves D, Augustine GJ, Fitzpatrick D, Katz LC, LaMantia AS, McNamara JO, Williams SM. Neuroscience. 2nd edition. Sunderland (MA): Sinauer Associates. 2001.

Pusch C, Zeitz C, Brandau O, Pesch K, Achatz H, Feil S, Scharfe C, Maurer J, Jacobi F, Pinckers A, Andreasson S, Hardcastle A, Wissinger B, Berger W, Meindl A. The complete form of X-linked congenital stationary night blindness is caused by mutations in a gene encoding a leucine-rich repeat protein. Nat Genet. 2000;26:324-327.

R

Reifler AN, Chervenak AP, Dolikian ME, Benenati BA, Li BY, Wachter RD, Lynch AM, Demertzis ZD, Meyers BS, Abufarha FS, Jaeckel ER, Flannery MP, Wong KY. All spiking, Sustained ON Displaced Amacrine Cells Receive Gap-Junction Input from Melanopsin Ganglion Cells. Curr Biol. 2015;25:2763-2773.

Reuter T. Fifty years of dark adaptation 1961-2011. Vision Res. 2011;51:2243-2262.

Raviola E, Gilula NB. Gap junctions between photoreceptor cells in the vertebrate retina. Proc Natl Acad Sci USA. 1973;70:1677-1681.

Richardson TM. Cytoplasmic and ciliary connections between the inner and outer segments of mammalian visual receptors. Vision Res.1969;9:727-731.

Rigaudiere F, Roux C, Lachapelle P, Rosolen SG, Bitoun, P, Gay-Duval A, Le Gargasson, JF. ERGs in female carriers of incomplete congenital stationary night blindness (I-CSNB). A family report. Doc Ophthalmol. 2003;107:203-212.

Rodieck RW. The first steps in seeing. Sunderland, Mass, Sinauer Associates.1998

S

Samardzija M, Tanimoto N, Kostic C, Beck S, Oberhauser V, Joly S, Thiersch M, Fahl E, Arsenijevic Y, von Lintig J, Wenzel A, Seeliger MW, Grimm C. In conditions of limited chromophore supply rods entrap 11-cis-retinal leading to loss of cone function and cell death. Hum Mol Genet. 2009;18:1266-1275.

Santos A, Humayun MS, de Juan E, Greenburg RJ, Marsh MJ, Klock IB, Milam AH. Preservation of the inner retina in retinitis pigmentosa. A morphometric analysis. Arch Ophthalmol. 1997;115:511-515.

Schneeweis DM, Schnapf JL. Photovoltage of rods and cones in the macaque retina. Science. 1995;268:1053-1056.

Seeliger MW, Grimm C, Ståhlberg F, Friedburg C, Jaissle G, Zrenner E, Guo H, Remé CE, Humphries P, Hofmann F, Biel M, Fariss RN, Redmond TM, Wenzel A. New views on RPE65 de fi ciency: the rod system is the source of vision in a mouse model of Leber congenital amaurosis. Nat Genet. 2001;29:70-74.

Seeliger MW, Brombas A, Weiler R, Humphries P, Knop G, Tanimoto N, Müller F. Modulation of rod photoreceptor output by HCN1 channels is essential for regular mesopic cone vision. Nat Commun. 2011;2:532.

Sothilingam V, Garcia Garrido M, Jiao K, Buena-Atienza E, Sahaboglu A, Trifunović D, Balendran S, Koepfli T, Mühlfriedel R, Schön C, Biel M, Heckmann A, Beck SC, Michalakis S, Wissinger B, Seeliger MW, Paquet-Durand F. Retinitis pigmentosa: impact of different Pde6a point mutations on the disease phenotype. Hum Mol Genet. 2015;24:5486-5499.

Sothilingam V, Michalakis S, Garcia Garrido M, Biel M, Tanimoto N, Seeliger MW. HCN1 Channels Enhance Rod System Responsivity in the Retina under Conditions of Light Exposure. PLoS One. 2016;11:e0147728.

Spalton DJ, Hitchings RA, Hunter PA. Atlas of clinical ophthalmology. 2nd edition Wolfe Publishing, London, UK. 1994.

Specht D, Wu SB, Turner P, Dearden P, Koentgen F, Wolfrum U, Maw M, Brandstätter JH, tom Dieck S. Effects of presynaptic mutations on a postsynaptic Cacna1s calcium channel colocalized with mGluR6 at mouse photoreceptor ribbon synapses. Invest Ophthalmol Vis Sci. 2009;50:505-515.

Strom T, Nyakatura G, Apfelstedt-Sylla E, Hellebrand H, Lorenz B, Weber B, Wutz K, Gutwillinger N, Rüther K, Drescher B, Sauer C, Zrenner E, Meitinger T, Rosenthal A, Meindl A. An L-type calcium-channel gene mutated in incomplete X-linked congenital stationary night blindness. Nat Genet. 1998;19: 260–263.

T

Tanimoto N, Muehlfriedel RL, Fischer MD, Fahl E, Humphries P, Biel M, Seeliger MW. Vision tests in the mouse: Functional phenotyping with electroretinography. Front Biosci (Landmark Ed). 2009;14:2730-2737.

Tanimoto N, Brombas A, Müller F, Seeliger MW. HCN1 channels significantly shape retinal photoresponses. Adv Exp Med Biol. 2012;723:807-812.

Tanimoto N, Sothilingam V, Euler T, Ruth P, Seeliger MW, Schubert T. BK channels mediate pathway-specific modulation of visual signals in the in vivo mouse retina. J Neurosci. 2012;32:4861-4866.

Tanimoto N, Sothilingam V, Seeliger MW. Functional phenotyping of mouse models with ERG. Methods Mol Biol. 2013;935:69-78.

Tanimoto N, Sothilingam V, Kondo M, Biel M, Humphries P, Seeliger MW. Electroretinographic assessment of rod- and cone-mediated bipolar cell pathways using flicker stimuli in mice. Sci Rep. 2015;5:10731.

Thomas MM, Lamb TD. Light adaptation and dark adaptation of human rod photoreceptors measured from the a-wave of the electroretinogram. J Physiol. 1999; 518:479-496.

Tomita T, Yanagida T. Origins of the ERG waves. Vision Res. 1981;21:1703-1707.

Travis GH. Mechanisms of cell death in the inherited retinal degenerations. Am J Hum Genet. 1998;62:503-508.

Tsukamoto Y, Morigiwa K, Ueda M, Sterling P. Microcircuits for night vision in mouse retina. J Neurosci. 2001;21:8616-8623.

Tsukamoto Y, Omi N. Some OFF bipolar cell types make contact with both rods and cones in macaque and mouse retinas. Front Neuroanat. 2014;8:105.

V

Veleri S, Lazar CH, Chang B, Sieving PA, Banin E, Swaroop A. Biology and therapy of inherited retinal degenerative disease: insights from mouse models. Dis Model Mech. 2015;8:109-129.

W

Wässle H, Boycott BB. Functional architecture of the mammalian retina. Physiol Rev. 1991;71:447-480.

Wässle H. Parallel processing in the mammalian retina. Nat Rev Neurosci. 2004;5:747-757.

Z

Zhang X, Cote RH. cGMP signaling in vertebrate retinal photoreceptor cells. Front Biosci. 2005;10:1191-1204.

III. Acknowledgements

First and foremost I owe my gratitude to Prof. Seeliger for providing me with the opportunity to complete my challenging PhD at his laboratory. I also want to thank him for given me another great opportunity to participate in national and international meetings which leaded to share valuable discussions with many collaboration partners.

I would further like to sincerely thank Prof. Nordheim for his pleasant and kind willingness to support my PhD.

My deep sense of gratefulness to Dr. Naoyuki Tanimoto who helped me getting started during the initial phases of my work and has taken many hours to guide me through the field of electroretinography. Thank you for the tremendous support and wonderful discussions and suggestions during the whole PhD period.

I am truly indebted to my close labmates Marina, Gudrun, Susanne and Regine who supported me in the institute and shared great moments in- and outside of work.

Furthermore, I would like to extend my sincere gratitude to all my collaboration partners. It has been a great privilege and experience for me.

Finally, I would like to say a heartfelt thank you to my parents and to my one and only sister Prarthana for the unfailing support which always keeps me very strong! I would like to express my very best and special thanks to my husband Senthil. He has been a constant source of strength and moral supporter for me. A deeply sincere thanks for his kind patience and understanding.

IV. Curriculum Vitae

Education

10/2004-04/2010	Diploma in Biology, University of Hohenheim, Germany Major subject: Physiology, final mark: 1.3, Minor subjects: Microbiology, final mark: 1.7; Plant Physiology and Biotechnology Biotechnology, final mark: 1.3 Diploma thesis "Charakterisierung des chemosensorischen Systems im Gastrointestinaltrakt: Anpassung an kritische Phasen der Nahrungsumstellung", final mark:1.3
Since 11/2010	Doctoral student, Division of Ocular Neurodegeneration, Institute for Ophthalmic Research, Tübingen, Germany

Memberships/Awards

Since 2010	Member of the Association for Research in Vision and Ophthalmology (ARVO)
01/2014	Recipient of the Swiss Retina Award for Young Scientist, Swiss Eye Research Meeting, Biel, Switzerland

Research Experience/International Recognition

01/2008-12/2008	Student research assistant, Membrane Physiology, Institute of Physiology, University of Hohenheim, Germany
01/2009-03/2010	Student research assistant, Physiology, Institute of Physiology, University of Hohenheim, Germany
10/2009-03/2010	Teaching assistant, Physiology, University of Hohenheim, Germany
05/2012	Assistant to Course Director, Education Course, Animal Electroretinography in Ophthalmic Research", Association for Research in Vision and Ophthalmology (ARVO) Annual Meeting in Fort Lauderdale, Florida, USA
11/2012	Assistant to Course Director, Advanced diagnostics for ocular diseases-exploring the retina using imaging and electrophysiology, (S&V Technologies AG, Acrivet Inc.)

List of Publications

1. **Sothilingam V**, Michalakis S, Garcia Garrido M, Biel M, Tanimoto N, Seeliger MW. HCN1 Channels Enhance Rod System Responsivity in the Retina under Conditions of Light Exposure. **PLoS One**. 2016;11:e0147728.

2. Schön C, Asteriti S, Koch S, **Sothilingam V**, Garcia Garrido M, Tanimoto N, Herms J, Seeliger MW, Cangiano L, Biel M, Michalakis S. Loss of HCN1 enhances disease progression in mouse models of CNG channel-linked retinitis pigmentosa and achromatopsia. **Hum Mol Genet**. 2016;25:1165-1175.

3. **Sothilingam V**, Garcia Garrido M, Jiao K, Buena-Atienza E, Sahaboglu A, Trifunović D, Balendran S, Koepfli T, Mühlfriedel R, Schön C, Biel M, Heckmann A, Beck SC, Michalakis S, Wissinger B, Seeliger MW, Paquet-Durand F. Retinitis pigmentosa: impact of different Pde6a point mutations on the disease phenotype. **Hum Mol Genet**. 2015;24:5486-5499.

4. Kohl S, Zobor D, Chiang WC, Weisschuh N, Staller J, Gonzalez Menendez I, Chang S, Beck SC, Garcia Garrido M, **Sothilingam V**, Seeliger MW, Stanzial F, Benedicenti F, Inzana F, Héon E, Vincent A, Beis J, Strom TM, Rudolph G, Roosing S, Hollander AI, Cremers FP, Lopez I, Ren H, Moore AT, Webster AR, Michaelides M, Koenekoop RK, Zrenner E, Kaufman RJ, Tsang SH, Wissinger B, Lin JH. Mutations in the unfolded protein response regulator ATF6 cause the cone dysfunction disorder achromatopsia. **Nat Genet**. 2015;47:757-765.

5. Tanimoto N, **Sothilingam V**, Kondo M, Biel M, Humphries P, Seeliger MW. Electroretinographic assessment of rod- and cone-mediated bipolar cell pathways using flicker stimuli in mice. **Sci Rep**. 2015;5:10731.

6. Katiyar R, Weissgerber P, Roth E, Dörr J, **Sothilingam V**, Garcia Garrido M, Beck SC, Seeliger MW, Beck A, Schmitz F, Flockerzi V. Influence of the β2-Subunit of L-Type Voltage-Gated Cav Channels on the Structural and Functional Development of Photoreceptor Ribbon Synapses. **Invest Ophthalmol Vis Sci**. 2015;56:2312-2324.

7. Weinl C, Wasylyk C, Garcia Garrido M, **Sothilingam V**, Beck SC, Riehle H, Stritt C, Roux MJ, Seeliger MW, Wasylyk B, Nordheim A. Elk3 deficiency causes transient impairment in post-natal retinal vascular development and formation of tortuous arteries in adult murine retinae. **PLoS One**. 2014;9:e107048.

8. Busskamp V, Krol J, Nelidova D, Daum J, Szikra T, Tsuda B, Jüttner J, Farrow K, Scherf BG, Alvarez CP, Genoud C, **Sothilingam V**, Tanimoto N, Stadler M, Seeliger M, Stoffel M, Filipowicz W, Roska B. miRNAs 182 and 183 are necessary to maintain adult cone photoreceptor outer segments and visual function. **Neuron**. 2014;83:586-600.

9. Michalakis S, Koch S, **Sothilingam V**, Garcia Garrido M, Tanimoto N, Schulze E, Becirovic E, Koch F, Seide C, Beck SC, Seeliger MW, Mühlfriedel R, Biel

M. Gene therapy restores vision and delays degeneration in the CNGB1(-/-) mouse model of retinitis pigmentosa. **Adv Exp Med Biol**. 2014;801:733-739.

10. Pellissier LP, Lundvig DM, Tanimoto N, Klooster J, Vos RM, Richard F, **Sothilingam V**, Garcia Garrido M, Le Bivic A, Seeliger MW, Wijnholds J. CRB2 acts as a modifying factor of CRB1-related retinal dystrophies in mice. **Hum Mol Genet**. 2014;23:3759-3771.

11. Alves CH, Pellissier LP, Vos RM, Garcia Garrido M, **Sothilingam V**, Seide C, Beck SC, Klooster J, Furukawa T, Flannery JG, Verhaagen J, Seeliger MW, Wijnholds J. Targeted ablation of Crb2 in photoreceptor cells induces retinitis pigmentosa. **Hum Mol Genet**. 2014;23:3384-3401.

12. Pellissier LP, Alves CH, Quinn PM, Vos RM, Tanimoto N, Lundvig DM, Dudok JJ, Hooibrink B, Richard F, Beck SC, Huber G, **Sothilingam V**, Garcia Garrido M, Le Bivic A, Seeliger MW, Wijnholds J. Targeted ablation of CRB1 and CRB2 in retinal progenitor cells mimics Leber congenital amaurosis. **PLoS Genet**. 2013;9:e1003976.

13. Tanimoto N, **Sothilingam V**, Gloeckner G, Bryda EC, Humphries P, Biel M, Seeliger MW. Auditory event-related signals in mouse ERG recordings. **Doc Ophthalmol**. 2014;128:25-32.

14. Michalakis S, Shaltiel L, **Sothilingam V**, Koch S, Schludi V, Krause S, Zeitz C, Audo I, Lancelot ME, Hamel C, Meunier I, Preising MN, Friedburg C, Lorenz B, Zabouri N, Haverkamp S, Garcia Garrido M, Tanimoto N, Seeliger MW, Biel M, Wahl-Schott CA. Mosaic synaptopathy and functional defects in Cav1.4 heterozygous mice and human carriers of CSNB2. **Hum Mol Genet**. 2014 ;23:1538-1550.

15. Knoflach D, Kerov V, Sartori SB, Obermair GJ, Schmuckermair C, Liu X, **Sothilingam V**, Garcia Garrido M, Baker SA, Glösmann M, Schicker K, Seeliger M, Lee A, Koschak A. Cav1.4 IT mouse as model for vision impairment in human congenital stationary night blindness type 2. **Channels (Austin)**. 2013;7:503-513.

16. Dudok JJ, Sanz AS, Lundvig DM, **Sothilingam V**, Garcia Garrido M, Klooster J, Seeliger MW, Wijnholds J. MPP3 regulates levels of PALS1 and adhesion between photoreceptors and Müller cells. **Glia**. 2013;61:1629-1644.

17. Favazza TL, Tanimoto N, Munro RJ, Beck SC, Garcia Garrido M, Seide C, **Sothilingam V**, Hansen RM, Fulton AB, Seeliger MW, Akula JD. Alterations of the tunica vasculosa lentis in the rat model of retinopathy of prematurity. **Doc Ophthalmol**. 2013;127:3-11.

18. Ait-Hmyed O, Felder-Schmittbuhl MP, Garcia-Garrido M, Beck S, Seide C, **Sothilingam V**, Tanimoto N, Seeliger M, Bennis M, Hicks D. Mice lacking Period 1 and Period 2 circadian clock genes exhibit blue cone photoreceptor defects. **Eur J Neurosci**. 2013;37:1048-1060.

19. Tanimoto N, **Sothilingam V**, Seeliger MW. Functional phenotyping of mouse models with ERG. **Methods Mol Biol**. 2013;935:69-78.

20. Hilgen G, Huebner AK, Tanimoto N, **Sothilingam V**, Seide C, Garcia Garrido M, Schmidt KF, Seeliger MW, Löwel S, Weiler R, Hübner CA, Dedek K. Lack of the sodium-driven chloride bicarbonate exchanger NCBE impairs visual function in the mouse retina. **PLoS One**. 2012;7:e46155.

21. Koch S, **Sothilingam V**, Garcia Garrido M, Tanimoto N, Becirovic E, Koch F, Seide C, Beck SC, Seeliger MW, Biel M, Mühlfriedel R, Michalakis S. Gene therapy restores vision and delays degeneration in the CNGB1(-/-) mouse model of retinitis pigmentosa. **Hum Mol Genet**. 2012;21:4486-4496.

22. Tanimoto N, **Sothilingam V**, Euler T, Ruth P, Seeliger MW, Schubert T. BK channels mediate pathway-specific modulation of visual signals in the in vivo mouse retina. **J Neurosci**. 2012;32:4861-4866.

23. Egger A, Samardzija M, **Sothilingam V**, Tanimoto N, Lange C, Salatino S, Fang L, Garcia-Garrido M, Beck S, Okoniewski MJ, Neutzner A, Seeliger MW, Grimm C, Handschin C. PGC-1α determines light damage susceptibility of the murine retina. **PLoS One**. 2012;7:e31272.

24. **Sothilingam V**, Hass N, Breer H. Candidate chemosensory cells in the stomach mucosa of young postnatal mice during the phases of dietary changes. **Cell Tissue Res**. 2011;344:239-249.

Related Presentations

1. Morphological and functional characterization of Crb2 mutant mice in vivo. Swiss Eye Research Meeting. Biel, Switzerland, Jan 27-28, **2011**

2. Crb2 In Retinal Development. The Association for Research in Vision and Ophthalmology (ARVO) Annual Meeting. Fort Lauderdale, Florida, USA. May 1-5, **2011**

3. In vivo functional analysis of Crb2 mutant mice. Crumbs In Sight Meeting, Crumbs Consortium. Amsterdam, Netherlands. May 22-23, **2011**

4. Recovery of ERG components in the Cngb1-/- model of RP following gene therapy. Swiss Eye Research Meeting. Biel, Switzerland, Jan 26-27, **2012**

5. In vivo morphological and functional characterization of conditional Mpp3-/- mice. Crumbs In Sight Meeting, Crumbs Consortium. Amsterdam, Netherlands. March 29-30, **2012**

6. Recovery of ERG Components in the Cngb1-/-Model of RP Following Gene Therapy. ARVO Annual Meeting. Fort Lauderdale, Florida, USA. May 1-10, **2011**

7. CNGB1 channelopathies: From Phenotype to Cure. Vorlesungsreihe: “Modelle erblicher Netzhauterkrankungen: Genetik, Pathophysiologie und Therapie” Tübingen, Germany. July 25, **2012**

8. Cyclic–nucleotide gated (CNG) channels play a key role in cGMP-related retinitis pigmentosa. ISCEV Symposium. Valencia, Spain. June 4-8, 2012

9. Functional Biomarkers for Successful Molecular Therapy of the Outer Retina in Retinal Degenerations. Swiss Eye Research Meeting Biel, Switzerland, Jan 24-25, **2013**

10. Functional Biomarkers for Successful Molecular Therapy of the Outer Retina in Retinal Degenerations. Vorlesungsreihe: Modelle erblicher Netzhauterkrankungen: Genetik, Pathophysiologie und Therapie. Tübingen, Germany. June 12, **2013**

11. Long-term preservation of cone vision following rod-specific gene therapy in experimental Retinitis Pigmentosa. Vorlesungsreihe: Progress in Neuroscience Research of the Retina and Inner Ear. Tübingen, Germany. Nov 28, **2013**

12. Long-term preservation of cone vision following rod-specific gene therapy in experimental Retinitis Pigmentosa. **Recipient of the Swiss Retina Award**. Swiss Eye Research Meeting. Biel, Switzerland, Jan 23-24, **2014**

13. Therapeutic cross-species efficacy of vector for human gene therapy in achromatopsia type 2 (ACHM2). ARVO Annual Meeting. Orlando, Florida, USA. May 4-8, **2014**

14. Targeting rod CNG channels as a goal for RP therapy. Vorlesungsreihe: Modelle erblicher Netzhauterkrankungen: Genetik, Pathophysiologie und Therapie. Tübingen, Germany. July 23, **2014**

15. HCN1: A Keyplayer to Counteract Rod Saturation. Swiss Eye Research Meeting. Biel, Switzerland, Jan 22-23, **2015**

16. HCN1: A Keyplayer to Counteract Rod Saturation. Vorlesungsreihe: Modelle erblicher Netzhauterkrankungen: Genetik, Pathophysiologie und Therapie. Tübingen, Germany. July 22, **2015**

V. Appendix

Paper I: Retinitis pigmentosa: impact of different Pde6a point mutations on the disease phenotype

Sothilingam V*, Garcia Garrido M*, Jiao K, Buena-Atienza E*, Sahaboglu A, Trifunović D, Balendran S, Koepfli T, Mühlfriedel R, Schön C, Biel M, Heckmann A, Beck SC, Michalakis S, Wissinger B**§, Seeliger MW**§, Paquet-Durand F**§

Published in Human Molecular Genetics
24:5486-5499 (2015)

Human Molecular Genetics, 2015, 1–14

doi: 10.1093/hmg/ddv275
Advance Access Publication Date: 17 July 2015
Original Article

ORIGINAL ARTICLE

Retinitis pigmentosa: impact of different *Pde6a* point mutations on the disease phenotype

Vithiyanjali Sothilingam[1,†], Marina Garcia Garrido[1,†], Kangwei Jiao[2,3,†], Elena Buena-Atienza[4], Ayse Sahaboglu[2], Dragana Trifunović[2], Sukirthini Balendran[4,‡], Tanja Koepfli[4,¶], Regine Mühlfriedel[1], Christian Schön[5], Martin Biel[5], Angelique Heckmann[6], Susanne C. Beck[1], Stylianos Michalakis[5], Bernd Wissinger[4,§], Mathias W. Seeliger[1,§] and François Paquet-Durand[2,§,*]

[1]Division of Ocular Neurodegeneration, Institute for Ophthalmic Research, Centre for Ophthalmology, University of Tuebingen, Schleichstr.4/3, Tuebingen 72076, Germany, [2]Cell Death Mechanisms Group, Institute for Ophthalmic Research, Centre for Ophthalmology, University of Tuebingen, Roentgenweg 11, Tuebingen 72076, Germany, [3]Second People's Hospital of Yunnan Province and Fourth Affiliated Hospital of Kunming Medical University, 176 Qingnian Road, Wuhua, Kunming, Yunnan 650021, China, [4]Molecular Genetics Laboratory, Centre for Ophthalmology, University Clinics Tuebingen, Roentgenweg 11, Tuebingen 72076, Germany, [5]Center for Integrated Protein Science Munich (CIPSM) at the Department of Pharmacy – Center for Drug Research, Ludwig-Maximilians-Universität München, Munich 81377, Germany and [6]GenOway, 181 Avenue Jean Jaures, Lyon 69362, France

*To whom correspondence should be addressed. Email: francois.paquet-durand@klinikum.uni-tuebingen.de (F.P.-D); bernd.wissinger@uni-tuebingen.de (B.W); mathias.seeliger@uni-tuebingen.de (M.W.S.)

Abstract

Mutations in the *PDE6A* gene can cause rod photoreceptors degeneration and the blinding disease retinitis pigmentosa (RP). While a number of pathogenic *PDE6A* mutations have been described, little is known about their impact on compound heterozygous situations and potential interactions of different disease-causing alleles. Here, we used a novel mouse model for the *Pde6a* R562W mutation in combination with an existing line carrying the V685M mutation to generate compound heterozygous *Pde6a* V685M/R562W animals, exactly homologous to a case of human RP. We compared the progression of photoreceptor degeneration in these compound heterozygous mice with the homozygous V685M and R562W mutants, and additionally with the D670G line that is known for a relatively mild phenotype. We investigated PDE6A expression, cyclic guanosine mono-phosphate accumulation, calpain and caspase activity, *in vivo* retinal function and morphology, as well as photoreceptor cell death and survival. This analysis confirms the severity of different *Pde6a* mutations and indicates that compound heterozygous mutants behave like intermediates of the respective homozygous situations. Specifically, the severity of the four different *Pde6a* situations may be categorized by the pace of photoreceptor degeneration: V685M (fastest) > V685M/R562W > R562W > D670G (slowest). While calpain activity was strongly increased in all four mutants, caspase activity was not.

†The authors wish it to be known that, in their opinion, the first three authors should be regarded as joint First Authors.
‡Present address: Department of Obstetrics and Gynaecology, Medical University of Vienna, Waehringer Guertel 18-20, 1090 Vienna, Austria.
¶Present address: CeGaT GmbH, Tübingen, Germany.
§These authors should be considered as equivalent corresponding authors.

Received: April 30, 2015. **Revised and Accepted:** July 9, 2015

This points to the execution of non-apoptotic cell death and may lead to the identification of new targets for therapeutic interventions. For individual RP patients, our study may help to predict time-courses for *Pde6a*-related retinal degeneration and thereby facilitate the definition of a window-of-opportunity for clinical interventions.

Introduction

Retinitis pigmentosa (RP) is a hereditary neurodegenerative disease of the retina which affects photoreceptors and is a major cause of early-onset blindness in the industrialized world (1).

The genetic mutations triggering RP usually lead to a disturbance of the phototransduction cascade, often associated with an elevation of cyclic guanosine mono-phosphate (cGMP) (2). In the dark, high guanylate cyclase activity increases cGMP levels (3). Phototransduction starts with a light-induced, conformational change of opsin molecules, causing sequential activation of transducin and phospho-diesterase-6 (PDE6), the latter of which subsequently reduces the intracellular cGMP concentration. High cGMP levels maintain cyclic-nucleotide-gated (CNG) cation channels in the open state, allowing Ca^{2+} influx (4). PDE6 activation reduces cGMP levels, thus closing CNG channels and causing hyperpolarization and signal transmission to second order neurons.

Genetic mutations affecting PDE6 function lead to an excessive accumulation of cGMP and subsequent rod photoreceptor death (5,6), followed by a mutation independent, secondary death of cone photoreceptors (7). In rod photoreceptors, PDE6 is composed of two catalytic subunits—alpha (A) and beta (B)—and in the inactive state associates with two inhibitory gamma subunits. When all mutations affecting any of the three PDE6 alpha, beta or gamma subunits are considered together, these are responsible for up to 4–8% of human RP patients (8–10). Previously, PDE6 dysfunction was investigated primarily in animal models affected by mutations in the *Pde6b* gene, such as the *rd1* (11) or the *rd10* mouse (12). A variety of *Pde6a* mutations are also known to cause RP (13) but, so far these have been relatively little studied.

RP animal models are normally studied in the homozygous state (e.g. as $Pde6b^{rd1/rd1}$) even though, in human RP patients, in outbred populations, homozygosity is relatively rare and, in fact, compound heterozygosity, where two different disease-causing alleles come together in one individual, is more frequent (*e.g.* $PDE6A^{V685M/R562W}$). To account for this, we have used various *Pde6a* mutant mice and studied the progression of retinal degeneration both in the homozygous and compound heterozygous situations. To facilitate a comparison with the human situation, we focussed on *Pde6a* mouse mutants for which homologous RP patients have previously been identified. This relates to point mutations resulting in an amino acid exchange in various positions of the PDE6A protein, i.e. R562W, D670G and V685M. For the sake of clarity, in the following these animal models will be referred to by the position of their respective mutations.

The previously reported *Pde6a* D670G and V685M mouse mutants have been generated by *N*-ethyl-*N*-nitrosourea (ENU) mutagenesis and were identified through a screen for altered fundus pigmentation (13). In this study, we generated and studied an additional *Pde6a* R562W-knock-in mutant. The generation of this mutant followed the identification of a human RP patient compound heterozygous for the c.1684C>T/p.Arg562Trp and c.2053G>A/p.Val685Met mutations in *PDE6A*. Therefore, the generation of the R562W-knock-in mutant gave the opportunity to study the exact homologous genotype of the patient through crossbreeding of the R562W-knock-in with the V685M mutant. We then used both homozygous and compound heterozygous *Pde6a* mutant animals to assess the relative impact of different genetic insults on the progression and the severity of retinal degeneration. The data generated here may serve as a reference for further pre-clinical studies in RP animal models and—extrapolated to the human situation—may guide future clinical trials for RP therapy development.

Material and Methods

Animals

All *Pde6a* mutants used were generated and maintained on the C57BL6/J strain background (wild type; wt), were housed under standard white cyclic lighting, had free access to food and water and were used irrespective of gender. The V685M (A.B6-*Tyr+/J-Pde6a*$^{nmf282/nmf282}$) and D670G (C57BL/6J- *Pde6a*$^{nmf363/363}$) animals were obtained from the Jackson Labs (Bar Harbor, MA, USA).

The R562W-knock-in mutant was generated by GenOway (Lyon, France) using standard procedures of homologous recombination in murine embryonic stem (ES) cells. Briefly, left arm and right arm homology fragments of 4066 bp (covering exon 10 to exon 12 and parts of the flanking introns of *Pde6a*) and of 3830 bp (covering exon 13 and parts of the flanking introns of *Pde6a*), respectively, were polymerase chain reaction (PCR) amplified from a C57BL/6-derived BAC clone carrying *Pde6a* sequences. To generate the knock-in mutation the 'CGG' arginine codon was replaced by a 'TGG' tryptophan codon at the respective position in exon 13 in the right arm homology fragment by *in vitro* mutagenesis. The cloned fragments were verified by Sanger sequencing and then assembled for the final targeting construct that comprised a neomycin positive selection cassette flanked by loxP sites and inserted in intron 12 between the left and right arm homology fragments, and a diphtheria toxin expression cassette for negative selection. The targeting construct was electroporated into C57BL/6-derived ES cells according to GenOway's electroporation procedures (i.e. 10^8 ES cells in the presence of 100 µg of linearized plasmid, 260 V, 500 µF). Positive selection was started 48 h after electroporation, by addition of 200 µg/ml of G418 (150 µg/ml of active component, Life Technologies, Inc.). Resistant clones were isolated and amplified in 96-well plates. Duplicates of 96-well plates were made. The set of plates containing ES cell clones amplified on gelatine were genotyped by both PCR and Southern blot analysis and the presence of the mutation was verified by sequencing. One fully characterized ES clone was used for injection into blastocysts of C57BL/6J-Tyr^{c-2J}/J mice and two highly chimeric male mice were obtained. These mice were mated with C57BL/6 cre deleter female mice to excise the neomycin selection cassette. The F1 progeny was tested for proper excision of the neomycin cassette by means of PCR and Southern blotting. Since the used C57BL/6-derived ES cells carry the *rd8* allele (14), we mated the F1 with C57BL/6J animals and then crossbred F2 animals to obtain homozygous R562W mice devoid of *rd8*.

For all animals used in this study, day of birth was considered as post-natal day (P) 0. All procedures carried out on animals were reviewed and approved by the competent authority (Regierungspräsidium Tuebingen). All efforts were made to minimize the number of animals used and their suffering.

Functional analysis of the p.R562W mutant gene

We used an established system for the functional expression of PDE6 protein based on a PDE6C/PDE5 fusion construct and the use of the baculovirus/Sf9 insect cell system for recombinant protein expression (15,16). The mutated construct bearing a tryptophan codon instead of an arginine codon at the site homologous to p.R562 of *Pde6a* was generated by *in vitro* mutagenesis (Quik Change *in vitro* Mutagenesis Kit from Agilent, Waldbronn, Germany). Generation of recombinant bacmids, transfection of Sf9 insect cells and viral amplifications were carried out according to the manufacturers' recommendations (Life Technologies/Invitrogen, Darmstadt, Germany). Lysis of cells and purification of recombinant protein was carried out as previously described (15) and PDE activity was measured using [^{3}H]-cGMP (GE Healthcare, Munich, Germany) as substrate (17). Briefly, 5 µg purified wt and mutant protein, respectively, were incubated in a total volume of 40 µl of 20 mM Tris–HCl pH8.0, 50 mM NaCl, 15 mM $MgSO_4$, 2 mM β-mercaptoethanol, 0.1 µM shrimp alkaline phosphatase and 5 µM [^{3}H]cGMP (100 000 cpm) for 10 min at room temperature. The reaction was stopped by the addition of 0.5 ml AG1-X2 anion exchange resin (Bio-Rad) in a 20% bed volume suspension. Samples were incubated with the resin for 10 min with occasional vortexing and then centrifuged at 9000*g* for 2 min. Two hundred and fifty microliter aliquots of the clear supernatant were removed and measured in a scintillation counter (Beckman LS 6000, Beckman Coulter GmbH, Krefeld, Germany).

RT-PCR and allelic quantification

Homozygous and heterozygous *Pde6a* R562W-knock-in mice were sacrificed at the age of P14 and P80, respectively. In addition, we used P13 and adult C57BL6 wt mice as control. Retinas were dissected from enucleated eyes and used to prepare total RNA. The tissue was lysed mechanically in a Precellys homogenizer (Peqlab Biotechnologie GmbH, Erlangen, Germany) and total RNA isolated through affinity chromatography on silica membrane (peqGold Total RNA Kit; Peqlab Biotechnologie GmbH).

Single-stranded cDNA was synthesized from 1–2 µg of total RNA by reverse transcription applying random hexamers for priming (Transcriptor First Strand cDNA Synthesis Kit, Roche, Mannheim, Germany). For qualitative reverse transcriptase-polymerase chain reaction (RT-PCR), we amplified 1/10 volume of the first-strand cDNA with primers MmPde6a_cDNA_ex12Fnw (5-ACGCGGAGTCATACGAAATC-3) and MmPde6a_cDNA_ex15Rnw (5-ATGATGCCTTTCCAAGATGG-3) or Pde6a_cDNA_Ex11 (5′-AGAG GTGTACGGCAAAGAGC-3′) and Pde6a_cDNA_Ex14 (5′-GTTGTT CGTGCCTCTGTGGT-3′) applying standard PCR conditions.

RT-PCR products were cloned into pCR2.1 using the TA Cloning Kit (Invitrogen/Life Technologies) and plasmid DNA purified from single bacterial clones was sequenced applying cycle sequencing and BigDye Terminator V1.1 chemistry (Applied Biosystems/Life Technologies). Sequencing products were separated on an ABI 3130XL capillary sequencer (Applied Biosystems/Life Technologies). Raw sequences were processed using Sequencing Analysis Software V5.2 (Applied Biosystems/Life technologies) and assembled into contigs using SeqMan (Lasergene, Madison, WI, USA).

Relative quantification between the R562W-knock-in allele and the wt allele was done by pyrosequencing. For relative quantification of allelic *Pde6a* transcripts, we amplified 1/10 volume of first-strand retinal cDNA of heterozygous mutant mice with primers Pde6a_Mm_Ex12–13_F (5′-TTCCACATCCCGCAAGAG-3′) and a 5′-biotinylated reverse primer Pde6a_Mm_Ex12–13_R (5-Bio-CCAGCAAGGAGAACATGGTC-3′) applying standard PCR conditions. For comparison, we amplified an exon 13 internal fragment of the Pde6a gene from genomic DNA of heterozygous R562W-knock-in mice (extracted from ear punches) with primers Pde6a_Mm_Ex13-DNA_F (5′-GTTCACAGGCCCTGGTGC-3′) and 5′ biotinylated Pde6a_Mm_Ex12–13_R (see above). PCR products were purified by immobilization on streptavidin coated sepharose beads (GE Healthcare) and vacuum filtration (Vacuum Manifold, Qiagen, Hilden, Germany). Single-stranded PCR products were sequenced with primer Pde6a_Mm_Ex12–13_S (5′-GAAT CACTTACCACAACTG-3′) on a Pyromark Q96 instrument according to the manufacturer's recommendations (Qiagen).

Minigene splicing assays

Minigene constructs were generated by cloning both allelic products of a PCR with primers *Eco*RI-PDE6A-MMf (5′-aaGAATTCT GTATCAGTACGACCCAAGAC-3′; *Eco*RI recognition site underlined) and *Bam*HI-PDE6A-MMr (5′-aaGGATCCGAGTTGTATACTT CTCTATTCTTGGAA-3′; *Bam*HI recognition site underlined) with genomic DNA of a heterozygous R562W-knock-in mutant into the *Eco*RI and *Bam*HI sites of the pSPL3 vector. The amplified fragment from the wt allele encompasses exon 13 of *Pde6a*, 424 bp of upstream intron 12 sequence, and 308 bp of downstream intron 13 sequence. The fragment from the knock-in allele covers an additional 96 bp insert (comprising a single loxP site and flanking multiple cloning site sequences derived from the targeting vector) inserted 247 bp upstream of exon 13. Further constructs were obtained by introducing the c.1684C>T/p.R562W mutation into the wt allele construct and by reverting the mutation in the knock-in allele construct through *in vitro* mutagenesis according to the manufacturer's protocol (Quik Change Mutagenesis Kit; Agilent). The inserts of the minigene constructs were verified by Sanger sequencing as outlined above. Purified plasmid DNA of the constructs were used to transfect HEK293 and 661W as follows: Cells were seeded in 6-well plates in Dulbecco's modified Eagle's medium (DMEM) (Gibco/Life Technologies) with 10% fetal bovine serum (Biochrom GmbH, Berlin, Germany) and the following day, at 80–90% confluency, cells were transfected with 4–10 µg plasmid DNA of the minigene construct using 20 µl Lipofectamine 2000 per well and OptiMEM® supplemented with GlutaMAX™ (Gibo/Life Technologies) as diluents and medium. After 6 h incubation, cells were harvested by trypsinization with 0.05% trypsin-ethylenediaminetetraacetic acid (Gibco/Life Technologies), centrifuged at 1500 rpm for 5 min and transferred to a 6 cm dish with DMEM supplemented with 10% fetal calf serum and antibiotics (10 ml/l of penicillin–streptomycin solution [P4333; Sigma-Aldrich Chemie GmbH, Munich, Germany] and 10 ml/l Amphotericin B [250 µg/ml in water; Biochrom AG]). Twenty-four hours post-transfection, cells were lysed and total RNA was extracted applying the peqGOLD Total RNA Kit (Peqlab Biotechnologie GmbH). Single-stranded cDNA was synthesized as outlined above and cDNA was amplified with primers SA2 (5′-ATCTCAGTGGTATTTGTGAGC-3′) and SD6 (5′-TCTGAGTCACC TGGACAACC-3′) applying standard PCR conditions. RT-PCR products obtained from transfected HEK293T cells were cloned into pCR2.1 using the TA Cloning Kit (Invitrogen/Life Technologies) and plasmid DNA isolated from single bacterial clones sequenced as outlined above.

Histology, immunohistochemistry and immunofluorescence

Animals were sacrificed in the morning (10–11 am), their eyes enucleated and fixed in 4% paraformaldehyde (PFA) in 0.1 M phosphate buffer (pH 7.4) for 45 min at 4°C. PFA fixation was

followed by cryoprotection in graded sucrose solutions (10, 20, 30%). Unfixed eyecups were directly embedded in cryomatrix (Tissue-Tek, Leica, Bensheim, Germany). Sagittal 12 µm sections were obtained and stored at –20°C.

For immunofluorescence, sections were incubated overnight at 4°C with primary rabbit antibody against PDE6A (Novus Biologicals, Cambridge, UK; # NBP1–87312), rabbit antibody against caspase-3 (Cell Signaling, Danvers, MA; #9664), or sheep antibody against cGMP (1:400; kindly provided by Harry Steinbusch, Maastricht, The Netherlands), then washed in PBS and incubated for 1 h with Alexa Fluor 488-conjugated, matching secondary antibodies (Molecular Probes, Inc. Eugene, USA). Negative controls were carried out by omitting the primary antibody. Sections were mounted with Vectashield (Vectorlabs, Burlingame, CA, USA) for microscopy.

Calpain activity and TUNEL assay

Calpain activity was investigated using an enzymatic *in situ* assay (18). Unfixed cryosections were incubated for 15 min in calpain reaction buffer (CRB; 25 mM HEPES, 65 mM KCl, 2 mM MgCl2, 1,5 mM CaCl2, 2 mM DTT) and then incubated at 35°C for 1 h in the dark in CRB with 2 mM fluorescent calpain substrate 7-amino-4-chloromethylcoumarin, t-BOC-Leucyl-L-methionine amide (Life technologies, Darmstadt, Germany; #A6520). Fluorescence was uncaged by calpain-dependent cleavage of t-Boc-Leu-Met-CMAC.

Terminal deoxynucleotidyl transferase dUTP nick end labelling (TUNEL) assay was performed using an *in situ* cell death detection kit (Fluorescein or TMR; Roche Diagnostics GmbH, Mannheim, Germany). For controls terminal deoxynucleotidyl transferase, enzyme was either omitted from the labelling solution (negative control), or sections were pre-treated for 30 min with DNAse I (Roche, 3 U/ml) in 50 mM Tris–HCl, pH 7.5, 1 mg/ml BSA to induce DNA strand breaks (positive control). While negative control gave no staining, positive control stained all nuclei in all layers of the retina (19).

Microscopy, cell counting and statistical analysis

Light and fluorescence microscopy were usually performed at room temperature on an Axio Imager Z.1 ApoTome Microscope, equipped with a Zeiss Axiocam MRm digital camera. Images were captured using Zeiss Axiovision 4.8 software; representative pictures were taken from central areas of the retina using a 20×/0.8 Zeiss Plan-APOCHROMAT objective. Adobe Photoshop CS3 (Adobe Systems Incorporated, San Jose, CA) was used for primary image processing.

For the quantifications of positively labelled cells (TUNEL, cGMP), pictures were captured on three entire sagittal sections for at least three different animals for each genotype and age using Mosaic mode of Axiovision 4.8 at 20× magnification. The average area occupied by a photoreceptor cell (i.e. cell size) for each genotype and age was determined by counting DAPI-stained nuclei in nine different areas (50 × 50 µm) of the retina. The total number of photoreceptor cells was estimated by dividing the outer nuclear layer (ONL) area by this average cell size. The number of positively labelled cells in the ONL was counted manually. We considered cells as positively labelled only if they showed a strong staining of either the photoreceptor nuclei (e.g. for TUNEL) or perinuclear areas (e.g. for cGMP, caspase-3). Values obtained are given as fraction of total cell number in ONL (i.e. as percentage) and expressed as mean ± standard error of the mean (SEM).

For the quantification of PDE6A protein expression, fluorescent pictures were loaded into ImageJ (Vers. 1.44; Wayne Rasband, National Institute of Mental Health, Bethesda, MA) and the line plot option was used to obtain maximum intensity values for the ONL and outer segment (OS) areas. The (unstained) ONL values were taken for background subtraction, the average pixel intensity in wt OS was arbitrarily set to 1; the mutant values were expressed as a function of that. For statistical comparisons, the unpaired Student *t*-test as implemented in Prism 5 for Windows (GraphPad Software, La Jolla, CA) was employed.

Non-invasive *in vivo* imaging and functional testing

A baseline characterization with electroretinography (ERG), spectral domain optical coherence tomography (SD-OCT) and scanning-laser ophthalmoscopy (SLO) was performed at 4 weeks of age. The groups were composed of four animals of each genotype.

Electroretinography

ERGs were recorded binocularly from different *Pde6a* mutants as described previously (20). Mice were dark-adapted overnight and anaesthetized using a combination of ketamine (66.7 mg/kg body weight) and xylazine (11.7 mg/kg body weight). Their pupils were dilated and single-flash ERG responses were obtained under scotopic (dark-adapted) and photopic (light-adapted with a background illumination of 30 cd/m^2, starting 10 min before recording) conditions. Single white-flash stimuli ranged from –4 to 1.5 log cd·s/m^2 under scotopic and from –1.0 to 1.5 log cd·s/m^2 under photopic conditions. Ten responses were averaged with inter-stimulus intervals of 5 s (for –4 to –0.5 log cd·s/m^2) or 17 s (for 0 to 1.5 log cd·s/m^2).

Spectral-Domain optical coherence tomography

Retinal structures of the still anesthetized animals were visualized via OCT imaging with a Spectralis^{TM} HRA + OCT (Heidelberg Engineering GmbH, Heidelberg, Germany). This device features a superluminescent diode at 870 nm as low coherence light source. Scans are acquired at a speed of 40 000 scans per second and each two-dimensional B-scan contains up to 1536 A-scans (21–23). The images were taken with the equipment set of 30° field of view and with the software Heidelberg Eye Explorer (HEYEX version 5.3.3.0, Heidelberg, Germany). Resulting images were exported as 8-bit colour bitmap files and processed with CorelDraw X3 (Corel corporation, Ottawa, ON, Canada).

Scanning-laser ophthalmoscopy

Eyes were kept moisturized with Methocel (Omnivision, Puchheim, Germany) so that SLO imaging was performed in the same session as OCT. It was carried out with a HRA 1 system (Heidelberg Engineering) according to previously described procedures (24). Briefly, the HRA 1 system features lasers in the short (visible) wavelength range (488 nm in both and 514 nm), and also in the long (infrared) wavelength range (795/830 nm and 785/815 nm). The 488 and 795 nm lasers are used for fluorescein (FLA) and indocyanine green (ICG) angiography, respectively. GFP excitation was detected in the autofluorescence mode at 488 nm with a 500 nm barrier filter.

Results

Functional analysis of the p.R562W mutation in PDE6A

To verify the pathogenicity and to assess the functional consequence of a recently identified new missense variant (p.R562W) in the PDE6A gene, we expressed the mutant PDE6 protein in Sf9 insect cells by using an established chimeric PDE6C/PDE5 construct (15). Purified recombinant protein was analyzed for cGMP

hydrolysis activity. In comparison with wt protein, the catalytic activity of R562W mutant protein was reduced to ~10% (Fig. 1).

Generation of a new mouse model for the R562W mutation

In order to study the retinal phenotype caused by the R562W mutation, we generated a *Pde6a*:R562W-knock-in mouse mutant applying state-of-the art homologous recombination in mouse ES cells. The knock-in allele bore the actual c.1684C>T/p.R562W mutation in exon 13 and, in addition, upstream, in intron 12, remnant sequences of the targeting process including a single loxP site flanked by 62 bp of sequence of the multiple cloning site derived from the targeting vector. We used heterozygous R562W-knock-in animals to test for proper expression of the mutant allele in the retina. Upon allelic quantification of *Pde6a* RT-PCR products, we found an excess of wt allele derived transcripts in heterozygous animals (Fig. 2A).

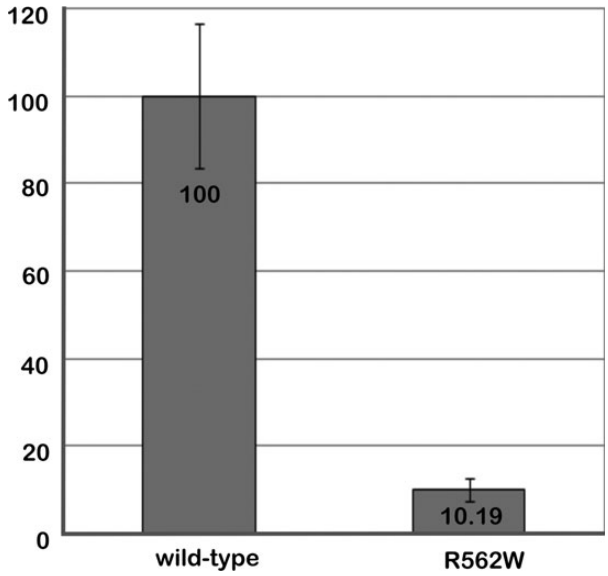

Figure 1. The R562W mutant PDE6 protein shows reduced catalytic activity. cGMP hydrolysis activity of wild-type and R562W mutant chimeric PDE6C/PDE5 protein was determined *in vitro* on purified recombinant protein. The bars were normalized to wild-type enzymatic activity (100%).

Further RT-PCR experiments with primers located in exon 12 and 14 revealed two major products in homozygous R562W mutants. The larger RT-PCR product was identical in size (403 bp) to the RT-PCR obtained from control animals, and the other ~100 bp smaller (Fig. 2B). Sequencing of cloned products from homozygous R562W mutant animals revealed that the smaller cDNA fragment lacks exon 13. Additionally, we performed RT-PCR experiments in heterozygous R562W animals. Sequencing of cloned RT-PCR products showed the absence of exon 13 in the smaller cDNA fragment while the larger cDNA fragment represented a mixture of correctly spliced wt and knock-in allele derived transcripts, respectively (Supplementary Material, Fig. S1). These findings indicated an incompletely penetrant splicing defect caused by the knock-in allele. Bioinformatic analysis suggested that the C>T transition created an exonic splicing silencer (ESS) site which most likely explained the impaired exon 13 splicing (data not shown). Skipping of exon 13 resulted in an in-frame deletion of the open reading frame and translated into a PDE6A protein shortened by 36 amino acid residues (p.541_576del), which lacks the amino-terminal portion of the catalytic domain including the first metal binding motif.

Since we could not rule out an effect of the resident modifications (loxP site and multiple cloning site sequences; loxP/MCS insert) in intron 12 in the knock-in allele on transcript splicing, we generated minigene constructs that include the murine exon 13 and 424 bp of upstream intron 12 and 309 bp of downstream intron 13 sequences inserted in to the pSPL3 exon trapping vector. Four different variants of the minigene constructs were cloned: (i) wt, (ii) wt exon 13 and the 96 bp loxP/MCS insert in intron 12, (iii) c.1684C>T/p.R562W mutation in exon 13 with wt intron 12 portion, and (iv) the knock-in allele (c.1684C>T/p.R562W and loxP/MCS insert in intron 12) (Supplementary Material, Fig. S2). Constructs were transfected into HEK293T cells and total RNA

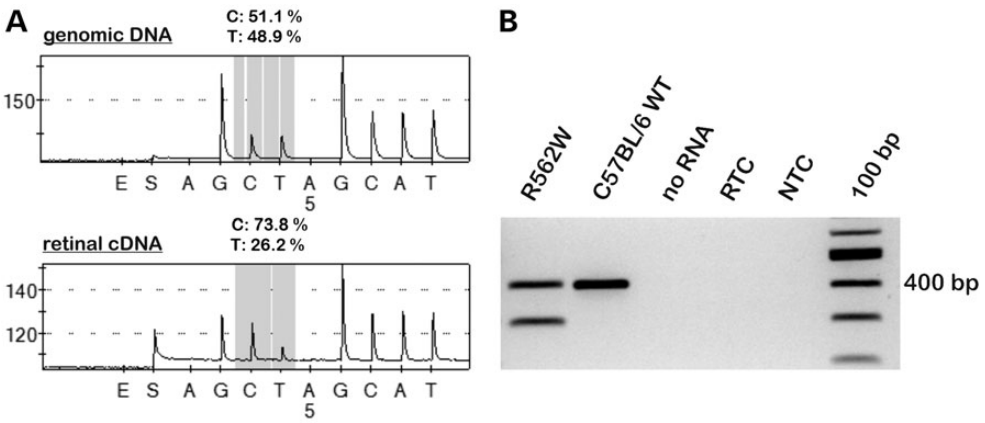

Figure 2. *Pde6a* cDNA analysis in the R562W-knock-in mouse mutant. (**A**) Pyrosequencing-based relative quantification of wild-type and R562W knock-in *Pde6a* alleles at the genomic DNA level (top) and in reverse transcribed retinal cDNA of a heterozygous *Pde6a*:R562W-knock-in mutant. Note that the assayed variant nucleotide position is the actual c.1684C>T mutation and that allelic quantification of cDNA was done on RT-PCR products with primers in exons 12 and 13. (**B**) Qualitative analysis of the integrity of retinal *Pde6a* transcripts in the *Pde6a*:R562W-knock-in mouse mutant. RT-PCR products with primers in exons 12 and 15 of *Pde6a* were amplified from retinal RNA of a homozygous *Pde6a*:R562W-knock-in mutant and a C57BL/6 wild-type control. The larger sized product of 403 bp is derived from correctly spliced transcripts and the smaller product represent mis-spliced transcripts lacking exon 13. Controls 'no RNA': w/o RNA in the DN*ase*I digestion and subsequent RT and PCR reactions, 'RTC': w/o RNA in the cDNA synthesis and subsequent PCR reaction, 'NTC': no template control for the PCR reaction. One hundred base pair ladder size standard is shown in the rightmost lane.

was prepared 24 h post-transfection. RT-PCR for the expression construct with primers located in flanking exons of the pSPL3 vector indicated that the splicing defect observed in the knock-in mouse mutant was caused by the c.1684C>T/p.R562W mutation and not primed or influenced by the modifications in intron 12 (Supplementary Material, Fig. S3). Given that a considerable proportion of exon 13 skipped transcripts were also expressed from the wt minigene construct in HEK293T cells, we re-performed minigene assays for the c.1684C>T/p.R562W mutant construct in the mouse cone photoreceptor-like cell line 661W. RT-PCR with RNA from transfected 661W cells showed a strongly reduced proportion of transcripts with exon 13 skipping from the wt minigene construct and roughly equal proportions of correctly spliced and exon 13 skipped transcripts from the mutant construct (Supplementary Material, Fig. S4). This corresponded to the findings in mutant mouse retina (Fig. 2B).

Decreased PDE6A expression causes cGMP accumulation and photoreceptor death

We first assessed the expression of the PDE6A protein in the retina of wt and *Pde6a* mutants, at post-natal day (PN) 11, i.e. a time-point just before the onset of photoreceptor degeneration and widespread destruction of the ONL. In wt retina PDE6A is present almost exclusively in photoreceptor OS. In contrast, in V685M, V685M/R562W and R562W PDE6A is essentially undetectable, with a faint, dot-like staining pattern in R562W OS indicative of a very low PDE6A protein expression. In D670G retina, PDE6A protein is detectable in OS; however, the amount of protein detected is clearly lower than in wt (Fig. 3A–E).

The decreased detection of PDE6A in mutant retinas correlated with an increased accumulation of cGMP (Fig. 3F–J). Wt retina did not show signs of important cGMP accumulation (wt: 0.003% cGMP-positive cells ± 0.003 SEM, $n = 6$), while in all four *Pde6a* mutants, the numbers of rod photoreceptors showing high levels of cGMP was elevated already at PN11 (V685M: 0.61% ± 0.04; V685M/R562W: 0.19% ± 0.06; R562W: 0.17% ± 0.08; D670G: 0.007% ± 0.002; $n = 3$ for all).

To further assess the progression of retinal degeneration in the various *Pde6a* mutants, we used the TUNEL assay to label dying photoreceptors and, conversely, quantified the number of rows of surviving photoreceptors (Fig. 4). In the V685M ONL, the percentage of TUNEL-positive cells peaks already at PN12, something that is also evidenced by the early and rapid loss of photoreceptor rows (Fig. 4B, G and L). In the compound heterozygous V685M/R562W and in the R562W, cell death peaked at PN15 although the peak amplitude was slightly lower in the R562W mutant (Fig. 4C, D, H, I, M and N). When compared with the V685M situation, this corresponded to a delay in the onset and progression of degeneration of ∼2 days in V685M/R562W retina and 4 days in R562W retina. The D670G mutant showed a relatively small peak of cell death at PN21 and also the slowest overall progression of degeneration among the four *Pde6a* mutant genotypes (Fig. 4E, J and O).

Retinal degeneration has frequently been associated with the execution of classical apoptosis and the activity of caspase-type proteases (25,26). However, more recent studies point to the activity of non-apoptotic and caspase-independent mechanisms of cell death in hereditary retinal degeneration (27) which may instead rely on the activity of Ca^{2+} activated calpain-type proteases (2,28). To address this question for the *Pde6a* mutants used here, we performed an immunostaining for activated caspase-3, a key effector in classical apoptosis. Since the chances for a positive detection of caspase-3 activity are highest when cell death is high, we focussed on the peaks of degeneration as assessed by the TUNEL assay. In the early post-natal wt, a low level of caspase-3 activity was present, likely relating to developmental cell death in rodent retina (29). Remarkably, none of the *Pde6a* mutants showed any significant increase of caspase-3 activity when compared with wt (Fig. 5A–E; quantification in K). An *in situ* assay for Ca^{2+} activated calpain-type proteases (28) revealed very low levels of activation in wt retina. In *Pde6a* mutants however, the numbers of photoreceptors cells showing calpain activation was dramatically increased (Fig. 5F–J). When we then assessed the progression of calpain activity over time, we found a strong temporal correlation between calpain activity and cell death (Fig. 5L).

Characterization of *Pde6a* mutants *in vivo*

The four *Pde6a* mutant lines were morphologically and functionally characterized *in vivo* by means of SLO and OCT imaging and ERG recording at the age of 4 weeks. In SLO imaging, overall fundus appearance was visualized with the green laser at 514 nm (Fig. 6A, F, K and P); the retinal vasculature was studied with angiography applying ICG (Fig. 6B, G, L and Q) and fluorescein (Fig. 6C, H, M and R) and the appropriate laser wavelengths (795 and 488 nm, respectively). Retinal layering was studied by means of OCT imaging (Fig. 6D, E, I, J, N, O, S and T). D670G mice revealed a heavily spotted fundus appearance in the native fundus imaging (Fig. 6A) as well as in the fluorescein angiography mode (Fig. 6C) whereas in the OCT analysis, a very thin ONL was visualized depicting the presence of only few photoreceptor rows (Fig. 6D and E). A spotty fundus was also found in the R562W mice (Fig. 6F) together with a further decrease in the retinal thickness where no outer retina was detected (Fig. 6I and J). Compound heterozygous V685M/R562W mice showed a heavily affected retinal fundus with large areas of degeneration (Fig. 6K and M). In these mutants, the retinal thickness was strongly decreased, which resulted in enhanced visibility of choroidal structures in each SLO imaging mode (Fig. 6K–M). Accordingly, the OCT analysis revealed a highly degenerated retina (Fig. 6N and O). V685M was the mouse line with the strongest degeneration, retinal and choroidal structures were difficult to distinguish due to the severe decrease in the retinal thickness (Fig. 6S and T). Altogether, a different degree of retinal degeneration was detected and a gradient based on the severity (from less to more affection) of the disease was established: D670G>R562W>V685M/R562W>V685M.

The *in vivo* morphological findings correlated well with the functional data obtained with ERG. Full-field ERG measurements under both scotopic and photopic conditions allow the assessment of retinal function (Fig. 7A and B). Depending on the extent of morphological alterations, different ranges of ERG recordings could be observed. Retinal function was mostly preserved in the D670G animals [blue box and whisker plot (B&W)], greatly reduced in the R562W mice (green B&W) and completely missing in the V685M mutant (red B&W). The V685M/R562W, as an intermediate mutant line, is positioned between the R562W and V685M variants. Scotopic and photopic ERG traces at the highest stimulus intensity (Fig. 7C) were similar to those of a $Rho^{-/-}$ animal used as a functional control for cone-only responses (20,30). A comparison of the size of ERG amplitudes of different *Pde6a* mutants with age-matched C57/BL6 wt mice revealed that amplitudes of *Pde6a* mutants were considerably smaller and represent one-third to one-fourth of wt animals (20). Taken together, these *in vivo* morphological and functional observations were closely matching the results obtained in *ex vivo* quantification of photoreceptor cell death and survival (Fig. 4).

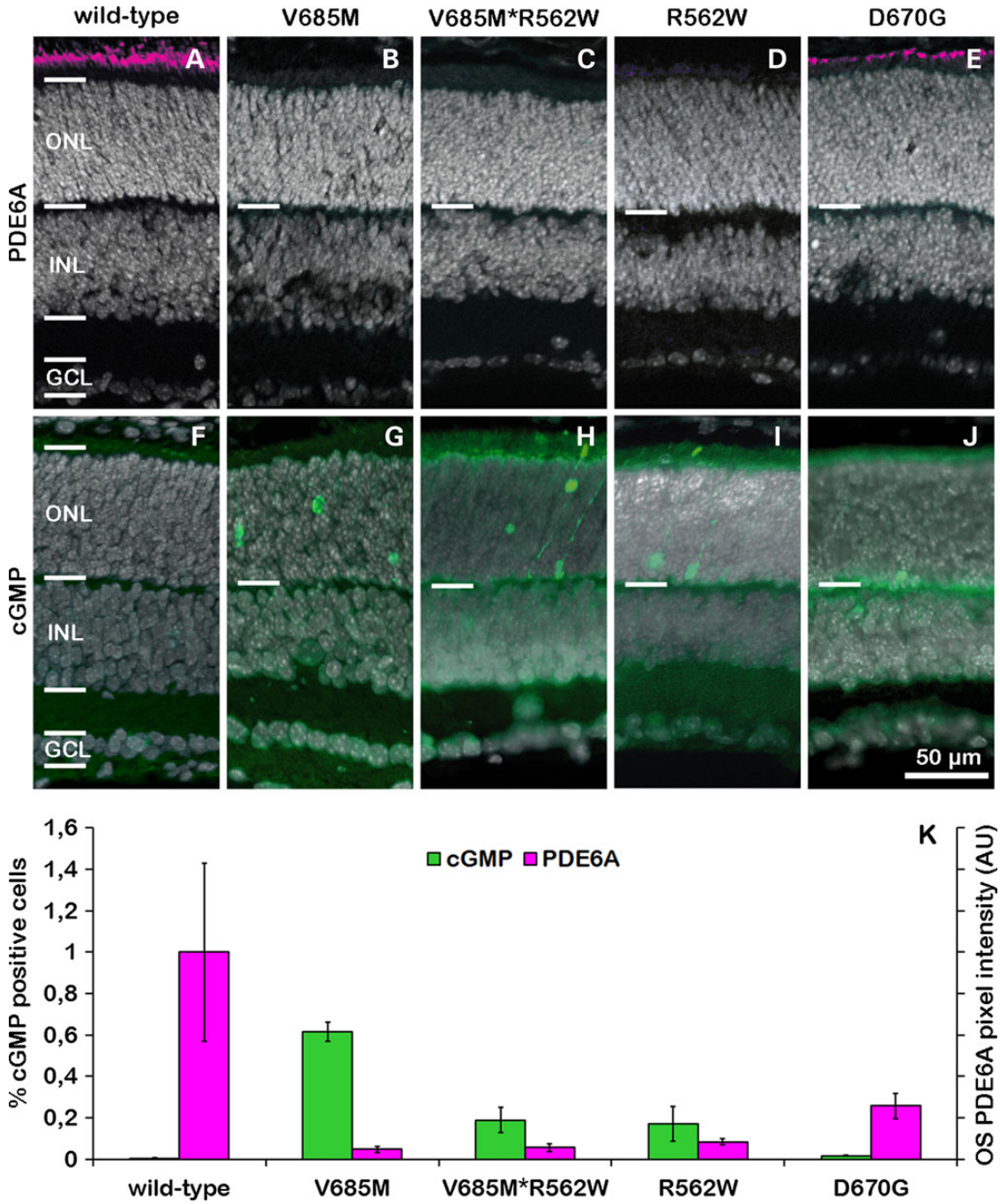

Figure 3. Loss of PDE6A expression causes cGMP accumulation. In the PN11 wild-type (wt) retina (**A**), immunostaining for PDE6A shows strong protein expression in photoreceptor OS. In contrast, at the same age, in V685M retina (**B**), the PDE6A protein is undetectable. Similarly, in the compound heterozygous V685M/R562W retina (**C**), the protein is essentially absent. In R562W retina, (**D**) small immunoreactive dots at the level of the OS may indicate a minimal protein expression. In the D670G mutant (**E**), however, there is a clear PDE6A protein expression; albeit at reduced levels when compared with wt. At PN11, wt retina is essentially negative for cGMP immunoreactivity (**F**). All *Pde6a* mutants, however, display individual rod photoreceptor cells that have accumulated large amounts of cGMP (**G–J**). The quantification of cGMP-positive cells in the ONL and the PDE6A pixel intensity in the OS (arbitrary units; AU) shows an inverse correlation (**K**). Images are representative for immunostaining performed on retinal sections from at least three independent animals for each genotype.

Discussion

In this report, we investigated the pathologic consequences of three different *Pde6a* point mutations for retinal photoreceptor degeneration. We analyzed the effects of these mutations on PDE6 activity, photoreceptor cGMP accumulation and progression and mechanisms of retinal degeneration. Previously, a variety of RP animal models have been generated and studied that carried human gene mutations homozygously (31–33). Here, we created an *in vivo* model carrying two different point mutations (*Pde6a* $^{V685M/R562W}$), exactly homologous to a human RP patient genotype, representing one of the first attempts to create a compound heterozygous, patient-matched

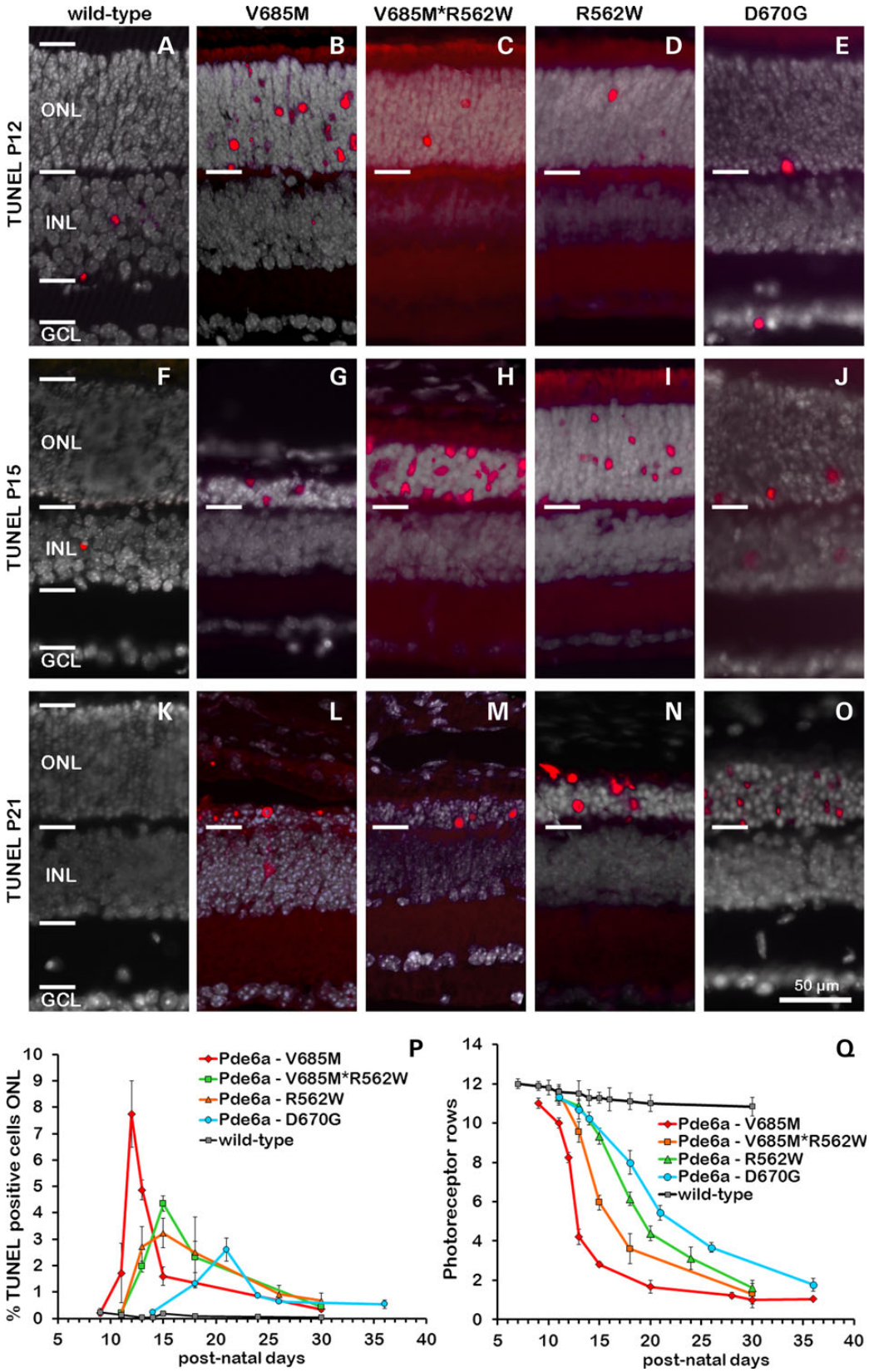

Figure 4. Photoreceptor cell death and survival. The TUNEL assay in the wt retina (**A**, **F** and **K**) occasionally labelled cells dying due to developmental processes. In contrast, in all *Pde6a* mutants (**B–E**, **G–J** and **L–O**), photoreceptor cell death was dramatically increased. The images show the situation at P12, P15 and P21, time-points corresponding to the peak of cell death for the different models. The line graph at the bottom left (**P**) illustrates the progression of photoreceptor cell death as evidenced by the TUNEL assay in the different *Pde6a* mutants. The peak times as well as the peak amplitudes correspond to the speed of retinal degeneration, which is illustrated by the loss of photoreceptors (**Q**). Images are representative for TUNEL assays performed on retinal sections from at least three independent animals, quantifications in P, Q include data from 3–7 animals per genotype and timepoint.

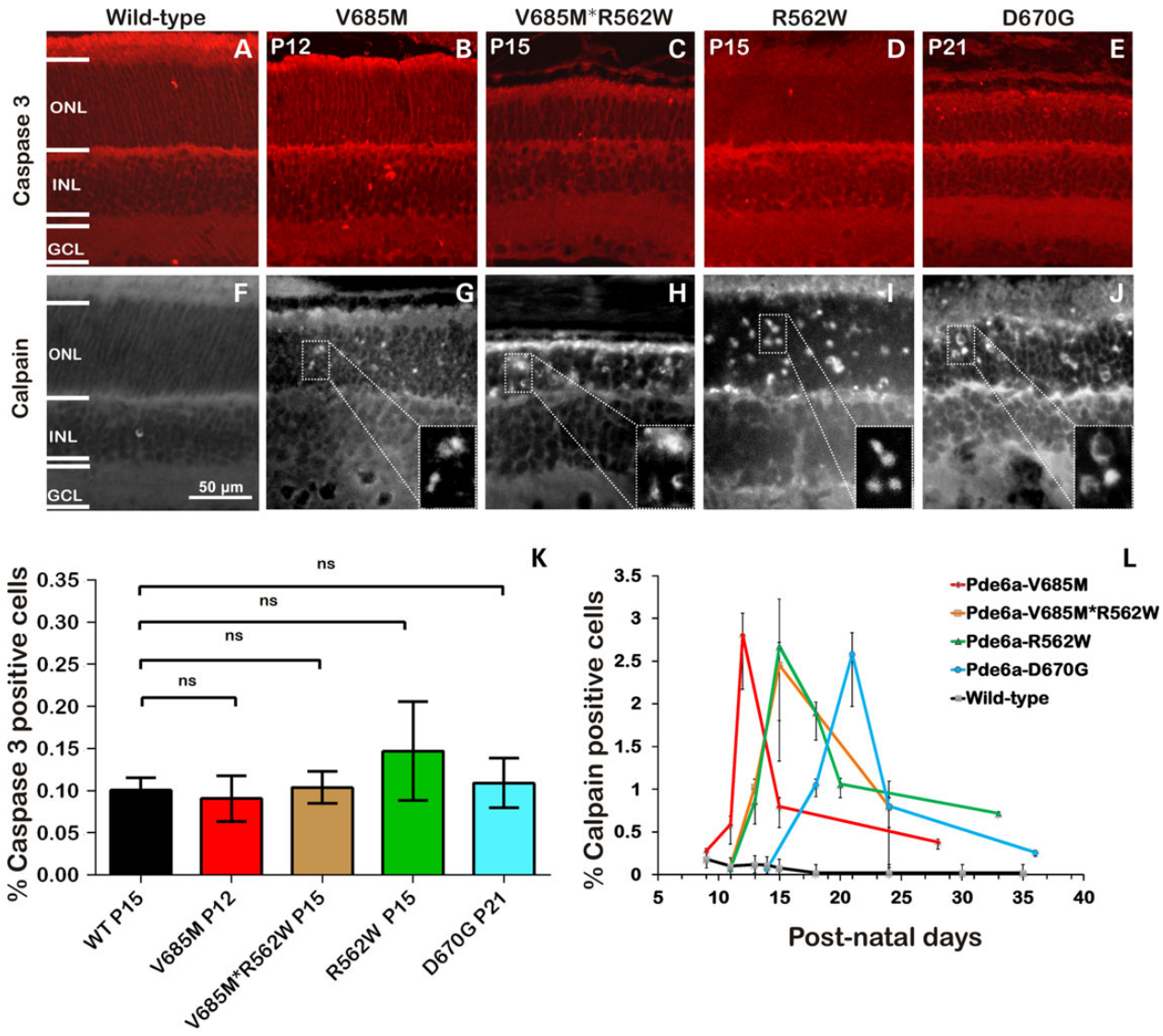

Figure 5. Photoreceptor degeneration in *Pde6a* mutants correlates with calpain not caspase activity. Immunofluorescence for activated caspase-3—a key marker for classical apoptosis—reveals no major differences between wild-type and mutant retinae (**A–E**). This is also illustrated by the quantification of caspase-3-positive cells, which shows only extremely low numbers of cells at the respective peaks of degeneration, with no significant (n.s.) differences to wt (**K**). In contrast, an *in situ* calpain activity assay reveals strong differences between wild-type (**F**) and all four *Pde6a* mutant genotypes (**G–J**). The progression of calpain activity was analyzed over time (**K**) and showed a strong correlation to the extent of cell death and the progression of retinal degeneration (cf. Fig. 4). Images shown are representative for at least three different stainings obtained at the respective mutant's peak of degeneration. Note that the differences in the progression of *Pde6a* mutant degenerations are also illustrated here by the differences in retinal ONL sizes. Data shown in K and L was obtained from observations made on 4–6 independent specimens for each genotype and timepoint.

basis for the development and assessment of individualized RP therapies.

Loss of PDE6 function, cGMP signalling and cell death

PDE6 is the main photoreceptor cGMP hydrolysing enzyme and displays the highest activity levels among all PDE's (34). Although excessive accumulation of cGMP has been found in various animal models for RP, it is particularly prominent in animals that carry mutations in PDE6 (2). However, it is still unclear to what extent different *PDE6* mutations cause cGMP accumulation and how this correlates with progression speed and severity of retinal degeneration. In all *Pde6a* mutants studied here the genetic defects led to a reduced PDE6 function as evidenced by an accumulation of cGMP. Compared with mutations where PDE6 function is abolished entirely, such as in the *rd1* mouse (35), the accumulation of cGMP in the *Pde6a* point-mutants examined here was less prominent.

High levels of cGMP are thought to cause an over-activation of CNG channels leading to excessive amounts of Ca^{2+}-influx (28,36). This is compatible with the observed increase in the numbers of photoreceptor cells showing a high degree of Ca^{2+}-activated calpain-type protease activity. Calpain activity is often associated with non-apoptotic forms of cell death (37) and in all *Pde6a* mutants it is strongly correlated in time with the progression of photoreceptor cell death. The relatively low amount of calpain activity-positive photoreceptors, when compared with the *rd1* mouse (38), likely reflects the lower extent of cGMP

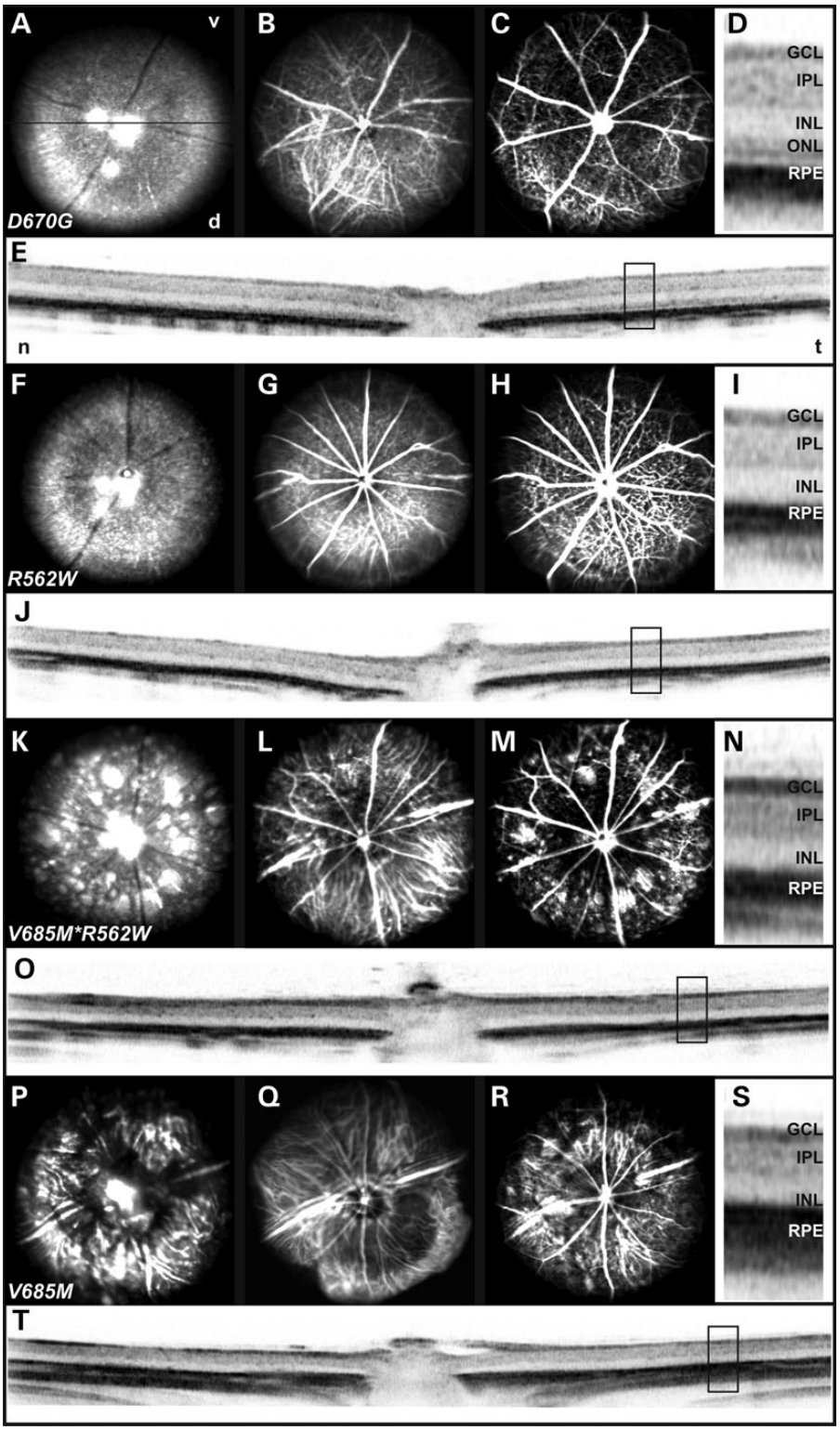

Figure 6. Retinal morphology in *Pde6a* mutants *in vivo*. D670G (**A–E**), R562W (**F–J**), V685M/R562W (**K–O**) and V685M (**P–T**) mutant mice were examined with SLO and SD-OCT at PN30. Examinations included fundus native imaging (A, F, K and P), ICG angiography (B, G, L and Q) and fluorescein angiography (C, H, M and R). For the OCT analyses, horizontal scans through the optic disc head are shown (E, J, O and T; magnifications; D, I, N and S). All of the mutants analysed revealed retinal degeneration. D670G mice showed several spots spread over the fundus (A), which were also visible in fluorescein angiography examination (C). Retinal thickness was also affected and a very thin ONL was detected (D and E). A similar fundus appearance (F–H) but a more severe decrease in the retinal thickness was found in the R562W mutants (I and J). V685M/R562W compound heterozygous mice showed large areas of retinal degeneration in native fundus imaging (K). The loss of retinal layers demonstrated in OCT imaging (O and N), allowed the enhanced visualization of choroidal structures (L and M). V685M exhibited a very severe retinal degeneration in both SLO and OCT imaging (P–T). GCL, ganglion cell layer, IPL, inner plexiform layer; INL, inner nuclear layer; ONL, outer nuclear layer; RPE, retinal pigment epithelium; d, dorsal; n, nasal; t, temporal; v, ventral.

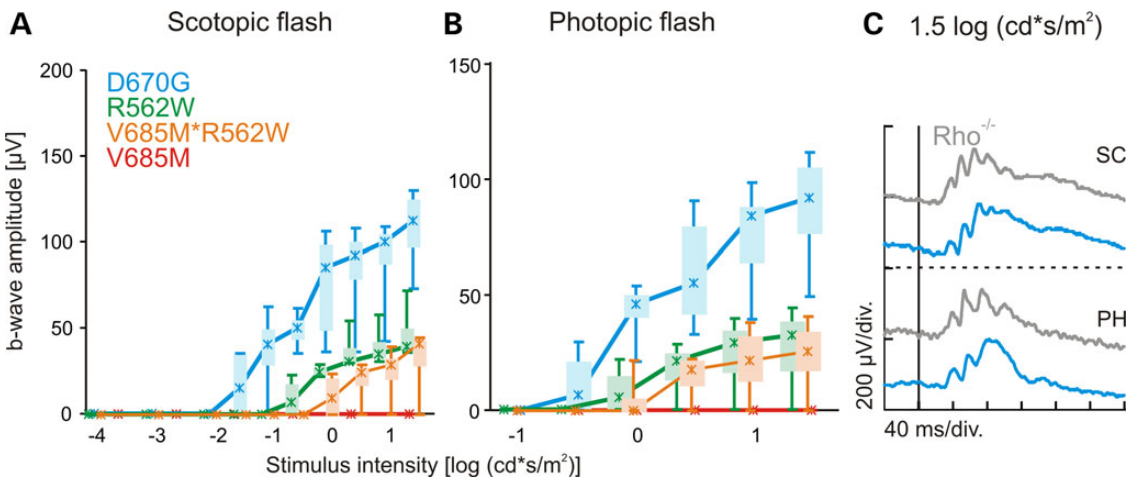

Figure 7. Functional assessment of different *Pde6a* mutants based on electroretinography. Quantitative evaluation of the scotopic [dark-adapted (**A**)] and photopic [light-adapted (**B**)] *b*-wave amplitude data, acquired at PN30 and shown as box-and whisker-plot (B&W), for the different *Pde6a* mutant lines. In B&W, boxes indicate the 25–75% quantile range, whiskers the 5 and 95% quantiles and asterisks the medians of the data. Scotopic (top) and photopic (bottom) single-flash ERG at 1.5 log (cd·s/m^2) maximal light intensity (**C**). ERGs from D670G mutant (blue) are similar to ERGs from a Rho$^{-/-}$ mouse, a valid model for pure cone function. D670G (blue), R562W (green), V685M/R562W (orange) and V685M mice (red).

accumulation and thus lower Ca^{2+}-influx. This may be particularly evident in the V685M mutant where the numbers of dying, TUNEL-positive cells exceeds the numbers of calpain activity positive cells by ~2:1. In the more slowly degenerating mutants the relative extent of calpain activity is more important, and reaches a ratio of ~1:1 in the D670G mutant. In either case, these results are suggestive of a causal involvement of calpain activity in the degenerative process.

Remarkably, in all four mutant genotypes the numbers of photoreceptors displaying high caspase-3 activity was very low, at wt levels, and not correlated to the progression of the mutation-induced degeneration. Since caspase-3 is key to the execution of numerous terminal proteolytic events in classical apoptotic cell death (27), this result indicates that apoptosis does not play any major role in *Pde6a* mutation-induced retinal degeneration. This is in agreement with a recent study on the prevalence of non-apoptotic cell death in 10 different rodent retinal degeneration models (2). Similar observations were also made in monkey retinal cell cultures subjected to hypoxia/reoxygenation where calpain proteolytic activity was in fact found to inactivate caspase-type proteases (39)

Overall, our results may provide important insights for potential therapy developments, suggesting the targeting of non-apoptotic processes, such as excessive cGMP-signalling or calpain activity as a feasible treatment approach.

Variable speed of progression, functional and degeneration phenotypes

The four different *Pde6a* mutants used here were found to have a variable pace of degeneration, corresponding to the effect of the genetic mutations on cGMP accumulation and—as deduced from this—PDE6 function.

Remarkably, there is a clear discrepancy between the extent of cGMP accumulation observed in *Pde6b* mutant *rd1* photoreceptors and *Pde6a* V685M photoreceptors. Even though the speed of photoreceptor loss is comparable in both RP models, and both PDE6 protein isoforms have been suggested to be enzymatically equivalent (40), in *rd1* retina 6–15% of photoreceptors show dramatic cGMP accumulation (6) compared with only 0.6% in V685M retina. The extent of *rd1* cGMP accumulation might be explained by a complete loss of PDE6 expression caused by the *rd1* mutation. In the V685M mutant a minor amount of residual PDE6 activity could prevent such a dramatic accumulation of cGMP; however, even a more moderate elevation of cGMP (undetectable by immunohistochemistry) would still result in rapid photoreceptor degeneration.

The phenotype of the novel R562W mutant is intermediate between that of the V685M and the D670G mutant. Unexpectedly, we found that the pathogenic effect of this underlying c.1684C>T substitution is twofold and at distinct levels: pre-mRNA splicing and protein enzymatic activity. The C>T transition (+64 of exon 13) is predicted to create an ESS site (–TGGTGG–) which results in an in-frame skipping of exon 13. The splicing defect induced by the mutation is only partially penetrant and therefore correctly spliced transcripts derived from the mutant allele, which accounts for ~50–60% of transcripts (Fig. 2B), will be translated into a full-length protein carrying the R562W substitution. This R562W mutant protein exhibits a reduction of its catalytic activity to ~10% compared with the WT protein. The shortened p.541_576del protein derived from *Pde6a* transcripts devoid of exon 13, lacks a strongly conserved segment of the protein's catalytic domain, including one of the two metal ion binding motifs which are important for functional activity (Supplementary Material, Fig. S5) (41). Therefore, we reason that the shortened protein may essentially be non-functional or with very strongly reduced activity. Moreover, protein stability of such shortened proteins is often reduced as also documented for other mouse models for retinal dystrophies (42). The findings with the R562W mutant complements prior reports of splicing defects in retinal PDE6 genes caused by single nucleotide exonic mutations such as the c.1814G>A/p.N605S in *Pde6b* in the *atrd3* mouse model (43) or the c.2368G>A/p.E790 K in the human *PDE6C* in a family with achromatopsia (44). It also emphasizes the need for a thorough transcript analysis of the mutant gene for a proper assessment of its consequences.

Typical for RP, the loss of the primarily affected rod photoreceptors was followed by a secondary loss of cone photoreceptors via a well-known but still aetiologically unresolved mechanism (45). Differences in rod loss among the mutants thus corresponded well to the functional data in Ganzfeld ERG at PN30,

although these essentially represent cone function. In particular, ERG amplitudes in the D670G mutants were similar to Rho$^{-/-}$ animals (30), while no more responses were left in V685M mutants. The results in the other lines were in between these extreme values. This correlation allows to provide an estimate of the minimal number of rod photoreceptors that still need to be physically present (i.e. surviving) in order to maintain residual cone photoreceptor function at a recordable level. In our setting, at least one intact row of rod photoreceptors was required in order to still preserve cone ERG at P30.

V685m/R562W: a new patient-matched, compound heterozygous animal model for RP

Current research on the mechanisms underlying recessive RP usually employs homozygous animal models, such as the *Pde6b*$^{rd1/rd1}$ mouse (11,46). In RP patients, in outbred populations, homozygosity is, however, less common than compound heterozygous mutations with two different disease-causing alleles (47,48). This creates incongruence between the currently used animal models for RP and the actual patient situation, in particular because the pathological consequences of compound heterozygous versus homozygous mutations are to date only poorly understood.

According to Muller (49), the action of recessive mutations may be explained be either constituting an amorph (classical *null* mutation) or a hypomorphic mutation, the latter being associated with lower amounts of the gene product or reduced function or activity. If the amounts of the gene product or its activity is strictly additive and proportional to the phenotypic outcome, then one would expect for compound heterozygous mutations an intermediate disease phenotype, which lies between the two respective homozygous disease phenotypes. However, this must not be necessarily true, for instance in traits that develop in a threshold-dependent manner. Moreover, one needs to consider situations of intra-allelic complementation in which different mutations in the same gene may 'neutralize' each other, a phenomenon most likely to occur in proteins that act as oligomers (50). Thus, comparative studies between homozygotes and compound heterozygotes bear important insights into the mode of action of individual mutations, potential interactions between different mutant proteins, and the correlation of the disease phenotype with the amount and functional activity of the mutant gene product.

Our results with the V685M/R562W retinal degeneration suggest that for the *Pde6a* gene a classic additive model for the interaction of the two mutations is valid, resulting in a proportional relationship between the amount or the functional activity of the mutant gene product and the phenotypic outcome. If generalized, this model enables to predict the outcome of an unknown genotype in terms of severity and disease progression if the phenotype of two adjoined genotypes in *Pde6a* is known. Our findings also demonstrate that a genotype–phenotype correlation with high predictability exists for *Pde6a*-associated retinal degeneration at least in murine mutants raised on the same genetic background. Therefore, the lack of consistent genotype–phenotype correlation sometimes observed in human RP patients is most likely due to secondary genetic factors and/or differences in lifestyle (51,52).

Nevertheless, our study provides a rational basis for predictions on human RP phenotypes and disease progression in compound heterozygous situations, provided the pathological consequences of at least one of the disease-causing alleles are known. This knowledge could be very valuable for patient counselling and also—if suitable therapeutic approaches become available in the future—for the determination of the best possible time-frame for therapeutic interventions.

The large genetic diversity in RP causing mutations—even if affecting the same gene—may cause very different degeneration phenotypes. Our detailed characterization of different homozygous and compound heterozygous mouse models for RP will provide a basis for further investigations, in particular on the development of future individualized therapies. The wide availability of a large variety of animal models will likely facilitate the generation of 'personalized' compound heterozygous animal models that match the human disease condition very closely. Such models could greatly speed up the development of a more personalized medicine in the field of retinal degenerations. For the individual RP patient, the prediction of time-courses for *Pde6a*-related retinal degeneration is currently of particular value. Upon availability of causative or symptomatic treatment options, the definition of a window-of-opportunity for clinical interventions will gain further importance.

Supplementary Material

Supplementary Material is available at *HMG* online.

Acknowledgements

We thank K. Masarini, N. Rieger and Britta Baumann for skilful technical assistance. We thank Dr Muayyad Al-Ubaidi (University of Oklahoma, Oklahoma City, USA) for kindly providing the 661W cell line.

Conflict of Interest statement. None declared.

Funding

This work was supported by the Kerstan Foundation (RD-CURE), the 2nd People's Hospital Of Yunnan Province and 4th Affiliated Hospital Of Kunming Medical University/China, Deutsche Forschungsgemeinschaft [DFG PA1751/4-1;7-1], Alcon Research Institute, and the European Commission [DRUGSFORD: HEALTH-F2-2012-304963; EyeTN: FP7-People-2012-ITN-317472].

References

1. Chizzolini, M., Galan, A., Milan, E., Sebastiani, A., Costagliola, C. and Parmeggiani, F. (2011) Good epidemiologic practice in retinitis pigmentosa: from phenotyping to biobanking. *Curr. Genomics*, **12**, 260–266.
2. Arango-Gonzalez, B., Trifunovic, D., Sahaboglu, A., Kranz, K., Michalakis, S., Farinelli, P., Koch, S., Koch, F., Cottet, S., Janssen Bienhold, U. *et al.* (2014) Identification of a common non-apoptotic cell death mechanism in hereditary retinal degeneration. *PLoS One*, **9**, e112142.
3. Olshevskaya, E.V., Ermilov, A.N. and Dizhoor, A.M. (2002) Factors that affect regulation of cGMP synthesis in vertebrate photoreceptors and their genetic link to human retinal degeneration. *Mol. Cell Biochem.*, **230**, 139–147.
4. Michalakis, S., Geiger, H., Haverkamp, S., Hofmann, F., Gerstner, A. and Biel, M. (2005) Impaired opsin targeting and cone photoreceptor migration in the retina of mice lacking the cyclic nucleotide-gated channel CNGA3. *Invest Ophthalmol. Vis. Sci.*, **46**, 1516–1524.
5. Farber, D.B. and Lolley, R.N. (1974) Cyclic guanosine monophosphate: elevation in degenerating photoreceptor cells of the C3H mouse retina. *Science*, **186**, 449–451.

6. Sahaboglu, A., Paquet-Durand, O., Dietter, J., Dengler, K., Bernhard-Kurz, S., Ekström, P., Hitzmann, B., Ueffing, M. and Paquet-Durand, F. (2013) Retinitis pigmentosa: rapid neurodegeneration is governed by slow cell death mechanisms. *Cell Death Dis.*, **4**, e488.
7. Hamel, C. (2006) Retinitis pigmentosa. *Orphanet. J Rare Dis.*, **1**, 40.
8. Bayes, M., Giordano, M., Balcells, S., Grinberg, D., Vilageliu, L., Martinez, I., Ayuso, C., Benitez, J., Ramos-Arroyo, M.A. and Chivelet, P., (1995) Homozygous tandem duplication within the gene encoding the beta-subunit of rod phosphodiesterase as a cause for autosomal recessive retinitis pigmentosa. *Hum. Mutat.*, **5**, 228–234.
9. Dryja, T.P., Rucinski, D.E., Chen, S.H. and Berson, E.L. (1999) Frequency of mutations in the gene encoding the alpha subunit of rod cGMP-phosphodiesterase in autosomal recessive retinitis pigmentosa. *Invest. Ophthalmol. Vis. Sci.*, **40**, 1859–1865.
10. Dvir, L., Srour, G., Abu-Ras, R., Miller, B., Shalev, S.A. and Ben-Yosef, T. (2010) Autosomal-recessive early-onset retinitis pigmentosa caused by a mutation in PDE6G, the gene encoding the gamma subunit of rod cGMP phosphodiesterase. *Am J Hum Genet.*, **87**, 258–264.
11. Keeler, C.E. (1924) The inheritance of a retinal abnormality in white mice. *Proc. Natl. Acad. Sci. U. S. A.*, **10**, 329–333.
12. Chang, B., Hawes, N.L., Hurd, R.E., Davisson, M.T., Nusinowitz, S. and Heckenlively, J.R. (2002) Retinal degeneration mutants in the mouse. *Vis. Res.*, **42**, 517–525.
13. Sakamoto, K., McCluskey, M., Wensel, T.G., Naggert, J.K. and Nishina, P.M. (2009) New mouse models for recessive retinitis pigmentosa caused by mutations in the Pde6a gene. *Hum. Mol. Genet.*, **18**, 178–192.
14. Mattapallil, M.J., Wawrousek, E.F., Chan, C.C., Zhao, H., Roychoudhury, J., Ferguson, T.A. and Caspi, R.R. (2012) The Rd8 mutation of the Crb1 gene is present in vendor lines of C57BL/6N mice and embryonic stem cells, and confounds ocular induced mutant phenotypes. *Invest. Ophthalmol. Vis. Sci.*, **53**, 2921–2927.
15. Grau, T., Artemyev, N.O., Rosenberg, T., Dollfus, H., Haugen, O.H., Cumhur, S.E., Jurklies, B., Andreasson, S., Kernstock, C., Larsen, M. *et al.* (2011) Decreased catalytic activity and altered activation properties of PDE6C mutants associated with autosomal recessive achromatopsia. *Hum. Mol. Genet.*, **20**, 719–730.
16. Muradov, K.G., Boyd, K.K., Martinez, S.E., Beavo, J.A. and Artemyev, N.O. (2003) The GAFa domains of rod cGMP-phosphodiesterase 6 determine the selectivity of the enzyme dimerization. *J. Biol. Chem.*, **278**, 10594–10601.
17. Natochin, M. and Artemyev, N.O. (2000) Mutational analysis of functional interfaces of transducin. *Methods Enzymol.*, **315**, 539–554.
18. Ekstrom, P.A., Ueffing, M., Zrenner, E. and Paquet-Durand, F. (2014) Novel in situ activity assays for the quantitative molecular analysis of neurodegenerative processes in the retina. *Curr. Med. Chem.*, **21**, 3478–3493.
19. Paquet-Durand, F., Silva, J., Talukdar, T., Johnson, L.E., Azadi, S., van Veen, T., Ueffing, M., Hauck, S.M. and Ekstrom, P.A. (2007) Excessive activation of poly(ADP-ribose) polymerase contributes to inherited photoreceptor degeneration in the retinal degeneration 1 mouse. *J. Neurosci.*, **27**, 10311–10319.
20. Tanimoto, N., Muehlfriedel, R.L., Fischer, M.D., Fahl, E., Humphries, P., Biel, M. and Seeliger, M.W. (2009) Vision tests in the mouse: functional phenotyping with electroretinography. *Front. Biosci.*, **14**, 2730–2737.
21. Fischer, M.D., Huber, G., Beck, S.C., Tanimoto, N., Muehlfriedel, R., Fahl, E., Grimm, C., Wenzel, A., Reme, C.E., van de Pavert, S.A. *et al.* (2009) Noninvasive, in vivo assessment of mouse retinal structure using optical coherence tomography. *PLoS One*, **4**, e7507.
22. Huber, G., Beck, S.C., Grimm, C., Sahaboglu-Tekgoz, A., Paquet-Durand, F., Wenzel, A., Humphries, P., Redmond, T.M., Seeliger, M.W. and Fischer, M.D. (2009) Spectral domain optical coherence tomography in mouse models of retinal degeneration. *Invest. Ophthalmol. Vis. Sci.*, **50**, 5888–5895.
23. Garcia, G.M., Beck, S.C., Muhlfriedel, R., Julien, S., Schraermeyer, U. and Seeliger, M.W. (2014) Towards a quantitative OCT image analysis. *PLoS One*, **9**, e100080.
24. Seeliger, M.W., Beck, S.C., Pereyra-Munoz, N., Dangel, S., Tsai, J.Y., Luhmann, U.F., van de Pavert, S.A., Wijnholds, J., Samardzija, M., Wenzel, A. *et al.* (2005) In vivo confocal imaging of the retina in animal models using scanning laser ophthalmoscopy. *Vis. Res.*, **45**, 3512–3519.
25. Chang, G.Q., Hao, Y. and Wong, F. (1993) Apoptosis: final common pathway of photoreceptor death in rd, rds, and rhodopsin mutant mice. *Neuron*, **11**, 595–605.
26. Sanges, D., Comitato, A., Tammaro, R. and Marigo, V. (2006) Apoptosis in retinal degeneration involves cross-talk between apoptosis-inducing factor (AIF) and caspase-12 and is blocked by calpain inhibitors. *Proc. Natl. Acad. Sci. U.S.A.*, **103**, 17366–17371.
27. Zeiss, C.J., Neal, J. and Johnson, E.A. (2004) Caspase-3 in postnatal retinal development and degeneration. *Invest. Ophthalmol. Vis. Sci.*, **45**, 964–970.
28. Paquet-Durand, F., Beck, S., Michalakis, S., Goldmann, T., Huber, G., Muhlfriedel, R., Trifunovic, D., Fischer, M.D., Fahl, E., Duetsch, G. *et al.* (2011) A key role for cyclic nucleotide gated (CNG) channels in cGMP-related retinitis pigmentosa. *Hum. Mol. Genet.*, **20**, 941–947.
29. Young, R.W. (1984) Cell death during differentiation of the retina in the mouse. *J. Comp Neurol.*, **229**, 362–373.
30. Jaissle, G.B., May, C.A., Reinhard, J., Kohler, K., Fauser, S., Lutjen-Drecoll, E., Zrenner, E. and Seeliger, M.W. (2001) Evaluation of the rhodopsin knockout mouse as a model of pure cone function. *Invest. Ophthalmol. Vis. Sci.*, **42**, 506–513.
31. Samardzija, M., Tanimoto, N., Kostic, C., Beck, S., Oberhauser, V., Joly, S., Thiersch, M., Fahl, E., Arsenijevic, Y., von Lintig, J. *et al.* (2009) In conditions of limited chromophore supply rods entrap 11-cis-retinal leading to loss of cone function and cell death. *Hum. Mol. Genet.*, **18**, 1266–1275.
32. Price, B.A., Sandoval, I.M., Chan, F., Simons, D.L., Wu, S.M., Wensel, T.G. and Wilson, J.H. (2011) Mislocalization and degradation of human P23H-rhodopsin-GFP in a knockin mouse model of retinitis pigmentosa. *Invest. Ophthalmol. Vis. Sci.*, **52**, 9728–9736.
33. Stuck, M.W., Conley, S.M. and Naash, M.I. (2014) The Y141C knockin mutation in RDS leads to complex phenotypes in the mouse. *Hum. Mol. Genet.*, **23**, 6260–6274.
34. Rybalkin, S.D., Hinds, T.R. and Beavo, J.A. (2013) Enzyme assays for cGMP hydrolyzing phosphodiesterases. *Methods Mol. Biol.*, **1020**, 51–62.
35. Bowes, C., Li, T., Danciger, M., Baxter, L.C., Applebury, M.L. and Farber, D.B. (1990) Retinal degeneration in the rd mouse is caused by a defect in the beta subunit of rod cGMP-phosphodiesterase. *Nature*, **347**, 677–680.
36. Fox, D.A., Poblenz, A.T. and He, L. (1999) Calcium overload triggers rod photoreceptor apoptotic cell death in chemical-induced and inherited retinal degenerations. *Ann. N.Y. Acad. Sci.*, **893**, 282–285.

37. Yamashima, T. (2004) Ca2+-dependent proteases in ischemic neuronal death: a conserved 'calpain-cathepsin cascade' from nematodes to primates. *Cell Calcium*, **36**, 285–293.
38. Paquet-Durand, F., Azadi, S., Hauck, S.M., Ueffing, M., van Veen, T. and Ekstrom, P. (2006) Calpain is activated in degenerating photoreceptors in the rd1 mouse. *J. Neurochem.*, **96**, 802–814.
39. Nakajima, E., Hammond, K.B., Rosales, J.L., Shearer, T.R. and Azuma, M. (2011) Calpain, not caspase, is the causative protease for hypoxic damage in cultured monkey retinal cells. *Invest. Ophthalmol. Vis. Sci.*, **52**, 7059–7067.
40. Muradov, H., Boyd, K.K. and Artemyev, N.O. (2010) Rod phosphodiesterase-6 PDE6A and PDE6B subunits are enzymatically equivalent. *J. Biol. Chem.*, **285**, 39828–39834.
41. He, F., Seryshev, A.B., Cowan, C.W. and Wensel, T.G. (2000) Multiple zinc binding sites in retinal rod cGMP phosphodiesterase, PDE6alpha beta. *J Biol. Chem.*, **275**, 20572–20577.
42. Chang, B., Khanna, H., Hawes, N., Jimeno, D., He, S., Lillo, C., Parapuram, S.K., Cheng, H., Scott, A., Hurd, R.E. *et al.* (2006) In-frame deletion in a novel centrosomal/ciliary protein CEP290/NPHP6 perturbs its interaction with RPGR and results in early-onset retinal degeneration in the rd16 mouse. *Hum. Mol. Genet.*, **15**, 1847–1857.
43. Muradov, H., Boyd, K.K., Kerov, V. and Artemyev, N.O. (2012) Atypical retinal degeneration 3 in mice is caused by defective PDE6B pre-mRNA splicing. *Vis. Res.*, **57**, 1–8.
44. Chang, B., Grau, T., Dangel, S., Hurd, R., Jurklies, B., Sener, E.C., Andreasson, S., Dollfus, H., Baumann, B., Bolz, S. *et al.* (2009) A homologous genetic basis of the murine cpfl1 mutant and human achromatopsia linked to mutations in the PDE6C gene. *Proc. Natl. Acad. Sci. U. S. A*, **106**, 19581–19586.
45. Kranz, K., Paquet-Durand, F., Weiler, R., Janssen-Bienhold, U. and Dedek, K. (2013) Testing for a gap junction-mediated bystander effect in retinitis pigmentosa: secondary cone death is not altered by deletion of connexin36 from cones. *PLoS One*, **8**, e57163.
46. Dalke, C. and Graw, J. (2005) Mouse mutants as models for congenital retinal disorders. *Exp. Eye Res.*, **81**, 503–512.
47. Glockle, N., Kohl, S., Mohr, J., Scheurenbrand, T., Sprecher, A., Weisschuh, N., Bernd, A., Rudolph, G., Schubach, M., Poloschek, C. *et al.* (2014) Panel-based next generation sequencing as a reliable and efficient technique to detect mutations in unselected patients with retinal dystrophies. *Eur. J. Hum. Genet.*, **22**, 99–104.
48. Huang, X.F., Huang, F., Wu, K.C., Wu, J., Chen, J., Pang, C.P., Lu, F., Qu, J. and Jin, Z.B. (2015) Genotype-phenotype correlation and mutation spectrum in a large cohort of patients with inherited retinal dystrophy revealed by next-generation sequencing. *Genet. Med.*, **17**, 271–278.
49. Muller, H. (1932) Further studies on the nature and causes of gene mutations. Proceedings of the 6th International Congress of Genetics, 213–255.
50. Fincham, J.R.S. (1977) Allelic complementation reconsidered. *Carlsberg Res. Commun.*, **42**, 421–430.
51. Berghmans, L.V., de Mendonca, R.H., Coppieters, F., de Oliveira, M.O. Jr, Takahashi, W.Y., Lissens, W., De, B.E. and Leroy, B.P. (2011) Discordance for retinitis pigmentosa in two monozygotic twin pairs. *Retina*, **31**, 1164–1169.
52. Walia, S., Fishman, G.A., Swaroop, A., Branham, K.E., Lindeman, M., Othman, M. and Weleber, R.G. (2008) Discordant phenotypes in fraternal twins having an identical mutation in exon ORF15 of the RPGR gene. *Arch. Ophthalmol.*, **126**, 379–384.

V. Appendix

Paper II: Gene therapy restores vision and delays degeneration in the CNGB1(-/-) mouse model of retinitis pigmentosa

Koch S, **Sothilingam V**, Garcia Garrido M, Tanimoto N, Becirovic E, Koch F, Seide C, Beck SC, Seeliger MW, Biel M, Mühlfriedel R[§], Michalakis S[§]

Published in Human Molecular Genetics
21:4486-4496 (2012)

Human Molecular Genetics, 2012, Vol. 21, No. 20 **4486–4496**
doi:10.1093/hmg/dds290
Advance Access published on July 16, 2012

Gene therapy restores vision and delays degeneration in the CNGB1$^{-/-}$ mouse model of retinitis pigmentosa

Susanne Koch[1], Vithiyanjali Sothilingam[2], Marina Garcia Garrido[2], Naoyuki Tanimoto[2], Elvir Becirovic[1], Fred Koch[1], Christina Seide[2], Susanne C. Beck[2], Mathias W. Seeliger[2], Martin Biel[1], Regine Mühlfriedel[2,*] and Stylianos Michalakis[1,*]

[1]Center for Integrated Protein Science Munich (CIPSM), Department of Pharmacy – Center for Drug Research, Ludwig-Maximilians-Universität München, Butenandtstr. 5-13, 81377 Munich, Germany and [2]Division of Ocular Neurodegeneration, Institute for Ophthalmic Research, Centre for Ophthalmology, University of Tübingen, Schleichstr. 4/3, 72076 Tübingen, Germany

Received May 29, 2012; Revised July 9, 2012; Accepted July 11, 2012

Retinitis pigmentosa (RP) is a group of genetically heterogeneous, severe retinal diseases commonly leading to legal blindness. Mutations in the CNGB1a subunit of the rod cyclic nucleotide-gated (CNG) channel have been found to cause RP in patients. Here, we demonstrate the efficacy of gene therapy as a potential treatment for RP by means of recombinant adeno-associated viral (AAV) vectors in the CNGB1 knockout (CNGB1$^{-/-}$) mouse model. To enable efficient packaging and rod-specific expression of the relatively large CNGB1a cDNA (~4 kb), we used an AAV expression cassette with a short rod-specific promoter and short regulatory elements. After injection of therapeutic AAVs into the subretinal space of 2-week-old CNGB1$^{-/-}$ mice, we assessed the restoration of the visual system by analyzing (i) CNG channel expression and localization, (ii) retinal function and morphology and (iii) vision-guided behavior. We found that the treatment not only led to expression of full-length CNGB1a, but also restored normal levels of the previously degraded CNGA1 subunit of the rod CNG channel. Both proteins co-localized in rod outer segments and formed regular CNG channel complexes within the treated area of the CNGB1$^{-/-}$ retina, leading to significant morphological preservation and a delay of retinal degeneration. In the electroretinographic analysis, we also observed restoration of rod-driven light responses. Finally, treated CNGB1$^{-/-}$ mice performed significantly better than untreated mice in a rod-dependent vision-guided behavior test. In summary, this work provides a proof-of-concept for the treatment of rod channelopathy-associated RP by AAV-mediated gene replacement.

INTRODUCTION

Retinitis pigmentosa (RP) is a family of hereditary eye disorders characterized by progressive retinal degeneration (1,2). RP primarily affects rod photoreceptors, but secondary to rods, cone photoreceptors also degenerate. Owing to the lack of rod functionality, patients suffer from night blindness at disease onset. Once cones are affected, the visual field becomes more and more constricted ('tunnel vision') and, finally, central vision is also impaired, leading eventually to complete blindness. Accordingly, clinical key symptoms of RP are night blindness, constricted visual fields, decreased visual acuity and color vision and enhanced glare sensitivity. The typical fundus picture includes dark pigmentary clumps ('bone spicules') and attenuated retinal vessels as well as retinal-pigment epithelium (RPE) atrophy. RP is genetically very heterogeneous and currently >50 RP genes are known. Many of the RP genes are preferentially or even exclusively expressed in rod photoreceptors (1). Only a minor fraction of the RP genes are specific for other retinal cell types, e.g. RPE cells. Early success of gene replacement therapy for

*To whom correspondence should be addressed. Tel: +49-7071-29-87784; Fax: +49-7071-29-4503; Email: regine.muehlfriedel@med.uni-tuebingen.de (R. Mühlfriedel); Tel: +49-89-2180-77325; Fax: +49-89-2180-77326; Email: michalakis@lmu.de (S. Michalakis).

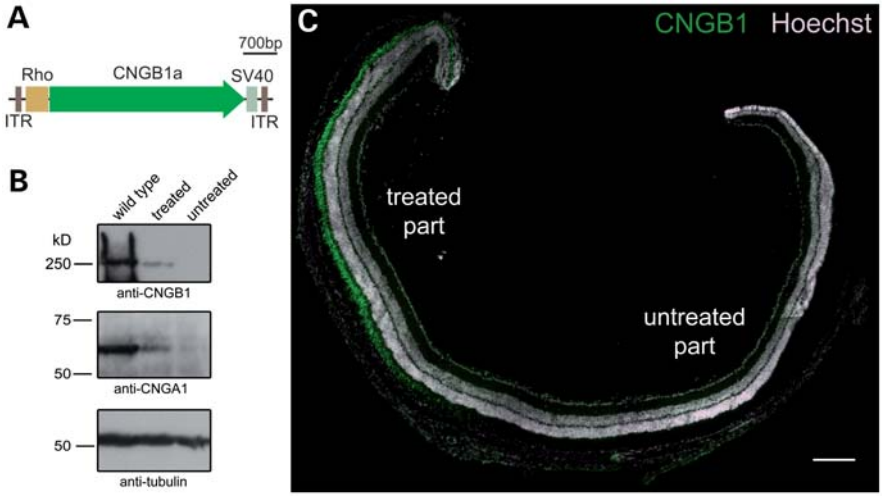

Figure 1. Subretinal delivery of CNGB1a using an optimized AAV vector results in the expression of full-length CNGB1a in photoreceptors. (**A**) Schematic representation of the Rho-CNGB1a AAV vector. The expression cassette within the two inverted terminal repeats (ITRs) includes a 471 bp mouse rhodopsin promoter fragment (Rho), the 3978 bp mouse CNGB1a cDNA and a 221 bp long SV40 polyA sequence. (**B**) Western blot analysis of retinal lysates from wild-type, treated and untreated CNGB1-deficient mice using an antibody against the C-terminus of CNGB1 demonstrates the expression of the CNGB1a (upper panel) and up-regulation of CNGA1 (middle panel) in treated CNGB1$^{-/-}$ mice. (**C**) Overview image showing expression and outer segment localization of CNGB1a in the treated part of a CNGB1$^{-/-}$ retina at 40 days after injection. The retinal slice was immunolabeled with an antibody directed against the C-terminus of CNGB1 (CNGB1, green). The cell nuclei were stained with the nuclear dye Hoechst 33342 (grey). Scale bar in (C) marks 200 μm.

RPE-specific mutations resulted in a number of clinical trials with promising results (3). However, as many of the disease-causing mutations concern (rod) photoreceptor-expressed genes, there is a need to develop treatments for photoreceptor-specific RP genes (1).

Mutations in the genes encoding the two rod cyclic nucleotide-gated (CNG) channel subunits cause autosomal recessive RP (arRP) (4). CNG channels are found in the plasma membrane of rod and cone photoreceptors and translate light-mediated concentration changes of the second messenger cyclic guanosine monophosphate (cGMP) into voltage and calcium signals (4). The rod CNG channel is a heterotetramer comprised of three CNGA1 subunits and one CNGB1 subunit (5). Mutations in CNGB1 (RP45 locus) are found in ~4% of arRP cases (1). Knockout of CNGB1 in mice results in a phenotype that recapitulates the principal pathology of RP patients. In particular, CNGB1 knockout mice lack rod photoreceptor function (6,7). This functional defect is accompanied by a progressive degeneration of rods, and, secondary to this, a degeneration of the cones (6,7). The degeneration progresses rather slow and results in loss of 10–20% of rods at 4 months, 30–50% at 6 months and 80–90% at 1 year of age. Finally, the loss of CNGB1a induces down-regulation of several proteins of the phototransduction cascade and degradation of the CNGA1 subunit (6,7). In the present study, we used CNGB1 knockout mice as a model for RP to evaluate adeno-associated virus (AAV)-mediated gene therapy as a potential treatment of RP caused by rod photoreceptor-specific gene mutations. We show here that our gene replacement approach was able to restore rod CNG channel expression and localization, to improve retinal function and vision-guided behavior and to delay retinal degeneration in CNGB1$^{-/-}$ mice.

RESULTS

Design and subretinal delivery of a gene therapy vector for rod-specific expression of CNGB1a

The relatively small packaging capacity (~5.2 kb) of AAV vectors (8–10) limits their use for the expression of large transgenes such as CNGB1a. Because of the large size of the CNGB1a cDNA (3978 bp), there is only limited space left for *cis*- and *trans*-regulatory elements. To achieve high expression rates at the smallest possible vector genome size, we decided to use only a single 221 bp long SV40 polyA sequence (see Materials and Methods) in combination with a 471 bp mouse rhodopsin promoter (−386 to +86) (11). This vector allowed the incorporation of the full-length CNGB1a cDNA without violating the 5.2 kb packaging limit of AAVs (8–10). We then packaged this construct (Fig. 1A) into viral vector particles with Y733F-modified AAV8 capsid (12) and injected ~10^{11} AAV genomic particles into the subretinal space of 2-week-old CNGB1$^{-/-}$ mice. The retinal site of treatment was monitored *in vivo* directly upon completion of the injection procedure and at subsequent time points using confocal scanning laser ophthalmoscopy (cSLO) (13) and optical coherence tomography (OCT) (14).

Restoration of CNG channel expression in rod outer segments of CNGB1$^{-/-}$ mice

We next analyzed the expression of CNGB1a in the retina of treated CNGB1$^{-/-}$ mice. In a western blot analysis, we confirmed that subretinal delivery of our AAV vector led to expression of the full-length CNGB1a protein migrating at the expected size of ~250 kDa (Fig. 1B, upper panel). In addition, the 63 kDa CNGA1 subunit that is completely degraded in

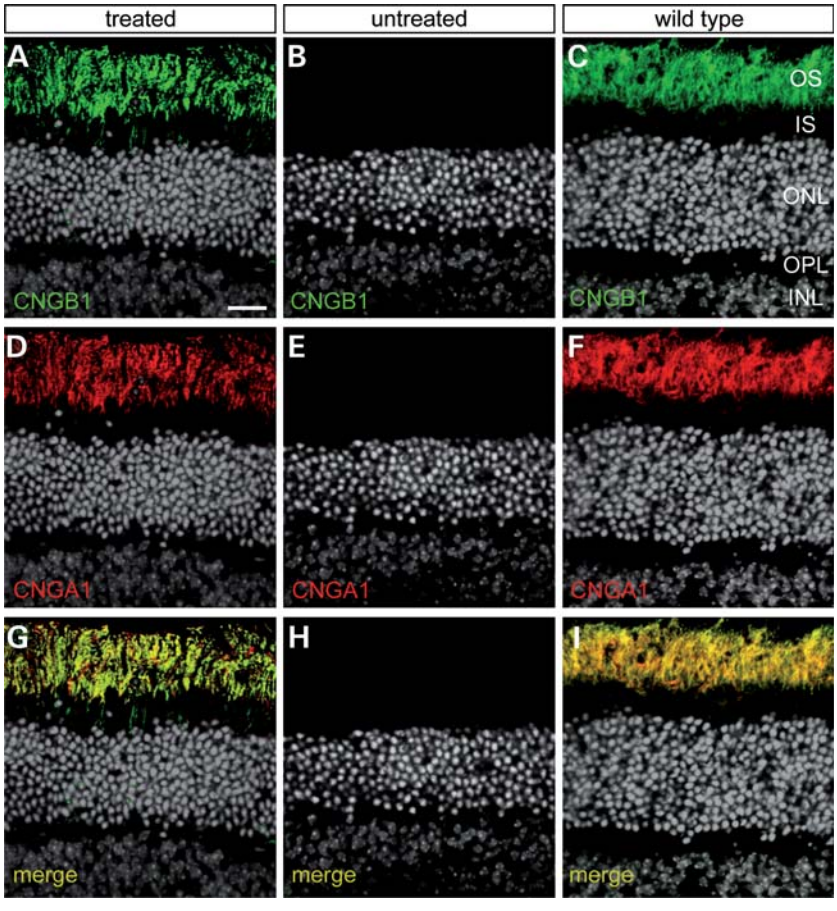

Figure 2. Analysis of CNG channel expression in the treated and untreated CNGB1$^{-/-}$ retina. Confocal scans from retinal slices immunolabeled with antibodies specific for CNGB1a (green) and CNGA1 (red). The treatment results in the expression of CNGB1a in rod outer segments of treated mice (**A**), which is absent in the untreated knockout retina (**B**). The CNGB1a expression levels in the treated knockout are comparable to wild-type (**C**). Viral CNGB1a expression also rescues the expression of CNGA1 in rod outer segments (**D**), which is down-regulated in the untreated knockout retina (**E**). Again, the levels of expression are comparable to wild-type (**F**). (**G**–**I**) Merged images of CNGA1 and CNGB1a signals (yellow). Both proteins co-localized in the outer segments from treated (G) and wild-type mice (I). Cell nuclei were stained with the nuclear dye Hoechst 33342 (grey) in all panels. INL, inner nuclear layer; IS, photoreceptor inner segments; ONL, outer nuclear layer; OPL, outer plexiform layer; OS, photoreceptor outer segments. The scale bar marks 20 μm.

CNGB1$^{-/-}$ mice was readily detectable in the injected retina (Fig. 1B, middle panel). Using immunohistochemistry, we detected virally encoded CNGB1a protein in the treated, but not the untreated part of the retina. Figure 1C shows a representative overview image of a CNGB1$^{-/-}$ retinal slice 40 days after treatment immunolabeled for CNGB1a. The treated area with high levels of CNGB1a expression corresponded to approximately one-third of the retina. The CNGB1a protein localized almost exclusively to rod outer segments, suggesting that transport mechanisms required for proper outer segment targeting of the channel are preserved in the treated knockout (Fig. 1C). Figure 2 shows high-resolution confocal scans from the treated (A, D and G) and untreated regions (B, E and H) of a CNGB1$^{-/-}$ retina as well as from wild-type control retina (C, F and I). Importantly, viral treatment not only restored expression of CNGB1a (Fig. 2A), but also restored levels of the previously missing endogenous CNGA1 protein (Fig. 2D), which now co-localized with CNGB1a in rod outer segments within the treated area (Fig. 2G). This suggests that AAV-mediated delivery of CNGB1a restored the expression of wild-type-like heterotetrameric CNG channels in rod outer segments of treated mice. Moreover, comparison with wild-type mice showed that the treatment led to almost wild-type levels of expression of CNGB1 and CNGA1 in treated CNGB1$^{-/-}$ mice (Fig. 2A, C, D and F). An improvement of photoreceptor outer segment morphology in the treated CNGB1$^{-/-}$ retina could also be detected *in vivo* using OCT (Fig. 3A and B). The typical outer retinal appearance in OCT with horizontal bands associated with the outer limiting membrane and the border between inner and outer segments (14,15) (arrow in Fig. 3A) was preserved in the treated eye (TE), but not in the untreated eye (UE). We also performed confocal microscopy on histological retinal sections labeled with the photoreceptor outer segment marker peripherin-2 to analyze the outer segment morphology in more detail (Fig. 3C and D). The labeling pattern and intensity of the anti-peripherin-2 antibody in the treated CNGB1$^{-/-}$ retina were comparable to the staining in the untreated. However, the length of the peripherin-2-positive outer segments was markedly increased in the treated (Fig. 3C) compared with the untreated (Fig. 3D) part of the CNGB1$^{-/-}$ retina.

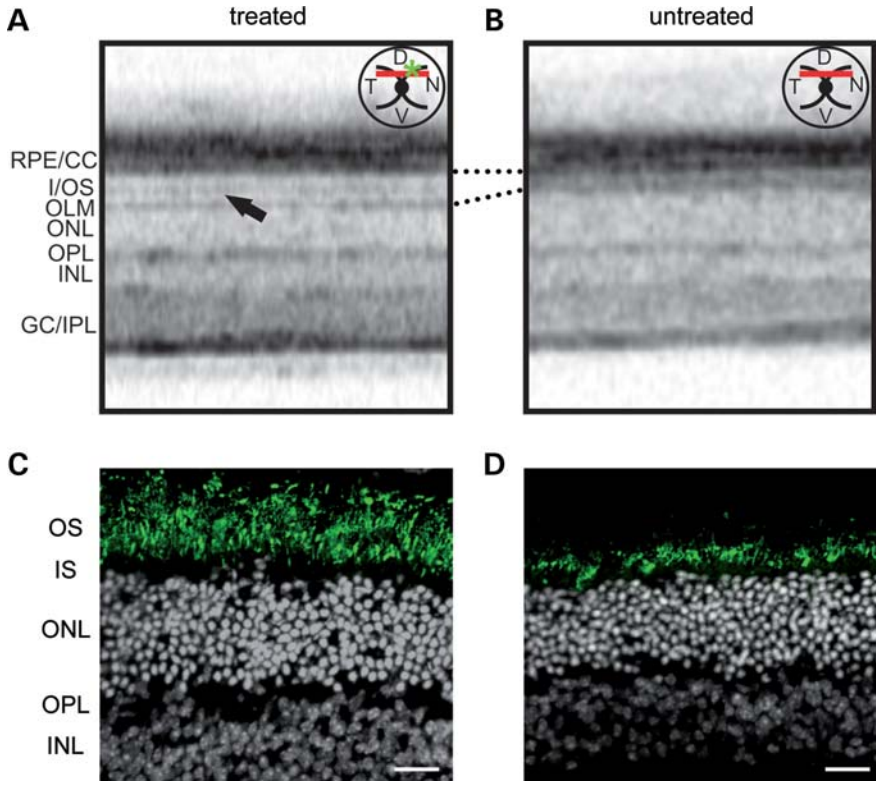

Figure 3. Effect of gene therapy on outer retinal morphology in *CNGB1*$^{-/-}$ mice. (**A**, **B**) Comparison of OCT data from TEs and UEs of the same representative CNGB1$^{-/-}$ mouse 2 months after injection. A schematic drawing of the mouse retina with the position of the injection site (green asterisk) and/or the OCT scan (red line) is shown in (A) and (B). D, dorsal; N, nasal; T, temporal; V, ventral. The typical outer retinal appearance in OCT with horizontal bands associated with the OLM and IS/OS border (marked with an arrow) was preserved in the TE (A), but not in the UE (B). The dotted lines between (A) and (B) mark the position of the lower margin of the RPE/choriocapillaris (CC) layer and the outer limiting membrane (OLM) in the treated (A) and untreated (B) retinas. The space between these two layers is markedly increased in the treated retina, indicating a distinct rescue of rod outer segment organization. (**C**, **D**) Confocal images from the treated (C) and untreated (D) CNGB1$^{-/-}$ retina immunostained with anti-peripherin-2 antibody (green) at 40 days after treatment. The outer segment length is increased in the treated (C) compared with the untreated (D) part. Cell nuclei were stained with the nuclear dye Hoechst 33342 (grey) in (C) and (D). GC/IPL, ganglion cell layer/inner plexiform layer; INL, inner nuclear layer; IS, photoreceptor inner segments; OPL, outer plexiform layer; ONL, outer nuclear layer; I/OS, inner/outer segment border; OS, photoreceptor outer segments. The scale bar in (C and D) marks 20 μm.

Restoration of rod photoreceptor function in treated CNGB1$^{-/-}$ mice

As expected, non-injected eyes (UEs) of 8-week-old CNGB1$^{-/-}$ mice did not show the usual responses to dim light stimuli in dark-adapted (scotopic) Ganzfeld electroretinography (ERG), reflecting a lack of regular rod system activity (Fig. 4A, middle panel). In contrast, distinct responses were present in eyes of CNGB1$^{-/-}$ mice that had received injections of CNGB1a AAV vector (TEs) (Fig. 4A, left panel and overlay in Fig. 4A, right panel). Figure 4B shows a statistical analysis of the ERG b-wave amplitude (which reflects mainly the activity of bipolar cells) for six TEs and UEs. It is again obvious that, in contrast to the controls, treated mice show substantial b-wave amplitudes, particularly at low light intensities (-4.0 to -2.0 log cd*s/m^2) where responses are entirely rod-driven.

For completeness, it should be mentioned that in a few cases, very small, irregular rod responses were present in CNGB1$^{-/-}$ mice as previously described (5), which are attributed to homomeric CNGA1 channels that have escaped degradation. This fact is, however, mainly of theoretical interest as these contributions were too small to have any perceivable impact on the results shown.

To further probe whether the responses of the rod to repetitive stimuli were also restored, a scotopic flicker flash intensity series was done (Fig. 4C and D). Contrary to UEs, a recovery of the rod-driven flicker ERG responses was observed in AAV TEs. In accordance with the approximate size of the treated area (about one-third of the total retina), rod-specific ERG amplitudes were about one-third of that in age-matched controls (Fig. 4E). It should further be noted that injections of CNGB1a AAVs had no effect on the light-adapted photopic ERG of CNGB1$^{-/-}$, indicating that the treatment including the technical procedure had no adverse effects on the cone system (data not shown).

AAV treatment restores rod-mediated vision-guided behavior in CNGB1$^{-/-}$ mice

Having shown by ERG that treated CNGB1$^{-/-}$ mice acquired the ability to generate rod-specific light-evoked signals and to activate rod bipolar cells, we asked whether this improvement on a retinal level might establish vision-guided behavior of the rod. We therefore used a simple water maze test to assess visual responsivity (see Materials and Methods). The mice were tested for five consecutive days in a cued water maze

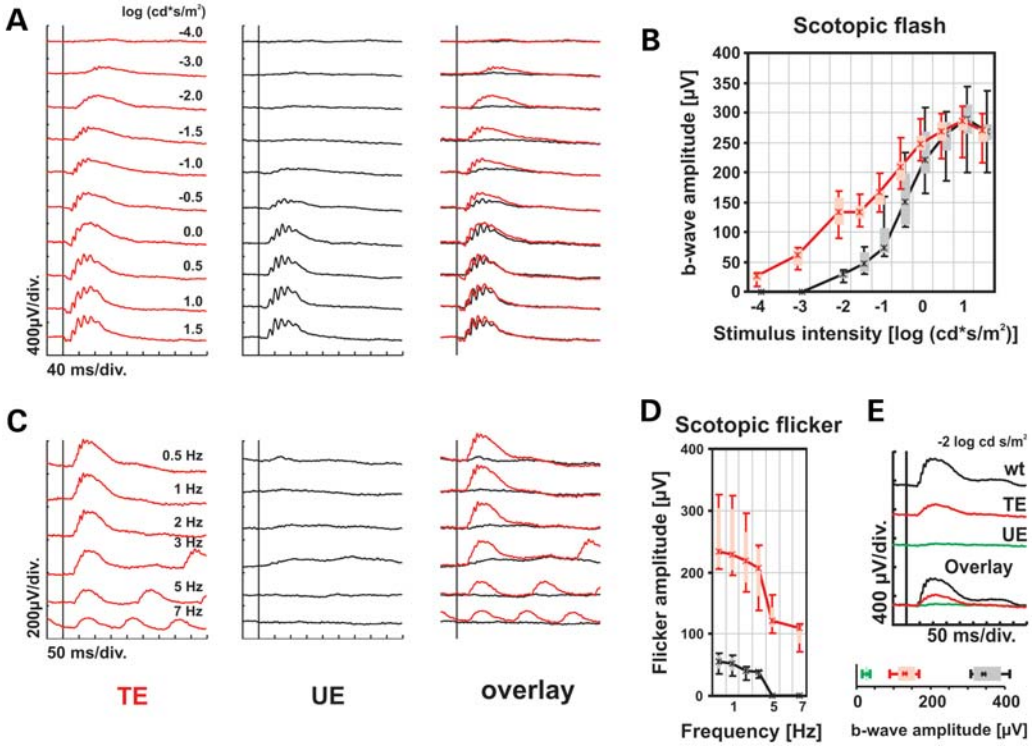

Figure 4. Effect of gene therapy on visual function in CNGB1$^{-/-}$ mice. Comparison of ERG data from TEs and UEs of the same individual CNGB1$^{-/-}$ mice ($n = 6$) treated at postnatal week 2 (PW 2). (**A**) Dark-adapted (scotopic) single-flash ERG intensity series of the treated (TE, red) and the untreated fellow eye (UE, black) of a representative CNGB1$^{-/-}$ mouse at 2 months after injection, together with a superposition to enhance visibility of differences (right column). The vertical line indicates the timing of the light stimulus in each panel. (**C**) Scotopic flicker ERG responses at a fixed rod-specific intensity (-2 log cd*s/m^2) from 0.5 to 7 Hz and the corresponding overlay. (**B**, **D**) The quantitative data of the entire group are shown as Box-and-Whisker plots, i.e. boxes indicate the 25 and 75% quantile range, whiskers indicate the 5 and 95% quantiles, and the asterisks indicate the median of the data. The amplitude data are plotted as a function of the logarithm of the flash intensity (B) and as a function of flash frequency (D). (**E**, top) Representative scotopic single-flash ERG responses at -2 log cd*s/m^2 recorded from a wild-type (wt) eye, TE, UE and a superposition. (E, bottom) The quantitative data of each group are shown as Box-and-Whisker plots as specified above. The results indicate a distinct rescue of rod functionality.

for their ability to navigate to a visible escape platform. On Days 1–3, the experiment was performed at dim light conditions (see Materials and Methods) to ensure that vision is totally conferred to the rod system. On Day 1, wild-type control mice needed 47.9 ± 10.6 s to navigate to the escape platform, but gradually improved their performance to 7.3 ± 1.1 s on Day 3 [$P = 0.0009$, one-way analysis of variance (ANOVA)] (Fig. 5A). An example swim path for a wild-type mouse on Day 3 is shown in Figure 5C. Based on the swimming abilities of the mice (mean swimming speed: 19.0 ± 1.8 cm/s) and the diameter (120 cm) of the water-filled tank, the swimming performance on Day 3 can be considered as the best achievable one. Untreated CNGB1$^{-/-}$ mice needed significantly longer than wild-type mice ($P < 0.001$, two-way ANOVA) and were not able to improve their performance significantly during the three test days (Day 1: 90.4 ± 8.1 s; Day 3: 67.9 ± 10.8 s; $P = 0.2660$, one-way ANOVA) (Fig. 5A; example swim path in Fig. 5C). In contrast, treated CNGB1$^{-/-}$ mice were clearly able to improve during the three test days (Day 1: 59.7 ± 11.0 s; Day 3: 23.1 ± 4.7 s; $P = 0.0127$, one-way ANOVA) and performed significantly better than untreated CNGB1$^{-/-}$ mice ($P = 0.0123$, two-way ANOVA) (Fig. 5A; example swim path in Fig. 5D). Treated mice showed slightly longer escape latencies than the wild-type mice, but did not significantly differ from wild-type in their overall performance ($P = 0.0834$, two-way ANOVA) (Fig. 5A). Also, the learning curves from treated and wild-type mice developed in parallel and had similar slopes (wild-type: −21.5 ± 5.4, treated: −18.3 ± 6.8; $P = 0.725$, *t*-test). Taken together, these findings suggest that treated CNGB1$^{-/-}$ mice gained the ability to navigate using information provided by the rod visual system.

We performed the test on Days 4 and 5 under normal light conditions (see Materials and Methods). Vision under these light conditions is mainly conferred by cone photoreceptors. As CNGB1$^{-/-}$ mice have preserved cone function until 6 months of age (6), we expected all animal groups to be able to navigate under these test conditions. Wild-type and treated CNGB1$^{-/-}$ mice performed better than untreated CNGB1$^{-/-}$ mice on Day 4, because they already learned the task under dim light conditions. However, untreated mice also started improving their performance until they reached similar levels of escape latencies like wild-type and treated mice on Day 5 (Fig. 5A).

During all tests, the mice were allowed to swim for up to 120 s. If a mouse did not find the platform within 120 s, it was considered as an 'error of omission'. Wild-type mice showed no (Day 3) or almost no (Day 2: 0.2 ± 0.2%) errors

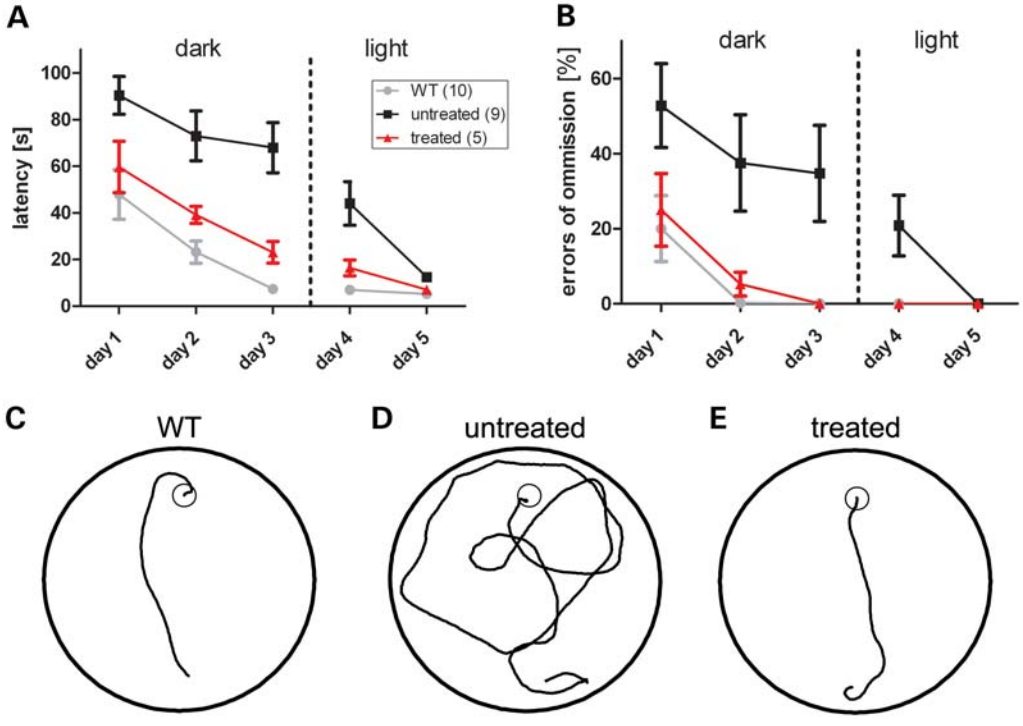

Figure 5. Effect of gene therapy on vision-guided behavior in CNGB1$^{-/-}$ mice. Treated mice show improved learning curves in a visual water maze that tests rod-mediated vision. (**A**, **B**) Latency to locate a swimming escape platform (A) and errors of omission (B) under dark (Days 1–3) and normal (Days 4 and 5) light conditions. In contrast to untreated CNGB1$^{-/-}$ mice (black), treated CNGB1$^{-/-}$ mice (red) significantly improved their performance during the first three test days in the dark. All treated mice successfully located the escape platform (e.g. performed without errors of omission) on Day 3. Their performance did not significantly differ from wild-type control mice (grey). On Days 4 and 5, the mice were tested under normal light conditions. As cone function is not impaired in young untreated CNGB1$^{-/-}$ mice (6), they were also able to improve their performance to the level of wild-type and treated CNGB1$^{-/-}$ mice on Day 5. (**C**–**E**) Example swim paths from wild-type (C), treated (D) and untreated (E) mice on Day 3.

of omission from the second test day onward (Fig. 5B). In contrast, untreated CNGB1$^{-/-}$ mice made errors of omission throughout the low-light condition test phase (Days 1–3) and the first day under normal light conditions (Day 4), and only improved to no more errors of omission on the second day under normal light conditions (Day 5) (Fig. 5B). As a clear indication for an improvement of rod-mediated vision, treated CNGB1$^{-/-}$ mice performed without any error of omission on Day 3 and had only 5.2 $\pm$ 3.2% errors of omission on Day 2 (Fig. 5B).

Gene therapy delays retinal degeneration in CNGB1$^{-/-}$ mice

RP patients and CNGB1$^{-/-}$ mice display a progressive retinal degeneration due to the loss of rod and cone photoreceptors, which needs to be ameliorated or halted in order to achieve long-term beneficial effects on vision. Having shown that our gene replacement therapy was able to restore rod photoreceptor function in ERG and to improve rod-mediated vision in the behavioral test, the question remained to what extent the treatment could also delay photoreceptor degeneration. Specifically, the progressive photoreceptor degeneration in CNGB1$^{-/-}$ mice results in thinning of the outer nuclear layer to about half the size of wild-type control mice at 6 months of age and to 1–2 rows of photoreceptors at 1 year (6). The wild-type retina contains 11–12 rows of photoreceptors. To test whether the treatment was able to delay the retinal degeneration, we isolated the retina at 12 months after injection and analyzed the retinal histology. Figure 6A shows an overview image from a representative retinal slice of a treated knockout mouse at 12 months after treatment labeled with a CNGB1-specific antibody and the nuclear dye Hoechst 33342. The region with no CNGB1a expression revealed the expected thinning of the outer nuclear layer. However, in the treated part with high levels of CNGB1a expression, 7–8 rows of photoreceptors remained, indicating that the treatment significantly delayed photoreceptor cell loss (Fig. 6A). In the untreated CNGB1$^{-/-}$ retina, Müller cells are activated and show high levels of glial fibrillary acidic protein (GFAP) immunoreactivity (Fig 6B) (6). In support of a beneficial effect on retinal degeneration, we observed a reduction of the GFAP signal to wild-type levels at 12 months after treatment (Fig. 6C and D). An overview image from a treated CNGB1$^{-/-}$ retina illustrating the treatment effect on Müller gliosis is shown in Figure 6E. The beneficial effects on retinal degeneration go along with the normalization of cGMP metabolism in the CNGB1$^{-/-}$ retina (Fig. 6G). Within the untreated part of the retina, a profound accumulation of cGMP can be detected in photoreceptors (Fig. 6F). In accordance with the functional data, expression of CNGB1a also lowered cGMP in photoreceptors to levels comparable to wild-type (Fig. 6G and H). As is typical for RP and its models, cone photoreceptors also start to

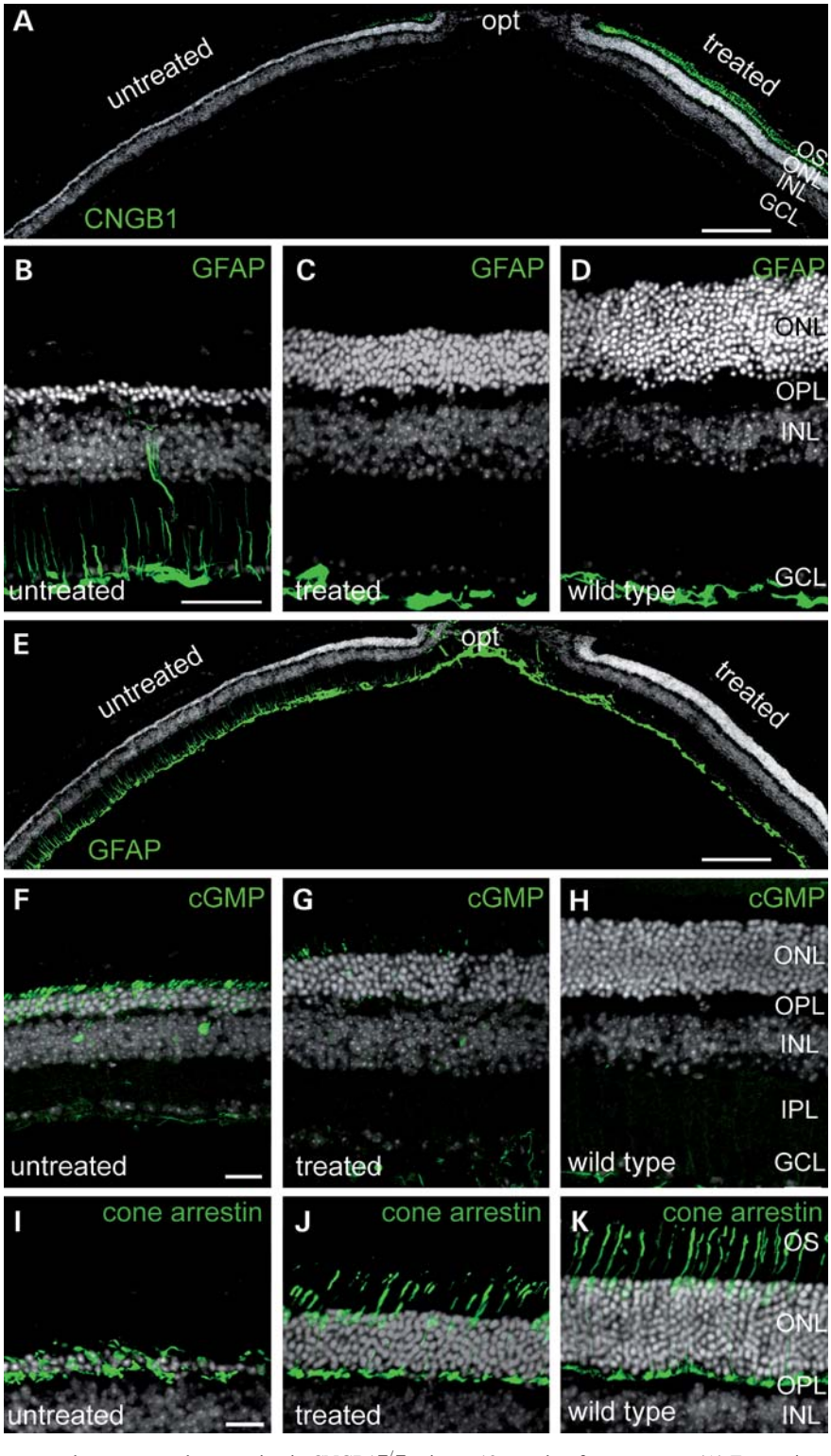

Figure 6. Effect of gene therapy on photoreceptor degeneration in CNGB1$^{-/-}$ mice at 12 months after treatment. (**A**) Expression of CNGB1a protein (green) in the CNGB1$^{-/-}$ retina delayed photoreceptor cell loss and thinning of outer nuclear layer (ONL) at 12 months after treatment. (**B**–**D**) Representative confocal images from untreated (B), treated (C) CNGB1$^{-/-}$ and wild-type (D) retinas immunolabeled for GFAP (green). The treatment decreased the activation of Müller glia cells (C) to levels comparable to wild-type (D). (**E**) Overview image spanning a larger portion of a treated CNGB1$^{-/-}$ retina showing the different levels of GFAP (green) in the treated and untreated parts. (**F**–**H**) Viral CNGB1a expression also lowered presumably deleterious levels of cGMP (green) in photoreceptors of treated mice 6 months after treatment (G) to levels comparable to wild-type (H). (**I**–**K**) Confocal scans from retinal slices immunolabeld for the specific 'cone marker' cone arrestin demonstrate the positive effect on cone morphology at 12 months after treatment (I–K). Cell nuclei were stained with the nuclear dye Hoechst 33342 (grey) in all panels. The scale bar marks 100 μm in (A) and (E), 50 μm in (B–D) and 20 μm in (F–K). GCL, ganglion cell layer; INL, inner nuclear layer; IPL, inner plexiform layer; OPL, outer plexiform layer; opt, optic nerve; ONL, outer nuclear layer; OS, photoreceptor outer segments.

degenerate in the CNGB1$^{-/-}$ mouse secondary to rods although they are primarily unaffected. In untreated mice, cone degeneration becomes evident after 6 months of age (6). To test for the beneficial effect of the treatment on cone photoreceptors, we stained the treated and untreated CNGB1$^{-/-}$ retina with the cone marker cone arrestin (16) at 12 months after injection. We found that in the treated CNGB1-deficient retina, the morphology of cones was positively affected (Fig. 6I–K).

DISCUSSION

RP is a family of hereditary eye diseases that affects the function and viability of rod photoreceptors resulting in night blindness and progressive retinal degeneration (1,2). The secondary degeneration of cone photoreceptors produces a corresponding loss of high-acuity vision that can eventually lead to complete blindness (1,2). Until recently, RP has been considered to be incurable. With the advent of AAV-mediated gene replacement therapy, several groups succeeded in restoration of retinal function in RP animal models (17,18). For one form of RP, Leber's congenital amaurosis caused by mutations in the RPE-specific gene RPE65, a gene replacement approach has already been translated from animal into clinical studies (19–21). For other forms of RP caused by mutations in photoreceptor-specific genes, the success rate of gene replacement therapy varied from modest, short-term effects to more pronounced and more stable therapeutic effects (17,18). This variability may be explained by the interaction of multiple factors such as the type of AAV (e.g. serotype, single- or double-stranded vector), the type of target cell (e.g. RPE, photoreceptors), the animal model in which the treatment is being tested, the rate of degeneration, the time point of treatment and the species specificity of the therapeutic transgenes, as well as the structure, localization and molecular function of the gene product (e.g. enzyme, receptor, ion channel). Another important consideration refers to the dosage of transgene expression. A minimum level of expression in the target cell is essential to achieve a therapeutic effect. However, overexpression of the therapeutic gene may also cause degeneration and cell death. For instance, gene therapy studies in RP mouse models with mutations in genes encoding the rod photoreceptor-specific phosphodiesterase have shown variable success rates ranging from partial rescue to more definite therapeutic effects (22–25). Due to the high degree of signal amplification and multi-facetted regulation of the phototransduction cascade (26), even subtle changes in expression levels may cause severe functional defects that influence the outcome of gene therapy. Thus, it appears that success rates of gene therapies for genes encoding proteins involved in the photoreceptor signal transduction cascade may require well-balanced transgene expression.

In this study, we present data on the successful restoration of vision in the CNGB1 knockout mouse model of RP using AAV-mediated gene therapy. The treatment resulted in efficient expression of high levels of full-length CNGB1a protein in rod photoreceptors that almost exclusively localized to outer segments. Importantly, this also resulted in the restoration of the previously degraded endogenous CNGA1 protein, which is the second subunit of the native rod CNG channel (5). Following treatment, both proteins co-localized in rod outer segments and formed regular CNG channel complexes in the transduced area of the CNGB1$^{-/-}$ retina. We have previously shown that the vast majority of homomeric CNG channels (e.g. CNGA1 or CNGA3 only) cannot be transported into the photoreceptor outer segments and are rapidly degraded (6,16,27). Only a minor fraction of CNGB1$^{-/-}$ rods (3 out of 35 recorded cells) (6) showed small (10–15% of wild-type) light responses. Accordingly, the levels of endogenous CNGA1 transcript and protein that are available for assembly with virally expressed CNGB1a seems to be the limiting factor that defines the amount of CNG channel complexes in the treated rod outer segments. Thus, the endogenous CNGA1 transcript levels act as an intrinsic safety barrier to ensure that the amounts of outer segment rod CNG channels cannot exceed wild-type levels, which may prevent deleterious changes in photoreceptor Ca^{2+} levels or membrane potential. In line with this, our treatment showed no adverse effects and revealed a prolonged preservation of photoreceptors up to the end of the follow-up period of 12 months.

In summary, the present study represents the first successful approach of restoration of vision in a retinal channelopathy model of RP. Importantly, we were able to demonstrate the restoration of visual system integrity and functionality by *in vivo* and *in vitro* analyses of retinal function and morphology, as well as vision-guided behavior. Our data are very encouraging to launch AAV-based gene therapy studies in human patients suffering from CNG channelopathies.

MATERIALS AND METHODS

Animals

Animals were housed under standard white cyclic lighting (200 lux), had free access to food and water and were used irrespective of gender. Lighting conditions were consistent across all groups and/or treatments. All procedures concerning animals were performed with permission of local authorities (Regierungspräsidium Tübingen and Regierung von Oberbayern) and in accordance with the ARVO Statement for the Use of Animals in Ophthalmic and Vision Research.

Cloning and production of rAAV vectors

Cloning and mutagenesis were performed by standard techniques. All sequence manipulations were confirmed by sequencing. To construct pAAV2.1-Rho-CNGB1a-SV40, we inserted a polymerase chain reaction (PCR)-amplified mouse Rhodopsin promoter (RhoF: 5′-GATCCTTAAGATGTGGAG AAG TGAATTTAGGGCCCAA-3′ and RhoR: 5′-GTATGTC GA CCACTGCGGCTGCTCGAAGGGGCTCCGCA-3′, PCR template: mouse genomic DNA) and a PCR-amplified SV40 late Poly A fragment [SV40F: 5′-TGTAGCGGCCGCAG ACATGATAAGATACATTGATGAGTT-3′, SV40R: 5′-TG TACTCGAGTACCACATTTGTAGAGGTTTTACTTGCT-3′, PCR template: psiCHECK-2 (Promega, Mannheim, Germany)] and PCR-amplified (mB1F: 5′-CCGGTACCGCCACCATG TTGGGCTGGGTCCAAAGG-3′, mB1R: 5′-GATCGCGGCC GCTCATGCACCTCACTCCGCC-3′, PCR template: mouse

retinal cDNA) full-length mouse CNGB1a cDNA into pAAV2.1-mcs (27). pAAV2/8 Y733F (12) encoding a Y733F-modified AAV8 capsid was obtained by site-directed mutagenesis (YF8F: 5′-GCCCCATTGGCACCCGTTTCCTCA CCCGTAATCTGTAATTG-3′, YF8R: 5′-CAATTACAGAT TACGGGTGAGGAAACGGGTGCCAATGGGGC-3′) using pAAV2/8 (28) as a template. Single-strand AAV vectors were produced by triple calcium phosphate transfection of 293T cells with pAdDeltaF6 (29), pAAV2/8Y733F and pAAV2.1-Rho-CNGB1a-SV40 plasmids followed by iodixanol gradient (30) purification. The 40–60% iodixanol interface was further purified and concentrated by ion exchange chromatography on a 5 ml HiTrap Q Sepharose column using an ÄKTA Basic FPLC system (GE Healthcare, Munich, Germany) according to previously described procedures, followed by further concentration using Amicon Ultra-4 Centrifugal Filter Units (Millipore, Schwalbach, Germany). Physical titers (in genome copies/ml) were determined by quantitative PCR of CNGB1 (B1aqF: 5′-GAACTGGAACTGCTGGCTGAT-3′\xEF\x80 and B1aqR: 5′-TGGAACACGGTGATGTCCAGGA-3′) using a LightCycler 480 (Roche Applied Science, Mannheim, Germany).

Subretinal rAAV injections

As previously described (27), mice were anesthetized by subcutaneous injection of ketamine (66.7 mg/kg) and xylazine (11.7 mg/kg), and their pupils were dilated with tropicamide eye drops (Mydriaticum Stulln; Pharma Stulln GmbH, Germany). One microliter of rAAV particles was injected into the subretinal space using the NanoFil Subretinal Injection Kit (WPI, Germany) equipped with a 34 gauge beveled needle. The injection was performed free hand under a surgical microscope (Carl Zeiss, Germany). Special care was taken to avoid damage of the lens. The success of the procedure was monitored immediately following the injections using SLO (13) and OCT (14). If the procedure was not successful (severe damage like a full retinal detachment), the mice were excluded from further analysis. At the given age, this concerned about one eye out of five.

Electroretinograms

ERG analysis was performed at 6 weeks to 4 months after injection according to the procedures described elsewhere (31,32). Single-flash intensity and flicker frequency series data were available from 11 animals (one eye treated, one eye untreated). Scotopic flicker ERG series data were available from 11 animals (one eye treated, one eye untreated).

Scanning laser ophthalmoscopy

Retinal structures were visualized via a cSLO [Heidelberg Retina Angiograph (HRA I)] according to previously described procedures (13). The HRA features two argon wavelengths (488 and 514 nm) in the short-wavelength range and two infrared diode lasers (795 and 830 nm) in the long-wavelength range. Laser wavelengths used for fundus visualization were: 514 nm (red-free channel) and 488 nm for autofluorescent images, with a barrier filter at 500 nm.

Spectral domain optical coherence tomography

Spectrum domain optical coherence tomography imaging was done with a commercially available Spectralis^{TM} HRA + OCT device (Heidelberg Engineering) featuring a broadband superluminescent diode at 870 nm as low coherent light source. Each two-dimensional B-scan recorded at 30° field of view consists of 1536 A-scans, which are acquired at a speed of 40 000 scans per second. Optical depth resolution is ∼7 μm with digital resolution reaching 3.5 μm. Imaging was performed using the proprietary software package Eye Explorer (version 3.2.1.0, Heidelberg Engineering). Retinal thickness was quantified using horizontal slides, located 1500 μm distant from the optic nerve head in the temporal hemisphere.

Immunohistochemistry

Immunohistochemical staining was performed at 40 days to 12 months after injection according to the procedures described previously (16). We used the following primary antibodies: rabbit anti-CNGB1 [C-AbmCNGB1 (6), 1:30 000], mouse anti-CNGA1 [2G11 (33), 1:30], mouse anti-peripherin-2 [Per5H2 (34), 1:1000], sheep anti-cGMP (35) (1:3000), Cy3-coupled anti-GFAP (16) (Sigma, Germany, 1:1000) and rabbit anti-cone arrestin (36) (1:300). Laser scanning confocal micrographs were taken using an LSM 510 meta microscope (Carl Zeiss, Germany) and images are presented as collapsed confocal z-stacks. Stainings were reproduced in ≥3 independent experiments.

Western blot

For protein isolation from mouse retinas, the retinas were homogenized using a mortar and suspended in homogenization buffer [2% sodium dodecyl sulfate (SDS), 50 mM Tris and proteinase inhibitor cocktail mix]. After heating at 95°C for 15 min followed by centrifugation at 1000*g* for 10 min at 4°C, the resulting supernatant was used in western blot analysis as previously described (16). The proteins were separated by 10% SDS-polyacrylamide gel electrophoresis followed by western blot analysis according to the standard procedures. The following antibodies were used: mouse anti-CNGB1 [1B4 (37), 1:30], mouse anti-CNGA1 [2G11 (33), 1:30] and mouse anti-Tubulin (1:2000; Dianova, Hamburg, Germany).

Visual water maze task

The Morris water maze test was originally described as a test for hippocampus-dependent learning (38) and used later with modifications as a test for vision-guided behavior (39). Mice were housed separately in an inverse 12 h light/dark cycle. The experiment was performed in dark. Mice were trained for 3 days (eight trials a day) to locate a stable platform (10 cm in diameter) at dim light conditions of 0.32 cd/m^2 to ensure that vision is totally conferred to the rod system. The platform was placed in a circular swimming pool (120 cm in diameter, 70 cm high, white plastic) filled with water. The starting position of the mouse was changed from trial to trial in a pseudorandom order, whereas the platform was kept in a constant location. Distal cues in the testing room and the

water maze, such as patterned cardboards, were provided as spatial references. Trials were terminated if the mouse climbed onto the platform or when it swam for 2 min. If the mouse did not find the platform, it was gently placed on the stable platform. After each trial, the mouse was left on the platform for 10 s undisturbed before warmed using a heating lamp and transferred to the home cage. On Days 4 and 5, the experiment was performed under light conditions (29.04 cd/m^2) to test cone vision-mediated behavior. The experiment was performed and analyzed blindly to the animal genotype.

Statistics

All values are given as mean $\pm$ SE, and N is the number of animals. Unless stated otherwise, an unpaired Student's t-test was performed for the comparison between two groups. Values of $P < 0.05$ were considered significant.

ACKNOWLEDGEMENTS

We thank Gudrun Utz, Pia Lacroix, Jennifer Schmidt and Elisabeth Schulze for excellent technical help, Dr Hildegard Büning for helpful discussion on AAV vectors, Drs James M. Wilson (University of Pennsylvania) and Alberto Auricchio (TIGEM) for the gift of AAV plasmids and Drs Robert Molday (University of British Columbia), Jan de Vente (University of Maastricht), Brigitte Pfeiffer-Guglielmi (University of Tübingen) and Wolfgang Baehr (University of Utah) for the gift of antibodies.

Conflict of Interest statement: None declared.

FUNDING

This work was supported by the Deutsche Forschungsgemeinschaft (DFG) (grant numbers Bi484/4-1 to M.B., Mi1238/1-2 to S.M., and Se837/5-2, Se837/6-2, Se837/7-1 to M.W.S.).

REFERENCES

1. Hartong, D.T., Berson, E.L. and Dryja, T.P. (2006) Retinitis pigmentosa. *Lancet*, **368**, 1795–1809.
2. Sahel, J., Bonnel, S., Mrejen, S. and Paques, M. (2010) Retinitis pigmentosa and other dystrophies. *Dev. Ophthalmol.*, **47**, 160–167.
3. Cideciyan, A.V. (2010) Leber congenital amaurosis due to RPE65 mutations and its treatment with gene therapy. *Prog. Retin. Eye Res.*, **29**, 398–427.
4. Biel, M. and Michalakis, S. (2007) Function and dysfunction of CNG channels: insights from channelopathies and mouse models. *Mol. Neurobiol.*, **35**, 266–277.
5. Biel, M. and Michalakis, S. (2009) Cyclic nucleotide-gated channels. *Handb. Exp. Pharmacol.*, **191**, 111–136.
6. Hüttl, S., Michalakis, S., Seeliger, M., Luo, D.G., Acar, N., Geiger, H., Hudl, K., Mader, R., Haverkamp, S., Moser, M. *et al.* (2005) Impaired channel targeting and retinal degeneration in mice lacking the cyclic nucleotide-gated channel subunit CNGB1. *J. Neurosci.*, **25**, 130–138.
7. Zhang, Y., Molday, L.L., Molday, R.S., Sarfare, S.S., Woodruff, M.L., Fain, G.L., Kraft, T.W. and Pittler, S.J. (2009) Knockout of GARPs and the beta-subunit of the rod cGMP-gated channel disrupts disk morphogenesis and rod outer segment structural integrity. *J. Cell Sci.*, **122**, 1192–1200.
8. Wu, Z.J., Yang, H.Y. and Colosi, P. (2010) Effect of genome size on AAV vector packaging. *Mol. Ther.*, **18**, 80–86.
9. Lai, Y., Yue, Y.P. and Duan, D.S. (2010) Evidence for the failure of adeno-associated virus serotype 5 to package a viral genome $\geq$8.2 kb. *Mol. Ther.*, **18**, 75–79.
10. Dong, B.A., Nakai, H. and Xiao, W.D. (2010) Characterization of genome integrity for oversized recombinant AAV vector. *Mol. Ther.*, **18**, 87–92.
11. Flannery, J.G., Zolotukhin, S., Vaquero, M.I., LaVail, M.M., Muzyczka, N. and Hauswirth, W.W. (1997) Efficient photoreceptor-targeted gene expression *in vivo* by recombinant adeno-associated virus. *Proc. Natl Acad. Sci. USA*, **94**, 6916–6921.
12. Petrs-Silva, H., Dinculescu, A., Li, Q., Min, S.H., Chiodo, V., Pang, J.J., Zhong, L., Zolotukhin, S., Srivastava, A., Lewin, A.S. *et al.* (2009) High-efficiency transduction of the mouse retina by tyrosine-mutant AAV serotype vectors. *Mol. Ther.*, **17**, 463–471.
13. Seeliger, M.W., Beck, S.C., Pereyra-Munoz, N., Dangel, S., Tsai, J.Y., Luhmann, U.F., van de Pavert, S.A., Wijnholds, J., Samardzija, M., Wenzel, A. *et al.* (2005) *In vivo* confocal imaging of the retina in animal models using scanning laser ophthalmoscopy. *Vision Res.*, **45**, 3512–3519.
14. Fischer, M.D., Huber, G., Beck, S.C., Tanimoto, N., Muehlfriedel, R., Fahl, E., Grimm, C., Wenzel, A., Reme, C.E., van de Pavert, S.A. *et al.* (2009) Noninvasive, *in vivo* assessment of mouse retinal structure using optical coherence tomography. *PLoS ONE*, **4**, e7507.
15. Spaide, R.F. and Curcio, C.A. (2011) Anatomical correlates to the bands seen in the outer retina by optical coherence tomography: literature review and model. *Retina*, **31**, 1609–1619.
16. Michalakis, S., Geiger, H., Haverkamp, S., Hofmann, F., Gerstner, A. and Biel, M. (2005) Impaired opsin targeting and cone photoreceptor migration in the retina of mice lacking the cyclic nucleotide-gated channel CNGA3. *Invest. Ophthalmol. Vis. Sci.*, **46**, 1516–1524.
17. den Hollander, A.I., Black, A., Bennett, J. and Cremers, F.P. (2010) Lighting a candle in the dark: advances in genetics and gene therapy of recessive retinal dystrophies. *J. Clin. Invest.*, **120**, 3042–3053.
18. Smith, A.J., Bainbridge, J.W. and Ali, R.R. (2012) Gene supplementation therapy for recessive forms of inherited retinal dystrophies. *Gene Ther.*, **19**, 154–161.
19. Bainbridge, J.W., Smith, A.J., Barker, S.S., Robbie, S., Henderson, R., Balaggan, K., Viswanathan, A., Holder, G.E., Stockman, A., Tyler, N. *et al.* (2008) Effect of gene therapy on visual function in Leber's congenital amaurosis. *N. Engl. J. Med.*, **358**, 2231–2239.
20. Cideciyan, A.V., Aleman, T.S., Boye, S.L., Schwartz, S.B., Kaushal, S., Roman, A.J., Pang, J.J., Sumaroka, A., Windsor, E.A., Wilson, J.M. *et al.* (2008) Human gene therapy for RPE65 isomerase deficiency activates the retinoid cycle of vision but with slow rod kinetics. *Proc. Natl Acad. Sci. USA*, **105**, 15112–15117.
21. Hauswirth, W.W., Aleman, T.S., Kaushal, S., Cideciyan, A.V., Schwartz, S.B., Wang, L., Conlon, T.J., Boye, S.L., Flotte, T.R., Byrne, B.J. *et al.* (2008) Treatment of Leber congenital amaurosis due to RPE65 mutations by ocular subretinal injection of adeno-associated virus gene vector: short-term results of a phase I trial. *Hum. Gene Ther.*, **19**, 979–990.
22. Bennett, J., Tanabe, T., Sun, D., Zeng, Y., Kjeldbye, H., Gouras, P. and Maguire, A.M. (1996) Photoreceptor cell rescue in retinal degeneration (RD) mice by *in vivo* gene therapy. *Nat. Med.*, **2**, 649–654.
23. Jomary, C., Vincent, K.A., Grist, J., Neal, M.J. and Jones, S.E. (1997) Rescue of photoreceptor function by AAV-mediated gene transfer in a mouse model of inherited retinal degeneration. *Gene Ther.*, **4**, 683–690.
24. Pang, J.J., Boye, S.L., Kumar, A., Dinculescu, A., Deng, W., Li, J., Li, Q., Rani, A., Foster, T.C., Chang, B. *et al.* (2008) AAV-mediated gene therapy for retinal degeneration in the rd10 mouse containing a recessive PDEbeta mutation. *Invest. Ophthalmol. Vis. Sci.*, **49**, 4278–4283.
25. Pang, J.J., Dai, X., Boye, S.E., Barone, I., Boye, S.L., Mao, S., Everhart, D., Dinculescu, A., Liu, L., Umino, Y. *et al.* (2011) Long-term retinal function and structure rescue using capsid mutant AAV8 vector in the rd10 mouse, a model of recessive retinitis pigmentosa. *Mol. Ther.*, **19**, 234–242.
26. Luo, D.G., Xue, T. and Yau, K.W. (2008) How vision begins: an odyssey. *Proc. Natl Acad. Sci. USA*, **105**, 9855–9862.
27. Michalakis, S., Mühlfriedel, R., Tanimoto, N., Krishnamoorthy, V., Koch, S., Fischer, M.D., Becirovic, E., Bai, L., Huber, G., Beck, S.C. *et al.* (2010) Restoration of cone vision in the CNGA3$^{-/-}$ mouse model of

congenital complete lack of cone photoreceptor function. *Mol. Ther.*, **18**, 2057–2063.
28. Gao, G.P., Alvira, M.R., Wang, L., Calcedo, R., Johnston, J. and Wilson, J.M. (2002) Novel adeno-associated viruses from rhesus monkeys as vectors for human gene therapy. *Proc. Natl Acad. Sci. USA*, **99**, 11854–11859.
29. Auricchio, A., Hildinger, M., O'Connor, E., Gao, G.P. and Wilson, J.M. (2001) Isolation of highly infectious and pure adeno-associated virus type 2 vectors with a single-step gravity-flow column. *Hum. Gene Ther.*, **12**, 71–76.
30. Grieger, J.C., Choi, V.W. and Samulski, R.J. (2006) Production and characterization of adeno-associated viral vectors. *Nat. Protoc.*, **1**, 1412–1428.
31. Seeliger, M.W., Grimm, C., Stahlberg, F., Friedburg, C., Jaissle, G., Zrenner, E., Guo, H., Reme, C.E., Humphries, P., Hofmann, F. *et al.* (2001) New views on RPE65 deficiency: the rod system is the source of vision in a mouse model of Leber congenital amaurosis. *Nat. Genet.*, **29**, 70–74.
32. Tanimoto, N., Muehlfriedel, R.L., Fischer, M.D., Fahl, E., Humphries, P., Biel, M. and Seeliger, M.W. (2009) Vision tests in the mouse: functional phenotyping with electroretinography. *Front Biosci.*, **14**, 2730–2737.
33. Molday, R.S., Molday, L.L., Dose, A., Clark-Lewis, I., Illing, M., Cook, N.J., Eismann, E. and Kaupp, U.B. (1991) The cGMP-gated channel of the rod photoreceptor cell characterization and orientation of the amino terminus. *J. Biol. Chem.*, **266**, 21917–21922.
34. Connell, G., Bascom, R., Molday, L., Reid, D., McInnes, R.R. and Molday, R.S. (1991) Photoreceptor peripherin is the normal product of the gene responsible for retinal degeneration in the rds mouse. *Proc. Natl Acad. Sci. USA*, **88**, 723–726.
35. Tanaka, J., Markerink-van Ittersum, M., Steinbusch, H.W. and De Vente, J. (1997) Nitric oxide-mediated cGMP synthesis in oligodendrocytes in the developing rat brain. *Glia*, **19**, 286–297.
36. Zhang, T., Baehr, W. and Fu, Y. (2012) Chemical chaperone TUDCA preserves cone photoreceptors in a mouse model of Leber congenital amaurosis. *Invest. Ophthalmol. Vis. Sci.*, **53**, 3349–3356.
37. Poetsch, A., Molday, L.L. and Molday, R.S. (2001) The cGMP-gated channel and related glutamic acid-rich proteins interact with peripherin-2 at the rim region of rod photoreceptor disc membranes. *J. Biol. Chem.*, **276**, 48009–48016.
38. Morris, R. (1984) Developments of a water-maze procedure for studying spatial learning in the rat. *J. Neurosci. Methods*, **11**, 47–60.
39. Pang, J.J., Chang, B., Kumar, A., Nusinowitz, S., Noorwez, S.M., Li, J., Rani, A., Foster, T.C., Chiodo, V.A., Doyle, T. *et al.* (2006) Gene therapy restores vision-dependent behavior as well as retinal structure and function in a mouse model of RPE65 Leber congenital amaurosis. *Mol. Ther.*, **13**, 565–572.

V. Appendix

Paper III: HCN1 Channels Enhance Rod System Responsivity in the Retina under Conditions of Light Exposure

Sothilingam V[§], Michalakis S, Garcia Garrido M, Biel M, Tanimoto N**, Seeliger MW**.

Published in PLoS One
11: e0147728 (2016)

PLOS | ONE

RESEARCH ARTICLE

HCN1 Channels Enhance Rod System Responsivity in the Retina under Conditions of Light Exposure

Vithiyanjali Sothilingam[1]*, Stylianos Michalakis[2], Marina Garcia Garrido[1], Martin Biel[2], Naoyuki Tanimoto[1☯], Mathias W. Seeliger[1☯]

1 Division of Ocular Neurodegeneration, Institute for Ophthalmic Research, Centre for Ophthalmology, Eberhard Karls University of Tübingen, Schleichstr. 4/3, D-72076, Tübingen, Germany, **2** Center for Integrated Protein Science Munich CIPSM, Department of Pharmacy-Center for Drug Research, Ludwig-Maximilians-Universität München, Butenandtstr. 5–13, D-81377, München, Germany

☯ These authors contributed equally to this work.
* Vithiyanjali.Sothilingam@med.uni-tuebingen.de

OPEN ACCESS

Citation: Sothilingam V, Michalakis S, Garcia Garrido M, Biel M, Tanimoto N, Seeliger MW (2016) HCN1 Channels Enhance Rod System Responsivity in the Retina under Conditions of Light Exposure. PLoS ONE 11(1): e0147728. doi:10.1371/journal.pone.0147728

Editor: Alfred S Lewin, University of Florida, UNITED STATES

Received: October 19, 2015

Accepted: January 7, 2016

Published: January 25, 2016

Data Availability Statement: All relevant data are within the paper.

Funding: This work was supported by the Deutsche Forschungsgemeinschaft (DFG), grants Se837/4-1, 5-2, and 6-2 and Open Access Publishing Fund of University of Tuebingen. The funders had no role in study design, data collection and analysis, decision to publish, or preparation of the manuscript.

Competing Interests: The authors have declared that no competing interests exist.

Abstract

Purpose

Vision originates in rods and cones at the outer retina. Already at these early stages, diverse processing schemes shape and enhance image information to permit perception over a wide range of lighting conditions. In this work, we address the role of hyperpolarization-activated and cyclic nucleotide-gated channels 1 (HCN1) in rod photoreceptors for the enhancement of rod system responsivity under conditions of light exposure.

Methods

To isolate HCN1 channel actions in rod system responses, we generated double mutant mice by crossbreeding *Hcn1*$^{-/-}$ mice with *Cnga3*$^{-/-}$ mice in which cones are non-functional. Retinal function in the resulting *Hcn1*$^{-/-}$ *Cnga3*$^{-/-}$ animals was followed by means of electroretinography (ERG) up to the age of four month. Retinal imaging via scanning laser ophthalmoscopy (SLO) and optical coherence tomography (OCT) was also performed to exclude potential morphological alterations.

Results

This study on *Hcn1*$^{-/-}$ *Cnga3*$^{-/-}$ mutant mice complements our previous work on HCN1 channel function in the retina. We show here in a functional rod-only setting that rod responses following bright light exposure terminate without the counteraction of HCN channels much later than normal. The resulting sustained signal elevation does saturate the retinal network due to an intensity-dependent reduction in the dynamic range. In addition, the lack of rapid adaptational feedback modulation of rod photoreceptor output via HCN1 in this double mutant limits the ability to follow repetitive (flicker) stimuli, particularly under mesopic conditions.

Conclusions

This work corroborates the hypothesis that, in the absence of HCN1-mediated feedback, the amplitude of rod signals remains at high levels for a prolonged period of time, leading to saturation of the retinal pathways. Our results demonstrate the importance of HCN1 channels for regular vision.

Introduction

The retina is able to respond to a wide range of light stimuli by the use of the two photoreceptor subtypes, rods and cones, whose signals converge at different sites in the retina. The highly sensitive rods are able to detect already very low amounts of light, whereas the less sensitive cones mainly contribute to perception under brighter light levels. At intermediate (mesopic) conditions, there is a considerable overlap of the two systems where both photoreceptor types contact onto the same downstream neurons [1, 2]. In order to facilitate a seamless, light-dependent transition from rod- to cone-dominated retinal signalling, their dynamic range has to be tightly controlled.

In the retina, the wide response range is implemented not only at the level of photoreceptors, but also downstream via the use of parallel, independent pathways and intensity-dependent convergence of signals at each stage of retinal processing [3–5]. The primary rod pathway operates at dim light conditions and connects rods via rod bipolar cells to AII amacrine cells and eventually the cone ON pathway. It also suppresses cone OFF signalling. The secondary rod pathway becomes operational at mesopic illuminations. Rod signals access the cone ON pathway via rod-cone electrical coupling through gap junctions [6–9]. In addition, horizontal connections at each level of signal processing (e.g. via gap junctions) are important for several aspects of vision [10].

The dynamic range of rod vision is further regulated by a number of feedback mechanisms. Here, we explored the actions of Hyperpolarization-activated and cyclic nucleotide-gated 1 (HCN1) channels in rods. HCN1 channels are strongly expressed in photoreceptor inner segments [11–13] and are activated after a short delay when light exposure closes CNG channels in the outer retina and hyperpolarizes the membrane potential of photoreceptors. Increased opening of HCN1 channels causes an inward current that drives the membrane potential back to the resting state [13–16]. In previous investigations, we have focused particularly on the importance of HCN1 channels for proper rod-cone-interaction [16]. Here, we studied the isolated rod-specific actions via a genetic impairment of cone function, as usually the intrusion of cone system contributions at higher light intensity renders a rod-specific analysis difficult [15, 16]. For this purpose, we crossbred *Hcn1*$^{-/-}$ mice [17] with *Cnga3*$^{-/-}$ mice [18] in order to obtain *Cnga3*$^{-/-}$ *Hcn1*$^{-/-}$ double knockout mice (DKO) with abolished cone function. The resulting DKOs were examined functionally by means of *in vivo* electrophysiology (ERG) using single flash and flicker paradigms under scotopic and mesopic conditions. *In vivo* retinal imaging, using optical coherence tomography (OCT) and scanning laser ophthalmoscopy (SLO), was also performed to exclude potential morphological alterations.

Materials and Methods

Ethics Statement

All the experimental procedures regarding animals were performed according to the ARVO Statement for the Use of Animals in Ophthalmic and Vision Research and the law of animal

experimentation issued by the German Government, and were finally approved by the local authorities (Regierungspraesidium Tuebingen).

Animals

Two mouse lines were used in this study: the *Cnga3*$^{-/-}$ single mutant [18] and *Cnga3*$^{-/-}$ *Hcn1*$^{-/-}$ double knockout line (DKO). DKOs were generated by crossbreeding single *Hcn1*$^{-/-}$ and *Cnga3*$^{-/-}$ animals and subsequent breeding of F1 heterozygotes. We identified double mutant mice in the F2 generation by PCR analysis of genomic DNA as described for the individual lines [17, 18]. All mice were examined at the age of 1 month because firstly retinal development is usually complete at this time point. Secondly, this time point is optimal for the analysis of primary functional changes due to a genetic defect in mice in-dependent of secondary changes (e.g degeneration) [19–21]. Lack of cone photoreceptor function due to a genetic ablation of the *Cnga3* gene has been found to secondarily induce synaptic remodelling to some degree [22]. Nevertheless, a functional alteration of rod system activity has so far not been described and was also not observed in previous studies involving ERG examinations [19–21]. So, this aspect remains at present of a theoretical nature.

Electroretinography (ERG)

ERGs were performed according to procedures described previously [19, 20] using a Ganzfeld bowl, a signal amplifier, and a PC-based control and recording unit (Toennies Multiliner Vision, Viasys Healthcare, Höchberg, Germany). Custom-made gold wire rings and stainless steel needles (SEI EMG, Cittadella, Italy) were used as active or reference and ground electrodes, respectively. ERGs were recorded binocularly from the corneal surface. Mice were dark-adapted over night. For anaesthesia, a combination of ketamine (66.7 mg per kg body weight) and xylazine (11.7 mg per kg body weight) was utilized. Pupils were dilated prior to the experiments (Mydriaticum Stulln, Stulln, Germany).

Single-flash ERG. Single flash responses were obtained under dark-adapted conditions (without any background illumination). Stimulus intensity from white flashes were categorized into low scotopic (0.1 and 1 mcd*s/m^2), high scotopic (10 mcd*s/m^2), low mesopic (0.03–0.3 cd*s/m^2) and high mesopic (1–25 cd*s/m^2) as described previously [23]. The intensity series was divided into ten steps of 0.5 or 1 log units and each trace were averaged from ten responses, with an inter-stimulus interval of 5 s (for $<$ 1 cd*s/ m^2) or 17 s (for 1 to 25 cd*s/ m^2). Band-pass filter frequencies were 0.3 and 300 Hz.

Steady-state flicker ERG. Dark-adapted flicker ERGs were performed with increasing frequency from 0.5 to 5 Hz at a fixed high mesopic intensity (3 cd*s/m^2) without background illumination [21]. Responses were averaged either 20 times (for 0.5, 1, 2, and 3 Hz) or 30 times (for 5 Hz) over time, i.e. steady-state recordings. Band-pass filter frequencies were 0.3 and 300 Hz.

Flicker ERG with a defined onset. A dark-adapted direct-current amplification (DC) flicker protocol was used at high scotopic conditions (10 mcd*s/m^2) with traces of 1s length [16] to assess the transition from the resting state towards steady-state conditions. For this analysis, 20 flicker responses were averaged for all frequencies.

This protocol allows to determine the range temporarily not available for light-driven responses due to the elevation of baseline (refractory range, RR), and the remaining dynamic range for light driven responses (DR).

In the DC protocol, the RR is given by the difference between the new flicker baseline at steady state and the baseline before stimulation as the reference. The DR is determined as the new amplitude of the flicker at steady state. Band-pass filter frequency settings for the DC protocol were 0 and 300 Hz.

Statistical analysis. The Mann-Whitney rank sum test was used in selected cases to test for statistical significance of differences between ERG amplitudes of *Cnga3*$^{-/-}$ single mutant and *Cnga3*$^{-/-}$ *Hcn1*$^{-/-}$ DKO mice. At a level of $p<0.05$, differences were considered to be statistically significant and marked with an asterisk (*) in respective figures. Lower p values were further marked with additional asterisks (** for $p<0.01$, and *** for $p<0.001$).

Scanning-Laser Ophthalmoscopy (SLO)

SLO imaging was performed with a HRA 1 system (Heidelberg Engineering, Heidelberg, Germany) in order to visualize the retinal structures of the anesthetized DKO animals (n = 6 eyes) according to previously described procedures [24]. Briefly, the HRA 1 features lasers in the short (visible) wavelength range (488 nm in both and 514 nm in HRA 1 only), and also in the long (infrared) wavelength range (795/830 nm and 785/815 nm). The 488 and 795 nm lasers are used for fluorescein (FLA) and indocyanine green (ICG) angiography, respectively.

Spectral-Domain Optical Coherence Tomography (SD-OCT)

SD-OCT imaging was performed in DKO mice (n = 6 eyes) in the same session as SLO and it was carried out with a Spectralis HRA+OCT device (Heidelberg Engineering GmbH, Heidelberg, Germany). This device features a super luminescent diode at 870 nm as low coherence light source. Scans are acquired at a speed of 40,000 scans per second and each two-dimensional B-scan contains up to 1536 A-scans. [25]. The images were taken with the equipment set of 30° field of view and with the software Heidelberg Eye Explorer (HEYEX version 5.3.3.0, Heidelberg, Germany).

Results

HCN1 Deficiency Leads to an Intensity-Dependent Prolongation of the Rod B-Wave

Before the functional analysis, we examined whether the lack of HCN1 channels in DKO mice influenced retinal morphology. *In vivo* imaging in DKO mice indicated no abnormalities in retinal structure, neither in SLO fundus images (Fig 1A–1D) nor in OCT cross sections (Fig 1E–1G).

Next, we asked whether lack of HCN1 channels in this rod-specific DKO line would cause an ERG phenotype similar to that found in non-selective *Hcn1*$^{-/-}$ models [16, 17]. Indeed, the absence of HCN1 channels resulted in unphysiologically prolonged b-wave signals which remained elevated even at 100 ms after light stimulation, corroborating our previous hypotheses. The results are summarized in Fig 2, a compilation of single flash ERGs of *Cnga3*$^{-/-}$ (left) and DKO animals (right) under dark-adapted conditions. For this purpose, we used *Cnga3*$^{-/-}$ mice as control animals since they were found to produce regular rod system response in previous studies involving ERG [19–21].

At low light intensities (Fig 2A; 0.1 and 1 mcd*s/m^2) ERG data were comparable between both mouse lines; however, a slight tendency towards the HCN1 phenotype was already visible in DKOs at 0.01 cd*s/m^2 (Fig 2A, right). At brighter light intensities, the prolongation became more pronounced (Fig 2A, right and Fig 2C, arrows). The b-wave amplitudes, determined from the trough to the peak of the positive deflection, were comparable between *Cnga3*$^{-/-}$ and DKO mice (Fig 2B). This is due to the fact that b-wave amplitude measurement does not include later parts of the response waveform, where most of the HCN1 phenotype is present (Fig 2A and 2C). In order to highlight the delayed response termination in DKO, we quantified ERG responses from both mouse lines at a later time-point (200 ms after stimulation) [16]. These data underline that a marked difference is already present at 0.01 cd*s/m^2 ($p = 0.038$), but further increases at 0.1 and 1 cd *s/m^2 ($p = 0.010$ for both intensities) (Fig 2D).

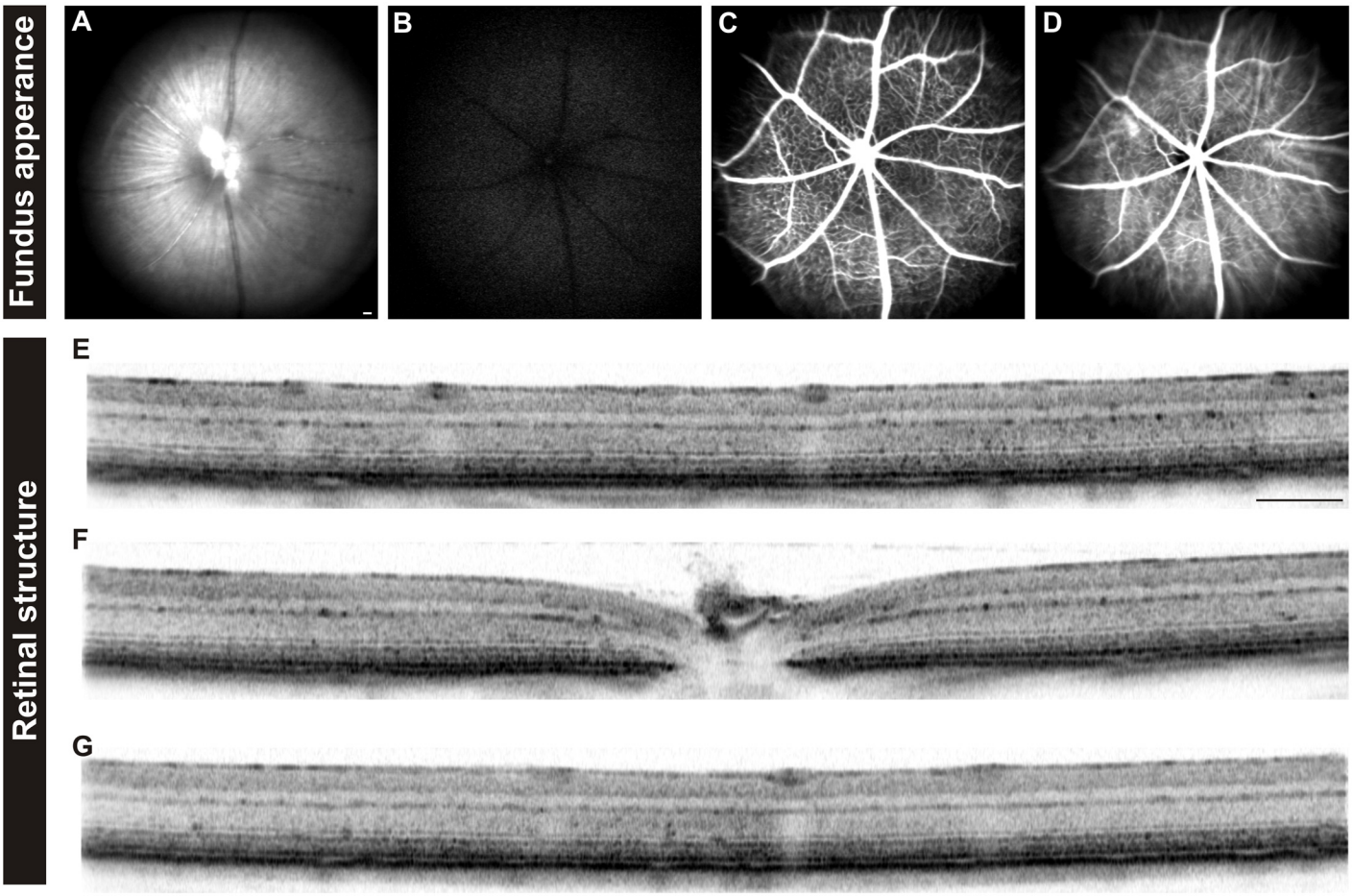

Fig 1. *In vivo* retinal imaging in *Cnga3*$^{-/-}$ *Hcn1*$^{-/-}$ DKO mice. DKO mice (n = 6 eyes) were examined with SLO (A-D) and OCT (E-G). Examinations included fundus native imaging (A), autofluorescence imaging (B), as well as fluorescein angiography (C) and indocyanine green angiography (D). For the OCT analyses, horizontal scans through the dorsal (E), central (F) and ventral part (G) of the retina are shown. *In vivo* imaging of the retina indicates that no signs of retinal degeneration, vascular alterations, or disturbances in the retinal layering of DKO mice. Scale bars (A-G): 200 μm.

doi:10.1371/journal.pone.0147728.g001

The intensity series in Fig 2 clearly showed the voltage-dependent activity of HCN1 channels in rod photoreceptor inner segments, since a substantial effect of HCN1-deficiency was discernible only at higher flash intensities above 30 mcd*s/m^2. In contrast, non-functional HCN1 channels do not affect rod photoreceptor outer segment currents, which was confirmed in *Hcn1*$^{-/-}$ mice [16]; similarly also in DKO mice, no differences were found in the analysis of the a-wave amplitude and implicit-time (data not shown).

In particular, a more detailed comparison between ERG amplitudes of the newly generated DKOs in this work and single *Hcn1*$^{-/-}$ recordings [16, 17] revealed that the prolongation of the b-wave was less pronounced in the DKOs than in *Hcn1*$^{-/-}$ mice, indicating that cone system contributions were indeed present in ERG signals of single mutant mice, whereas these signals were absent in DKOs.

HCN1-Deficiency Reduces the FFF at High Scotopic Conditions

In DKOs, the prolongation of b-waves in the dark-adapted intensity series led us to suppose that, due to the lack of internal HCN1-mediated feedback, rod system responses may be transiently saturated. In ERG, this would become noticeable as a reduced ability to respond to

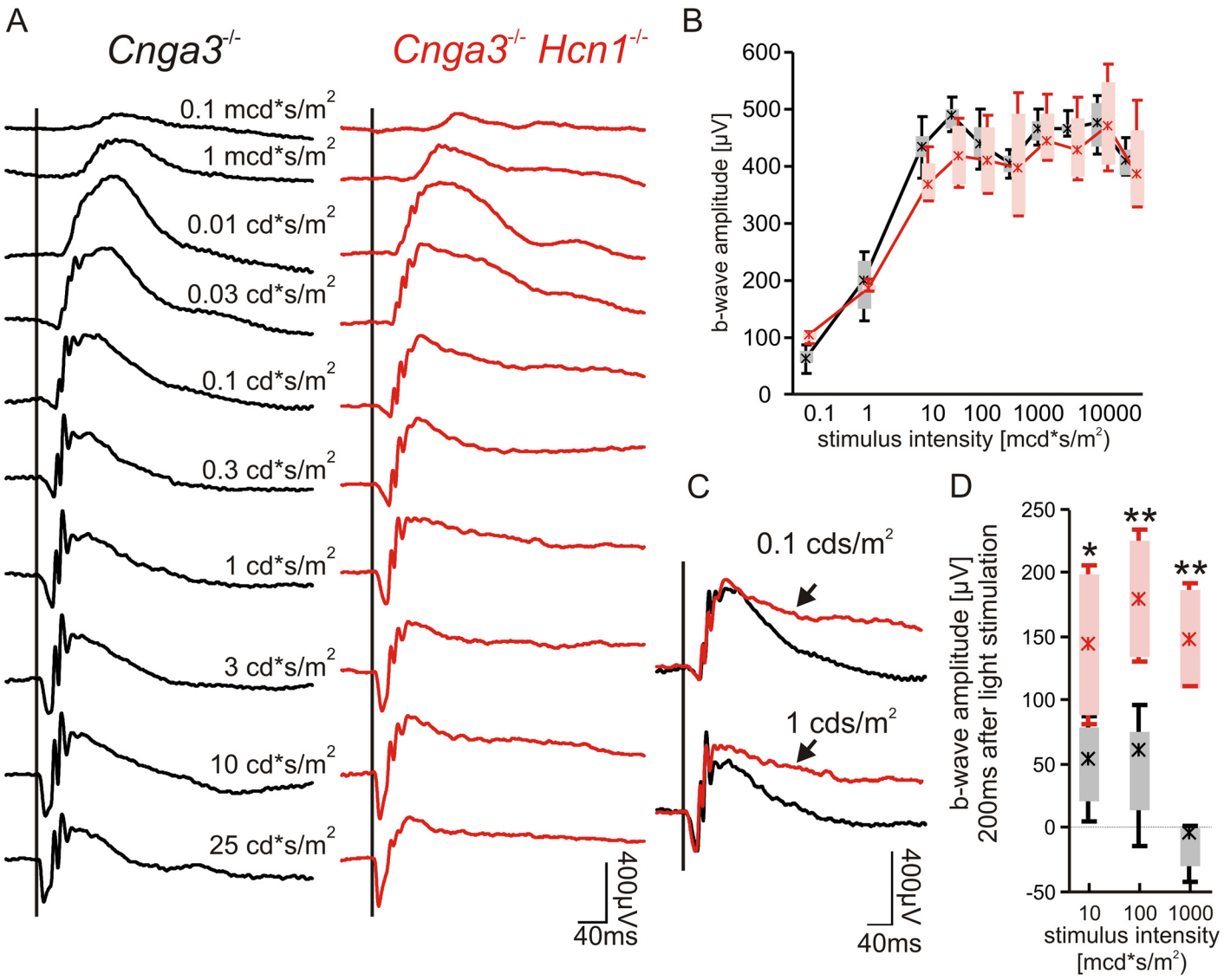

Fig 2. Effect of HCN1 on dark-adapted single flash ERG. (A) Representative ERG traces of an intensity series for a *Cnga3*$^{-/-}$ (left) and a DKO (right) mouse. (B) Quantitative evaluation of b-wave amplitudes (box-and-whisker-plots) for the entire group of *Cnga3*$^{-/-}$ (n = 8 eyes) and DKO (n = 4 eyes). Boxes: 25%-75% quantile range, whiskers: 5% and 95% quantiles, asterisks: median. (C) Superpositions of selected ERG recordings from *Cnga3*$^{-/-}$ mice and DKOs at 0.1 (top) and 1 (bottom) cd*s/m^2. (D) Amplitudes of selected single flash ERG traces 200 ms after stimulus onset. Statistically significant differences are indicated with asterisks (*p<0.05 for 0.01 cd*s/m^2 and **p = 0.01 for 0.1 and 1 cd *s/m^2. Lack of HCN1 leads to an unphysiological prolongation of the b-waves in DKOs at high light intensities.

doi:10.1371/journal.pone.0147728.g002

repetitive stimuli, i.e. a lowered flicker fusion frequency (FFF). To investigate this hypothesis, we assessed the transition from the resting state to steady-state conditions by recording single traces of flicker ERG with a defined onset. This enabled us to retain information about the signal baseline before and during light stimulation, including the refractory range (RR) and the remaining dynamic range (DR).

Two key factors that influence the flicker ERG are the signal baseline level and the basal DR, which are illustrated in Fig 3A. In a frequency series, signal baseline level (Fig 3A, red line) is increasingly elevated whenever single ERG responses are unable to reach the initial level before onset of the following response (dotted line), creating a refractory range (RR) spanned by the

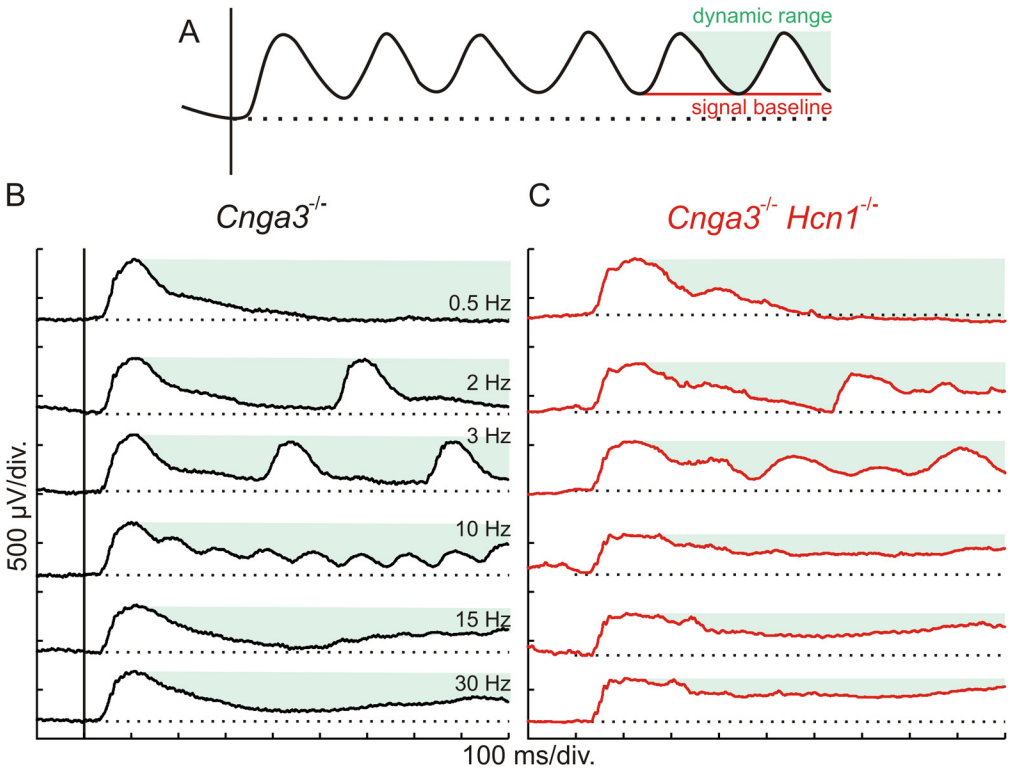

Fig 3. Effect of HCN1 on flicker fusion frequency under high scotopic conditions. (A) Scheme of an ERG flicker response, highlighting characteristic parameters of the record: the dynamic range (DR, green shaded area), the signal baseline (red line) and the baseline prior to the stimulus (dotted black line). (B, C) Scotopic direct current ERGs of a *Cnga3*$^{-/-}$ and a DKO mouse under high scotopic conditions (0.01 cd*s /m^2). In *Cnga3*$^{-/-}$ controls (B), increasing inability of the rod system response to reach signal baseline decreases the DR, leading to a flicker fusion frequency (FFF) of about 15Hz. The additional prolongation of the rod response due to HCN1 deficiency limits its DR to a much greater extent and thus reduces the FFF (C). In total, DC measurements were performed in n = 6 eyes for Cnga3$^{-/-}$ mice and n = 4 eyes for DKO mice.

doi:10.1371/journal.pone.0147728.g003

original baseline (dotted line) and the new baseline level. An increase in RR does in turn reduce the DR (green shaded area) for subsequent responses.

The flicker response characteristics of *Cnga3*$^{-/-}$ and DKOs are presented in Fig 3B and 3C. In *Cnga3*$^{-/-}$ animals, the rod system was able to follow high flicker frequencies up to about 12–18 Hz. In the representative flicker series shown here, the FFF was slightly above 15Hz and traces at frequencies above FFF were close to single flash-like responses. In contrast, the prolongation of the rod system response due the lack of HCN1 channels caused a remarkable reduction of the FFF in DKOs down to 7-10Hz, together with an elevation of the baseline abnormally increasing with frequency (Fig 3C). At frequencies above the FFF, the flicker ERG signal remained elevated with no remaining DR, resulting in a step-like response as described for *Hcn1*$^{-/-}$ in our previous study [17]. These data corroborate the important role of HCN1 channels in rod vision. In particular, HCN1 channels enable the rod system to resolve higher frequencies by extending their DR at the photoreceptor level at intensities of 0.01 cd*s/m^2 and above.

HCN1-Deficiency Reduces the FFF at High Mesopic Conditions

Finally, we addressed the question whether the lack of HCN1 influences the FFF also under high mesopic conditions at 3 cd*s/m^2. We used conventional steady-state ERG flicker recordings, where responses were continuously averaged. The normal rod system is able to respond under these conditions only to low temporal frequencies of up to 3 Hz (Fig 4A, red bar) [21].

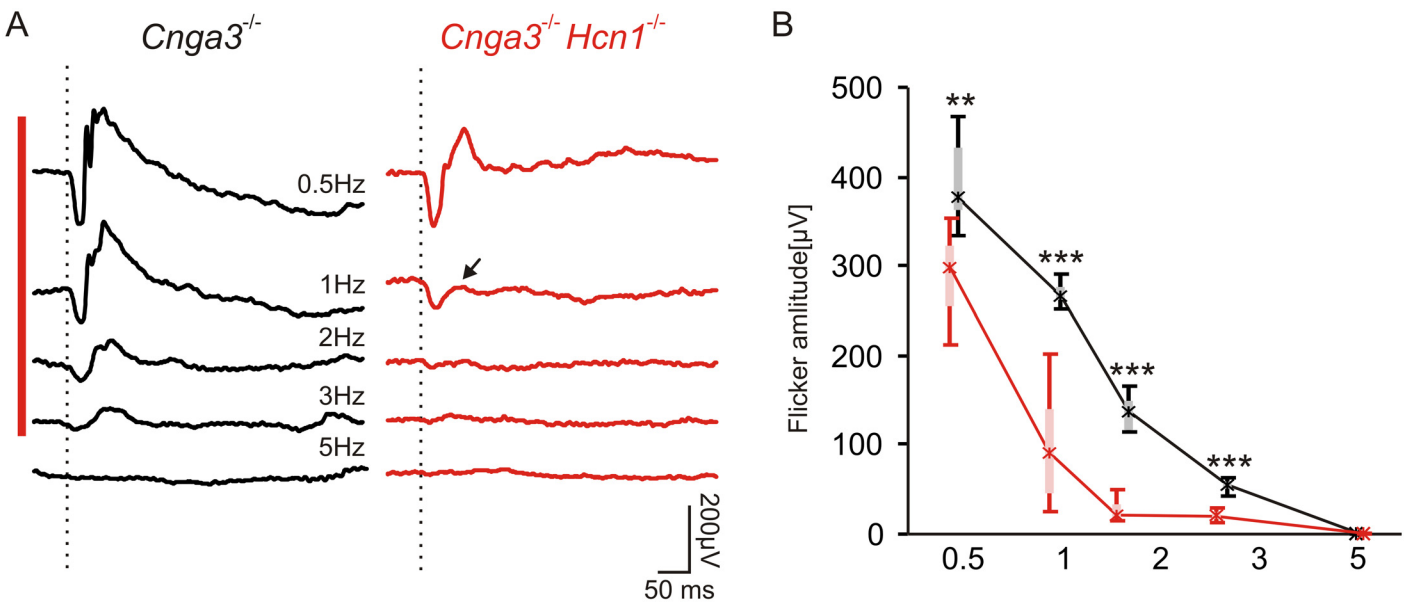

Fig 4. Rod flicker ERG under high mesopic conditions. (A) Steady-state flicker ERG of a *Cnga3*$^{-/-}$ (left) and a DKO (right) mouse under high mesopic conditions (3 cd*s/m^2). (B) Quantification of flicker ERG amplitudes of *Cnga3*$^{-/-}$ (n = 8 eyes) and DKOs (n = 8 eyes), indicating a strong reduction of rod flicker responses in DKO mice. Boxes: 25%-75% quantile range, whiskers: 5% and 95% quantiles, asterisks: median. Statistically significant differences are indicated with asterisks (**p<0.01 for 0.5 Hz and ***p<0.001 for 1–3 Hz). HCN1 deficiency reduces the ability to follow flicker under high mesopic conditions even further (A, red bar).

doi:10.1371/journal.pone.0147728.g004

In DKO, ERG responses were even more reduced with increasing frequency (Fig 4A, right), with a tendency to a stronger reduction of the positive deflection relative to the negative deflection (Fig 4A right, arrow). A summary of flicker amplitude data from *Cnga3*$^{-/-}$ and DKO mice, including the analysis of the positive deflection (Fig 4B), further illustrates the significant reduction in FFF at 0.5 Hz ($p = 0.002$) and above ($p<0.001$ for 1–3 Hz).

Discussion

In this study, we investigated the role of HCN1 channels in rod photoreceptors for the enhancement of rod system responsivity under conditions of light exposure. To isolate HCN1 channel actions in rod system responses, we generated *Hcn1*$^{-/-}$ *Cnga3*$^{-/-}$ double knockout mice. The *Cnga3*$^{-/-}$ line is a model of achromatopsia type 2 and particularly specific in the removal of any light-activated cone signalling, while the rod system stays functionally intact [18]. *Hcn1*$^{-/-}$ *Cnga3*$^{-/-}$ double knockout mice thus allow to study rod-driven visual activity in HCN1-deficient mutants. We found that a lack of HCN1-mediated feedback in rod photoreceptor cells indeed prolongs rod responses and saturates the downstream retinal network during bright light stimulation (Fig 2). In ERG analyses, this was noticeable as a reduced dynamic range (DR) and a lowered flicker fusion frequency (FFF, Figs 3 and 4). Feedback mechanisms are common strategies of the mammalian retina to avoid saturation of the neuronal network. A further example is the triad of synapses between rod bipolar cells and AII and A17 amacrine cells. These triads modulate rod bipolar output signals and consequently influence the saturation of rod vision [23]. When comparing these adaptive mechanisms, they appear to share the same goal: To avoid saturation without compromising sensitivity. Evolutionary, one may speculate that the maximal sensitivity of vision in darkness is an advantage that is equally helpful to the ability to rapidly perceive light-evoked signals again following a saturating stimulus, both for predators and prey.

With more and more details about the functional components of photoreceptors emerging, modelling of entire cells comes within reach. Our rod-specific *in vivo* data does provide first-hand information for the implementation of such models and generally for computational studies dealing with saturation of the rod system.

In summary, we show that HCN1 channel feedback enhances the dynamic range of the rod system in order to limit the period of saturation following bright light exposure, while leaving rod sensitivity untouched. The newly generated *Cnga3*$^{-/-}$ *Hcn1*$^{-/-}$ double mutant is a valuable specific model and a crucial building block to understand and model the role of HCN1 channels in shaping mammalian vision.

Acknowledgments

The authors wish to thank Gudrun Utz and Pia Lacroix for their technical assistance. This work was supported by the Deutsche Forschungsgemeinschaft (DFG, grants Se837/4-1, 5–2, and 6–2).

Author Contributions

Conceived and designed the experiments: VS NT MWS. Performed the experiments: VS NT MGG. Analyzed the data: VS NT MGG. Contributed reagents/materials/analysis tools: SM MB. Wrote the paper: VS NT MWS.

References

1. Sharpe LT, Stockman A. Rod pathways: the importance of seeing nothing. Trends Neurosci. 1999; 22:497–504 PMID: 10529817
2. Wässle H. Parallel processing in the mammalian retina. Nat Rev. Neurosci. 2004; 5:747–757 PMID: 15378035
3. Rieke F, Rudd ME. The challenges natural images pose for visual adaptation. Neuron. 2009; 64:605–16. doi: 10.1016/j.neuron.2009.11.028 PMID: 20005818
4. Völgyi B, Deans MR, Paul DL, Bloomfield SA et al. Convergence and segregation of the multiple rod pathways in mammalian retina. J Neurosci. 2004; 24:11182–92 PMID: 15590935
5. Kolb H. The organization of the outer plexiform layer in the retina of the cat: electron microscopy observations. J Neurocytol. 1977; 6:131–153. PMID: 856949
6. Abd-El-Barr MM, Pennesi ME, Saszik SM, Barrow AJ, Lem J, Bramblett DE et al. Genetic dissection of rod and cone pathways in the dark-adapted mouse retina. J Neurophysiol. 2009; 102:1945–55. doi: 10.1152/jn.00142.2009 PMID: 19587322
7. Lee EJ, Han JW, Kim HJ, Kim IB, Lee MY, Oh SJ et al. The immuncyto-chemical localization of connexin 36 at rod and cone gap junctions in the guinea pig retina. Eur J Neurosci. 2003; 18:2925–2934. PMID: 14656288
8. Feigenspan A, Janssen-Bienhold U, Hormuzdi S, Monyer H, Degen J, Söhl GI et al. Expression of connexin36 in cone pedicles and OFF-cone bipolar cells of the mouse retina. J Neurosci. 2004; 24:3325–3334. PMID: 15056712
9. Raviola E, Gilula NB. Gap junctions between photoreceptor cells in the vertebrate retina. Proc Natl Acad Sci. USA. 1973; 70:1677–1681. PMID: 4198274
10. Nelson R. Cat cones have rod input: a comparison of the response properties of cones and horizontal cell bodies in the retina of the cat. J Comp Neurol. 1977; 172:109–135. PMID: 838876
11. Müller F, Scholten A, Ivanova E, Haverkamp S, Kremmer E, Kaupp UB. HCN channels are expressed differentially in retinal bipolar cells and concentrated at synaptic terminals. Eur J Neurosci. 2003; 17:2084–96. PMID: 12786975
12. Ivanova E, Müller F. Retinal bipolar cell types differ in their inventory of ion channels. Vis Neurosci. 2006; 23:143–54. PMID: 16638168
13. Della Santina L, Piano I, Cangiano L, Caputo A, Ludwig A, Cervetto L et al. Processing of retinal signals in normal and HCN deficient mice. PLOS ONE. 2012; 7:e29812. doi: 10.1371/journal.pone.0029812 PMID: 22279546

14. Barrow AJ, Wu SM. Low-conductance HCN1 ion channels augment the frequency response of rod and cone photoreceptors. J Neurosci 2009; 29:5841–5853. doi: 10.1523/JNEUROSCI.5746-08.2009 PMID: 19420251

15. Knop GC, Seeliger MW, Thiel F, Mataruga A, Kaupp UB, Friedburg C et al. Light responses in the mouse retina are prolonged upon targeted deletion of the HCN1 channel gene. Eur J Neurosci. 2008; 28:2221–2230. doi: 10.1111/j.1460-9568.2008.06512.x PMID: 19019198

16. Seeliger MW, Brombas A, Weiler R, Humphries P, Knop G, Tanimoto N. Modulation of rod photoreceptor output by HCN1 channels is essential for regular mesopic cone vision. Nat Commun. 2011; 2:532. doi: 10.1038/ncomms1540 PMID: 22068599

17. Nolan MF, Malleret G, Lee KH, Gibbs E, Dudman JT, Santoro B et al. The hyper-polarization-activated HCN1 channel is important for motor learning and neuronal integration by cerebellar Purkinje cells. Cell. 2003; 115:551–64. PMID: 14651847

18. Biel M, Seeliger MW, Pfeifer A, Kohler K, Gerstner A, Ludwig A et al. Selective loss of cone function in mice lacking the cyclic nucleotide-gated channel CNG3. Proc Natl Acad Sci U S A. 1999; 96:7553–7. PMID: 10377453

19. Tanimoto N, Muehlfriedel RL, Fischer MD, Fahl E, Humphries P, Biel M et al. Vision tests in the mouse: Functional phenotyping with electroretinography. Front Biosci (Landmark Ed). 2009; 14:2730–7.

20. Tanimoto N, Sothilingam V, Seeliger MW. Functional phenotyping of mouse models with ERG. Methods Mol Biol. 2013; 935:69–78. doi: 10.1007/978-1-62703-080-9_4 PMID: 23150360

21. Tanimoto N, Sothilingam V, Kondo M, Biel M, Humphries P, Seeliger MW. Electroretinographic assessment of rod- and cone-mediated bipolar cell pathways using flicker stimuli in mice. Sci Rep. 2015; 5:10731 doi: 10.1038/srep10731 PMID: 26029863

22. Haverkamp S, Michalakis S, Claes E, Seeliger MW, Humphries P, Biel M et al. Synaptic plasticity in CNGA3(-/-) mice: cone bipolar cells react on the missing cone input and form ectopic synapses with rods. J Neurosci. 2006; 26:5248–55. PMID: 16687517

23. Tanimoto N, Sothilingam V, Euler T, Ruth P, Seeliger MW, Schubert T. BK channels mediate pathway-specific modulation of visual signals in the in vivo mouse retina. J Neurosci. 2012; 32:4861–6 doi: 10.1523/JNEUROSCI.4654-11.2012 PMID: 22492042

24. Seeliger MW, Beck SC, Pereyra-Munoz N, Dangel S, Tsai JY, Luhmann UF et al. In vivo confocal imaging of the retina in animal models using scanning laser ophthalmoscopy. Vision Res. 2005; 45: 3512–9. PMID: 16188288

25. Fischer MD, Huber G, Beck SC, Tanimoto N, Muehlfriedel R, Fahl E et al. Noninvasive, in vivo assessment of mouse retinal structure using optical coherence tomography. PLOS ONE. 2009; 4:e7507. doi: 10.1371/journal.pone.0007507 PMID: 19838301

V. Appendix

Paper IV: Mosaic synaptopathy and functional defects in Cav1.4 heterozygous mice and human carriers of CSNB2

Michalakis S, Shaltiel L, **Sothilingam V**, Koch S, Schludi V, Krause S, Zeitz C, Audo I, Lancelot ME, Hamel C, Meunier I, Preising MN, Friedburg C, Lorenz B, Zabouri N, Haverkamp S, Garcia Garrido M, Tanimoto N, Seeliger MW, Biel M, Wahl-Schott CA[§].

Published in Human Molecular Genetics
21:4486-4496 (2014)

Human Molecular Genetics, 2013 ***1–13***
doi:10.1093/hmg/ddt541

Mosaic synaptopathy and functional defects in Cav1.4 heterozygous mice and human carriers of CSNB2

Stylianos Michalakis[1], Lior Shaltiel[1], Vithiyanjali Sothilingam[2], Susanne Koch[1], Verena Schludi[1], Stefanie Krause[1], Christina Zeitz[3,4,5], Isabelle Audo[3,4,5,6,7], Marie-Elise Lancelot[3,4,5], Christian Hamel[8], Isabelle Meunier[8], Markus N. Preising[9], Christoph Friedburg[9], Birgit Lorenz[9], Nawal Zabouri[10], Silke Haverkamp[10], Marina Garcia Garrido[2], Naoyuki Tanimoto[2], Mathias W. Seeliger[2], Martin Biel[1] and Christian A. Wahl-Schott[1,*]

[1]Center for Integrated Protein Science Munich (CIPSM) and Department of Pharmacy—Center for Drug Research, Ludwig-Maximilians-Universität München, 81377 Munich, Germany [2]Division of Ocular Neurodegeneration, Institute for Ophthalmic Research, Centre for Ophthalmology, University of Tübingen, 72076 Tübingen, Germany [3]INSERM, UMR_S968, Paris F-75012, France [4]CNRS, UMR_7210, Paris F-75012, France [5]UPMC Univ Paris 06, UMR_S 968, Institut de la Vision, Paris F-75012, France [6]Centre Hospitalier National d'Ophtalmologie des Quinze-Vingts, INSERM-DHOS CIC 503, Paris F-75012, France [7]UCL-Institute of Ophthalmology, London EC1V 9EL, UK [8]CHRU, Genetics of Sensory Diseases, Montpellier 34091, France [9]Department of Ophthalmology, Justus-Liebig-University Giessen, Universitätsklinikum Giessen and Marburg GmbH, Giessen Campus, 35392 Giessen, Germany [10]Neuroanatomy, Max-Planck-Institute for Brain Research, 60438 Frankfurt/M, Germany

Received September 6, 2013; Revised and Accepted October 24, 2013

Mutations in *CACNA1F* encoding the α_1-subunit of the retinal Cav1.4 L-type calcium channel have been linked to Cav1.4 channelopathies including incomplete congenital stationary night blindness type 2A (CSNB2), Åland Island eye disease (AIED) and cone-rod dystrophy type 3 (CORDX3). Since *CACNA1F* is located on the X chromosome, Cav1.4 channelopathies are typically affecting male patients via X-chromosomal recessive inheritance. Occasionally, clinical symptoms have been observed in female carriers, too. It is currently unknown how these mutations lead to symptoms in carriers and how the retinal network in these females is affected. To investigate these clinically important issues, we compared retinal phenotypes in Cav1.4-deficient and Cav1.4 heterozygous mice and in human female carrier patients. Heterozygous *Cacna1f* carrier mice have a retinal mosaic consistent with differential X-chromosomal inactivation, characterized by adjacent vertical columns of affected and non-affected wild-type-like retinal network. Vertical columns in heterozygous mice are well comparable to either the wild-type retinal network of normal mice or to the retina of homozygous mice. Affected retinal columns display pronounced rod and cone photoreceptor synaptopathy and cone degeneration. These changes lead to vastly impaired vision-guided navigation under dark and normal light conditions and reduced retinal electroretinography (ERG) responses in *Cacna1f* carrier mice. Similar abnormal ERG responses were found in five human *CACNA1F* carriers, four of which had novel mutations. In conclusion, our data on Cav1.4 deficient mice and human female carriers of mutations in *CACNA1F* are consistent with a phenotype of mosaic CSNB2.

*To whom correspondence should be addressed at: Department Pharmazie, Pharmakologie für Naturwissenschaften, Ludwig-Maximilians-Universität München, Butenandtstr. 5-13, D-81377 München, Germany. Tel: +49 89218077654; Fax: +49 89218077326; Email: christian.wahl@cup.uni-muenchen.de

INTRODUCTION

Retinal photoreceptors and bipolar cells contain a highly specialized type of synapse designated ribbon synapse (1,2). Neurotransmitter release in these synapses is controlled via graded and sustained changes in membrane potential that are maintained throughout the duration of a light stimulus. Cav1.4 L-type Ca^{2+} channels are the main channel subtype converting these analog input signals into corresponding tonic glutamate release (3–6). Cav1.4 channels are tailored to this function since they display very slow voltage-dependent inactivation (VDI) and a lack of Ca^{2+}-dependent inactivation (CDI). Cav1.4 channels are multisubunit complexes consisting of the principal α_1 and the auxiliary β_{2a} and $\alpha 2\delta$ subunits (3,7). The α_1 subunit of retina-specific Cav1.4 voltage-gated L-type calcium channels is encoded by the X-chromosomal *CACNA1F* gene. Mutations in *CACNA1F* have been identified in patients suffering from congenital stationary night blindness type 2 (CSNB2; incomplete X-linked CSNB; OMIM: 300 071) (8,9), Åland Island eye disease (AIED; OMIM: 300 600) (10,11) and X-linked cone-rod dystrophy (CORDX3; OMIM: 300 476) (12). These channelopathies display similar electroretinographic changes that indicate a loss of neurotransmission from rods to bipolar cells, which is consistent with a loss of Cav1.4 function in rod photoreceptor synapses. In addition, some patients present with varying degrees of cone photoreceptor impairments. Deletion of Cav1.4 in mice leads to profound visual impairment. These mice also seem to have a variable phenotype but in general a more severe phenotype than human patients (13–16).

Cav1.4 channelopathies are transmitted by X-chromosomal inheritance. Therefore, males are affected far more frequently than females. Clinical symptoms have occasionally been observed also in carrier females (17,18). Interestingly, the c.2234T>C, p.Ile745Thr *CACNA1F* mutation (17,19) revealed a severe retinal phenotype in a large New Zealand family with male children showing abnormal color vision and reduced intellectual abilities. More importantly, female carriers presented with abnormal ERGs. The authors argued that the presence of symptoms in female carriers may relate to the specific mutation which results in increased, rather than loss of, activity of the Cav1.4 calcium channel. A mouse model for this particular mutation has been described (14), but the phenotypes of males and females have not yet been reported.

In the present study, we set out to further explore the phenotype observed in female carriers of loss of function mutation in *CACNA1F*. To this end, we addressed this clinically important issue by a comparative analysis of retinal phenotypes in Cav1.4 deficient and Cav1.4 heterozygous mice and compared these results to the clinical information obtained from human female carriers presenting with four novel mutations in *CACNA1F*.

RESULTS

Retinal and visual function in Cav1.4 deficient mice

In the wild-type retina, Cav1.4 protein localizes to rod and cone photoreceptor synapses within the outer plexiform layer (opl) and to a lesser extent to rod bipolar cell synapses in the inner plexiform layer (ipl) (Fig. 1A). In retinas from Cav1.4 deficient

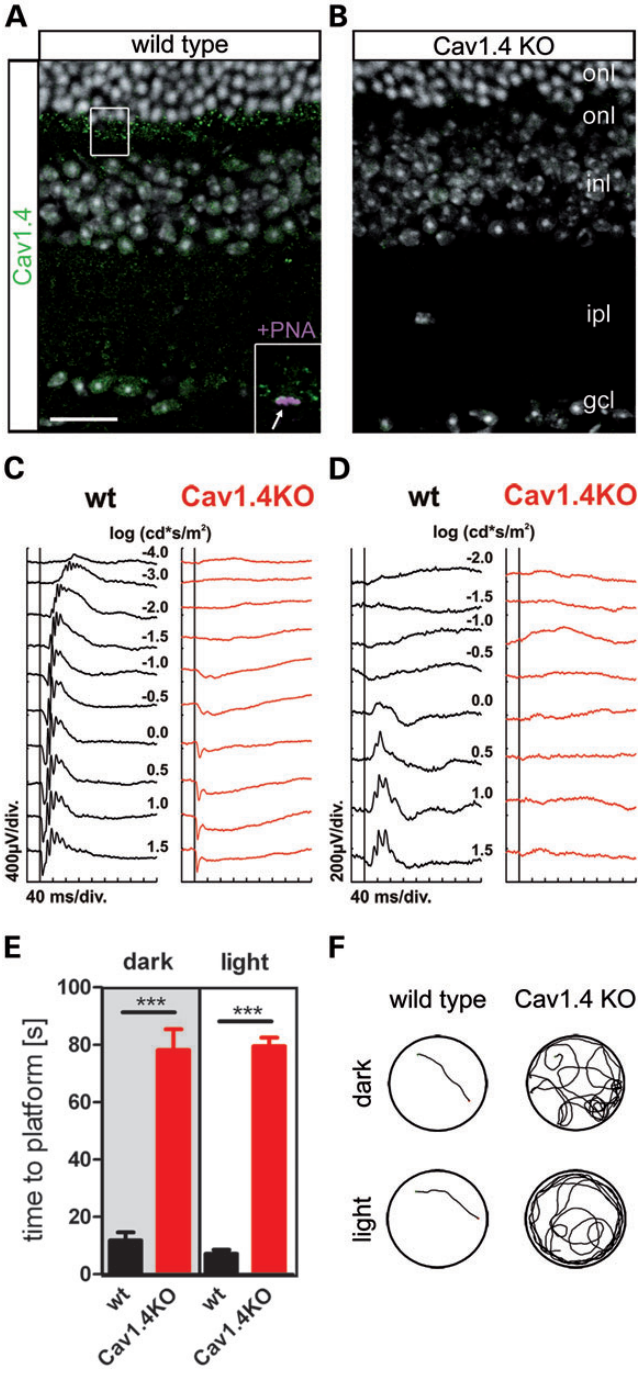

Figure 1. Visual function in *Cacna1f*-knockout mice. (**A** and **B**) Confocal scans of vertical retinal sections from wild-type (A) and *Cacna1f* knockout (Cav1.4-KO) mice (B) labeled with a Cav1.4-specific antibody (green). Cell nuclei were stained with the nuclear dye Hoechst 33342 (grey). Inlay in (A): magnification view on the outer plexiform layer (opl) region marked with a white rectangle illustrating the partial co-localization of the Cav1.4 signal (green) with the cone pedicle marker peanut agglutinin (PNA, magenta). (**C** and **D**) Electroretinographic analysis of retinal function in Cav1.4-KO mice. Representative Ganzfeld-ERG intensity series from dark-adapted (C) and light-adapted (D) wild-type (wt, black traces) and Cav1.4-KO mice (red traces). (**E** and **F**) Performance of Cav1.4-KO mice in a visual water-maze behavioral task. (E) Latency to locate a visible platform under dark (left two bars) and normal light conditions (right two bars). (F) Example swimming paths under dark (upper part) and normal light conditions (lower part). The scale bar marks 20 µm. gcl, ganglion cell layer; inl, inner nuclear layer; ipl, inner plexiform layer; onl, outer nuclear layer.

(Cav1.4-KO) mice (14), Cav1.4 immunoreactivity was not longer present in the opl and the ipl (Fig. 1B). Most immunoreactivity observed in the opl of wild-type retina corresponds to rod photoreceptor synapses. However, double labeling with the cone pedicle marker peanut agglutinin (PNA) revealed that cone photoreceptor synapses are also Cav1.4 immunopositive (Fig. 1A inlay).

The overall retinal function of Cav1.4-KO mice was evaluated by Ganzfeld Electroretinography (ERG) using stimulation protocols to isolate rod- (Fig. 1C) or cone-driven (Fig. 1D) light responses. In the dark-adapted (scotopic) part of the protocol, in which cones are non-responsive, the b-wave component and oscillatory potentials were completely absent in ERG recordings of Cav1.4-KO mice when compared with wild-type mice throughout the stimulus range (Fig. 1C). However, the amplitude and the threshold of the a-wave in Cav1.4-KO mice were similar to wild-type. In the light-adapted (photopic) part of the ERG, in which rods are non-responsive due to desensitization, the b-wave component and oscillatory potentials were also completely absent in Cav1.4-KO mice (Fig. 1D). The absence of a scotopic and photopic b-wave in the Cav1.4-KO mice is consistent with a defect in neurotransmission from both rod and cone photoreceptors to second-order neurons, particularly bipolar cells.

The functional significance of the observed defects in the ERG responses was evaluated by testing the visual performance of Cav1.4-KO mice in a vision-guided water-maze behavioral task. The latency to navigate to a visible platform under dark and normal light conditions was significantly increased in Cav1.4-KO when compared with wild-type mice (Fig. 1E). Moreover, in 37.5 $\pm$ 9.1% of the trials in the dark and 27.3 $\pm$ 4.4% of the trials during light Cav1.4-KO mice did not manage to find the platform within the test period of 2 min (scored as error of omission). In contrast all wild-type mice reached the platform within time in all test trials. Wild-type mice dramatically improved their visual performance on day 2 to a maximum, which could not be further improved during the third test day under dark light conditions (Supplementary Material, Fig. S2A). Under normal light conditions (day four) no further improvement was observed (Supplementary Material, Fig. S2A). In contrast to wild-type mice, Cav1.4-KO mice struggled to locate the platform and showed no improvement during the three successive test days under dark or on the fourth test day under normal light conditions. Consistent with the increased latency of Cav1.4-KO mice the swimming path was much longer (Fig. 1F). To exclude that residual cone function could not be detected in this test paradigm in Cav1.4-KO mice, we tested another group of animals for three consecutive days solely under normal light conditions. Again, wild-type mice displayed a robust learning curve, whereas Cav1.4-KO mice did not show any improvement (Supplementary Material, Fig. S2B), confirming that cone function is also strongly compromised in Cav1.4-KO mice.

Synaptopathy in Cav1.4 deficient mice

Having characterized the functional defects in Cav1.4-KO mice, we set out to analyze the changes of the retinal network architecture of Cav1.4-KO mice at the morphological level. It is well established that second order retinal neurons, e.g. bipolar cells (BC) and horizontal cells (HC) respond to a number of pathological conditions by extending sprouting processes into the outer nuclear layer (onl) (20–23). Staining of wild-type retinas for the horizontal and amacrine cell marker calbindin showed strong labeling of horizontal cell bodies and a dense plexus of horizontal cell processes in the opl (Fig. 2A). In contrast, in retinas of Cav1.4-KO mice calbindin staining was reduced in the opl and numerous elongated horizontal cell neurites extended far into the outer nuclear layer (onl) (Fig. 2B). This phenomenon was also observed in aged animals (Fig. 2C) confirming that it is not restricted to certain age periods. In wild-type retinas, stainings by PKCα, a rod bipolar cell marker, displayed regular arborization of bipolar cell dendrites restricted to the opl (Fig. 2D). In contrast, in retinas of Cav1.4-KO mice, rod bipolar cell dendrites extended beyond the opl, far into the onl (Fig. 2E). Moreover, the staining revealed compromised morphology of rod BC synapses in the ipl of Cav1.4-KO mice (Fig. 2D and E). The PKCα antibody also labels cone outer segments (upper part in Fig. 2D and E), which appear disorganized in Cav1.4-KO mice. The irregular outgrowth of HC and BC neurites concurred with a marked thinning of the opl in Cav1.4-KO retinas when compared with wild-type retina. This was particularly evident in retinal slices stained with the nuclear dye Hoechst 33342 as thinning of the gap between the outer and inner nuclear layers (Fig. 2A–C).

Together, these findings indicate disturbed synaptic contacts between photoreceptors and second order neurons. We therefore performed a set of stainings to evaluate the distribution of presynaptic markers in the Cav1.4-KO retina. The vesicular glutamate transporter 1 (vGlut1) labels rod spherules and cone pedicles in the opl as well as axon terminals of bipolar cells in the ipl (24). The complexins (Cplx) 3 and 4 label cone pedicles or rod and cone synapses, respectively (25). Stainings for vGlut1 (Fig. 2F and G), Cplx3 and Cplx4 (Fig. 2H–K) confirmed a greatly reduced immunoreactivity in the opl and an increased punctuate staining in the onl in Cav1.4-KO mice when compared with wild-type control mice. These results are consistent with a retraction of photoreceptor synapses from the opl into the onl. In addition, the vGlut1 staining revealed a markedly reduced labeling of rod BC synapses in the knockout (Fig. 2F and G), which is in line with the reduction of PKCα stainings in rod BC synapses of Cav1.4-KO mice (Fig. 2E).

Cone photoreceptor degeneration in Cav1.4 deficient mice

We next analyzed whether the severe synaptic pathology is associated with additional changes of photoreceptor morphology. To this end, we labeled wild-type and knockout retinas with rod and cone photoreceptor markers. The rod phototransduction cascade protein rod arrestin (also known as visual arrestin or S-antigen) revealed similar expression and localization in outer segments of wild-type and mutant retinas (Fig. 3A and B). However, the synaptic fraction of rod arrestin labeling (arrows in Fig. 3A) was lost from the opl and partially found in the onl (arrows in Fig. 3B). In contrast, labeling of Cav1.4-KO retinas for the cone photoreceptor-specific homologue cone arrestin revealed a loss of immunosignal compared with wild-type mice (Fig. 3C and D). Specific labeling of cone photoreceptor extracellular matrix by peanut agglutinin (PNA) revealed a loss of cone pedicles in the opl while the morphology of the cone inner and outer segments was normal (Fig. 3E and F).

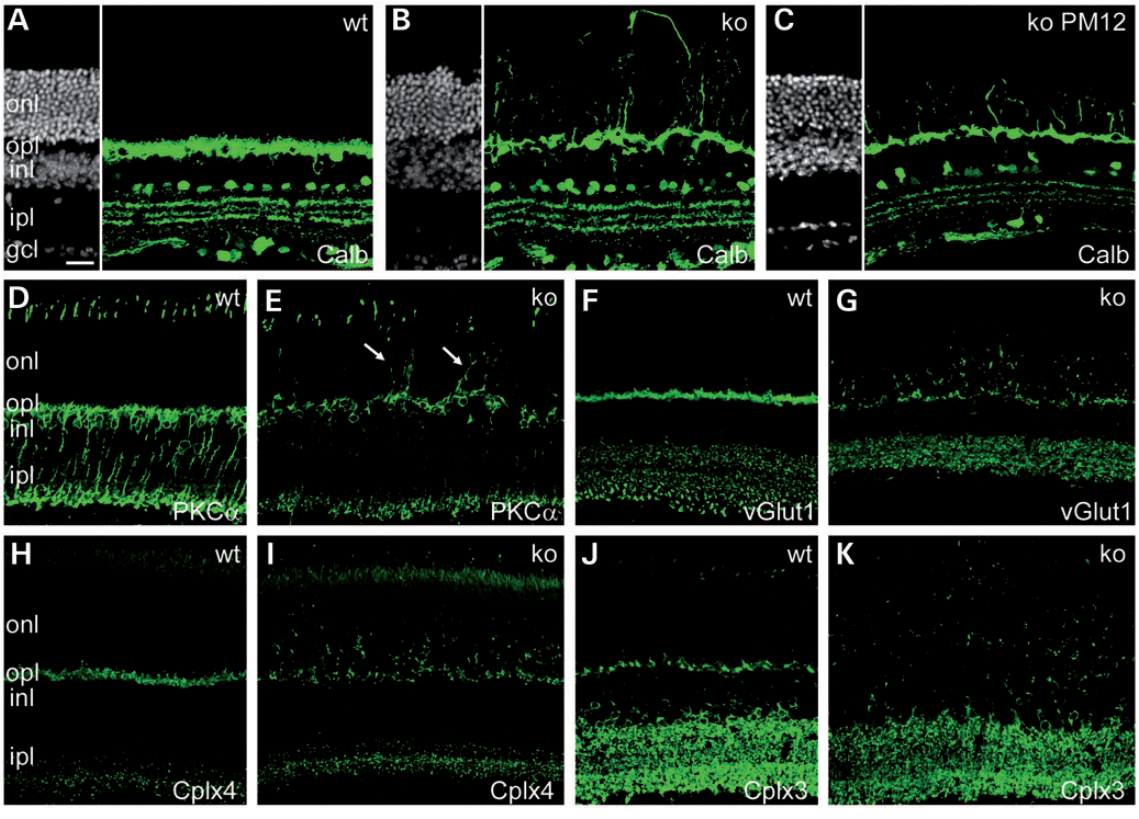

Figure 2. Synaptic changes in *Cacna1f* deficient mice. Confocal scans of vertical retinal sections from wild-type (wt) and Cav1.4-KO (ko) mice. (**A**–**C**) Immunolabeling of horizontal and amacrine cells with calbindin (Calb, green, right parts in A–C). The cell nuclei were stained with the dye Hoechst 33342 (grey) to illustrate the retinal layers (left part in A–C). Horizontal cell neurites extend deep into the outer nuclear layer (onl) in young (6-week-old) (B) and aged (12-month-old, PM 12) ko mice (C). (**D** and **E**) Retinal sections from 6-week-old wt and ko mice immunolabeled with the rod bipolar cell marker protein kinase C alpha (PKCα) (D and E), as well as with the presynaptic markers vesicular glutamate transporter 1 (vGlut1) (**F** and **G**), complexin 4 (Cplx4) (**H** and **I**) and complexin 3 (cplx3) (**J** and **K**). PKCα staining demonstrates pronounced growth of rod bipolar cell dendrites into the onl of Cav1.4-KO mice (arrows in E). Note that PKCα also labels cone outer segments (upper part in D and E), which appear disorganized in the ko (E). The presynaptic markers (F–K) also reveal a disperse redistribution of rod (vGlut1 and Cplx4) and cone (Cplx3) presynaptic elements from the outer plexiform layer (opl) to the onl in the ko (G, I and K). inl, inner nuclear layer; ipl, inner plexiform layer. The scale bar shown in (A) marks 20 μm.

In order to examine whether down-regulation of cone arrestin reflected ongoing cone degeneration, we labeled wild-type and Cav1.4-KO retinas for the Müller glial cell-specific glial fibrillary acid protein (GFAP). In wild-type retina GFAP is only found in Müller glial cell endfeet (Fig. 3G). In contrast, strongly GFAP-positive stress fibers appear in Müller glial cells of Cav1.4-KO mice (Fig. 3H) indicating the presence of a reactive gliosis. A similar reactive gliosis can also be observed in classical mouse models of cone degeneration (21,26).

Together these findings indicate that the synaptopathy in the Cav1.4-KO mouse has no obvious effect on rod outer segment morphology, but is associated with an overall compromised cone photoreceptor morphology and cone degeneration.

Morphological changes in Cav1.4 heterozygous mice (carriers)

Having defined the morphological changes in the Cav1.4-KO retina, we next set out to study whether morphological changes are also present in heterozygous female mice (Cav1.4$^{+/-}$). Distribution of Cav1.4 protein was patchy, characterized by islets of Cav1.4 immunoreactivity and areas without Cav1.4 immunoreactivity next to each other (Fig. 4A–C).

To test the hypothesis that this could result in mosaic synaptic defects in heterozygous mice, we stained for calbindin (Fig. 4D–F), vGlut1 (Fig. 4G–I) and complexin 3 (Fig. 4J–L). This revealed a similar patchy pattern of changes in synaptic morphology. Specifically, retinal network columns with compromised morphology were radially oriented and displayed outgrowths of horizontal cell neurites and bipolar cell dendrites into the onl and thinning of the opl, whereas neighboring non-affected network columns revealed wild-type-like appearance (Fig. 4D–L). Moreover, in affected Cav1.4-KO-like retinal columns of the heterozygous retina, we also observed a loss of cone pedicles (Fig. 4M), down-regulation of cone arrestin (Fig. 4N) and reactive gliosis (Fig. 4O).

We next wondered how the synaptic contacts between photoreceptors and second order neurons are organized in Cav1.4 heterozygous mice, in particular at the border regions between healthy and affected retina. We therefore analyzed retinal slices double-labeled with specific pre- and postsynaptic markers. Figure 5A–C shows images for PKCα and Ctbp2 (Fig. 5A). Ctbp2 is a marker of the photoreceptor synaptic ribbon and labels characteristic horseshoe-shaped structures in rod and cone photoreceptor synapses (27). While Ctbp2 is still expressed in the Cav1.4-KO (data not shown) and in affected

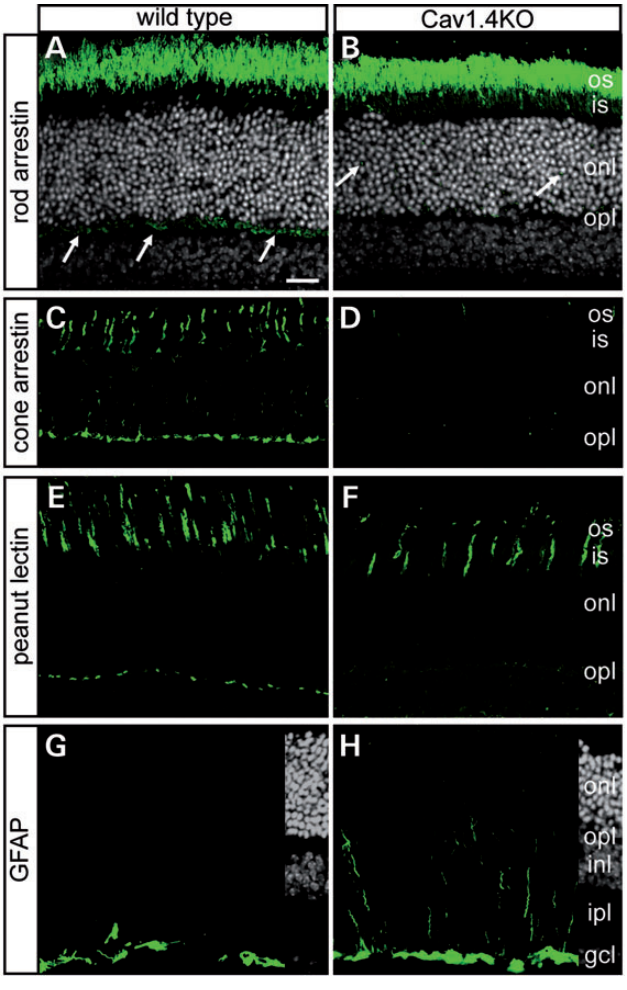

Figure 3. Photoreceptor morphology in *Cacna1f* deficient mice. Confocal scans of vertical retinal sections from 6-week-old wild-type and Cav1.4-KO mice labeled for rod arrestin (**A** and **B**), cone arrestin (**C** and **D**), peanut agglutinin (**E** and **F**) and GFAP (**G** and **H**). (A and B) The outer segment expression and localization of rod arrestin is not compromised in the KO. However, the synaptic fraction of rod arrestin labeling (arrows in A) was lost from the outer plexiform layer (opl) and was partially found in the outer nuclear layer (onl) (arrows in B). Cell nuclei were stained with the nuclear dye Hoechst 33342 (grey). (C and D) Cone arrestin is markedly downregulated throughout the cone cells in the KO (D). (E and F) Peanut lectin staining of cone photoreceptor extracellular matrix reveals a loss of cone pedicles, but preservation of cone inner and outer segment (is, os) morphology. (G and H) Induction of GFAP-positive stress fibers in the KO retina. Right part in panels (G and H) are Hoechst 33342 (grey) images of the respective retinal slices. The scale bar marks 20 μm. gcl, ganglion cell layer; inl, inner nuclear layer; ipl, inner plexiform layer; onl, outer nuclear layer.

parts of the Cav1.4$^{+/-}$ retina (Fig. 5A), the normal signal is decreased in the opl and appears redistributed throughout the onl. Other presynaptic markers relocate similarly (e.g. vGlut1). Interestingly, most of the ectopic Ctbp2 signal in the affected area also had aberrant morphology (Fig. 5B and C). However, ectopic Ctbp2 staining in the onl that was in close proximity to PKCα-positive rod BC dendrite, have an appearance similar to the Ctbp2 signal in the wild-type (data not shown) or healthy parts of the opl in the heterozygous retina (Fig. 5C). Another pair of pre- and postsynaptic markers that we analyzed was vGlut1 and the Cav1.1 voltage-gated L-type calcium channel α_1 subunit (also known as Cacna1 s) (Fig. 5D and E). Cav1.1 localizes to ON BC dendrites in the wild-type and in the non-affected part of the Cav1.4 heterozygous retina (Fig. 5D). In contrast, it is strongly down-regulated in the Cav1.4-KO (14) and the affected part of the Cav1.4 heterozygous retina (Fig. 5D). Interestingly, ectopic Cav1.1 signal could also be seen throughout the onl in the border region between affected and healthy areas of the Cav1.4 heterozygous retina (Fig. 5D and E) suggesting the formation of ectopic synapses between ON BCs within affected retinal columns lacking normal input and neighboring non-affected photoreceptors (Fig. 8).

Functional changes in Cav1.4 heterozygous mice (carriers)

We next assessed the retinal function in Cav1.4$^{+/-}$ mice in analogy to Cav1.4-KO mice. Scotopic ERGs were characterized by reduced b-wave amplitudes and, superimposed on them, oscillatory potentials throughout the stimulus range in the carrier mice when compared with the wild-type (Fig. 6A and B). However, the threshold of the b-wave as well as the amplitude and the threshold of the a-wave were normal in Cav1.4$^{+/-}$ mice. A similar reduction in the b-wave amplitude was also observed for the photopic ERGs (Fig. 6C and D). These findings are characteristic for a functional defect in the transmission of visual signals from rod and cone photoreceptors to bipolar cells in Cav1.4$^{+/-}$ mice.

We also tested whether this impaired retinal processing had any influence on the ability of Cav1.4$^{+/-}$ mice to navigate in a visual water maze. Indeed, the performance of Cav1.4$^{+/-}$ mice under dark conditions was in between the wild-type and Cav1.4-KO mice (Fig. 6E and F), as judged by both, the latency to locate the platform (Fig. 6E) and the errors to find the platform during the trial (errors of omission) (Fig. 6F). Under normal light conditions the phenotype was somewhat milder since heterozygous mice had only slightly increased latencies and did not make any error of omissions (Fig. 6G and H).

CACNA1F mutations and phenotypes in male patients and female carriers

Given the morphological and functional defects in Cav1.4$^{+/-}$ carrier mice, we investigated visual function and morphology in five females carrying *CACNA1F* mutations from families seen by two different clinical centers (Fig. 7; Supplementary Material, Fig. S3). Four of the mutations were novel. The mutation spectrum comprised two missense mutations in exons 6 and 16 (c.764G>A, p.Gly255Glu and c.2090T>C, p.Leu697Pro), which are predicted to cause exchanges of amino acid residues in transmembrane segment S5 of domain I (p.Gly255Glu) and in the pore loop of domain II (p.Leu697Pro). In addition, three mutations were identified, which were predicted either to result in mRNA decay or in a truncated Cav1.4 channel protein: In the mutation (c.2821dupC, p.Leu941Profs*115) a duplication in exon 23 is predicted to cause a frameshift at amino acid residue 941 (segment S3 of domain III), which changes the 115 following amino acid residues. After these 115 residues the protein is truncated. In the mutation (c.4547_4549delinsCC, p.Leu1516Profs*9), a deletion/insertion in exon 39 is predicted to cause a frameshift at the amino acid residue 1516 (proximal

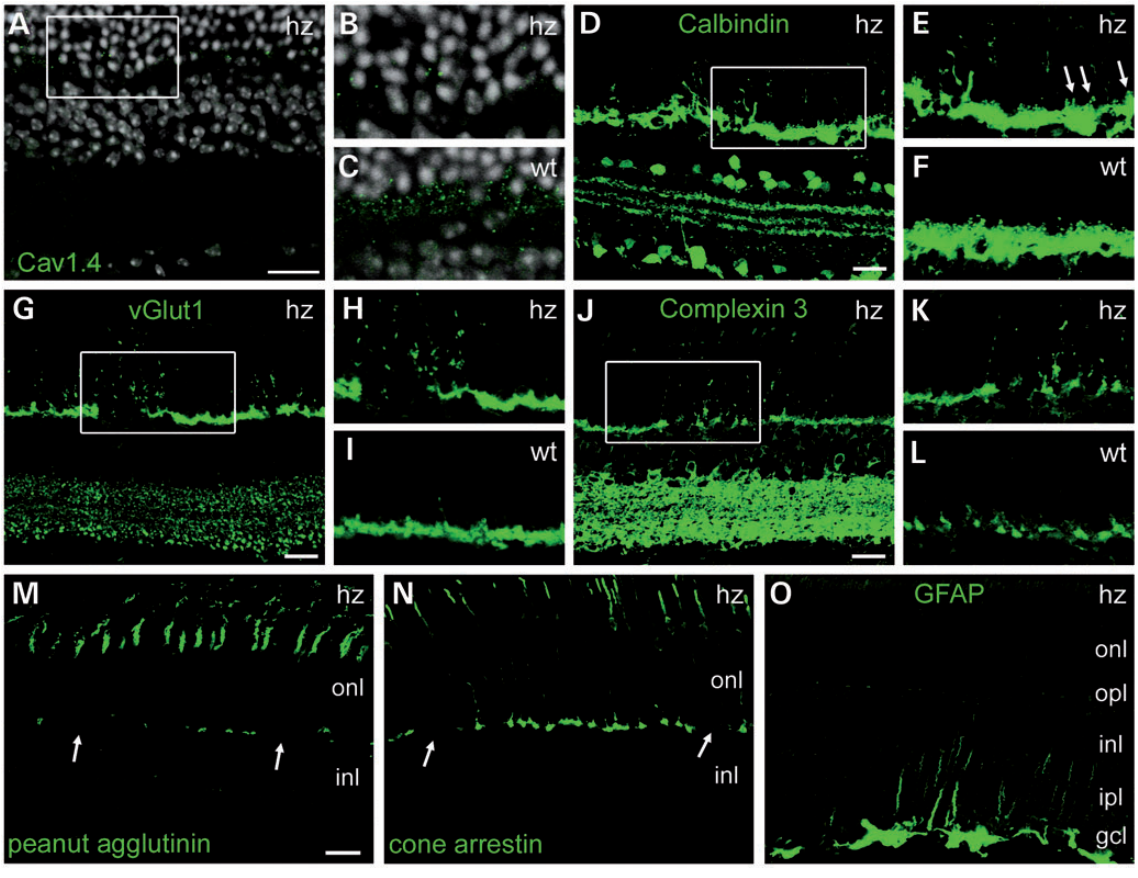

Figure 4. Mosaic synaptopathy in *Cacna1f* heterozygous mice. Confocal scans of vertical retinal sections from Cav1.4 heterozygous (hz) mice. (**A**) Representative image from an hz mouse labeled with a Cav1.4-specific antibody (green). (**B**) Magnification view on the outer plexiform layer region marked with a white rectangle in (A). (**C**) Magnification view on the corresponding region from a wild-type control mouse labeled with a Cav1.4-specific antibody (green). Cell nuclei in (A–C) were stained with the nuclear dye Hoechst 33342 (grey). (**D**–**L**) Retinal sections from hz (D and E, G and H and J–H) and wt (F, I and L) mice immunolabeled for calbindin (Calb, D–F), vGlut1 (G–I) and complexin 3 (cplx3) (J–L). The hz mice show a pronounced mosaic (patchy) photoreceptor synaptopathy. The regions marked with a white rectangle in panels (D, G and J) are shown in (E, H and K), respectively. (F, I and L) show corresponding immunostainings from wt. (**M**–**O**) Representative image from hz mice labeled for peanut agglutinin (M), cone arrestin (N) and GFAP (O) reveal a mosaic loss of synaptic cone structures and reactive gliosis in the hz. The scale bar marks 20 μm. gcl, ganglion cell layer; inl, inner nuclear layer; ipl, inner plexiform layer; onl, outer nuclear layer; opl, outer plexiform layer.

C-terminus), which changes the nine following amino acid residues. After these nine residues, the protein is truncated. Mutation c.2928+1G>A has been reported before (IVS24+1) (28). The location of the mutations in the Cav1.4 channel protein is shown in Supplementary Material, Figure S3.

All carriers showed visual abnormalities of variable extent (Table 1). Importantly, all carriers had a variable degree of ERG changes (Fig. 7). While rod function reached the lower normal range in some, cone function never reached more than half the normal size (Fig. 7, Table 1). The clinical symptoms and the pathological ERG changes of carrier females were consistent with the phenotype of incomplete CSNB. This phenotype co-segregated in affected male patients and was present at the heterozygous state in all female carriers (Table 1, Fig. 7).

DISCUSSION

Neurotransmission from photoreceptors to bipolar cells relies on calcium-triggered release of glutamate from photoreceptor synaptic terminals (1,2). The major calcium entry pathway in presynaptic terminals of photoreceptors and bipolar cells is thought to be a voltage-gated L-type calcium channel containing the Cav1.4 α1 subunit, which is encoded by the X-chromosomal *CACNA1F* gene. In this study, we analyzed the retinal phenotypes in Cav1.4-KO and Cav1.4 heterozygous mice and in human female carrier patients. ERG tests and behavioral test of visual performance suggest homozygous Cav1.4-KO mice are essentially blind. In these mice, a pronounced synaptopathy, characterized by retraction of rod and cone photoreceptor synapses, sprouting of second-order neurons, formation of ectopic synapses and pronounced degeneration and loss of cone, but not of rod photoreceptors were present. These findings indicate that Cav1.4 channels are essential for both rod and cone neurotransmission and the functional and structural integrity of photoreceptor synapses in mice. This conclusion is in line with results reported for a Cav1.4-KO mouse model, which was genetically independently engineered and previously characterized (13,29).

Our analysis of Cav1.4 heterozygosity in Cav1.4-KO mice revealed several new aspects of Cav1.4 channel dysfunction *in vivo*. First, they suggest that retinal function in the heterozygous Cav1.4 retina is impaired, because the affected 'knockout' retinal columns do not contribute to light detection, processing and transmission through the visual pathway (Fig. 8). The

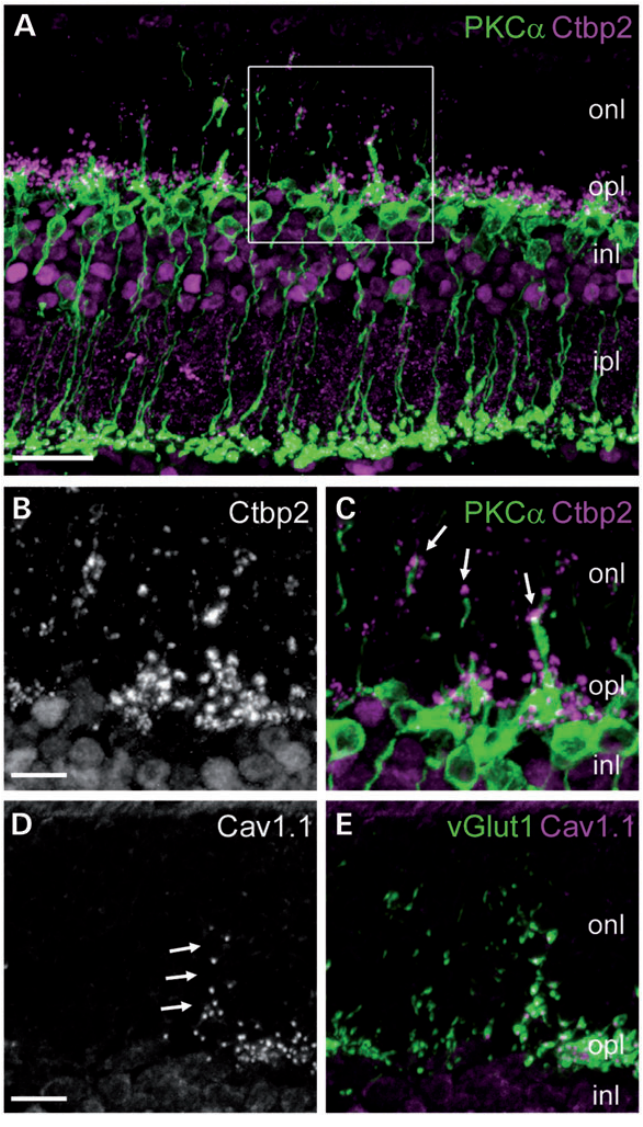

Figure 5. Pre- and postsynaptic changes in *Cacna1f* heterozygous mice. Confocal scans of vertical retinal sections from Cav1.4 heterozygous (hz) mice double-labeled for a combination of pre- and postsynaptic marker proteins. (**A**) Immunostaining for the ribbon synapse marker C-terminal binding protein 2 (Ctbp2, magenta) and PKCα (green). Ctbp2 labels ipl cell bodies as well as inl and opl synapses. In the non-affected parts the Ctbp2 signal of photoreceptor synapses is restricted to the opl. In the affected parts PKCα-positive dendrites grow into the onl and Ctbp2 is re-distributed throughout the onl. (**B** and **C**) High resolution images of the area marked with a rectangle in (A). (B) Ctbp2 (grey) signal only. (C) Merged image for Ctbp2 (magenta) and PKCα (green). The arrows mark ectopic Ctbp2-positive structures in close proximity to the tips of outgrown PKCα-positive rod bipolar cell dendrites. (**D** and **E**) Co-immunostaining for the postsynaptic L-type calcium channel subunit 1.1 (Cav1.1) and vGlut1. The arrows point to Cav1.1-positive puncta at the border of the affected area. (D) Cav1.1 signal (grey) only. (E) Merged image for Cav1.1 (magenta) and vGlut1 (green). The scale bar marks 10 μm. inl, inner nuclear layer; onl, outer nuclear layer; opl, outer plexiform layer.

prerequisite of this idea is the presence of a retinal mosaic in Cav1.4 heterozygous mice, characterized by radial retinal columns of Cav1.4-KO morphology was present in the Cav1.4-KO mouse retina side by side to radial columns of wild-type-like morphology. It is very likely that this mosaic like pattern is caused by differential X-chromosomal inactivation prior to the onset of neurogenesis (30). When the X-chromosome is inactivated in early retinal precursor cells, those cells with inactivation of the wild-type *Cacna1f*- gene would lead to cells deficient of Cav1.4 in carriers. Clonal descendents of retinal precursor cells inherit the X-active status of their ancestors and these clones are precisely organized in radial columns (30–32). Importantly, the morphological changes observed in affected columns of carrier mice included the synaptopathy as well as the degenerative changes of cone photoreceptors. Given the presence of radial Cav1.4-KO columns, it is likely that the vertical flow of visual information is compromised and cannot be compensated by neighboring unaffected and functional retinal cells.

Secondly, we provide evidence that aberrant crosstalk originating from the border areas between affected and non-affected retinal columns could interfere with normal retinal processing. In line with this hypothesis, ectopic synapses are formed between neurites originating from second order neurons within the affected retinal column and rod photoreceptor somata in non-affected columns (Fig. 8).

On a functional level, Cav1.4 heterozygous mice revealed reduced amplitudes of ERG b-waves and oscillatory potentials and a compromised performance in the vision-guided behavior which was in between that of wild-type and Cav1.4-KO mice. Notably, this phenotype was observed under scotopic and photopic light conditions arguing for defects in rod and cone function. We noticed that the phenotype of carrier mice was more pronounced at the level of vision-guided behavior than in the ERG. This might be attributable to significant disturbance of retinal network signaling in carrier mice (Fig. 8).

In humans, most X chromosomal diseases do not lead to clinical symptoms in carrier females (33). However, exceptions are retinal diseases like specific subtypes of X-linked retinitis pigmentosa (34) and Choroideremia (35). In carriers for CSNB2 associated with mutations in *CACNA1F* clinically detectable signs are relatively rare (10,17,18). Here, we present five female carriers which had decreased cone-specific ERG responses. These carriers had independent *CACNA1F* mutations, four of which were novel. From the structural point of view, it is very likely that the frameshift mutations lead to a loss of Cav1.4 function. The specific functional consequences of the two point mutations are not known. The presence of symptoms in female carrier heterozygous for different mutations in *CACNA1F* supports the hypothesis of X-inactivation. Furthermore, variable expressivity of symptoms observed in different carriers is consistent with differential X-inactivation. Finally, the observation that not all carriers in the families of a given mutation are affected suggests partial penetrance which also agrees with X-chromosomal inactivation. Together, these clinical data suggest that X-inactivation rather than a specific effect of a mutation is responsible for the specific clinical presentation of an individual carrier. Supposed the morphological changes observed in the retina of Cav1.4 heterozygous mice are also present in the human retina of Cav1.4 carrier females, one would expect impaired vertical processing of visual information in affected retinal network columns. In addition, aberrant crosstalk between affected and non-affected retinal columns would lead to erroneous visual signal processing. However, one needs to take into account that the human retina differs in many ways from the mouse retina. For instance, human daylight vision

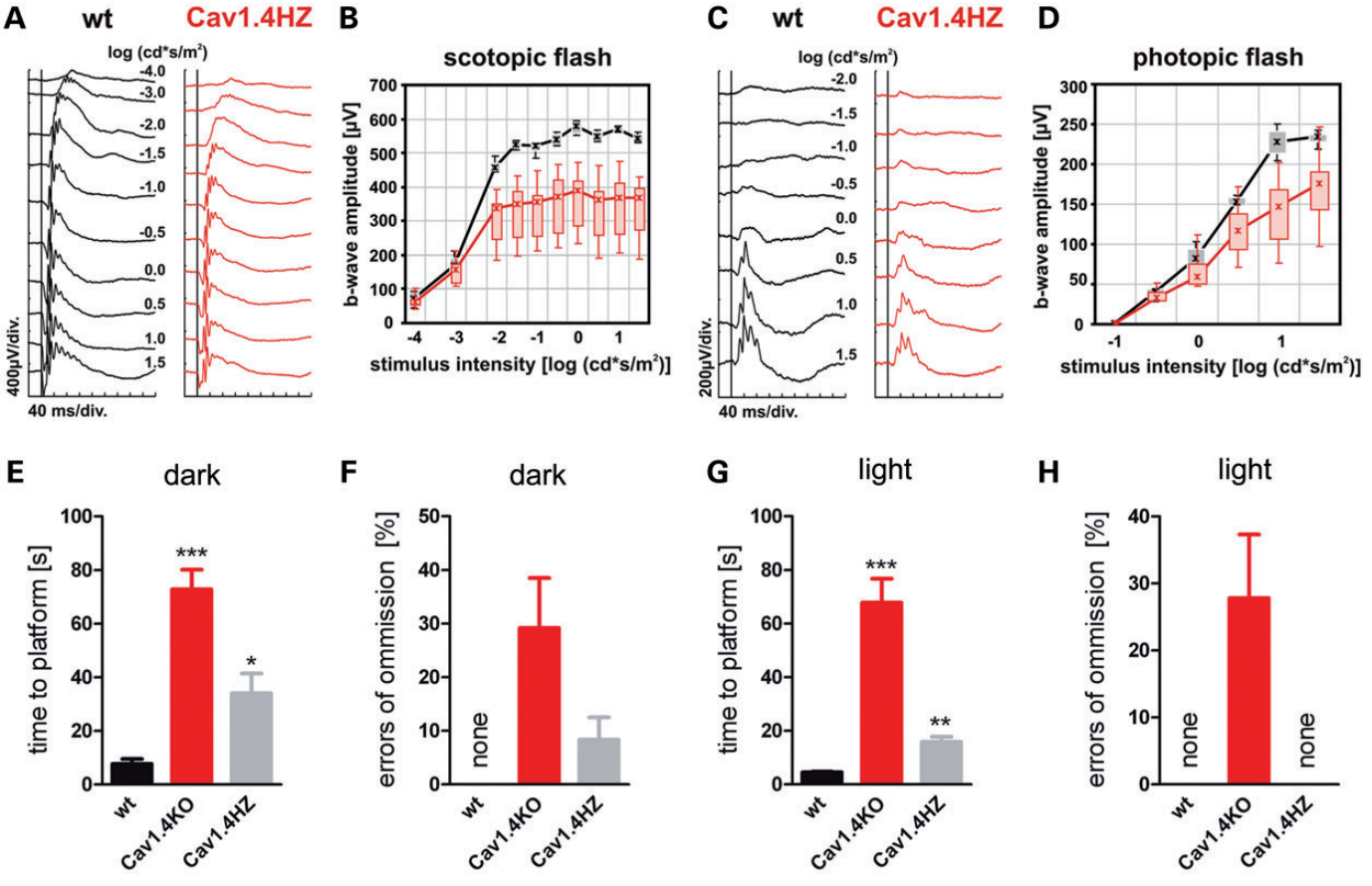

Figure 6. Visual function in *Cacna1f* heterozygous mice. (**A**–**D**) Electroretinographic analysis of retinal function in Cav1.4 HZ mice. Representative Ganzfeld-ERG intensity series from dark-adapted (A) and light-adapted (C) wild-type (wt, black traces) and Cav1.4 HZ mice (red traces). (B and D) Quantitative data of the entire group shown as Box-and-Whisker plots, i.e. boxes indicate the 25 and 75% quantile range, whiskers indicate the 5 and 95% quantiles and the asterisks indicate the median of the data. The amplitude data are plotted as a function of the logarithm of the flash intensity. (**E**–**H**) Performance of Cav1.4 HZ mice (grey) in a visual water-maze behavioral task under dark (E and F) or normal light conditions (G and H). Wild-type (wt, black) and Cav1.4-KO mice (red) are show for comparison. (E and G) Latency to locate a visible platform under dark (E) and normal light conditions (G). (F and H) Errors of ommision under dark (F) and normal light conditions (H).

mainly depends on the foveal/macular cone photoreceptors. Moreover, it is still not clear whether human cones (or rods) express other L-type VDCCs (e.g. Cav1.3) in addition to Cav1.4 that might compensate for the loss of Cav1.4 function. These reasons could at least partially explain why the phenotype in mice has such deleterious effects whereas in humans it is hardly noticed subjectively.

Our study provides the first comprehensive description of morphological and functional changes in female carriers due to mutations in *CACNA1F* affecting the Cav1.4 channel. Our data indicate that *CACNA1F* heterozygosity in female carrier mice and humans have significant consequences for both rod and cone-mediated vision and that this functional impairment is presumably caused by X-chromosomal inactivation of the wild-type Cav1.4 allele. Finally, our study helps to explain previously not understood complaints of mutant Cav1.4 carriers.

MATERIALS AND METHODS

Animals

We used Cav1.4-KO mice obtained from Dr Marion Maw, University of Otago, Dunedin, New Zealand (14). In these mice, the *Cacna1f* locus was globally disrupted through homologous recombination by a Cre/loxP-based deletion of exons 14–17 which encode the transmembrane helices 8–12 located in domain 2 of the channel protein (14). The deletion of exon 14–17 of the Cav1.4 gene was confirmed at the level of genomic DNA by Southern blot analysis (Supplementary Material, Fig. S1A and B). Cav1.4-KO mice (Cav1.4-KO) were born at the expected Mendelian ratio, were fertile and showed no immediately visible behavioral and physical abnormalities.

Immunohistochemistry

Immunohistochemical staining was performed on retinal cryosections according to the procedures described previously (21).

Briefly, after enucleation, the eyes were pierced with a needle and fixed for 5 min with 4% paraformaldehyde (PFA) in 0.1 M phosphate buffer (PB). Subsequently, the cornea and lens were removed and the remaining eye cut was fixed for 45 min in 4% PFA/PB, then washed three times in 0.1 M PB and incubated overnight in 30% sucrose/PB. After embedding in tissue freezing medium (Tissue-Tek O.C.T Compound, Sakura Finetech), vertical cryosections were cut at 10 µm and stored at −20°C until

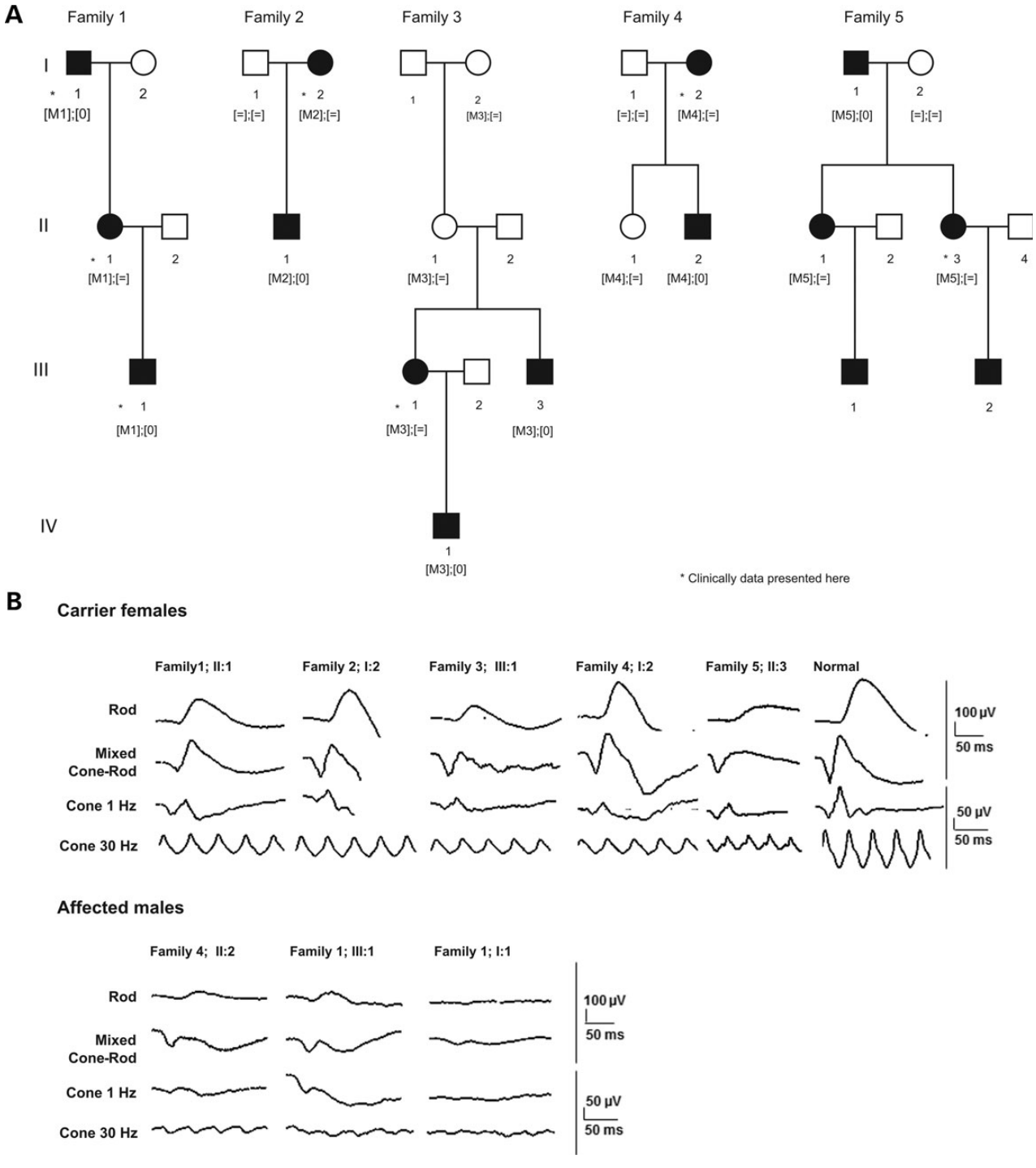

Figure 7. Visual function in human CSNB patients carrying *CACNA1F* mutations (**A**) Pedigrees of incomplete CSNB patients and carriers with *CACNA1F* mutations and co-segregation analysis in available family members. Filled symbols represent affected and unfilled unaffected individuals. Squares depict males, circles females. Stars mark individuals for whom we present the clinical data. Equation symbols represent unaffected alleles. (**B**) Electroretinograms (ERG) of carriers and male patients set-up to stimulate: I. rods (dark adapted, $0.01^{*}cd^{*}m^{-2}s$), II. cones and rods (dark adapted, $3^{*}cd^{*}m^{-2}$ s); III. and IV. cones (light adapted, 3 $cd^{*}m^{-2}$ s, 1 Hz and 30 Hz). Compared with normal responses displayed in the last column, carriers had a variable *b*-wave responses under rod conditions. Those with markedly low *b*-waves (RP1214 and 1344.01) did not reach a larger *b*- than *a*-wave for the mixed cone-rod condition ('negative' ERG). Under rod suppression by light adaptation no carrier reached more than about 50% of the normal response to either single flashes (1 Hz) or flicker (30 Hz). Responses of all three affected males were much smaller under both dark and light adapted condition.

use. The retina slices were rehydrated with 0.1 M PB and then fixed for 10 min with 4% PFA. After washing three times with 0.1 M PB, the slices were incubated with primary antibody overnight at 4°C in a solution of 0.1 M PB, 5% Chemiblocker (Millipore) and 0.3% Triton X. Next, the slices were again washed three times with 0.1 M PB, before proceeding with

Table 1. Clinical details of carriers

Family number, internal reference number	CACNA1F mutation found in son	Exon/ Intron	Sex, age	History	Refractive error RE, LE	VA; RE; LE	ERG
Family 1, Mo802,	c.2821dupC => p.Leu941Pfs*115 heterozygote	Ex 23	F, 34	Strabismus in childhood, surgery, amblyopia right eye	+2.50/0.75/90° +1.25 sph	0.3* 1.0	Electronegative cone response, decreased 30-Hz flickers amplitudes, rod responses in the lower range
Family 2, Mo1189,	c.2090T>C => p.Leu697Pro heterozygote	Ex 16	F, 22	Amblyopia left eye, needs relatively strong lights	+2.50/−0.50/80° +5.00/−0.50/20°	1.0 0.7*	Electronegative cone response, decreased 30-Hz flickers amplitudes, rod responses in the normal range
Family 3, Mo1214,	c.4547_4549delinsCC => p.Leu1516Profs*9 heterozygote	Ex 39	F, 31	Refractive surgery at age 28 years for astigmatism	0/−1.25/55° −0.25/−0.25/100°	0.9 0.9	Highly electronegative cone response, half decreased 30-Hz flickers amplitudes, decreased rod responses
Family 4 Mo1242,	c.764G>A => p.Gly255Glu heterozygote	Ex 6	F, 34	—	—	—	Decreased cone response, decreased 30-Hz flickers amplitudes, rod responses in the normal range
Family 5 Gi1344.01	c.2928+1G>A => 4S24+1 heterozygote	In 24	F, 51	Photophobic for bright light	−0.25/−0.5/152° −1.75/−0.75/8°	0.7 0.7	Negative ERG: rod, mixed and cone b-waves about $\frac{1}{2}$ of normal, a-waves normal. Rod b-wave delayed.

Refractive errors (sph spherical/cylindrical diopters/and axes) and corresponding visual acuity (VA); Electroretinograms (ERGs) were all below mean normal amplitudes, latencies unchanged except for rod response Family 5; II:3. Two carriers had abnormal fundus appearance: In Family 4; I:2 the color of the peripheral retina appeared slightly heterogenous; equally, Family 5; II:3 had overall light fundus pigmentation, in the LE circular chorioretinal atrophy of one optic disc diameter (disease unrelated). In both eyes, no macular reflex was seen and optic discs were pale. This was confirmed by spectral-domain optical coherence tomography which illustrated a shallow foveal pit and partial optic atrophy with thinning of the retinal nerve fiber layer around the optic disc. Fundus autofluorescence, was slightly irregular (sparkled higher and lower FAF) around the macula, while Family 1; II:1 had a normal appearance. RE right eye; LE left eye; —, data not obtained; One carrier (Family 5; II:3) named symptoms, i.e. sensitivity to bright light. One carrier (Gi1344.01) had moderate myopia. Carriers Family 5; II:3 and Family 3; III:1 did not reach normal visual acuity despite best correcting glasses.
*Visual acuity reduced due to amblyopia in squinting eye.

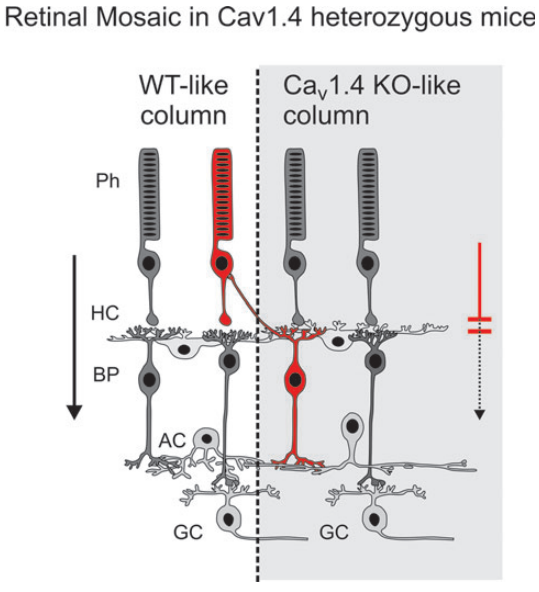

Figure 8. Model for pathological retinal information processing in Cav1.4 heterozygous mice. Retinal mosaic in Cav1.4 heterozygous mice showing a wild-type like retinal column (left part of the figure) and a Cav1.4-KO like retinal column (right part of the figure). Affected 'knockout' retinal columns do not contribute to light detection, processing and transmission through the visual pathway (arrow on the right). Aberrant crosstalk at the border areas between affected and non-affected retinal columns interfere with normal retinal processing. Formation of ectopic synapses between neurites originating from second order neurons within the affected retinal column and rod photoreceptor somata in non-affected columns (Red rod photoreceptor and red bipolar neuron). Ph, rod photoreceptor; BP, bipolar cell; GZ, ganglion cell; HZ, horizontal cell; AZ, amacrine cell.

secondary detection using Alexa 488 anti-mouse or rabbit IgG $F(ab')_2$ fragments (Cell Signaling Technology) or anti-guinea pig IgG (Mobitec) or Cy3 anti-mouse or anti-rabbit IgG (Jackson Immunoreagents). The cell nuclei were stained with Hoechst 33342. Finally, the sections were washed with 0.1 M PB and covered with coverslips.

The following primary antibodies were used: rabbit anti-Cav1.4 (Cav1.4 Pep3; 1:1000) (14), mouse anti-Cav1.1 (Millipore, clone mab1A, 1:5000), rabbit anti-calbindin (Swant, Bellinzona, Switzerland; 1:2000) (23), rabbit anti-cone arrestin (1:300) (23,36), rabbit anti-complexin 3 (1:1000) (25), rabbit anti-complexin 4 (1:20 000) (25), mouse anti-Ctbp2 (BD Biosciences, 1:10 000), Cy3-coupled anti-GFAP (Sigma, Germany; 1:1000) (21), mouse anti-PKCα (clone MC5, Leinco Technologies, Inc.; 1:50) (21), rabbit anti-PKCα; Sigma, 1:1000), mouse anti-rhodopsin (anti-rhodopsin Clone 1D4; Thermo Scientific; 1:150) (37), mouse anti-vGlut1 (NeuroMab, clone N28/9; 1:1000), guinea pig anti-vGlut1 (Millipore, 1:50 000), FITC-peanut agglutinin (PNA, Sigma-Aldrich, 1:100) (21) was used as a cone marker. Confocal images were collected at a Zeiss LSM 510 laser scanning microscope (Carl Zeiss, Germany) and images are presented as collapsed confocal z-stacks. The stainings were reproduced in ≥3 independent experiments.

Electroretinograms in mice

ERG analysis was performed according to procedures described elsewhere (38,39).

Visual water maze task

Mice were housed separately in an inverse 12 h light/dark cycle. The experiment was performed in the dark cycle. Mice were trained for 3 days (eight trials a day) to locate a stable platform (10 cm in diameter) at dim light conditions of 0.3 cd/m^2 to ensure that vision is totally conferred to the rod system. The platform was placed in a circular swimming pool (120 cm in diameter, 70 cm high, white plastic) filled with water. The starting position of the mouse was changed from trial to trial in a pseudo-random order whereas the platform was kept in a constant location. Distal cues in the testing room and the water maze, such as patterned cardboards, were provided as spatial references. Trials were terminated if the mouse climbed onto the platform or when it swam for 2 min. If the mouse did not find the platform, it was gently placed on the stable platform. After each trial, the mouse was left on the platform for 10 s undisturbed before warmed using a heating lamp and transferred to the home cage. On day 4, 5 and 6, the experiment was performed under light conditions (29 cd/m^2) to test cone vision mediated behavior. In a second experiment, we tested another group of animals for three consecutive days under normal light conditions (29 cd/m^2) only to exclude any behavioral adaptation effects on the cone function test. The experiments were performed and analyzed blindly to the animal genotype.

Mutation analysis

Total genomic DNA was extracted from peripheral leukocytes in blood samples by standard salting out procedure or according to the manufacturer's recommendation (Puregen Kit; Qiagen, Courtaboeuf, France).The 48 exons of *CACNA1F* (RefSeq: AJ006216) were amplified on 50 µl genomic DNA using 33 fragments (oligonucleotide sequences and exact conditions can be obtained on request) with a polymerase (HotFire, Solis Biodyne, Estonia). The PCR products were enzymatically purified (ExoSAP-IT, USB Corporation, Cleveland, OH, USA purchased from GE Healthcare, Orsay, France) and sequenced with a commercially available sequencing mix (BigDyeTerm v1.1 CycleSeq kit, Applied Biosystems, Courtaboeuf, France). The sequenced products were purified on a pre-soaked Sephadex G-50 (GE Healthcare) 96-well multiscreen filter plate (Millipore, Molsheim, France), the purified product analyzed on an automated 48-capillary sequencer (ABI 3730 Genetic analyzer, Applied Biosystems) and the results interpreted by applying a software (SeqScape, Applied Biosystems). At least 192 commercially available control samples were used to validate the pathogenicity of the novel sequence variants (Human random control panel 1–3, Health Protection Agency Culture Collections, Salisbury, UK).

Phenotypic characterization of patients and carriers

Patients had standard ophthalmological examination (refractometry, visual acuity, slit-lamp examination, applanation tonometry, funduscopy with pupil dilatation). Optical coherence tomography (OCT) was obtained in Montpellier using a time domain OCT (TD-OCT, Stratus model 3000, Carl Zeiss Meditec, CA, USA, software version 3.0) and in Giessen using a spectral domain OCT (SD-OCT, Spectralis, Heidelberg

Enginieering, Heidelberg, Germany). Fundus autofluorescence was imaged with a confocal laser ophthalmoskop (HRA2 in Montpellier and HRA3 in Gießen; both by Heidelberg Engineering, Heidelberg, Germany). Full-field ERGs were recorded under pupil dilatation using the MonPackOne (Metrovision, Pérenchies, France) with bipolar contact lens electrodes (Montpellier) or a ColorDome Ganzfeld stimulator with an ESPION-system and DTL-Electrodes (Diagnosys UK Ltd, Impington, Cambridge, UK) in line with recommendatations of the International Society for Clinical Electrophysiology of Vision (http ://www.iscev.org/standards/index.html).

SUPPLEMENTARY MATERIAL

Supplementary Material is available at *HMG* online.

ACKNOWLEDGEMENTS

We thank Kathrin Rötzer, Gudrun Utz and Elisabeth Schulze for excellent technical help, Drs Marion Maw (University of Otago) and Susanne tom Dieck (Max Planck Institute for Brain Research) for providing Cav1.4 KO mice and Cav1.4 antibodies and Drs Wolfgang Baehr (University of Utah) and Kerstin Reim (Max Planck Institute of Experimental Medicine, Göttingen) for the gift of antibodies. The monoclonal antibody anti-vGlut1 N28/9 was obtained by the UC Davis/NIH NeuroMab Facility.

Conflict of Interest statement. None declared.

FUNDING

This work was supported by the Deutsche Forschungsgemeinschaft (DFG) (WA 2597/2-1); Foundation *Voir et Entendre* (C.Z.), Prix Dalloz for *'la recherche en ophtalmologie*' (C.Z.), Ville de Paris and Region Ile de France, LABEX LIFESENSES [reference ANR-10-LABX-65] supported by French state funds managed by the ANR within the *Investissements d'Avenir programme* [ANR-11-IDEX-0004-0].

REFERENCES

1. Matthews, G. and Fuchs, P. (2010) The diverse roles of ribbon synapses in sensory neurotransmission. *Nat. Rev. Neurosci.*, **11**, 812–822.
2. Heidelberger, R., Thoreson, W.B. and Witkovsky, P. (2005) Synaptic transmission at retinal ribbon synapses. *Prog. Retin. Eye Res.*, **24**, 682–720.
3. Baumann, L., Gerstner, A., Zong, X., Biel, M. and Wahl-Schott, C. (2004) Functional characterization of the L-type Ca2+ channel Cav1.4alpha1 from mouse retina. *Invest Ophthalmol. Vis. Sci.*, **45**, 708–713.
4. Wahl-Schott, C., Baumann, L., Cuny, H., Eckert, C., Griessmeier, K. and Biel, M. (2006) Switching off calcium-dependent inactivation in L-type calcium channels by an autoinhibitory domain. *Proc. Natl Acad. Sci. USA*, **103**, 15657–15662.
5. McRory, J.E., Hamid, J., Doering, C.J., Garcia, E., Parker, R., Hamming, K., Chen, L., Hildebrand, M., Beedle, A.M., Feldcamp, L. *et al.* (2004) The CACNA1F gene encodes an L-type calcium channel with unique biophysical properties and tissue distribution. *J. Neurosci.*, **24**, 1707–1718.
6. Koschak, A., Reimer, D., Walter, D., Hoda, J.C., Heinzle, T., Grabner, M. and Striessnig, J. (2003) Cav1.4alpha1 subunits can form slowly inactivating dihydropyridine-sensitive L-type Ca2+ channels lacking Ca2+-dependent inactivation. *J. Neurosci.*, **23**, 6041–6049.
7. Ball, S.L., Powers, P.A., Shin, H.S., Morgans, C.W., Peachey, N.S. and Gregg, R.G. (2002) Role of the beta(2) subunit of voltage-dependent calcium channels in the retinal outer plexiform layer. *Invest. Ophthalmol. Vis. Sci.*, **43**, 1595–1603.
8. Strom, T.M., Nyakatura, G., Apfelstedt-Sylla, E., Hellebrand, H., Lorenz, B., Weber, B.H., Wutz, K., Gutwillinger, N., Ruther, K., Drescher, B. *et al.* (1998) An L-type calcium-channel gene mutated in incomplete X-linked congenital stationary night blindness. *Nat. Genet.*, **19**, 260–263.
9. Bech-Hansen, N.T., Naylor, M.J., Maybaum, T.A., Pearce, W.G., Koop, B., Fishman, G.A., Mets, M., Musarella, M.A. and Boycott, K.M. (1998) Loss-of-function mutations in a calcium-channel alpha1-subunit gene in Xp11.23 cause incomplete X-linked congenital stationary night blindness. *Nat. Genet.*, **19**, 264–267.
10. Jalkanen, R., Bech-Hansen, N.T., Tobias, R., Sankila, E.M., Mantyjarvi, M., Forsius, H., de la Chapelle, A. and Alitalo, T. (2007) A novel CACNA1F gene mutation causes Aland Island eye disease. *Invest. Ophthalmol. Vis. Sci.*, **48**, 2498–2502.
11. Vincent, A., Wright, T., Day, M.A., Westall, C.A. and Heon, E. (2011) A novel p.Gly603Arg mutation in CACNA1F causes Aland island eye disease and incomplete congenital stationary night blindness phenotypes in a family. *Mol. Vis.*, **17**, 3262–3270.
12. Jalkanen, R., Mantyjarvi, M., Tobias, R., Isosomppi, J., Sankila, E.M., Alitalo, T. and Bech-Hansen, N.T. (2006) X linked cone-rod dystrophy, CORDX3, is caused by a mutation in the CACNA1F gene. *J. Med. Genet.*, **43**, 699–704.
13. Mansergh, F., Orton, N.C., Vessey, J.P., Lalonde, M.R., Stell, W.K., Tremblay, F., Barnes, S., Rancourt, D.E. and Bech-Hansen, N.T. (2005) Mutation of the calcium channel gene Cacna1f disrupts calcium signaling, synaptic transmission and cellular organization in mouse retina. *Hum. Mol. Genet.*, **14**, 3035–3046.
14. Specht, D., Wu, S.B., Turner, P., Dearden, P., Koentgen, F., Wolfrum, U., Maw, M., Brandstatter, J.H. and tom Dieck, S. (2009) Effects of presynaptic mutations on a postsynaptic Cacna1s calcium channel colocalized with mGluR6 at mouse photoreceptor ribbon synapses. *Invest. Ophthalmol. Vis. Sci.*, **50**, 505–515.
15. Chang, B., Heckenlively, J.R., Bayley, P.R., Brecha, N.C., Davisson, M.T., Hawes, N.L., Hirano, A.A., Hurd, R.E., Ikeda, A., Johnson, B.A. *et al.* (2006) The nob2 mouse, a null mutation in Cacna1f: anatomical and functional abnormalities in the outer retina and their consequences on ganglion cell visual responses. *Vis. Neurosci.*, **23**, 11–24.
16. Doering, C.J., Rehak, R., Bonfield, S., Peloquin, J.B., Stell, W.K., Mema, S.C., Sauve, Y. and McRory, J.E. (2008) Modified Ca(v)1.4 expression in the Cacna1f(nob2) mouse due to alternative splicing of an ETn inserted in exon 2. *PLoS One*, **3**, e2538.
17. Hemara-Wahanui, A., Berjukow, S., Hope, C.I., Dearden, P.K., Wu, S.B., Wilson-Wheeler, J., Sharp, D.M., Lundon-Treweek, P., Clover, G.M., Hoda, J.C. *et al.* (2005) A CACNA1F mutation identified in an X-linked retinal disorder shifts the voltage dependence of Cav1.4 channel activation. *Proc. Natl Acad. Sci. USA*, **102**, 7553–7558.
18. Rigaudiere, F., Roux, C., Lachapelle, P., Rosolen, S.G., Bitoun, P., Gay-Duval, A. and Le Gargasson, J.F. (2003) ERGs in female carriers of incomplete congenital stationary night blindness (I-CSNB). A family report. *Doc. Ophthalmol.*, **107**, 203–212.
19. Hope, C.I., Sharp, D.M., Hemara-Wahanui, A., Sissingh, J.I., Lundon, P., Mitchell, E.A., Maw, M.A. and Clover, G.M. (2005) Clinical manifestations of a unique X-linked retinal disorder in a large New Zealand family with a novel mutation in CACNA1F, the gene responsible for CSNB2. *Clin. Exp. Ophthalmol.*, **33**, 129–136.
20. Dick, O., tom Dieck, S., Altrock, W.D., Ammermuller, J., Weiler, R., Garner, C.C., Gundelfinger, E.D. and Brandstatter, J.H. (2003) The presynaptic active zone protein bassoon is essential for photoreceptor ribbon synapse formation in the retina. *Neuron*, **37**, 775–786.
21. Huttl, S., Michalakis, S., Seeliger, M., Luo, D.G., Acar, N., Geiger, H., Hudl, K., Mader, R., Haverkamp, S., Moser, M. *et al.* (2005) Impaired channel targeting and retinal degeneration in mice lacking the cyclic nucleotide-gated channel subunit CNGB1. *J. Neurosci.*, **25**, 130–138.
22. Lewis, G.P., Linberg, K.A. and Fisher, S.K. (1998) Neurite outgrowth from bipolar and horizontal cells after experimental retinal detachment. *Invest. Ophthalmol. Vis. Sci.*, **39**, 424–434.
23. Koch, S., Sothilingam, V., Garcia Garrido, M., Tanimoto, N., Becirovic, E., Koch, F., Seide, C., Beck, S.C., Seeliger, M.W., Biel, M. *et al.* (2012) Gene therapy restores vision and delays degeneration in the CNGB1(-/-) mouse model of retinitis pigmentosa. *Hum. Mol. Genet.*, **21**, 4486–4496.

24. Haverkamp, S., Ghosh, K.K., Hirano, A.A. and Wassle, H. (2003) Immunocytochemical description of five bipolar cell types of the mouse retina. *J. Comp. Neurol.*, **455**, 463–476.
25. Landgraf, I., Muhlhans, J., Dedek, K., Reim, K., Brandstatter, J.H. and Ammermuller, J. (2012) The absence of Complexin 3 and Complexin 4 differentially impacts the ON and OFF pathways in mouse retina. *Eur. J. Neurosci.*, **36**, 2470–2481.
26. Michalakis, S., Geiger, H., Haverkamp, S., Hofmann, F., Gerstner, A. and Biel, M. (2005) Impaired opsin targeting and cone photoreceptor migration in the retina of mice lacking the cyclic nucleotide-gated channel CNGA3. *Invest. Ophthalmol. Vis. Sci.*, **46**, 1516–1524.
27. tom Dieck, S., Altrock, W.D., Kessels, M.M., Qualmann, B., Regus, H., Brauner, D., Fejtova, A., Bracko, O., Gundelfinger, E.D. and Brandstatter, J.H. (2005) Molecular dissection of the photoreceptor ribbon synapse: physical interaction of Bassoon and RIBEYE is essential for the assembly of the ribbon complex. *J. Cell Biol.*, **168**, 825–836.
28. Boycott, K.M., Maybaum, T.A., Naylor, M.J., Weleber, R.G., Robitaille, J., Miyake, Y., Bergen, A.A., Pierpont, M.E., Pearce, W.G. and Bech-Hansen, N.T. (2001) A summary of 20 CACNA1F mutations identified in 36 families with incomplete X-linked congenital stationary night blindness, and characterization of splice variants. *Hum. Genet.*, **108**, 91–97.
29. Raven, M.A., Orton, N.C., Nassar, H., Williams, G.A., Stell, W.K., Jacobs, G.H., Bech-Hansen, N.T. and Reese, B.E. (2008) Early afferent signaling in the outer plexiform layer regulates development of horizontal cell morphology. *J. Comp. Neurol.*, **506**, 745–758.
30. Reese, B.E. and Galli-Resta, L. (2002) The role of tangential dispersion in retinal mosaic formation. *Prog. Retin. Eye Res.*, **21**, 153–168.
31. Reese, B.E., Harvey, A.R. and Tan, S.S. (1995) Radial and tangential dispersion patterns in the mouse retina are cell-class specific. *Proc. Natl Acad. Sci. USA*, **92**, 2494–2498.
32. Reese, B.E. and Tan, S.S. (1998) Clonal boundary analysis in the developing retina using X-inactivation transgenic mosaic mice. *Semin. Cell Dev. Biol.*, **9**, 285–292.
33. Migeon, B.R. (2006) The role of X inactivation and cellular mosaicism in women's health and sex-specific diseases. *JAMA*, **295**, 1428–1433.
34. Wegscheider, E., Preising, M.N. and Lorenz, B. (2004) Fundus autofluorescence in carriers of X-linked recessive retinitis pigmentosa associated with mutations in RPGR, and correlation with electrophysiological and psychophysical data. *Graefes Arch. Clin. Exp. Ophthalmol.*, **242**, 501–511.
35. Preising, M.N., Wegscheider, E., Friedburg, C., Poloschek, C.M., Wabbels, B.K. and Lorenz, B. (2009) Fundus autofluorescence in carriers of choroideremia and correlation with electrophysiologic and psychophysical data. *Ophthalmology*, **116**, 1201. –1209 e1201–1202.
36. Zhang, T., Baehr, W. and Fu, Y. (2012) Chemical chaperone TUDCA preserves cone photoreceptors in a mouse model of Leber congenital amaurosis. *Invest. Ophthalmol. Vis. Sci.*, **53**, 3349–3356.
37. Molday, R.S. and MacKenzie, D. (1983) Monoclonal antibodies to rhodopsin: characterization, cross-reactivity, and application as structural probes. *Biochemistry*, **22**, 653–660.
38. Seeliger, M.W., Grimm, C., Stahlberg, F., Friedburg, C., Jaissle, G., Zrenner, E., Guo, H., Reme, C.E., Humphries, P., Hofmann, F. *et al.* (2001) New views on RPE65 deficiency: the rod system is the source of vision in a mouse model of Leber congenital amaurosis. *Nat. Genet.*, **29**, 70–74.
39. Tanimoto, N., Muehlfriedel, R.L., Fischer, M.D., Fahl, E., Humphries, P., Biel, M. and Seeliger, M.W. (2009) Vision tests in the mouse: Functional phenotyping with electroretinography. *Front. Biosci. (Landmark Ed)*, **14**, 2730–2737.

V. Appendix

Paper V: Cav1.4 IT mouse as model for vision impairment in human congenital stationary night blindness type 2

Knoflach D, Kerov V, Sartori SB, Obermair GJ, Schmuckermair C, Liu X, **Sothilingam V**, Garcia Garrido M, Baker SA, Glösmann M, Schicker K, Seeliger M, Lee A, Koschak A[§]

Published in Channels (Austin)
7:503-513 (2013)

RESEARCH PAPER

Channels 7:6, 503–513; November/December 2013; © 2013 Landes Bioscience

Cav1.4 IT mouse as model for vision impairment in human congenital stationary night blindness type 2

Dagmar Knoflach[1], Vasily Kerov[2,8], Simone B Sartori[3], Gerald J Obermair[5], Claudia Schmuckermair[3], Xiaoni Liu[2], Vithiyanjali Sothilingam[4], Marina Garcia Garrido[4], Sheila A Baker[8], Martin Glösmann[7], Klaus Schicker[1], Mathias Seeliger[4], Amy Lee[2], and Alexandra Koschak[1,*]

[1]Medical University Vienna; Centre for Physiology and Pharmacology; Department of Neurophysiology and Pharmacology; Vienna, Austria; [2]University of Iowa; Department of Molecular Physiology & Biophysics; Iowa City, IA USA; [3]University of Innsbruck; Institute of Pharmacy, Pharmacology and Toxicology; Center for Chemistry and Biomedicine; Innsbruck, Austria; [4]University of Tübingen, Institute for Ophthalmic Research; Centre for Ophthalmology; Division of Ocular Neurodegeneration; Tübingen, Germany; [5]Medical University Innsbruck; Division of Physiology; Innsbruck, Austria; [6]Department of Histology and Institute of Bioengeneering; Universidad Miguel Hernández; Alicante, Spain; [7]University of Veterinary Medicine; Vetcore; Vienna, Austria; [8]University of Iowa; Department of Biochemistry; Iowa City, IA USA

Keywords: CSNB2, L-type calcium channel, channelopathies, gain-of-function, retinal

Mutations in the *CACNA1F* gene encoding the Cav1.4 Ca^{2+} channel are associated with X-linked congenital stationary night blindness type 2 (CSNB2). Despite the increasing knowledge about the functional behavior of mutated channels in heterologous systems, the pathophysiological mechanisms that result in vision impairment remain to be elucidated. This work provides a thorough functional characterization of the novel IT mouse line that harbors the gain-of-function mutation I745T reported in a New Zealand CSNB2 family.[1] Electroretinographic recordings in IT mice permitted a direct comparison with human data. Our data supported the hypothesis that a hyperpolarizing shift in the voltage-dependence of channel activation—as seen in the IT gain-of-function mutant[2]—may reduce the dynamic range of photoreceptor activity. Morphologically, the retinal outer nuclear layer in adult IT mutants was reduced in size and cone outer segments appeared shorter. The organization of the outer plexiform layer was disrupted, and synaptic structures of photoreceptors had a variable, partly immature, appearance. The associated visual deficiency was substantiated in behavioral paradigms. The IT mouse line serves as a specific model for the functional phenotype of human CSNB2 patients with gain-of-function mutations and may help to further understand the dysfunction in CSNB.

Introduction

Cav1.4 L-type Ca^{2+} channels (LTCCs) are the most abundant in the retina and localized at the specialized ribbon synapses formed between photoreceptors and second-order neurons.[3,4,5,6] Their low voltage activation range and slow inactivation properties due to the lack of calcium-dependent inactivation[7] render Cav1.4 channels perfectly suited to ensure sustained neurotransmitter release which is modulated by light stimuli.

Human genetic analyses indicate an essential role for Cav1.4 in vision. So far, more than 50 different mutations in *CACNA1F*, the gene coding for the Cav1.4 channel, have been found to cause congenital stationary night blindness type 2 (CSNB2) in human patients (for review see ref. 8). The majority of mutations are predicted to form non-functional channels, often because of structural changes like premature truncations that are incompatible with channel function. However, also gain-of-function mutations have been reported and characterized biophysically in transfected mammalian cells or *Xenopus* oocytes.[2,9,10,11] Data on functional implications in their native retinal environment remain still scarce. Cav1.4 gain-of-function mutations promote enhanced Ca^{2+} entry through the channel due to a strong hyperpolarizing shift in the voltage-dependence of activation which as well as slowed voltage-dependent inactivation. The so far most pronounced hyperpolarizing shift in Cav1.4 channel activation (around 30 mV) was found in mutation I745T (IT), which was identified in a New Zealand family. The affected family members were described to show an unusually severe CSNB2 phenotype—usually comprising low visual acuity, myopia, nystagmus, and variable levels of night blindness (clinically diagnosed by a reduction in the ERG b-wave)—which was associated with intellectual disability in males. In heterozygote females, clinical and functional abnormalities were also present.[2] 'Enhanced activity', as observed in gain-of-function mutations, implies an unwarranted positive connotation because it does not necessarily result in improved signaling but in a loss-of-control of existing signaling pathways important e.g., in developmental processes. Herein, we present the functional dysregulation and morphological consequences observed in retinas from IT mice. These findings correlate with impaired visual function in behavioral paradigms seen in these mice. Our data show that the IT mouse line, in contrast to

*Correspondence to: Alexandra Koschak; Email: alexandra.koschak@meduniwien.ac.at
Submitted: 08/30/2013; Accepted: 09/03/2013
http://dx.doi.org/10.4161/chan.26368

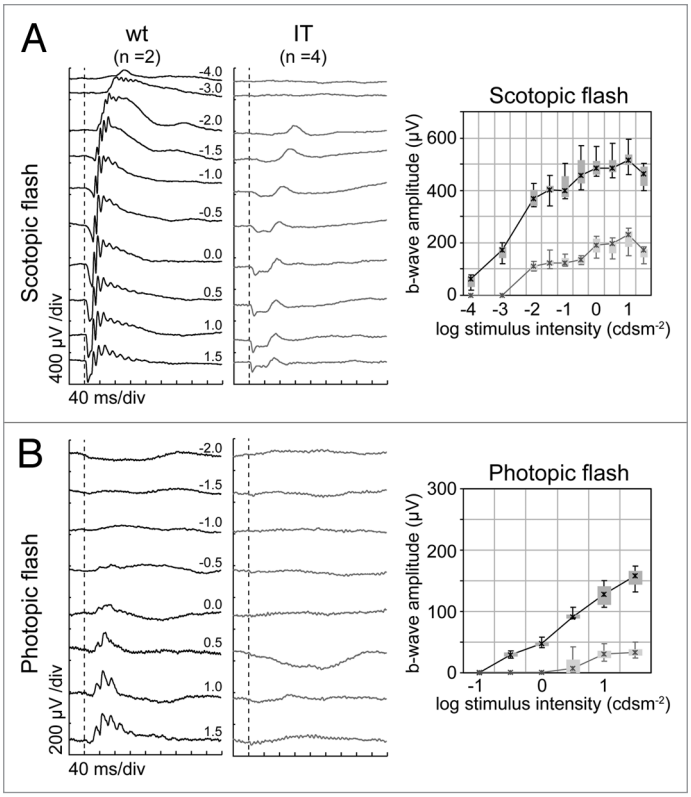

Figure 1. Functional assessment of wt and IT mouse retinas in vivo based on ERG. Left column: Representative Ganzfeld-ERG intensity series for dark-adapted (scotopic, [**A**]) and light-adapted (photopic, [**B**]) responses in wt (black) and IT mice (gray). Right column: Quantitative evaluation of the scotopic (**A**) and photopic (**B**) b-wave amplitude data for the entire group (wt, n = 2; IT, n = 4).

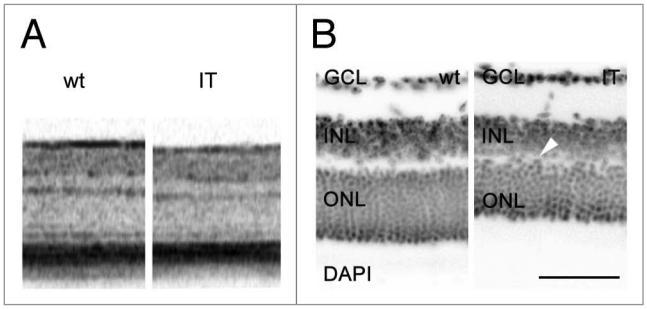

Figure 2. Morphological assessment of wt and IT mouse retinas. (**A**) In vivo OCT analysis of wt and IT mouse retinas, indicating (i) a reduction of the photoreceptor-containing outer nuclear layer (ONL), and (ii) a less expressed patterning of the inner/outer segment (IS/OS) border. (**B**) Retinal slices of adult wt (left) and IT (right) mice were stained with DAPI to show the nuclei. Light microscopic pictures from wt and IT were aligned at the GCL. Exemplar sections were taken from slices showing the same eccentricity. The reduction in the thickness of the ONL and INL in IT mice is evident (in [µm] for wt and IT respectively: ONL: 56 vs. 35; INL: 37 vs. 22). The arrow indicates the obvious misorganisation of the OPL. ONL, outer nuclear layer, INL, inner nuclear layer, GCL, ganglion cell layer. Scale bar 50 µm.

other mouse models characterized so far,[12] very well reflects the functional phenotype described in a family with the Cav1.4 I745T point mutation.[1]

Results

Rod and cone photoreceptor activity in wt and IT mice

Ganzfeld ERG recordings allow both dark adapted (scotopic) measurements to study rod-driven activity and light adapted (photopic) recordings to obtain information about the contribution of the cone system.[16] We found that adult IT animals very well matched their human CSNB2 counterparts in terms of the functional pattern resembling incomplete CSNB. Both rod and cone single flash responses (**Fig. 1A and B**) as well as the flicker ERG amplitude (not shown) were reduced. In contrast, the negative components of the scotopic standard flash response were smaller than those found in other CSNB models, and a minute but distinct positive peak indicated a remaining b-wave component. However, identical differences were found in patients carrying the exact same mutation.[1] The IT mouse line is therefore a representative model for human CSNB2 caused by the I745T mutation.

Morphological characteristics in Cav1.4 wild type (wt) and IT mouse retinas

Optical coherence tomography (OCT) of retinal substructures/layers in vivo indicated a distinct reduction in the outer plexiform layer (OPL) thickness in the mutant mice (**Fig. 2A**). This finding is in line with our histomorphological analysis (**Fig. 2B**). Specifically, a DAPI staining was performed on retinal sections of adult (2 mo-old) mice to compare the thickness of the retina as well as that of the major retinal layers at three different eccentricities in wt and IT. At comparable eccentricities, the rows of nuclei in the outer nuclear layer (ONL) were counted. Gross retinal structure and layering were normal in IT mice. All retinal layers were present. However, the number of rows of nuclei in the ONL was lower in IT than in wt mice resulting in a reduction in the thickness of the ONL and the total retinal thickness (**Fig. 2B**). OCT further revealed a less expressed patterning of the inner/outer segment (IS/OS) border that is indicative of irregular outer retinal layering (**Fig. 2A**).

We assessed potential aberrations in cone morphology by labeling with peanut agglutinin (PNA), a lectin preferentially binding cone-photoreceptor associated domains of the interphotoreceptor matrix[30,31] and glycogen phosphorylase (glypho), which stains cones from their outer segments to their pedicles.[32] PNA labeling demonstrated that outer segments were present and of normal appearance (**Fig. 3A**). However, and in accordance with the decreased thickness of the ONL, the overall length of cones was shorter in IT mice. PNA-positive pedicles were also observed in the IT retina (**Fig. 3A**, arrowheads), with no obvious dissimilarity to the wt retina. No decrease in the number of cones was evident (as also indicated in **Fig. 4C**). In the wt retina anti-glypho stained the inner segments of cone photoreceptors, known sites of high energy consumption, as well as cone pedicles (**Fig. 3B**, left). Cone photoreceptors in IT mice were shorter with shorter outer and inner segments and pedicles that appeared larger than in wt retina

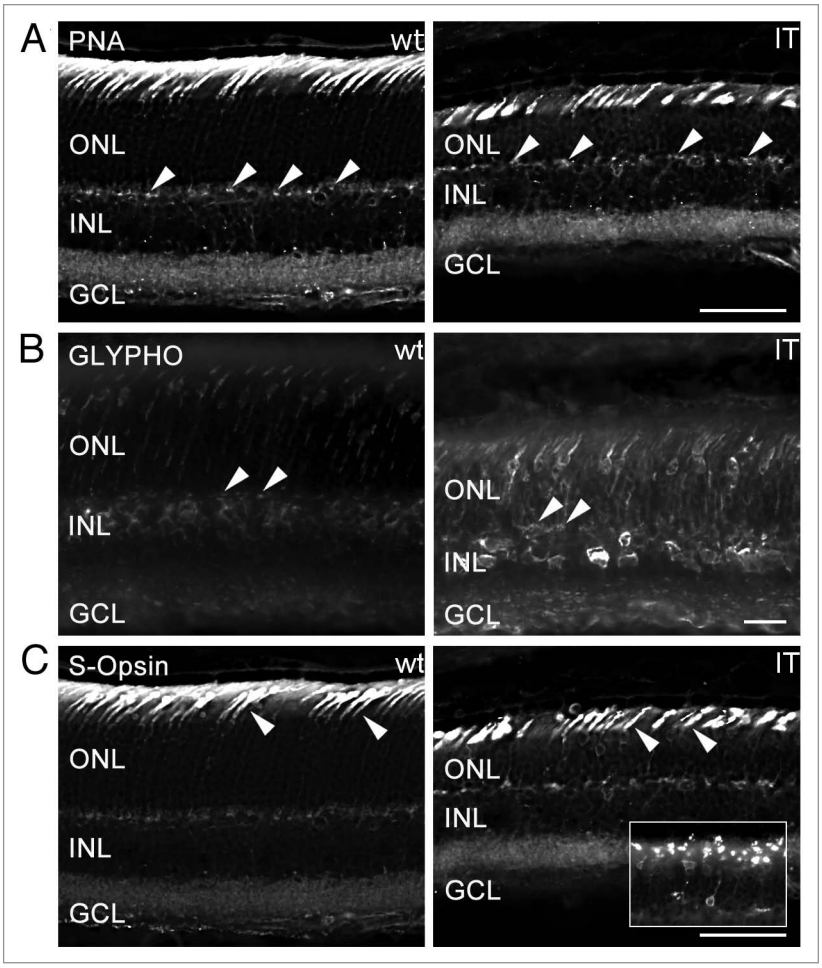

Figure 3. Effect of the IT mutation on adult mouse cones. Immunohistochemical analyses were performed on P74–81 (11-week old mice) mice using cone-specific markers and vertical sections were analyzed by wide-field fluorescence light microscopy. (**A**) PNA staining shows cones with normal appearance but shorter outer segments. Arrowheads indicate comparable staining of cone pedicle invaginations in wt (C57BL/6N) and IT mice. Scale bar 50 µm (**B**) Glypho also strongly labels the cone terminals. In IT mice immunostaining was pronounced throughout the cytoplasm from the outer segment to the synaptic pedicle. Arrowheads indicate enlargement of pedicles. Scale bar 20 µm. (**C**) S-opsin staining experiments for wt and IT retinas. The inset shows a sprouted cone (left), a mislocalized cone cell body (middle) and an enlarged cone pedicle (right). Scale bar 50 µm.

(**Fig. 3B**, right, arrowheads). Notably, glypho signal was consistently higher in the IT mutant, both in the inner and outer retina. Using the S-opsin marker sc14363 we found S-opsin expression clearly visible in the cone outer segments in the ventral wt retina as well as their pedicles (**Fig. 3C**, left). Consistent with our glypho staining cones were shorter in IT mice (**Fig. 3C**, right, arrowheads). As seen in the inset of **Figure 3C**, indeed we found a few cones that appeared to sprout, a phenomenon seen also in KO mice at different ages.[33]

We further examined the photoreceptor synaptic phenotype and investigated Cav1.4 expression in co-localization experiments with the synaptic ribbon protein CtBP2/Ribeye in wt and IT mice (**Fig. 4**). In adult wt retina, Cav1.4 co-localized in the characteristically horseshoe-shaped synapses in the OPL, whereas in IT retinas staining was disperse extending also into the ONL. The synaptic morphology resembled immature synapses with shorter but rather linear shape; in some ribbons elongated or regular horseshoe appearance was preserved (**Fig. 4A**). Immunofluorescence with the bipolar cell marker PKC-α also demonstrated the presence of ectopic synapses that were protruding into the ONL of IT retinas whereas in wt mice no sprouting of rod bipolar dendrites was observed (**Fig. 4B**). Ribeye/PNA co-staining was comparable in wt and IT retinas (**Fig. 4C**).

Expression profile of calcium channels in wt and IT mouse retinas

To test whether the insertion of a mutation in the *CACNA1F* gene induced changes in the expression of other Cav channel subunits we performed qRT-PCR experiments from adult wt and IT mice. All Cav α_1 subunits except Cav1.1 were reliably expressed in IT mouse retinas, although at different expression levels (**Fig. 5**). Cav1.4, β_2, and $\alpha_2\delta$-4 were by far the most abundantly expressed isoforms in IT mice. Even though suggested from previous independent publications[34,35] this finding has not been shown before in direct comparison using the same tissue samples. The total amount of calcium channel transcripts in IT mice was not significantly different from wt but an approximately 25% reduction in the expression of Cav1.4

Table 2. Behavioral measures assessed in diverse tests of anxiety in wt and IT mice. Data are presented as means ± SEM

	wt, n = 13	IT, n = 11	Student t test	
Open field test			t value	p value
center entries (n)	34 ± 2	41 ± 4	1.230	0.232
center time (s)	143 ± 15	132 ± 15	0.499	0.623
distance traveled (cm)	2634 ± 105	2873 ± 160	1.284	0.213
Elevated plus maze				
latency to first open arm entry (s)	23 ± 4	18 ± 3	10.861	0.401
open arm entries (n)	9 ± 1	8 ± 1	0.234	0.818
open arm time (%)	43 ± 8	35 ± 9	0.617	0.544
total arm entries (n)	23 ± 2	22 ± 3	0.106	0.917
Light/dark test				
latency to first entry into the lit area (s)	53 ± 13	71 ± 34	0.548	0.589
entries into the lit area (n)	16 ± 2	13 ± 2	1.174	0.253
time spent in the lit area (s)	167 ± 17	185 ± 29	0.568	0.576
distance traveled (cm)	2811 ± 200	2781 ± 273	0.568	0.576

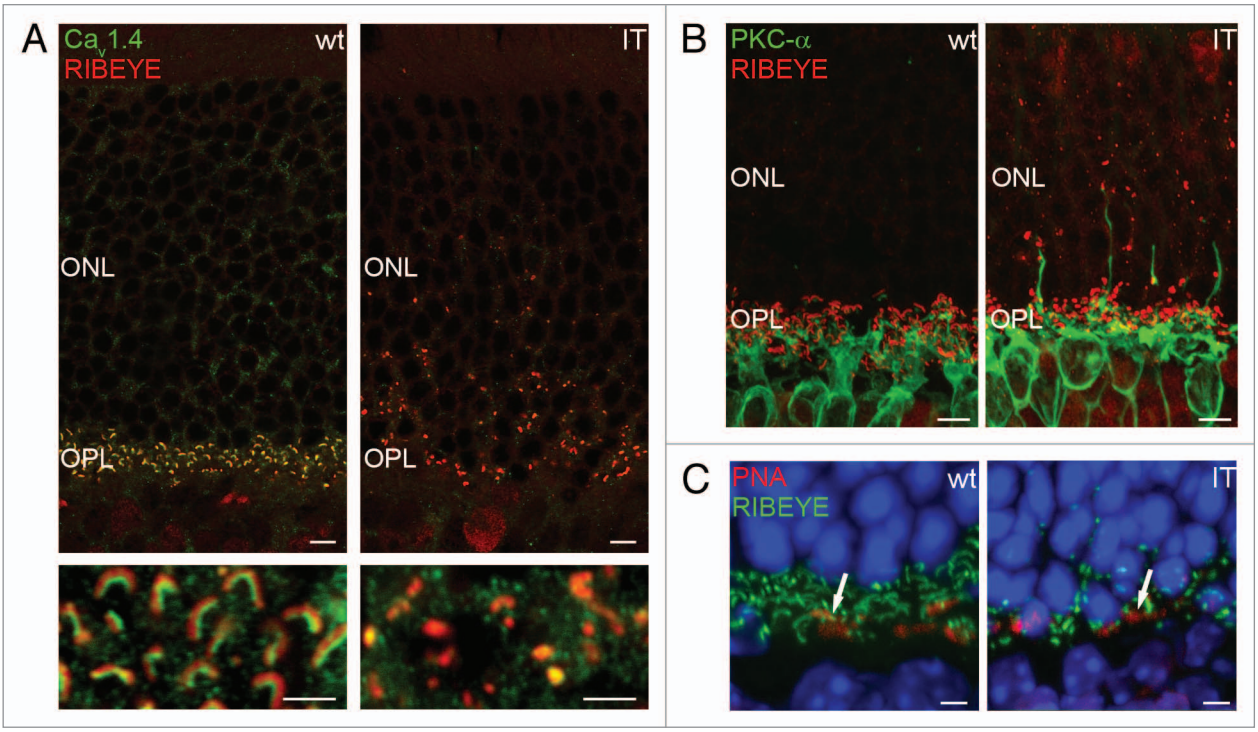

Figure 4. Photoreceptor synapses in adult wt and IT mice. (**A**) Immunofluorescence double-labeling of Cav1.4 (green) and the synaptic protein RIBEYE (red) in wt (right) and IT (left) mice. Wt mice show mature horseshoe-shaped ribbons whereas IT synapses were variable in morphology. (**B**) Co-staining with the rod bipolar cell maker PKCα (green) and CtBP2/Ribeye (red). Ectopic synapses in the outer nuclear layer (ONL) were observed only in IT mice (right). (**C**) Similar PNA staining (red) of cone synapses together with RIBEYE (green) in wt (left) and IT (right) mice. Scale bar 2 µm.

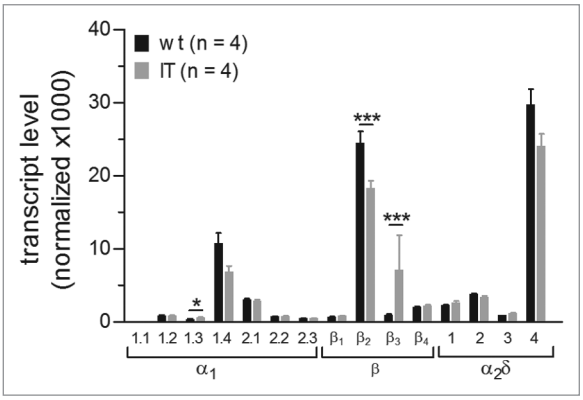

Figure 5. Expression profiles of voltage-activated Ca^{2+} channels in mouse retina of IT mice. The mRNA expression profiles of all high voltage-activated Ca^{2+} channel α_1, β, and $\alpha_2\delta$ subunit isoforms were determined in retinas of adult wt (black) and IT (gray) mice. Transcript levels (i.e., number of molecules per sample; see Material and Methods) of the individual experiments were normalized to the expression of the control genes Gapdh and Sdha. Log10 transformed transcript levels were analyzed by 2-way ANOVA: genotype, $F_{(1)} = 1.6$, $p = 0.208$; gene, $F_{(13)} = 131.5$, $p < 0.001$; genotype*gene, $F_{(13)} = 3.3$, $p < 0.001$; p values are derived from Holm-Sidak posthoc analysis. Data are presented as mean ± SEM. Note that in comparison to wt, expression of Cav1.4 trended to be less in IT mice ($p = 0.05$).

($p = 0.05$), β_2, and $\alpha_2\delta$-4 was evident in IT mice (**Fig. 5**). This finding may reflect a loss of photoreceptors, which was consistent also with our staining experiments (**Fig. 2**). In 2 out of 4 IT mice analyzed expression levels of the auxiliary β_3 subunit were 5-fold and 20-fold higher when compared with the other wt and IT mice, respectively (data not shown). This result is a plausible explanation for the highly significant increase of β_3 expression in IT mice ($p < 0.001$). Intriguingly, although transcripts for Cav1.3 account for only 2% of total α_1 subunits in wt they were significantly higher expressed in IT ($p = 0.03$). The isoforms Cav2.1, β_4 and $\alpha_2\delta$-2, which have previously been shown to be co-expressed in the cerebellum[25] also show comparable expression levels in the retina as implicated previously.[36]

Behavioral phenotype of IT mice

Finally, we investigated the role of Cav1.4 in visual function subjecting mice to established behavioral paradigms. Since these tests were all locomotion-based, we first screened for possible alterations in motor function. Wt and IT mice did not differ in novelty-induced locomotor activity (i.e., the distance traveled in the open field test and light/dark test or the total arm entries in the elevated plus maze test) as compared with wt (**Table 2**). Next, we assessed the visual performance of wt and IT mice subjecting them to the visual platform test of the Morris water maze[37] (**Fig. 6**). The escape latency (latency to reach and climb the platform) gradually decreased with the increasing number of trials performed (repeated measures ANOVA: $F(\text{trial})_{7,154} = 10.689$, $p < 0.001$) in both genotypes ($F(\text{trial} \times \text{genotype})_{7,154} = 0.445$, $p = 0.872$). However, in IT mice the latency was greatly

increased as compared with wt ($F(genotype)_{1,22}$ = 60.149, p < 0.001), pointing towards poor visual function of IT mice. In order to exclude a specific deficit in learning or memory-related processes as a cause for the impaired performance in the visible platform task of the Morris water maze, we tested the animals in an auditory cued fear-conditioning paradigm. Conditional responses, as indicated by freezing behavior, increased to the same extent in wt and IT mice upon 3 CS-footshock pairings (repeated measures ANOVA: $F(pairing)_{4,88}$ = 62.502, p < 0.001; $F(genotype)_{1,22}$ = 0.430, p = 0.519; $F(pairing \times genotype)_{4,88}$ = 0.6189, p = 0.650). On the next day in a novel context presentation of the CS alone did not elicit different freezing levels between the 2 genotypes suggesting normal learning capabilities of IT mice (percent freezing: wt 46.9 ± 5.5, IT 40.8 ± 5.2, t = 0.807, p = 0.428). Stimulated by human studies showing that the loss of vision has an impact on emotionality,[38,39,40] we also investigated the anxiety-related behavior of IT mice. No differences in any anxiety-related parameter including the entries into or time spent in the center of the open field, the latency, entries and time in the open arms of the elevated plus maze or the latency, entries into and time spent in the light compartment of the light/dark test were observed as compared with wt (**Table 2**).

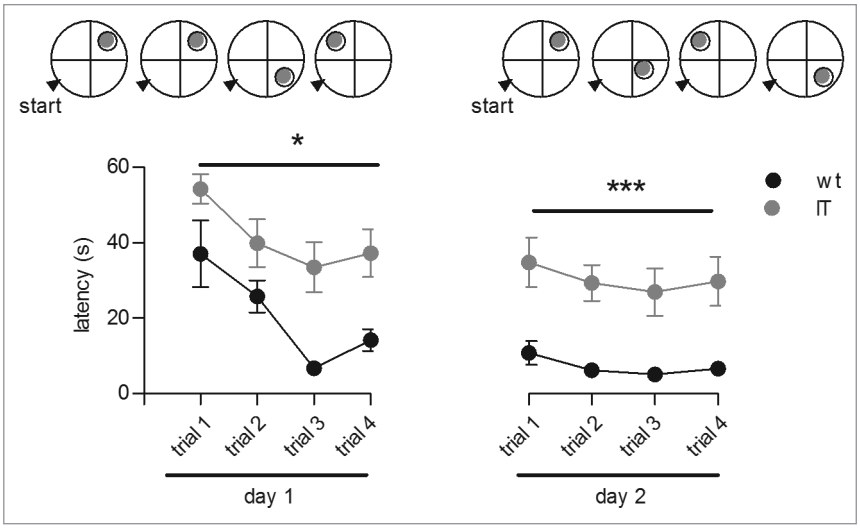

Figure 6. Behavioral phenotype of adult wt and IT mice. Performances of mice (latency to escape from the pool onto the platform) in the visible platform test of the Morris water maze task during 4 trials per day over 2 training days are shown. The fixed starting position of the mice is indicated by a black arrow while the varying positions of the platform are indicated by gray circles. Data represent the mean ± SEM; n = 13 for wt mice (black circles) and n = 11 for IT mice (gray circles). * p < 0.0.5 and *** p < 0.001 using a repeated-measures ANOVA and a post Fisher LSD test.

Discussion

Gain-of-function mutation I745T results in a loss of visual function

ERGs from Cav1.4 KO mice under scotopic and photopic conditions predicted a virtual lack of retinal transmission of electrical signals at the first synapse, affecting both rod and cone photoreceptors.[12] Recent data[33] also provided evidence that rod photoreceptor synapses in these mice remain immature which could inhibit photoreceptor synaptic transmission. Our data show that the level of synaptic maturation in adult IT mice, in contrast, was variable. Most synapses were abnormal, round, or elongated. However, some showed the horseshoe-like shape typical for mature wt synapses. In these cells specifically, a gain-of-function may limit the dynamic range of photoreceptor responses to an extent that would reduce but not completely suppress retinal signaling as seen in our ERG recordings. The marked leftward shift in the activation curve found in heterologously expressed IT channels[2] might increase the basal calcium levels in photoreceptors, due to higher activity at depolarized membrane potentials in the absence of light. Such high Ca^{2+} levels near the release sites could also lead to an increase in the time needed to shut-off glutamate release upon light exposure resulting in increased response latencies.

Our immunohistochemical data show cone anomalies similar to KO mice previously described.[33,41] Glypho, an enzyme that catalyzes the rate-limiting step in glycogenolysis (in brain but also retinal Müller glial cells and cones[42,43,44]) represents a main limited energy reserve.[45] The apparent stronger immunofluorescence signal in the cones and likely in surrounding cells in the IPL suggests that these cell types sense metabolic stress and show a higher need for glycogen breakdown. Although seen to a much lesser extent, the presence of potential degenerative signs is in line with a recent report on KO mice.[33]

The visually guided behavior tests supported our functional and structural findings. IT mice displayed increased escape latencies in the cued version of the Morris Water maze confirming poor visual ability. The performance of IT mice was comparable to that of animals with naturally occurring retinal degeneration including rd12 mice[37] and mice of the FVB/NJ, DBA/2, C3H, NIH Swiss and Black Swiss mice strains owen.[46,47] The Morris Water maze paradigm was used for assessing visual function.[48,49,50] Due to its primary field of application which is testing for spatial learning deficits in rodents[51] we wished to exclude the possibility that a cognitive deficit may underlie their bad performance. We therefore subjected wt and IT mice to an auditory cued fear-conditioning paradigm where vision is not essential. Indeed, both genotypes did not differ in fear learning or memory which is in line with other models of impaired vision owen.[46,52,53]

Additional information on retinal calcium channels obtained from the IT model

The expression profiling supported findings that Cav1.4 but also Cav1.3[5,54-63] and Cav1.2 [4,5] LTCCs are expressed in the retina. Interestingly, Cav1.3 channels were upregulated in IT. The retinal Cav1.3 distribution pattern is, however, controversial. Some studies showed accumulation in the inner segments of photoreceptors, OPL, INL, or GCL, whereas another reported Cav1.3

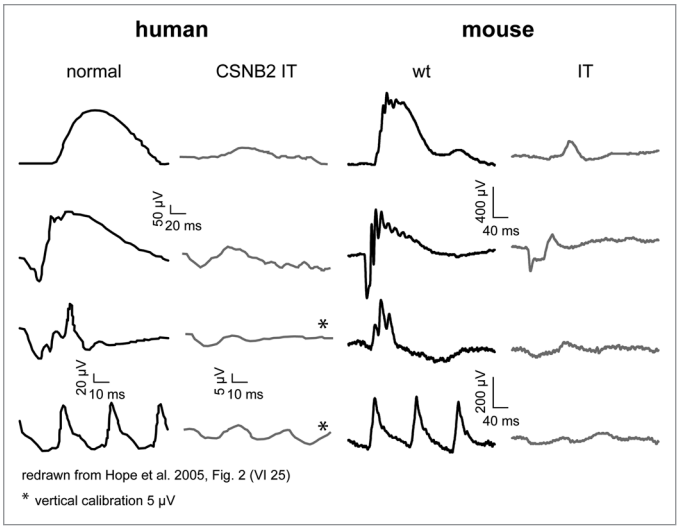

Figure 7. Functional comparison of human and murine subjects affected by the I745T mutation. Ganzfeld ERG recordings from a normal subject (left) and a patient with incomplete CSNB carrying the CACNA1F mutation I745T (center left) were redrawn form the original records (ref. 3). They correlate rather well with the murine data of wt (C57BL/6N; center right) and IT mice (right). The set of records follows the human ERG diagnostic standard as issued by the International Society for Clinical Electrophysiology of Vision (ISCEV; www.iscev.org/standards). From top to bottom, traces in each column represent the scotopic single flash response, the scotopic mixed response, the photopic single flash response, and the photopic 30 Hz flicker ERG. The murine records were obtained with identical paradigms.

expression across retinal cell layers.[5] Therefore, the role of Cav1.3 remains ambiguous. A contribution of Cav1.3 to ERG light peak regulation in the pigment retinal epithelium (RPE) is reported.[64] Though in our preparation the RPE was never included. Cav1.3 channels are also subject to rapid glutamate-induced internalization, likely to serve as a protective negative feedback mechanism[62] implying a role in other processes than synaptic transmission. Upregulation of Cav1.3 channels may be part of a potential compensatory mechanism in IT. The high level of expression of Cav2.1, β_4, and $\alpha_2\delta$-2 in IT retinas is intriguing. Although retinal pathway involvement in the adaptation mechanism to circadian phase-shift has been excluded previously in Cav2.1-mutated migraine mice[65] this hypothesis was never directly tested. The mammalian retina contains a clock that generates molecular circadian rhythms independent of the suprachiasmatic nucleus master clock,[66] but a calcium channel contribution was so far only reported for Cav1.2.[67,68]

IT mice serve as a good model for the functional phenotype seen in human patients

The Ganzfeld ERG recordings, both dark adapted (scotopic) and light adapted (photopic), suggest that there is a very close match between rod and cone system responses in CSNB2 patients carrying the I745T mutation[1] and the IT mouse line (**Fig. 7**). The functional pattern in both resembles a form of incomplete CSNB; rod and cone single flash responses as well as the flicker ERG were typically altered. The particular feature in I745T mutants, presumably associated with the gain-of-function nature of the disorder, is that the negative components of the scotopic standard flash response are smaller than those found in other CSNB types, but on the other hand a distinct remaining b-wave component is present. The comparison with the human data clearly underlines that the IT mouse line is a specific model for the functional phenotype seen in respective patients.

Materials and Methods

Animals

Animals were group-housed under standard laboratory conditions (12:12 light/dark cycle with lights on at 07:00 h, 22 ± 2 °C, 50–60% humidity) with pelleted food and water available ad libitum. All experiments were designed to minimize animal suffering as well as the number of animals used and were approved by the national ethical committee on animal care and use (Austrian Federal Ministry for Science and Research; BMWF-66.008/0016-II/3b/2012) and the Institutional Animal Care and Use Committee at the University of Iowa. Animals were killed by cervical dislocation in compliance with international laws and policies or by carbon dioxide exposure followed by cervical dislocation as approved by the Institutional Animal Care and Use Committee at the University of Iowa. All ERG and OCT procedures in animals were performed in accordance with the ARVO Statement for the Use of Animals in Ophthalmic and Vision Research with permission of local authorities (Regierungspräsidium Tübingen).

Cav1.4 mouse lines

We used a mouse model made by Dr Marion Maw (University of Otago) which carries the mutation I745T in the CACNA1F gene identified in a New Zealand CSNB2 family (IT).[4] Mouse tail biopsies were collected from all mice before and after the experiment for genotyping. Only male mice were investigated. Genomic DNA was isolated using buffer containing 10 mM Tris (pH 8.8), 50 mM KCl and 0.1% Triton X-100. We controlled for the IT allele and the corresponding wt alleles, as well as the rd8 mutant allele. IT mice were checked with following specific primers fwd-CACTCCAGACATCCTGCTGA and rev-GTCAACCCATGCTGTCTCCT. The PCR product for the wt allele has a length of 288-bp and the one for the IT allele 449-bp. PCR reaction was performed in a total volume of 20 µl, containing 2 µl DNA eluate, 0.2 µM fwd and rev primer, 0.025 U GoTaq DNA Polymerase (Promega), 1.5 mM MgCl, and 200 µM dNTPs. The following reaction cycle was used: 95 °C 4 min, 40 cycles of 9 5°C for 30 s, 63 °C for 30 s and 72 °C for 45 s, with a final extension at 72 °C for 10 min. Because the background of both IT and wt littermates as non-littermate wt controls was C57BL/6N we also genotyped for the rd8 mutation allele[13] which was amplified with fwd – CCCCTGTTTGCATGGAGGAAACTTGGAAG and rev-GCCCCATTTGCACACTGATGAC (224-bp product). The following PCR program was used for this assay: 94°C for 5 min, followed by 35 cycles at 94 °C for 30 s, 65 °C for 30 s, 72 °C for 30 s and a final elongation step of 72 °C for 7 min. The wt allele was amplified with fwd-GTGAAGACAGCTACAGTTCTGATC and rev-GCCCCATTTGCACACTGATGAC (220 bp product size). For the mutant allele

a PCR reaction of 25 µl was applied; containing 2 µl DNA, 1.6 µM forward and reverse primer, 0.02 U GoTaq DNA Polymerase (Promega), 1.2 mM MgCl and 100 µM dNTPs. The following PCR program was used: 94 °C for 5 min, followed by 35 cycles at 94 °C for 30 s, 65 °C for 30 s, 72 °C for 30 s. and a final elongation step of 72 °C for 7 min. The wt allele was amplified as follows: 25 µM reaction volume containing 2 µl DNA, 0.8 µM fwd primer and 1.6 µM rev primer, 0.02 U GoTaq DNA Polymerase (Promega), 1.2 mM MgCl, and 100 µM dNTPs. For the wt allele, DNA was denaturated at 94°C for 5 min, followed by 35 cycles of 94 °C for 30 s, 58 °C for 30 s, 72 °C for 30 s followed by extension at 72 °C for 7 min. Mice used in the study were either heterozygous or homozygous for the mutated allele; the wt retinal phenotype was without pathological findings.

Table 1. Markers investigated in immunofluorescence studies

Primary antibodies /markers	Dilution	Company
glycogen phosphorylase (glypho)	1:2000	Gift from Dr Hamprecht (Pfeiffer-Guglielmi et al., 2003)
sc-14363/blue sensitive cone opsin	1:200	Santa Cruz Biotechnology Inc. Heidelberg, Germany
biotinylated peanut agglutinin (PNA)	1:25	Vector Laboratories, California, USA
DAPI	1:10000	Sigma, St. Louis, MO
rabbit/mouse PKC-α	1:500	Santa Cruz, Dallas, Texas and Sigma, St. Louis, MO
rabbit/mouse RIBEYE	1:500	Covance, Princeton, NJ and BD bioscience, San Jose, CA
rabbit Cav1.4	1:1000	Custom-made (Dr Amy Lee)
Secondary antibodies		
Alexa Fluor® 488 Donkey Anti-Goat IgG	1:300 or 1:1000	Life Technologies, Grand Island, NY
Alexa Fluor ® 594 Goat Anti Guinea Pig IgH	1:300	Life Technologies, Grand Island, NY
Alexa Fluor ® 568-Goat Anti-mouse IgG	1:1000	Life Technologies, Grand Island, NY
Streptavidin, Alexa Fluor® 546 conjugate	1:300	Life Technologies, Grand Island, NY

Immunocytochemisty

Fixation and embedding

Eleven week old mice were sacrificed in the morning by cervical dislocation and decapitation. Eyes were removed, opened at the sclero-corneal rim and fixed for 15 min in 4% paraformaldehyde (PFA) in phosphate-buffered saline (PBS, 1 × , pH 7.4). After removal of cornea and lens, the eyecups were fixed for 2 h in 4% PFA/1 × PBS at room temperature (RT), rinsed in 1 × PBS (4 changes), and cryoprotected in increasing concentrations of sucrose (10% and 20% in 1 × PBS). Eyecups were embedded in a 1:1 mixture of 20% sucrose in 1x PBS and OCT medium (Tissue-Tek, Sakura) for 2 d at RT. Sections of 16 µm thickness were collected on to Superfrost Plus slides, air-dried for 24 h and stored at – 20°C until further use.

Immunofluoroescence

Sections were washed 3 times with washing buffer (1 × PBS, 0.1% Triton X-100, and 0.05% NaN_3). For primary antibody labeling or PNA, the tissue was blocked with 1% bovine serum albumin (BSA, Sigma) in 1 × PBS, 0.1% Triton X-100 and 0.05% NaN_3 for 30 min at RT. Primary antibody incubation and PNA staining was performed overnight at 4°C. Sections were washed 3 times in washing buffer, incubated with the secondary antibody for 1 h at RT, washed 3 times and counterstained with DAPI before mounting in Aqua-Poly/Mount (Polysciences). Primary and secondary antibodies and PNA were used in dilutions listed in **Table 1**. Micrographs or series of microsgraphs were taken with a Zeiss Axiovert 200M (Carl Zeiss). Images were adjusted for brightness and contrast and assembled using Photoshop CS5 (Adobe). Z-stacks were taken in 0.1 µm intervals and deconvolved with Huygens Essential (Scientific Volume Imaging B.V.) software. Processing of synaptic connections was done essentially as described previously.[14] In some experiments Hoechst stain (1:1000) was applied along with secondary antibodies. Confocal microscopy was performed using a Fluoview 1000 confocal microscope (Olympus) with 60X or 100X oil-immersion objectives or a Zeiss LSM710 confocal microscope with a Plan-Neofluar 63x/1.4 oil-immersion objective (Carl Zeiss). For consistency among figures, the red and green colors were switched using Adobe Photoshop.

Electroretinography

The functional implications of the I745T mutation was assessed in the IT mouse line in vivo with electroretinography (ERG). ERGs were recorded binocularly from animals at the age of 6 weeks postnatally as described previously.[15,16] Mice were anaesthetized using Ketamine (66.7 mg/kg body weight) and Xylazine (11.7 mg/kg body weight). Their pupils were dilated and single flash ERG responses were obtained under scotopic (dark-adapted overnight) and photopic (light-adapted with a background illumination of 30 cdm^{-2} starting 10 min before recording) conditions. Single white-flash stimuli ranged from – 4 to 1.5 log $cdsm^{-2}$ under dark-adapted and from – 2 to 1.5 log $cdsm^{-2}$ under light-adapted conditions. Ten responses were averaged with inter-stimulus intervals of 5 s (for – 4 to – 0.5 log $cdsm^{-2}$) or 17 s (for 0 to 1.5 log $cdsm^{-2}$). Responses to trains of flashes (flicker) were obtained under dark – adapted conditions using a fixed intensity (0.5 log $cdsm^{-2}$, resembling the International Society for Clinical Electrophysiology of Vision standard flash (ISCEV SF) intensity.[17] Flicker responses were averaged 30 times, and band-pass filter cut-off frequencies were 0.3 and 300 Hz for all ERG recordings. ERGs were obtained in n = 4 IT and n = 2 wt control animals.

Spectral Domain Optical Coherence Tomography

Spectral Domain Optical Coherence Tomography (SD-OCT) imaging was done with a commercially available Spectralis™ HRA+OCT device (Heidelberg Engineering) featuring a broadband superluminescent diode at 870 nm as low coherent light source. Each 2-dimensional B-scan recorded at 30° field of view consists of 1536 A-scans, which are acquired at a speed of 40000

scans per second. Optical depth resolution is approximately 7 μm with digital resolution reaching 3.5 μm. Imaging was performed using the proprietary software package Eye Explorer (version 3.2.1.0, Heidelberg Engineering). OCTs were recorded binocularly from animals at the age of 6 weeks postnatally as described previously.[18,19]

Quantitative RT-PCR

Whole retinas, brain and muscle from 8 week old wt and mutant mice were dissected. Tissue was collected and flash frozen in liquid nitrogen. For control PCRs, tsA-201 cells were transfected with cDNA encoding Cav1.4 (Accession number JF701915). Total RNA of either mouse retinas or transfected tsA-201 was isolated with RNeasy Plus Mini Kit, (Qiagen) with an extra purification step with RNase-Free DNase Set (Qiagen). For total RNA isolation of brain and muscle RNeasy Lipid Tissue Midi Kit or respectively muscle RNeasy Fibrous Tissue Midi Kit were used. cDNA synthesis was performed with RT-PCR first strand synthesis (Fermentas, ThermoScientific). For cDNA synthesis of retina, total RNA eluate, for muscle and brain 35ng/μl of RNA eluate was used. Qualitative PCRs were conducted using cDNA in the following range: retina 25 – 116 ngμl^{-1}, brain and muscle: 35 ngμl^{-1} and transfected cells 1.5 – 1.9 μgμl^{-1}. Specific primer for Cav1.1, 1.2, 1.4 as well as various splice forms of Cav1.3 were tested.[20,21,22,23,24] *Taqman RT-PCR* on cDNA obtained from retinas (see above) was performed according to a previously developed protocol.[25] The relative abundance of different Cav subunit transcripts was assessed by TaqMan quantitative PCR (qRT-PCR) using a standard curve method based on PCR products of known concentration in combination with normalization using the most stable control genes as previously described.[25] TaqMan gene expression assays specific for all high-voltage activated Ca^{2+} channel subunits (α_1, β, and $\alpha_2\delta$) were designed to span exon–exon boundaries, and were purchased from Applied Biosystems. The following assays were used [name (gene symbol), assay ID (Applied Biosystems)]: Cav1.1 (Cacna1s), Mm00489257_m1; Cav1.2 (Cacan1c), Mm00437953_m1; Cav1.3 (Cacna1d), Mm01209919_m1; Cav1.4 (Cacna1f), Mm00490443_m1; Cav2.1 (Cacna1a), Mm00432190_m1; Cav2.2 (Cacna1b), Mm00432226_m1; Cav2.3 (Cacna1e), Mm00494444_m1; β_1 (Cacnb1), Mm00518940_m1; β_2 (Cacnb2), Mm00659092_m1; β_3 (Cacnb3), Mm00432233_m1; β_4 (Cacnb4) Mm00521623_m1; $\alpha_2\delta$-1 (Cacna2d1), Mm00486607_m1; $\alpha_2\delta$-2 (Cacna2d2), Mm00457825_m1; $\alpha_2\delta$-3 (Cacna2d3), Mm00486613_m1; $\alpha_2\delta$-4 (Cacna2d4), Mm01190105_m1. The endogenous control genes included were [name (gene symbol), assay ID (Applied Biosystems)]: γ-cytoplasmic actin (ACTB), Mm00607939_s1; β-2-microglobulin (B2M), Mm00437762_m1; glyceraldehyde-3-phosphate dehydrogenase (GAPD), Mm99999915_g1; hypoxanthine phosphoribosyl-transferase 1 (HPRT1), Mm00446968_m1; succinate dehydrogenase complex, subunit A (SDHA), Mm01352363_m1; tata box binding protein (TBP), Mm00446973_m1; transferrin receptor (TFRC), Mm00441941_m1. The qRT-PCR (50 cycles) was performed in duplicates using 10–20 ng total RNA equivalents of cDNA and the specific TaqMan gene expression assay for each 20 μl reaction in TaqMan Universal PCR Master Mix (Applied Biosystems). Measurements were performed on four independent RNA preparations from each genotype. Analyses were performed using the 7500 Fast System (Applied Biosystems). The cycle threshold (Ct) values for each Cav gene expression assay were recorded for each individual preparation. To allow a direct comparison between the expression levels in different tissues, we normalized all experiments to Gapdh and Sdha, which were determined to be most stable expressed reference genes across all preparations and time points.[26] Subsequently normalized molecule numbers were calculated for each Cav subunit from their respective standard curve.[25]

Behavioral experiments

All behavioral experiments were performed between 09:00 and 14:00 h after the animals had been habituated to the testing room for at least 24 h. In order to decrease the number of animals used, the behavioral experiments, with at least 2 d of rest between each, were performed in the same animals in the following order: (1) animals were tested in the open field test,[27,28] light/dark test[28] and the elevated plus maze test,[5] (2) their visual function was assessed in a modified Morris water maze test involving a visible escape platform[5] and (3) auditory fear conditioning was used to assess (vision-independent) learning capabilities.[29]

Open field

Mice were individually placed into the periphery of an open field (41 × 41 × 41 cm, floor illumination 150 lx) whose area was divided into a 28 × 28 cm central zone. The entries into the central zone, the time spent in the central zone and the overall distance traveled by the mice were measured during the 10 min exploration time by using an automated activity monitoring system (TruScan, Coulbourn Instruments).

Light/dark test

The white, aversive compartment (41 × 20.5 × 41 cm, floor illumination 400 lx) and the dark, safe compartment (41 × 20.5 × 41 cm covered by a black top, floor illumination 10 lx) of the testing arena were connected by a small opening (7 × 7 cm) located in the center of the partition at floor level. Animals were individually placed into the dark compartment facing away from the opening and allowed to freely explore the apparatus for 10 min. The latency to the first entry into the lit compartment, the number of entries and time spent in the lit compartment and the overall distance traveled by each mouse was automatically registered (TruScan, Coulbourn Instruments).

Elevated plus maze test

The 5 min test was performed on a plus-shaped maze which was elevated (73 cm) from the floor and consisted of 2 open arms (à 30 × 6 cm; 100 lx), two closed arms (à 30 × 6 × 17 cm; illuminated with red light), and a central neutral zone (6 × 6 cm). Animals were placed onto the neutral zone of the maze facing a closed arm and their locomotor behavior was continuously recorded by a tracking system (TSE Technical and Scientific Equipment GmbH) connected to a camera positioned above the maze. The latency to the first open arm entry, the number of open arm entries, the percentage of time spent on the open arms and the distance traveled were analyzed.

Visible platform test of the Morris water maze

Mice were placed into a circular pool (1.2 min in diameter) filled with water (23 °C) and illuminated at 40 lx. Starting from a fixed position they were allowed to escape by climbing onto a platform (10 cm diameter) placed just above the water and marked with a flag for facilitating visualization. The animals were allowed to stay on the platform for additional 10 s. In case the animal was not able to locate the platform, it was gently guided to it by the experimenter. On each of 2 consecutive days animals performed four 60 s trials separated by 60 min. The location of the platform was changed after each trial. The latency to reach the platform was recorded.

Auditory fear conditioning

In the conditioning context (25 × 25 × 30 cm chamber with transparent walls and a metal rod floor cleaned with water, floor illumination 300 lx; TSE) mice received three pairings (2 min inter-pairing interval) of an auditory 30 s white noise conditioned stimulus (CS; 10 kHz, 80 dB) and a co-terminating 2 s mild foot shock (0.6 mA). Twenty-four hours after the auditory fear conditioning 3 CSs separated by 5 s were presented to mice for a fear expression test in a novel context (25 × 25 × 30 cm chamber with black walls and a solid gray cleaned with ethanol, floor illumination 10 lx; TSE). The time remaining in freezing behavior during the CS presentations was manually determined by an observer blind to the genotype.

Statistics

All values are presented as mean ± SEM for the indicated number of experiments (n). For multiple comparisons of in vitro data statistical significance was determined by a 1-way analysis of variance (ANOVA) followed by Bonferroni multiple-comparison or the Dunnett post-hoc test. For comparisons of 2 groups, data were analyzed by the Student t test as indicated for individual experiments. Behavioral data were statistically analyzed using repeated-measures ANOVA followed by post Fisher's LSD test or the unpaired Student t test. In qRT-PCR experiments, data were organized and analyzed using MS Excel and SigmaStat (Systat Software, Inc.) statistical software. Statistical significance was determined on log10 transformed expression levels using 2-way-ANOVA followed by Holm-Sidak posthoc comparison. Statistical significance was set at $p < 0.05$.

Disclosure of Potential Conflicts of Interest

No potential conflicts of interest were disclosed.

Acknowledgments

We thank Stefanie Geisler and Stefan Kummer for excellent technical assistance and Peter Ahnelt for helpful discussions. This work was supported by the Austrian Science Fund (FWF P-22528 to Koschak A), SFB F44 (F4402 to Koschak A, F4406 to Obermair GJ), P24079-B21 (to Obermair GJ) the German Research Council DFG (Se837/6–2), the National Institutes of Health (DC009433 and HL87120 to Lee A, DC010362 [Iowa Center for Molecular Auditory Neuroscience], EY020542 to Baker SA) and the Medical University Vienna.

References

1. Hope CI, Sharp DM, Hemara-Wahanui A, Sissingh JI, Lundon P, Mitchell EA, Maw MA, Clover GM. Clinical manifestations of a unique X-linked retinal disorder in a large New Zealand family with a novel mutation in CACNA1F, the gene responsible for CSNB2. Clin Experiment Ophthalmol 2005; 33:129-36; PMID:15807819; http://dx.doi.org/10.1111/j.1442-9071.2005.00987.x
2. Hemara-Wahanui A, Berjukow S, Hope CI, Dearden PK, Wu SB, Wilson-Wheeler J, Sharp DM, Lundon-Treweek P, Clover GM, Hoda JC, et al. A CACNA1F mutation identified in an X-linked retinal disorder shifts the voltage dependence of Cav1.4 channel activation. Proc Natl Acad Sci U S A 2005; 102:7553-8; PMID:15897456; http://dx.doi.org/10.1073/pnas.0501907102
3. Morgans CW. Localization of the alpha(1F) calcium channel subunit in the rat retina. Invest Ophthalmol Vis Sci 2001; 42:2414-8; PMID:11527958
4. Specht D, Wu SB, Turner P, Dearden P, Koentgen F, Wolfrum U, Maw M, Brandstätter JH, tom Dieck S. Effects of presynaptic mutations on a postsynaptic Cacna1s calcium channel colocalized with mGluR6 at mouse photoreceptor ribbon synapses. Invest Ophthalmol Vis Sci 2009; 50:505-15; PMID:18952919; http://dx.doi.org/10.1167/iovs.08-2758
5. Busquet P, Nguyen NK, Schmid E, Tanimoto N, Seeliger MW, Ben-Yosef T, Mizuno F, Akopian A, Striessnig J, Singewald N. CaV1.3 L-type Ca2+ channels modulate depression-like behaviour in mice independent of deaf phenotype. Int J Neuropsychopharmacol 2010; 13:499-513; PMID:19664321; http://dx.doi.org/10.1017/S1461145709990368
6. Mercer AJ, Chen M, Thoreson WB. Lateral mobility of presynaptic L-type calcium channels at photoreceptor ribbon synapses. J Neurosci 2011; 31:4397-406; PMID:21430141; http://dx.doi.org/10.1523/JNEUROSCI.5921-10.2011
7. Koschak A, Reimer D, Walter D, Hoda JC, Heinzle T, Grabner M, Striessnig J. Cav1.4alpha1 subunits can form slowly inactivating dihydropyridine-sensitive L-type Ca2+ channels lacking Ca2+-dependent inactivation. J Neurosci 2003; 23:6041-9; PMID:12853422
8. Stockner T, Koschak A. What can naturally occurring mutations tell us about Ca(v)1.x channel function? Biochim Biophys Acta 2013; 1828:1598-607; PMID:23219801; http://dx.doi.org/10.1016/j.bbamem.2012.11.026
9. McRory JE, Hamid J, Doering CJ, Garcia E, Parker R, Hamming K, Chen L, Hildebrand M, Beedle AM, Feldcamp L, et al. The CACNA1F gene encodes an L-type calcium channel with unique biophysical properties and tissue distribution. J Neurosci 2004; 24:1707-18; PMID:14973233; http://dx.doi.org/10.1523/JNEUROSCI.4846-03.2004
10. Hoda JC, Zaghetto F, Koschak A, Striessnig J. Congenital stationary night blindness type 2 mutations S229P, G369D, L1068P, and W1440X alter channel gating or functional expression of Ca(v)1.4 L-type Ca2+ channels. J Neurosci 2005; 25:252-9; PMID:15634789; http://dx.doi.org/10.1523/JNEUROSCI.3054-04.2005
11. Peloquin JB, Rehak R, Doering CJ, McRory JE. Functional analysis of congenital stationary night blindness type-2 CACNA1F mutations F742C, G1007R, and R1049W. Neuroscience 2007; 150:335-45; PMID:17949918; http://dx.doi.org/10.1016/j.neuroscience.2007.09.021
12. Mansergh F, Orton NC, Vessey JP, Lalonde MR, Stell WK, Tremblay F, Barnes S, Rancourt DE, Bech-Hansen NT. Mutation of the calcium channel gene Cacna1f disrupts calcium signaling, synaptic transmission and cellular organization in mouse retina. Hum Mol Genet 2005; 14:3035-46; PMID:16155113; http://dx.doi.org/10.1093/hmg/ddi336
13. Mattapallil MJ, Wawrousek EF, Chan CC, Zhao H, Roychoudhury J, Ferguson TA, Caspi RR. The Rd8 mutation of the Crb1 gene is present in vendor lines of C57BL/6N mice and embryonic stem cells, and confounds ocular induced mutant phenotypes. Invest Ophthalmol Vis Sci 2012; 53:2921-7; PMID:22447858; http://dx.doi.org/10.1167/iovs.12-9662
14. Haeseleer F, Imanishi Y, Maeda T, Possin DE, Maeda A, Lee A, Rieke F, Palczewski K. Essential role of Ca2+-binding protein 4, a Cav1.4 channel regulator, in photoreceptor synaptic function. Nat Neurosci 2004; 7:1079-87; PMID:15452577; http://dx.doi.org/10.1038/nn1320
15. Seeliger MW, Zrenner E, Apfelstedt-Sylla E, Jaissle GB. Identification of Usher syndrome subtypes by ERG implicit time. Invest Ophthalmol Vis Sci 2001; 42:3066-71; PMID:11687556
16. Tanimoto N, Muehlfriedel RL, Fischer MD, Fahl E, Humphries P, Biel M, Seeliger MW. [Landmark Ed]. Front Biosci 2009; 14:2730-7; http://dx.doi.org/10.2741/3409
17. Marmor MF, Holder GE, Seeliger MW, Yamamoto S; International Society for Clinical Electrophysiology of Vision. Standard for clinical electroretinography (2004 update). Doc Ophthalmol 2004; 108:107-14; PMID:15455793; http://dx.doi.org/10.1023/B:DOOP.0000036793.44912.45

18. Fischer MD, Huber G, Beck SC, Tanimoto N, Muehlfriedel R, Fahl E, Grimm C, Wenzel A, Remé CE, van de Pavert SA, et al. Noninvasive, in vivo assessment of mouse retinal structure using optical coherence tomography. PLoS One 2009; 4:e7507; PMID:19838301; http://dx.doi.org/10.1371/journal.pone.0007507
19. Huber G, Beck SC, Grimm C, Sahaboglu-Tekgoz A, Paquet-Durand F, Wenzel A, Humphries P, Redmond TM, Seeliger MW, Fischer MD. Spectral domain optical coherence tomography in mouse models of retinal degeneration. Invest Ophthalmol Vis Sci 2009; 50:5888-95; PMID:19661229; http://dx.doi.org/10.1167/iovs.09-3724
20. Koschak A, Obermair GJ, Pivotto F, Sinnegger-Brauns MJ, Striessnig J, Pietrobon D. Molecular nature of anomalous L-type calcium channels in mouse cerebellar granule cells. J Neurosci 2007; 27:3855-63; PMID:17409250; http://dx.doi.org/10.1523/JNEUROSCI.4028-06.2007
21. Singh A, Gebhart M, Fritsch R, Sinnegger-Brauns MJ, Poggiani C, Hoda JC, Engel J, Romanin C, Striessnig J, Koschak A. J Biol Chem 2008
22. Sinnegger-Brauns MJ, Huber IG, Koschak A, Wild C, Obermair GJ, Einzinger U, Hoda JC, Sartori SB, Striessnig J. Expression and 1,4-dihydropyridine-binding properties of brain L-type calcium channel isoforms. Mol Pharmacol 2009; 75:407-14; PMID:19029287; http://dx.doi.org/10.1124/mol.108.049981
23. Baig SM, Koschak A, Lieb A, Gebhart M, Dafinger C, Nürnberg G, Ali A, Ahmad I, Sinnegger-Brauns MJ, Brandt N, et al. Loss of Ca(v)1.3 (CACNA1D) function in a human channelopathy with bradycardia and congenital deafness. Nat Neurosci 2011; 14:77-84; PMID:21131953; http://dx.doi.org/10.1038/nn.2694
24. Bock G, Gebhart M, Scharinger A, Jangsangthong W, Busquet P, Poggiani C, Sartori S, Mangoni ME, Sinnegger-Brauns MJ, Herzig S, et al. Functional properties of a newly identified C-terminal splice variant of Cav1.3 L-type Ca2+ channels. J Biol Chem 2011; 286:42736-48; PMID:21998310; http://dx.doi.org/10.1074/jbc.M111.269951
25. Schlick B, Flucher BE, Obermair GJ. Voltage-activated calcium channel expression profiles in mouse brain and cultured hippocampal neurons. Neuroscience 2010; 167:786-98; PMID:20188150; http://dx.doi.org/10.1016/j.neuroscience.2010.02.037
26. Willems E, Leyns L, Vandesompele J. Standardization of real-time PCR gene expression data from independent biological replicates. Anal Biochem 2008; 379:127-9; PMID:18485881; http://dx.doi.org/10.1016/j.ab.2008.04.036
27. Singewald N, Sinner C, Hetzenauer A, Sartori SB, Murck H. Magnesium-deficient diet alters depression – and anxiety-related behavior in mice—influence of desipramine and Hypericum perforatum extract. Neuropharmacology 2004; 47:1189-97; PMID:15567428; http://dx.doi.org/10.1016/j.neuropharm.2004.08.010
28. Sartori SB, Whittle N, Hetzenauer A, Singewald N. Magnesium deficiency induces anxiety and HPA axis dysregulation: modulation by therapeutic drug treatment. Neuropharmacology 2012; 62:304-12; PMID:21835188; http://dx.doi.org/10.1016/j.neuropharm.2011.07.027
29. Sartori SB, Hauschild M, Bunck M, Gaburro S, Landgraf R, Singewald N. Enhanced fear expression in a psychopathological mouse model of trait anxiety: pharmacological interventions. PLoS One 2011; 6:e16849; PMID:21386891; http://dx.doi.org/10.1371/journal.pone.0016849
30. Blanks JC, Johnson LV. Specific binding of peanut lectin to a class of retinal photoreceptor cells. A species comparison. Invest Ophthalmol Vis Sci 1984; 25:546-57; PMID:6715128
31. Johnson LV, Hageman GS. Enzymatic characterization of peanut agglutinin-binding components in the retinal interphotoreceptor matrix. Exp Eye Res 1987; 44:553-65; PMID:3109930; http://dx.doi.org/10.1016/S0014-4835(87)80163-X
32. Haverkamp S, Wässle H, Duebel J, Kuner T, Augustine GJ, Feng G, Euler T. The primordial, blue-cone color system of the mouse retina. J Neurosci 2005; 25:5438-45; PMID:15930394; http://dx.doi.org/10.1523/JNEUROSCI.1117-05.2005
33. Zabouri N, Haverkamp S. Calcium channel-dependent molecular maturation of photoreceptor synapses. PLoS One 2013; 8:e63853; PMID:23675510; http://dx.doi.org/10.1371/journal.pone.0063853
34. Wycisk KA, Budde B, Feil S, Skosyrski S, Buzzi F, Neidhardt J, Glaus E, Nürnberg P, Ruether K, Berger W. Structural and functional abnormalities of retinal ribbon synapses due to Cacna2d4 mutation. Invest Ophthalmol Vis Sci 2006; 47:3523-30; PMID:16877424; http://dx.doi.org/10.1167/iovs.06-0271
35. Ball SL, McEnery MW, Yunker AM, Shin HS, Gregg RG. Distribution of voltage gated calcium channel β subunits in the mouse retina. Brain Res 2011; 1412:1-8; PMID:21831364
36. Kamphuis W, Hendriksen H. Expression patterns of voltage-dependent calcium channel alpha 1 subunits (alpha 1A-alpha 1E) mRNA in rat retina. Brain Res Mol Brain Res 1998; 55:209-20; PMID:9582423; http://dx.doi.org/10.1016/S0169-328X(97)00363-X
37. Pang JJ, Chang B, Kumar A, Nusinowitz S, Noorwez SM, Li J, Rani A, Foster TC, Chiodo VA, Doyle T, et al. Gene therapy restores vision-dependent behavior as well as retinal structure and function in a mouse model of RPE65 Leber congenital amaurosis. Mol Ther 2006; 13:565-72; PMID:16223604; http://dx.doi.org/10.1016/j.ymthe.2005.09.001
38. Fenwick E, Rees G, Pesudovs K, Dirani M, Kawasaki R, Wong TY, Lamoureux E. Social and emotional impact of diabetic retinopathy: a review. Clin Experiment Ophthalmol 2012; 40:27-38; PMID:21575125; http://dx.doi.org/10.1111/j.1442-9071.2011.02599.x
39. Kempen GI, Zijlstra GA. Clinically Relevant Symptoms of Anxiety and Depression in Low-Vision Community-Living Older Adults. Am J Geriatr Psychiatry 2013; PMID:23567435; http://dx.doi.org/10.1016/j.jagp.2012.08.007
40. Renieri G, Pitz S, Pfeiffer N, Beutel ME, Zwerenz R. Changes in quality of life in visually impaired patients after low-vision rehabilitation. Int J Rehabil Res 2013; 36:48-55; PMID:22890293; http://dx.doi.org/10.1097/MRR.0b013e328357885b
41. Raven MA, Orton NC, Nassar H, Williams GA, Stell WK, Jacobs GH, Bech-Hansen NT, Reese BE. Early afferent signaling in the outer plexiform layer regulates development of horizontal cell morphology. J Comp Neurol 2008; 506:745-58; PMID:18076080; http://dx.doi.org/10.1002/cne.21526
42. Ignacio PC, Baldwin BA, Vijayan VK, Tait RC, Gorin FA. Brain isozyme of glycogen phosphorylase: immunohistological localization within the central nervous system. Brain Res 1990; 529:42-9; PMID:2282504; http://dx.doi.org/10.1016/0006-8993(90)90809-P
43. Nihira M, Anderson K, Gorin FA, Burns MS. Primate rod and cone photoreceptors may differ in glucose accessibility. Invest Ophthalmol Vis Sci 1995; 36:1259-70; PMID:7775103
44. Pfeiffer-Guglielmi B, Francke M, Reichenbach A, Fleckenstein B, Jung G, Hamprecht B. Glycogen phosphorylase isozyme pattern in mammalian retinal Müller (glial) cells and in astrocytes of retina and optic nerve. Glia 2005; 49:84-95; PMID:15390095; http://dx.doi.org/10.1002/glia.20102
45. Osorio-Paz I, Sánchez-Chávez G, Salceda R. Control of glycogen content in retina: allosteric regulation of glycogen synthase. PLoS One 2012; 7:e30822; PMID:22363495; http://dx.doi.org/10.1371/journal.pone.0030822
46. Owen EH, Logue SF, Rasmussen DL, Wehner JM. Assessment of learning by the Morris water task and fear conditioning in inbred mouse strains and F1 hybrids: implications of genetic background for single gene mutations and quantitative trait loci analyses. Neuroscience 1997; 80:1087-99; PMID:9284062; http://dx.doi.org/10.1016/S0306-4522(97)00165-6
47. Clapcote SJ, Lazar NL, Bechard AR, Roder JC. Effects of the rd1 mutation and host strain on hippocampal learning in mice. Behav Genet 2005; 35:591-601; PMID:16184487; http://dx.doi.org/10.1007/s10519-005-5634-5
48. O'Steen WK, Spencer RL, Bare DJ, McEwen BS. Analysis of severe photoreceptor loss and Morris water-maze performance in aged rats. Behav Brain Res 1995; 68:151-8; PMID:7654301; http://dx.doi.org/10.1016/0166-4328(94)00168-F
49. Spencer RL, O'Steen WK, McEwen BS. Water maze performance of aged Sprague-Dawley rats in relation to retinal morphologic measures. Behav Brain Res 1995; 68:139-50; PMID:7654300; http://dx.doi.org/10.1016/0166-4328(94)00167-E
50. Koch S, Sothilingam V, Garcia Garrido M, Tanimoto N, Becirovic E, Koch F, Seide C, Beck SC, Seeliger MW, Biel M, et al. Gene therapy restores vision and delays degeneration in the CNGB1(-/-) mouse model of retinitis pigmentosa. Hum Mol Genet 2012; 21:4486-96; PMID:22802073; http://dx.doi.org/10.1093/hmg/dds290
51. D'Hooge R, De Deyn PP. Applications of the Morris water maze in the study of learning and memory. Brain Res Brain Res Rev 2001; 36:60-90; PMID:11516773; http://dx.doi.org/10.1016/S0165-0173(01)00067-4
52. Bolivar VJ, Pooler O, Flaherty L. Inbred strain variation in contextual and cued fear conditioning behavior. Mamm Genome 2001; 12:651-6; PMID:11471061; http://dx.doi.org/10.1007/s003350020039
53. Clapcote SJ, Lazar NL, Bechard AR, Wood GA, Roder JC. NIH Swiss and Black Swiss mice have retinal degeneration and performance deficits in cognitive tests. Comp Med 2005; 55:310-6; PMID:16158906
54. Taylor WR, Morgans C. Localization and properties of voltage-gated calcium channels in cone photoreceptors of Tupaia belangeri. Vis Neurosci 1998; 15:541-52; PMID:9685206; http://dx.doi.org/10.1017/S0952523898153142
55. Morgans CW, El Far O, Berntson A, Wässle H, Taylor WR. Calcium extrusion from mammalian photoreceptor terminals. J Neurosci 1998; 18:2467-74; PMID:9502807
56. Morgans CW. Calcium channel heterogeneity among cone photoreceptors in the tree shrew retina. Eur J Neurosci 1999; 11:2989-93; PMID:10457194; http://dx.doi.org/10.1046/j.1460-9568.1999.00719.x
57. Firth SI, Morgan IG, Boelen MK, Morgans CW. Localization of voltage-sensitive L-type calcium channels in the chicken retina. Clin Experiment Ophthalmol 2001; 29:183-7; PMID:11446465; http://dx.doi.org/10.1046/j.1442-9071.2001.00401.x
58. Welch NC, Wood S, Jollimore C, Stevens K, Kelly ME, Barnes S. High-voltage-activated calcium channels in Muller cells acutely isolated from tiger salamander retina. Glia 2005; 49:259-74; PMID:15472989; http://dx.doi.org/10.1002/glia.20113
59. Cristofanilli M, Mizuno F, Akopian A. Disruption of actin cytoskeleton causes internalization of Ca(v)1.3 (alpha 1D) L-type calcium channels in salamander retinal neurons. Mol Vis 2007; 13:1496-507; PMID:17893673

60. Henderson D, Doerr TA, Gottesman J, Miller RF. Calcium channel immunoreactivity in the salamander retina. Neuroreport 2001; 12:1493-9; PMID:11388436; http://dx.doi.org/10.1097/00001756-200105250-00039
61. Xiao H, Chen X, Steele EC Jr. Abundant L-type calcium channel Ca(v)1.3 (alpha1D) subunit mRNA is detected in rod photoreceptors of the mouse retina via in situ hybridization. Mol Vis 2007; 13:764-71; PMID:17563731
62. Mizuno F, Barabas P, Krizaj D, Akopian A. Glutamate-induced internalization of Ca(v)1.3 L-type Ca(2+) channels protects retinal neurons against excitotoxicity. J Physiol 2010; 588:953-66; PMID:20123787; http://dx.doi.org/10.1113/jphysiol.2009.181305
63. Kersten F, van Wijk E, van Reeuwijk J, van der Zwaag B, Maerker T, Peters T, Katsanis N, Wolfrum U, Keunen J, Roepman R, et al. Invest Ophthalmol Vis Sci 2009; PMID:19959638
64. Wu J, Marmorstein AD, Striessnig J, Peachey NS. Voltage-dependent calcium channel CaV1.3 subunits regulate the light peak of the electroretinogram. J Neurophysiol 2007; 97:3731-5; PMID:17376851; http://dx.doi.org/10.1152/jn.00146.2007
65. van Oosterhout F, Michel S, Deboer T, Houben T, van de Ven RC, Albus H, Westerhout J, Vansteensel MJ, Ferrari MD, van den Maagdenberg AM, et al. Enhanced circadian phase resetting in R192Q Cav2.1 calcium channel migraine mice. Ann Neurol 2008; 64:315-24; PMID:18825664; http://dx.doi.org/10.1002/ana.21418
66. Storch KF, Paz C, Signorovitch J, Raviola E, Pawlyk B, Li T, Weitz CJ. Intrinsic circadian clock of the mammalian retina: importance for retinal processing of visual information. Cell 2007; 130:730-41; PMID:17719549; http://dx.doi.org/10.1016/j.cell.2007.06.045
67. Ko ML, Liu Y, Shi L, Trump D, Ko GY. Circadian regulation of retinoschisin in the chick retina. Invest Ophthalmol Vis Sci 2008; 49:1615-21; PMID:18385082; http://dx.doi.org/10.1167/iovs.07-1189
68. Shi L, Ko ML, Ko GY. Rhythmic expression of microRNA-26a regulates the L-type voltage-gated calcium channel alpha1C subunit in chicken cone photoreceptors. J Biol Chem 2009; 284:25791-803; PMID:19608742; http://dx.doi.org/10.1074/jbc.M109.033993